

Copyright is owned by the Author of the thesis. Permission is given for a copy to be downloaded by an individual for the purpose of research and private study only. The thesis may not be reproduced elsewhere without the permission of the Author.



MASSEY
UNIVERSITY
TE KUNENGA KI PŪREHUROA

UNIVERSITY OF NEW ZEALAND

THE DEVELOPMENT OF OPTICAL
NANOMACHINES
FOR STUDYING MOLECULES

A THESIS PRESENTED IN PARTIAL FULFILMENT OF THE REQUIREMENTS FOR THE
DEGREE OF
DOCTOR OF PHILOSOPHY
IN
MECHATRONICS ENGINEERING
AT MASSEY UNIVERSITY, PALMERSTON NORTH,
NEW ZEALAND.

Philippa-Kate Andrew

2022

Contents

ABSTRACT	xx
DEDICATION	xxi
QUOTE	xxii
ACKNOWLEDGEMENTS	xxiii
1 INTRODUCTION	1
1.1 PROBLEM STATEMENT	2
1.2 THESIS OVERVIEW	2
1.3 KEY CONTRIBUTIONS	3
1.4 COLLABORATORS AND CO-AUTHORS	3
1.5 PUBLICATIONS USED IN THIS THESIS	5
1.6 SELECTED PRESENTATIONS	5
2 OPTICAL MICROMACHINES FOR BIOLOGICAL STUDIES	6
2.0.1 DECLARATION	7
2.1 OPTICAL MICROMACHINES FOR BIOLOGICAL STUDIES	8
2.1.1 INTRODUCTION	8
2.1.2 AN INTRODUCTION TO THE THEORY OF OPTICAL TWEEZERS	9
2.1.3 FIRST APPLICATIONS AND IMPACT ON FIELDS	13
2.1.4 OPTICAL TRAPPING: CONCERNS FOR BIOLOGICAL RESEARCH	15
2.1.5 OPTICAL MICROROBOTS	18
2.1.5.1 POTENTIAL TOOLS FOR BIOLOGICAL STUDIES	18
2.1.5.2 ACHIEVEMENTS TO DATE AND CHALLENGES	20
2.1.5.3 EFFECTS OF MICROROBOT SHAPE	24
2.1.6 CHOICE OF OPTICAL TWEEZERS FOR MICROROBOTICS	27
2.1.7 LOOKING TO THE FUTURE	29

2.1.8	CONCLUSIONS	30
3	FUNCTIONAL OPTICAL MICROMACHINES	33
3.1	PREMISE	33
3.2	TWO PHOTON ABSORPTION POLYMERISATION (TPAP)	35
3.2.1	THE NANOSCRIBE PHOTONIC PROFESSIONAL GT2	37
3.3	THE OPTICAL TWEEZERS SETUP	40
3.3.1	HOOKEAN SPRING MODEL OF OPTICAL TWEEZERS	44
3.4	PRELIMINARY DESIGN WORK AND RESULTS	45
3.4.1	SAMPLE PREPARATION AND OPTICAL TRAPPING CONFIGURATION	48
3.4.2	FIRST LEVER RESULTS	51
3.4.3	SECOND ITERATION OF LEVER DESIGNS	53
3.4.4	FURTHER CHANGES TO LEVER DESIGNS	57
3.4.4.1	KEY FEATURES OF MICROLEVERS	58
3.4.4.2	SUPPORTED AND UNSUPPORTED MICROLEVERS	59
3.4.4.3	IMPROVING MICROLEVER FUNCTIONALITY	61
3.5	DESIGN OF OPTICAL MICROMACHINES FOR USE IN BIOLOGI- CALLY RELEVANT ENVIRONMENTS	69
3.5.1	DECLARATION	69
3.5.2	INTRODUCTION	69
3.5.3	METHODS	71
3.5.3.1	THEORY	71
3.5.3.2	DESIGN AND MANUFACTURE	72
3.5.3.3	EXPERIMENTAL	76
3.5.4	RESULTS AND DISCUSSION	78
3.5.5	CONCLUSIONS	83
4	DNA STRETCHING	84
4.1	DNA AS A MECHANICAL OBJECT	84
4.1.1	THE FREELY-JOINTED CHAIN	84
4.1.2	THE WORM-LIKE CHAIN MODEL	86
4.2	TRADITIONAL DNA STRETCHING PROTOCOL	87
4.2.1	MODIFYING THE DUAL-TRAP PROTOCOL	89
4.3	OPTICAL MICROLEVER-ASSISTED DNA STRETCHING	94
4.3.1	DECLARATION	96

4.3.2	INTRODUCTION	96
4.3.3	DESIGN OF MICROLEVERS	98
4.3.4	EXPERIMENTAL METHOD AND MATERIALS	99
4.3.4.1	OPTICAL TWEEZERS SET-UP	99
4.3.4.2	LEVER PRINTING	100
4.3.4.3	SAMPLE PREPARATION	101
4.3.4.4	DNA STRETCHING PROTOCOL	101
4.3.5	RESULTS AND DISCUSSION	103
4.3.5.1	LEVER-ASSISTED STRETCHES	103
4.3.5.2	TRACKING LEVER MOVEMENT	106
4.3.5.3	STRETCHES USING TWO BEADS	106
4.3.5.4	DISCUSSION OF THE LEVER-ASSISTED METHOD	107
4.3.6	CONCLUSIONS	108
4.4	FURTHER WORK	109
4.4.1	DOUBLE LEVER ASSISTED STRETCHES	109
4.4.2	MEASURING FORCE AMPLIFICATION USING DNA STRETCHING	114
5	GIVING OPTICAL TWEEZERS A MECHANICAL ADVANTAGE	118
5.1	DEVELOPING AN OPTICAL MICROLEVER FOR STABLE AND UNSUPPORTED FORCE AMPLIFICATION	119
5.1.1	DECLARATION	119
5.1.2	INTRODUCTION	120
5.1.3	LEVER DESIGN	122
5.1.4	OPTICAL TWEEZERS SET-UP	126
5.1.5	EXPERIMENTATION AND RESULTS	127
5.1.5.1	QUANTIFYING OUT OF PLANE MOVEMENT . . .	127
5.1.5.2	AMPLIFYING FORCE	131
5.1.6	CONCLUSIONS	134
6	CONCLUSIONS AND FUTURE WORK	135
6.1	THESIS SCOPE AND SUMMARY	135
6.2	FUTURE WORK BASED ON THIS THESIS	136
6.2.1	DOUBLE-LEVER-ASSISTED DNA STRETCHING	136
6.2.2	COMPARISON OF OPTICAL TRAPPING EFFECTS ON DNA	137
6.2.3	QUANTITATIVE ANALYSIS OF TPAP EFFECTS ON OPTICAL MICROROBOTS	138

6.2.4	IMPROVING MODELLING OF FORCES ON MICROLEVERS	138
A	NANOSCRIBE PRINT SETTINGS	140
A.0.0.1	PRINTING CONFIGURATION AND DIRECTION . .	142
A.0.0.2	LASER SCAN MODE, Z-POSITION ADJUSTMENT AND HATCHING DIRECTION	144
A.0.0.3	THIN-WALLED SHAPES	145
B	LAYOUT OF LARGE SAMPLES USED FOR CHAPTER 3	148
C	DRC FORMS FOR PUBLICATIONS IN THIS THESIS	151
	Bibliography	156

List of Tables

3.1	Key Features of the objectives used for high resolution direct laser writing with the PPTG2	37
3.2	The features of the first successfully rotating microlever.	51
3.3	Variations of the second iteration of levers, and the code used to label them.	55
3.4	Printing parameters used for levers in Fig. 3.20 and Fig. 3.21.	62
3.5	Adaptive slicing mode parameters used to produce smooth levers.	66
3.6	Features of levers used in this study.	75
3.7	Tris-Buffered Saline Concentrations Used for Trapping	78
5.1	Variable features of the levers used in this work.	126
5.2	Mean Transferred and Applied Forces	134
B.1	Sample layout for Sample 1A. Inner radius of the levers was 900 nm larger than the radius of the centre axle.	149
B.2	Sample Layout for 1C (IP-L 780) and 1D (IP-Dip). All levers were printed with a scanning speed of 10 mm/s and a vertical gap of 1.4 μm	150

List of Figures

2.1	Optical tweezer theory treats the force associated with the focussed laser beam as two components, which can be visualised as resulting from the intense focussing of the light.	11
2.2	Three different methods for stretching a DNA tether with optical tweezers can be seen in this figure: the translating slide method (a), using an anchoring micropipette (b) and using two separate optical traps (c). Reproduced with permission from Reference [1]. ©2014 American Chemical Society.	15
2.3	The inclusion of a thin metallic layer inside a 3D printed chamber leads to the movement of silica and polystyrene payload particles through convection. Reproduced from Villangca et al. [2], under Creative Commons license NC ND 4.0.	23
2.4	Asavei et al. produced an optical “paddle wheel” held in place using two 1070 nm optical traps and driven with a separate 780 nm beam. Reproduced from “Optically trapped and driven paddle-wheel”, [3], under Creative Commons license CC BY 3.0. (Top): Schematic of the device. (Bottom): Stills taken from a video of the device in action, where the position of the 780 nm beam is shown with a red x.	25
2.5	Illustration of the interaction of the optical tweezers with differently shaped low-refractive index particles, and the impact of the position of the beam waist. In (a) and (c) the object shape and the beam waist position act to push the object out of the trap, whereas in (b) the incident forces are balanced on the inner walls of the ring, and the position of the beam waist in the Z direction acts to pull the object towards the waist, producing a stable trap. M_i is the incident momentum, M_o is the outgoing momentum and M_d is the momentum transferred from the light to the object. Reproduced with permission from Reference [4] ©The Optical Society.	27
2.6	Simple schematic of holographic optical tweezers, based on the authors’ laboratory set-up.	28

2.7	A free-floating microrobot, such as this lever, equipped with a sharp tip, could be used to apply amplified forces for measuring cell membrane stiffness. At least two traps are necessary for this, one fixed trap to hold the microlever in place near the cell and another to move the lever arm.	32
3.1	The highly focused, pulsed infrared lasers used for TPAP allow for the polymerisation of tiny voxels of resin at a time, in contrast with the 360 nm ultraviolet sources commonly used for conventional, 2D photolithography.	36
3.2	Nanoscribe's PPGT2 allows the user to define points for polymerisation directly (point by point) or use DeScribe's import wizard to define a recipe for an already designed .stl file.	39
3.3	The optical tweezers setup used for this work included both HOT and a pair of higher power traps, one of which was fixed in place and the other which could be steered by positioning a mirror using a piezo controller.	42
3.4	The three initial levers: (a) a first-class pin-jointed lever, (b) a second-class pin-jointed lever and (c) a simple cantilever.	46
3.5	The initial concept for a simple cantilever, with a much thinner segment of the beam acting as an elastic joint. All measurements are in micrometres.	47
3.6	The results of SolidWorks simulation indicated that forces near the limit of the HP trap's powers would be insufficient to usefully bend the cantilevers (despite the dramatic looking bend that the simulation animation produces).	48
3.7	The borosilicate microprobes pictured above a sample populated with levers printed using IP-L 780.	49
3.8	The depth limitations of the optical traps required different orientations for the levers printed with IP-Dip and IP-L 780.	50
3.9	Lowering the laser power used for polymerisation resulted in a well-defined vertical gap, but sagging lever arms. Additionally, this SEM image seems to show resin sagging in the lever ring, as well as along the arm. Image by Dr Daniel Fan, 2018.	52
3.10	The design that produced the first successfully rotating levers was supported with four long, thin pillars of resin. These were easily detached from the substrate, but not easily removed from the levers.	52
3.11	Stills from a screen recording of the first successfully optically manipulated lever. It seemed that the trap (shown in green) was pushing the lever around, rather than actually trapping the lever, potentially due to scattering effects from the flat surfaces of the lever.	53

3.12	The second group of levers were designed to have lever arms with equal length on either side of the pivot. There were 30 μm long from end-to-end, with dimensions shown in (a). The two types of pins used were the “A” (angled) pins, marked (b) in this figure and the “B” (flat) pins, marked (c) here.	54
3.13	Test results from the Group A microlevers, for the milliQ water manual turn test (with the microprobe) and with the optical tweezers.	56
3.14	Test results from the Group B microlevers, for the milliQ water manual turn test (with the microprobe) and with the optical tweezers.	56
3.15	The first attempt at attaching a functionalised microbead to the especially printed pocket at the end of the lever. (a) The microbead appeared to be attached when the optical trap was holding it in place, seemingly against the lever. (b) However, when the trap was switched off the bead was shown to not be attached. Additionally, the micrographs shown here illustrate one of the problems with using the same sample for multiple experiments in liquid environments: namely the colonisation of the sample by bacteria.	58
3.16	While changes were made to the levers to improve their functionality, the key features were chosen specifically for the goals of this project. In this diagram, the explanation for these key features is given. The SEM image in the inset shows an excellent view of the lateral gap between lever arm and axle, due to removal of the top of the pin.	59
3.17	Attempts to remove supports using the borosilicate microprobe were largely unsuccessful, with the supports instead being detached from the substrate, and then bent out of the way.	60
3.18	Attempting to print levers with gaps between the supports and the lever arm did not yield promising results, with some distortion of the lever visible.	61
3.19	A designed gap of 800 nm was not sufficient to create more easily removed supports, but did have the effect of deforming the levers printed.	62
3.20	The relationship between laser dose and voxel size in TPAP means that different ranges of laser power produce the most effective results for different geometries. Here this manifests as a difference in range of power required to produce functional microlevers. The data shown on the graph are the combined averages taken from three samples with three levers printed at each laser power.	63

3.21	In this SEM image, the narrow window of laser power for optimum functionality can be seen, as some of the levers have rotated without requiring manipulation after printing. This can be seen as a difference in orientation, from the 0° printing direction to almost 90°. The upper group, which was printed with a 1.0 μm lateral gap, also appears to show a decrease in functionality at around 37% laser power, indicating that the separation between parts may be compromised by increased voxel size at this laser power.	64
3.22	Lever sagging and hogging seen when using 90°hatch angle and offset. .	64
3.23	Lever deformity seen when using 0°hatch angle and offset. The poor sphere shape was of particular concern.	65
3.24	The printing parameters outlined in Table 3.4 seemed to be insufficient for producing levers with high quality surface finish, although the overall lever shape was good.	65
3.25	A high magnification image of a lever’s pocket seems to show the effect of the fixed hatching and slicing distance, as well as the lack of contour. .	66
3.26	Changing the slicing mode from fixed to adaptive, and introducing two contours in the printing settings resulted in vastly improved lever smoothness and pocket quality, as shown in this image.	67
3.27	Ridges were printed on the tops of pillars in order to determine repeatability when printing thin ridges, as well as how this varied when the printing laser power was adjusted.	67
3.28	Evaluation of the thickness of the different ridges with respect to the laser power used to print them revealed that the average thickness varied only slightly, with high variability within the samples that used the same power. The average size of the features remained roughly consistent at just over 200 nm.	68
3.29	The dependence of the Debye length on the concentration of TBS, according to (3).	73
3.30	The basic design was a first-class lever, with equal length arms. Three spherical features are positioned as trapping handles, and a pocket is positioned at the end of the lever. All measurements are in micrometres.	74
3.31	Five variations of the basic 1:1 lever were used in this study. Two of these designs featured no supporting structures, while the other three were supported using either straight or tapered supports. Additionally, centre-pin height, vertical gap size and lever arm thickness varied between designs.	74
3.32	The “No Supports” type lever under SEM.	75

3.33	The optical trapping set-up used for the work. This diagram was previously published in [5].	77
3.34	Trapping was performed using a holographic optical trap, placed on one of the “inner” trapping handles, as shown here with the red “x” in (a). If a full turn was not possible in this configuration, or if the lever moved out of focus due to the unbalanced force, then two traps were used, as shown in (b).	77
3.35	Lever performance was simply grouped into three categories: successful, multiple 360° turns (top); response to the optical trap but no full turns, where out-of-plane movement and limited rotation are counted (middle); and stuck levers (bottom).	79
3.36	The ridges added to the centre-pin served to keep overlapping area small, and increase vertical separation. However, the size of the outer cut-out on the lever arm was the same diameter as the outside of the pin, meaning that “cupping” of the centre pin during settling would actually increase the contact area between parts.	80
3.37	In this case it is possible to see the support structures flexing against the lever turning. Due to the strength of adhesion between the substrate and the supports, a full turn was impossible, but the supports were flexible enough to allow slight twisting and rotation around the axis. The red arrows point to two of the supports, showing a slight change in position and angle.	80
3.38	Unsupported levers required two traps to ensure planar rotation. In these stills from the trapping videos for NS levers in milliQ water the difference between trapping using a single trap (left) and symmetric rotating traps (right) can be clearly seen.	81
3.39	Microbeads could be successfully attached to functional levers at 5% TBS. Before attachment (a) and after (b).	82
4.1	The FJC breaks a polymer of length L into N equal-length segments of length b . The end-to-end vector for the entire polymer is R and the vector for each segment is represented by r_i , where $i = 1, 2, \dots, N$	85
4.2	The possible configurations of DNA are many at the equilibrium state, but the probability distribution of these changes as the polymer is extended. Stretching DNA thus allows researchers to determine characteristic properties of the molecule, even when using simple models such as the FJC.	86

4.3	The persistence length is defined as the distance between points at which the tangent angles are no longer correlated. The zoomed in view in the magenta circle shows the persistence length as the distance between the two points marked by crosses, with the tangent angles indicated by θ_1 and θ_2	87
4.4	The HOT system was used to stretch dsDNA in a low-power dual trap assay in a 10% TSB solution, and the results were fit to the WLC model to test whether stretches could be performed in such a solution. (a) The beads are brought close together to allow a tether to form before one is pulled away to create a stretch. (b) When a stretch is created, the bead in the stationary trap moves out of the trap centre, which allows the force-extension to be measured.	90
4.5	A short series of low-force DNA stretches were performed using the dual-trap configuration with the HOT, and a 10% TSB solution, in order to evaluate the possibility of performing DNA stretches in a low-ionic strength environment.	91
4.6	Initial attempts at adding AD beads to the samples used higher concentrations than were required, resulting in the levers becoming covered in microbeads.	92
4.7	(a) The Hough circle transform was used to detect circles at the start of a sequence of images, and centre-of-mass tracking was then used to monitor the movement of these points over the course of the sequence. (b) A lever at the start of a sequence of oscillations, where the entire lever appears to be in focus. (c) A lever at the peak of oscillations, the lever still appears to be in focus and the trapped end remains in the optical trap, indicating that the lever is not sticking as it moves around the pivot.	94
4.8	(a) In the ideal case microlevers remained trapped over multiple waveform cycles, and displayed the same motion. Here it can be noted that the Free End (where the AD bead is attached using the pocket) demonstrates motion with 2x the amplitude of the input waveform (measured using the motion of the pivot). (b) Events that disrupt the trap, such as a free microbead flying into the trap, in this case, cause noticeable differences to the levers' movement. Of particular note is the disruption to the position of the trapped handle, circled in red.	95

4.9	(a) The familiar dumbbell assay moves functionalised microbeads apart, using optical tweezers to stretch DNA. (b) The microlevers used for this work have a pocket for attaching a microbead, and offer a simple mechanism for distancing the trap from the target. (c) The modified assay, using a microlever to distance one of the traps.	97
4.10	The levers used for the DNA stretching were made with the dimensions shown.	98
4.11	(a) The supported levers used for DNA stretching had tapered supports that narrowed at the bottom, but otherwise shared the same dimensions as the unsupported levers shown in (b). The supports in the SEM image are pointed out by red arrows in the diagram.	99
4.12	The optical tweezers setup used for this study consisted of two separate lasers, with dichroic mirrors used to reflect the beams into the objective.	100
4.13	(a) and (b) show an anti-digoxigenin coated bead being guided into the pocket of a lever. (c) shows the borosilicate microprobe setup on the microscope, and (d) shows the borosilicate probe being used to turn a microlever with a bead in its pocket. This process was useful for testing how firmly the beads were attached, as well as freeing seized levers. . . .	102
4.14	Scattering interactions of bent supports occasionally led to levers being “pushed up” out of the plane, as in (a). (b) shows a supported lever spontaneously reorientating in the optical trap, resulting in the entire lever being slightly angled around the y (long) axis, rather than being flat in the x-y plane. (c) shows an unsupported lever, appearing to be well focused and flat in plane. Comparisons such as this validated the use of unsupported levers for this work.	104
4.15	Compilation of stretches performed using supported levers. These stretches demonstrated the difficulty of repeating a stretch with a single DNA duplex, as often over the course of the experiment more DNA attaches, leading to a narrowing of the force-extension curve.	105
4.16	Compilation of stretches performed using unsupported levers. These stretches were performed with a 10x lower concentration of DNA, indicating that the problem of multiple strands attaching could be overcome for DNA-assisted stretches.	105

4.17	It was difficult to perform multiple stretch repetitions with the levers, due to the difficulty of restricting the stretches to a regime that would not pull the streptavidin bead out of the trap, and the possibility of the lever seizing during the stretch. Here a particularly successful lever was tracked, which resulted in three stretch repetitions. A 2.0 μm , 0.1 Hz triangle wave was applied and data were recorded at 50 fps.	107
4.18	Performing DNA stretches with microbeads allowed for a comparison of lever-assisted stretches with a more traditional method, here results are shown for 12 stretches performed using the fixed bead method. The stretches performed using this method show the same kind of multiple-strand behaviour seen in the supported lever results.	107
4.19	In previous work regarding the functionality of microlevers in challenging, salty environments, only a fraction of levers worked well. Therefore, samples were printed with 20 pairs of microlevers to increase the chances that both levers would be able to turn, which is necessary for lever-assisted DNA stretching. A large “F” was printed on all samples over the course of this project, for ease of locating the levers for SEM imaging, and to provide orientation information, as “F” has no rotational symmetry.	110
4.20	(a) Levers were printed with a slight offset (4 μm) in the X direction, in order to allow for contact between microbeads when they were attached to the printed pockets. (b) The first concept for double lever-assisted DNA stretches involved trapping the microlevers at the handle furthest from the pockets.	110
4.21	Attaching the 1.26 μm diameter streptavidin beads to the levers proved problematic due to interference to the optical traps, likely due to the shape of the pockets on the microlevers.	111
4.22	Stills taken from a montage of attempted DNA stretching with a double microlever configuration revealed problems with the concept. (a), (b) and (c) demonstrate lever mobility in response to movement of the top (a and b) and bottom (c) traps. (d) and (e) show the microbeads becoming stuck together, an occurrence that revealed the sensor trap’s lack of sensitivity in this configuration.	112

4.23	(a) The actuator lever was changed to be asymmetric, allowing for the possibility of force-amplification, a thin ridge around the inner radius of the lever arm was added to try to increase the time that the lever remained functional for, and the lateral and vertical gaps were decreased in order to try to reduce tolerance in the pin joint. (b) The sensor lever was changed to a “half lever” with the same lateral gap as the actuator lever, as well as an area reducing ridge. Both the actuator and sensor levers were printed with “centred” pockets, in the hope that this would make bead attachment quicker and easier.	113
4.24	(a) An SEM image of the new paired levers for attempted double-lever-assisted DNA stretching. The clear radius of the pockets was especially good to see. (b) The concept for the stretch included making use of the ratios between the distance between the force application points (the microbeads) and the trap positions from the lever axles.	113
4.25	The comparative lack of flexibility of the high power optical tweezers, compared with the holographic optical tweezers, meant that the levers started in non-ideal positions (compared to the horizontal starting point imagined in Fig. 4.24. Fixed trap position is shown in red, while the steered trap is shown in violet. (a) The difference between the Z position of the fixed and steered components of the trap means that when the steered position is aligned with the camera focus, the fixed trap is out of focus. Here the bead attached to the sensor lever was actually stuck to the underside of the lever rather than perfectly in the pocket, meaning it remained somewhat in focus. (b) In this image the handle mid-way along the lever is being used to control the position of the sensor lever, which seems to allow for better matching of the microbeads in the lever pockets. However, it results in more out-of-plane movement of the microlever overall.	115
4.26	Single-lever DNA stretching, with the option for force amplification was seen as one way to investigate the use of DNA as a metrology standard, and to test the amplification abilities of the microlevers. (a) The expected scenario with an un-amplified HOT trap: the force is too low to displace the strep bead from the HP trap, and a low-force stretch, as well as displacement of the lever, is the result. (b) Moving the HOT trap so that it has a mechanical advantage against the HP trap was thought of as a method to amplify forces, hopefully allowing for force measurement based on displacement from the HP trap.	116

4.27	Attempting to perform DNA stretches using the HOT to move the microlever, and the high power tweezers to trap a free streptavidin bead did not work well. (a) The high power of the optical trap resulted in multiple beads being trapped at once, leading to the seemingly out-of-focus trap seen here, and making alignment with the levers difficult (circled in magenta). (b) Like free microbeads, the levers themselves were pulled into the high powered trap when alignment with the trapped strep beads was attempted (circled in magenta). Position of the holographic trap is marked by a violet “x”.	117
5.1	Our experiment uses a two-trap set-up to test and quantify optical force amplification (a), with the hope that such levers could become useful tools in areas such as molecule stretching (b) and cell studies (c).	120
5.2	The basic design for levers in this work featured an “effort arm” twice as long as the shorter “output arm”. The longer side also featured two spherical handles, to be used for optical trapping, to allow for comparison between force applied with an equal lever arm ratio and a force applied using the 2:1 arm ratio. The lateral and vertical gaps, shown in dark blue and magenta respectively, are important for the functionality of the lever, as inadequate separation between parts leads to a greater likelihood of adhesion between parts.	123
5.3	A short test using a series of levers with outsize centre pins (concept shown in a) showed a decrease in success rate with increasing area (b), despite the levers with larger area also having larger lateral gaps. Gap size was incremented by 0.2 μm , from 1.0 to 1.6 μm . Overlapping area was calculated per the shaded area shown in (b, inset), based on the projected vertical area of the lever arm on the pin, when in a perfectly centred position.	125
5.4	(a) The levers used for this study had different handle shapes, which were referenced by 2H, 3H or 3OH in the naming convention used. (b) an SEM image showing the successful printing of the ridge that was used to reduce contact between the centre axis and the inner radius of the lever arm.	126
5.5	The setup was equipped with two lasers for creating separate optical traps. This forms two optical tweezers: one holographic and dynamic and the other fixed. The fixed trap was attenuated using a neutral density filter.	127

5.6	The levers were oscillated in the Y-direction, for 10 cycles using the piezo stage, with the goal of monitoring out-of-plane movement over the course of these oscillation.	128
5.7	Tracking the movement of the lever over the course of the experiment provided an easy method for selecting frames to compare to each other. In this case 100 frames were selected from the peaks and the troughs of the pivot’s movement, respectively. This plot also shows the inconsistent phase shift between the free end of the lever and the oscillating pivot, which is attributed to the tolerance of the pin joint.	129
5.8	Strips across the image were used to quantify a change in focus as the levers were moved back and forth to test trap stability. Correlation of the Fourier power spectra of these strips was calculated for the “flat” (a) and “rotated” (b) cases, which corresponded with the beginning and peak of oscillations respectively.	130
5.9	The calculated trap stiffness for the 3 μm trap handles was much lower than for the 2 μm handles at the same trapping powers, while the values for the 2 μm handles were comparable to values for 2 μm polystyrene beads.	131
5.10	The calculated trap stiffness for the fixed high power trap was much higher than for the HOT trap, as expected.	132
5.11	Force amplification could be measured successfully at three different laser powers, with results shown vertically offset in order to make separate lines clearer.	132
A.1	Just as in conventional printing, DeScribe allows the user to set the slicing distance for a job.	141
A.2	The hatching configuration can be set in DeScribe, and both the angle and hatch separation are important for the overall result.	142
A.3	The final screen of the DeScribe .stl import process allows the user to set the name that will be used to identify the associated files, as well as letting them set several printing parameters. The yellow warning symbols seen in this screenshot are displayed as job and data files already exist for this filename. In order to avoid overwriting when changing printing parameters, the data and job file names should be edited to reflect the chosen parameters, to keep track of design iterations.	143

A.4	The Z direction for printing is conventionally set to be “upwards” for the oil-immersion method and “downwards” for DiLL. The PPGT2 uses the refractive index mismatch between the substrate and the resin to find the interface, in both cases. In DiLL, the resin itself is used as the lens immersion media, rather than the index-matched oil used for the oil-immersion method.	144
A.5	Accidental bubbling of resist, caused by too-high laser dose. While such bubbling is generally considered undesirable, it can also provide interesting possibilities for creating features that are generally unprintable. .	146

Nomenclature

AD Anti-digoxygenin. Also abbreviated as anti-dig

bp Base pair

DLVO Theory Theory explaining aggregation of aqueous dispersions.
Named for Derjaguin, Landau, Verwey and Overbeek

dsDNA Double stranded Deoxyribonucleic acid

FJC Freely-Jointed Chain

HOT Holographic Optical Tweezers

PPGT2 Nanoscribe Photonic Professional GT 2

SLM Spatial Light Modulator

Strep Streptavidin

TPAP Two Photon Absorption Polymerisation

WLC Worm-like Chain

ABSTRACT

Optical tweezers have been used for a number of applications since their invention by Arthur Ashkin in 1986, and are particularly useful for biological and biophysical studies due to their exceptionally high spatial and force-based resolution. The same intense laser focus that allows light to be used as a tool for micro-nanoscale manipulation also has the potential to damage the objects being studied, and the extremely high force resolution is coupled with the limitation of very low forces. There is potential to overcome these drawbacks of optical manipulation through making use of another laser based technique: two-photon absorption polymerisation (TPAP). This thesis has brought these together to demonstrate the uses of optical nanomachines as helpful tools for optical tweezer studies. The project was highly interdisciplinary, concerning the intersection of optical trapping, 3D micromachine design and development, and DNA stretching. The thesis was based around the strategy of first developing micro-robots and demonstrating their manipulation using optical tweezers, then adjusting the design for specific applications. Microlevers were developed for lever-assisted DNA stretching and amplification of optical forces. The influence of design features and TPAP parameters on microlever functionality was investigated; particularly the influence of overlapping area and presence of supports, and the effects of differently shaped "trapping handles". These features were important as lever functionality was tested in solutions of different ionic strength, and stable trapping of the levers was required for force amplification. DNA stretching was chosen as a target application for distanced-application of optical forces due to its status as a well-known and characterised example of single-molecule studies with optical tweezers. Amplification of optical forces was also seen as an application that could demonstrate the utility of optical micromachines, and microlevers with a 2:1 lever arm ratio were developed to produce consistent, two-fold amplification of optical forces, in a first for unsupported, pin-jointed optical micro-robotics. It is hoped that in the future fully-remote, micromachine-assisted studies will extend optical tweezer studies of laser-sensitive subjects, as well as increasing the forces that can be applied, and the results obtained in this thesis are encouraging. All in all, the thesis confirms the potential of optical micromachines for aiding studies using optical tweezers, and demonstrates concrete progress in both design and application.

DEDICATION

*For Jordan Ambrose Andrew, Maxine Exton, Wilf Cameron Exton, Caiti Spence and
E. J. Banbury.*

QUOTE

“Reality so often fails when it comes to small, satisfying details, she thought.”

- Sir Terry Pratchett, *Nation*

ACKNOWLEDGEMENTS

A PhD is the achievement of one, but it's the fault of many, and so I am crediting the many people who had a vital role in this undertaking. I will undoubtedly leave people out, and I will realise once it is printed, submitted to the library and I have proofread it once again, perfectly happy. Therefore, let's all agree to charitably pretend that I managed to express my gratitude adequately to everyone, at some stage. Feel free to skip this, writing conventions will be defenestrated.

I'm grateful to my supervisors, Ebu and Bill, who managed to find ways to keep the wheels turning despite the rubber continuously threatening to come off the tyres. I'm also incredibly grateful to Allan Raudsepp, who I would have liked to have had formally added to my supervision team, for his patience, help and incredible depth and breadth of knowledge. "Dankjewel" to Urs Stauffer, for hosting my project and for being my promoter at the TU Delft, and to the inimitable Daniel Fan, who was a fantastic day supervisor. Likewise, my sincerest thanks and appreciation to Volker Nock, who is one of the most energetic and kindest researchers in the Southern Hemisphere, and who continues to entertain my ideas. Thank you as well to my examiners, I am so grateful for your time and effort in examining this thesis. Many, many thanks to Gary Turner and Lisa Kent, for their help and the stellar job they do as research engineers/technicians. Likewise, I would like to show my appreciation for the fantastic admin and IT staff I have relied on so frequently: Glenda Rosoman, Dilantha Punchihewa, Nick Look and Mark Adams. I also extend my thanks to the first person who made me think that I could do research at a higher level: the newly minted Professor Paul Docherty.

Superbedankt to all the friends I made in Delft, including Daniel, but this time in his capacity as a friend and source of ever-hilarious anecdotes. The Beboppers: Sona, Raj, Milan, W. I. L. Lawrie, Kristie- the best work wife I could have ever had, without whom I would have felt the need to tell random passers-by all my thoughts- Nicole, Gertjan, Stefan, Xavi and, of course, the newly Dutch Deniz. Thank you for being wonderful, and continuing to allow me to lurk in the group chat. In addition, thanks to the talented and brilliant students and postdocs from PME 2019: Irek, Ata, Stein, Andrea, Andre, Ali, Saleh and Tomas. Many thanks for all the lunch-time conversations and the coffee-breaks.

While we are on the subject of friends, colleagues and comrades: I thank my beloved Palmy Family.

- The Lunch League: TY, David and Paul Chambonniere.
- My big sister in science: Rayén, for absolutely everything.
- My favourite Canadian: Esther Onguta.
- Costume queen Lisa Souhoka (*superbedankt* also for the bike, surfboard and clothes!).
- The only good landlord and my first friend in this city: Joe Mills. I owe you so much.
- Alexis and Olivia, for the boardgame nights, friendship, tea and baked goods.
- *Merci beaucoup* to Alexis for convincing Liam to come to my birthday party.
- Davide for the curated memes, commiseration, sourdough and limoncello.
- Paul Ogbuigwe. Hamilton doesn't deserve your elegance.
- Sebbe Linnenkugel and Florencia Yedro.
- Eli Gray-Stuart.
- My partner, Liam. You are one of the best people on earth. I am so lucky to be with you.

Thank you also to Dylan and Sam, for being exceptional friends/flatmates and for sharing the love of Axel, Fly and Ash, those dogs got me through a lot.

Thank you to the MacDiarmid Institute and the beautiful people of MESA. I cannot imagine a more impressive group. Special mention to the Massey group: Sam Brooke, Ludwig Petters, Ben Westberry, Shikeale Harris, Sashi Ramamirtham, Susav Pradhan, Nimisha Mohandas and Josiah Cleland. Special thanks also to the fantastic, far-flung friends I have made through the MacD activities: WE ARE THE SYSTEM.

Thank you also to Sonja Willemse, I just want to acknowledge everything you have been through. Things should be more just.

My friends are everything to me, and so I want to take a moment to recognise the old ones. Thank you Khayla Te Maro (née Welch), Caiti Spence, Faith Holloway, Emma Banbury (and Theo), Thomas Wallace, Andrew Liang, Ariel Yap, Kate Unwin, Tom Miliken, Flo Everett, Praise Li and Skye Amaryllis. I would not have survived to this point without you!

There's a joke about PhDs that if you don't have a mental illness when you start, one will be provided for you. So it is only appropriate that I give my sincere thanks to Steven Buhr, for the very necessary therapy sessions and the coping strategies- they have helped me more than I can say. Thank you also to Angela Barr, for helping me to cope with similar problems in high school. Your work is absolutely vital.

Finally, thank you always to *my gesin*, especially my parents, for the love, support, guidance and all the impossible to articulate things they are to me. Of course, I include the best boys: Hobbes and Jabu. Thank you as well to *my familie*, I am proud to be one of you.

In high school Classics, I read that the ancient Romans used to end prayers by saying "And to any other gods, as yet unmentioned, who might have a stake in these things". I cannot find a source for this supposed practice, but I am going to borrow it: thank you to anyone I have forgotten to mention.

Chapter 1

INTRODUCTION

Understanding of materials and processes is limited by the spatial and temporal resolution of the tools available, as well as the forces that can be applied and the dexterity of manipulation. Advances in visualisation techniques, such as the invention of the scanning tunnelling and atomic force microscopes [6, 7] and improvements in optical microscopy [8] have facilitated the progress of research into micro and nanoscale structures, systems and processes. This has applications for research in a diverse range of specialisations including some within the vast fields of biomedical research [9], material science [10] and soft matter studies [11]. Tools have also been developed for interacting with increasingly small subjects previously out of reach. These developments can be attributed to manufacturing methods and novel materials developed due to the drive toward increasingly small and low-cost electronics [12, 13, 14], as well as strides made in visualising micro and nanoscale subjects. Such developments have enabled miniaturisation of components and machines, as micro and nanoscale components have become easier to manufacture. The ability to observe subjects at the nanoscale has been facilitated by improvements in optical microscopy which aimed to tackle the problem of the diffraction limit [15], and technologies that take advantage of forces that are weak at the macroscale but produce significant effects on microscale and sub-microscale objects. These technologies enable the undertaking of nanoscale manipulation and measurement, such as the use of the momentum of light to develop optical tweezers [16]. The potential for the use of optical tweezers in biological studies has been of interest to researchers, with studies into the mechanical properties of DNA and its processes leading to improved understanding of the fundamental molecule. However, the use of optical tweezers in biological studies is not without its challenges; particularly the low maximum forces which can be applied, and the potential for damage to the sample, as it is exposed to the high intensity laser trap. This project makes use of optical tweezers and nanoscale 3D printing to develop optical nanorobots that can be used to facilitate the investigation of molecules: specifically, their mechanical properties. While there is

some confusion about the definition of the terms “nanorobot” and “nanomachine” they are defined in the context of this project as being machines that can move nanoscale objects and produce nano-resolution movement: i.e. control displacement to less than a micron. Despite this definition, the tools used in this project may be referred to as micro-levers, micromachines or microrobots, depending on the application and the scale that is relevant for the part of the project.

1.1 PROBLEM STATEMENT

The aim of the project was to realise the potential of optical nanorobotics in single-molecule studies. As such, using optical nanorobots as end-effectors in force-extension studies of molecules was one of the main goals. Another goal was to utilise the mechanical advantage made available by optical nanorobots to amplify optical forces. Currently, the capabilities of optical tweezers are limited by the power of the laser used to create the optical traps, and the number of traps that the set-up allows for. However, trapping using higher powers has been associated with increased risk of damage to the biological samples being examined. The forces applied by optical tweezers are generally in the range of 10^{-14} to 10^{-10} Newtons, which is too low to access a number of interesting, force-triggered events that have been demonstrated in single-molecule studies, such as conformational rearrangements of sugar rings that have been demonstrated with AFM. Therefore, the purpose of this project is to demonstrate the utility of optical nanorobotics for enhancing the capabilities of optical tweezers. The two main opportunities for optical nanorobots are in enabling indirect optical manipulation, hopefully reducing the potential for laser-induced damage to biological subjects, and in amplifying optical forces by introducing mechanical advantage.

1.2 THESIS OVERVIEW

This thesis by publication presents a narrative view of the project. As such it begins with a short introduction and problem statement, which has laid out the main aims that drove the work. The key contributions of the work to the field of optical nanorobotics and biophysics have then been listed, along with the publications and presentations that have resulted from the project, and which have been used to form the backbone of the subsequent chapters. A literature review of optical manipulation strategies and microrobots for biological studies is then presented in order to assist the reader in understanding the project. Following this introduction and review, the work regarding the specific goals of the project is presented in three chapters: functional optical microrobots, optical nanomachines for DNA stretching and advanced tasks with optical nanomachines. Each of these chapters have been built around published articles, and

additional material has been added to link the articles together to form an understandable narrative, as well as to include material important for the reader's comprehension. Finally, the closing chapter reiterates the key results of the project and considers the implications of the research moving forward. The layout of this thesis is intended to demonstrate the cumulative nature of the research, and the way in which each milestone built upon the preceding work. As this is a thesis by publication, methods used for each section of the project have been gathered within the chapter covering the work they were used for. This is intended to help the reader navigate the thesis, particularly in the case of future students reading the thesis for practical information on specific methods or sections of work, as well as those reading for understanding of the topic.

1.3 KEY CONTRIBUTIONS

The key contributions of this thesis are:

- The successful printing of unsupported high aspect ratio optical microlevers that can be manipulated with relatively low force optical tweezers.
- Design of functional levers for use in salty aqueous solutions, bearing in mind the role of ions in screening electrostatic interactions, which results in increasing chance of lever adhesion and seizing.
- Successful adaptation of the dumbbell assay for DNA stretching to incorporate microlevers, leading to the first microlever-assisted DNA stretch.
- Amplification of optical forces using a pin-jointed microlever, and characterisation of spherical handles as most useful for stable, in-plane trapping of high-aspect ratio shapes.

1.4 COLLABORATORS AND CO-AUTHORS

The work presented in this thesis is my own, and all design, experimentation, analysis and imaging was performed by me, Philippa-Kate Andrew, unless otherwise explicitly stated. However, the project would not have been successful without the inputs of the co-authors who have been named in the declaration statements for each paper. They are additionally named here, along with their institute affiliation at the time of the work.

- Dr Daniel Fan, who provided supervision and training during a research stay at the Technische Universiteit Delft during the project. In addition, Dr Fan assisted with the design and printing of the first iterations of the optical microlevers. Dr

Fan was with the Department of Precision and Micro Engineering, Technische Universiteit Delft, 2600 AA Delft, The Netherlands.

- Dr Allan Raudsepp, whose primary contributions were providing training for the optical tweezers, and direct supervision and assistance with the DNA stretching studies. Dr Raudsepp was with the School of Fundamental Sciences, Massey University, Palmerston North 4442, New Zealand.
- Matthew Lofroth, who tested lever functionality using facilities at Massey University during the TU Delft research stay. Mr Lofroth was affiliated with the Department of Mechanical and Electrical Engineering, Massey University, Palmerston North 4442, New Zealand.
- Dr Volker Nock, who printed microlevers from designs I developed, and provided supervision during research visits at the University of Canterbury. Dr Nock was with the Department of Electrical and Computer Engineering, University of Canterbury, Christchurch, New Zealand.
- Prof. dr. Urs Staufer, who acted as the promoter and main supervisor during my research stay at the TU Delft. Prof. dr. Staufer was with the Department of Precision and Micro Engineering, Technische Universiteit Delft, 2600 AA Delft, The Netherlands.
- Dr Ebubekir “Ebu” Avci, who served as the main supervisor for the project. Dr Avci also performed sample preparation for lever testing during my stay at the TU Delft. Dr Avci was with the Department of Mechanical and Electrical Engineering, Massey University, Palmerston North 4442, New Zealand.
- Prof. Martin A. K. “Bill” Williams, who served as the biophysics-based cosupervisor for the project. Prof. Williams was with the School of Fundamental Sciences, Massey University, Palmerston North 4442, New Zealand.
- In addition to their other contributions, Dr Avci and Prof. Williams secured the funding for this project. This work was supported by the Marsden Fund Council from New Zealand Government funding, managed by Royal Society Te Aparangi (MAU1714).
- Dr Avci, Prof. Williams and Dr Nock were also affiliated with the MacDiarmid Institute for Advanced Materials and Nanotechnology, Wellington 6140, New Zealand, where Dr Avci is an associate investigator and Prof. Williams and Dr Nock are principal investigators.

1.5 PUBLICATIONS USED IN THIS THESIS

- **P-K. Andrew**, M.A.K. Williams, E. Avci, “Optical Micromachines for Biological Studies”. *Micromachines* 2020, 11, 192.
- **P-K. Andrew** et al., “Design of Optical Micromachines for Use in Biologically Relevant Environments*,” 2020 IEEE/ASME International Conference on Advanced Intelligent Mechatronics (AIM), 2020, pp. 2039-2045.
- **P-K. Andrew**, A. Raudsepp, D. Fan, U. Staufer, M.A.K. Williams, E. Avci, “Optical Microlever Assisted DNA Stretching”. *Optics Express* 2021, 29, 16, pp. 25836-25847.
- **P-K. Andrew**, A. Raudsepp, V. Nock, D. Fan, M. A. K. Williams, U. Staufer, E. Avci, “Developing an Optical Microlever for Stable and Unsupported Force Amplification,” 2022 International Conference on Manipulation, Automation and Robotics at Small Scales (MARSS), 2022, pp. 1-8, doi: 10.1109/MARSS55884.2022.9870464.

1.6 SELECTED PRESENTATIONS

- “**Manufacturing Microrobots to Aid in Optical Tweezer Studies of Single Molecules**”, *Talk at MinacNed International Micro Nano Conference 2019*, Utrecht, Netherlands, 2019.
- “**Laser Enabled Microrobotics**”, *Talk presented at the mid-central NZ IEEE Student Symposium*, Wellington, New Zealand, 2020. (*Runner-up: Best Presentation*).
- “**Optical Micromachines for Molecule Stretching**”, *Presented at the MacDiarmid Institute Symposium and Future Leaders’ Forum 2021*, Rotorua, New Zealand, (*Best Student Presentation*).
- “**Optical Micromachines for Biophysical Studies**”, *Talk presented at the 2021 Nanoscribe GmbH User Meeting, held virtually on 9 September 2021*.
- “**Giving Light the Mechanical Advantage**”, *Talk presented online after the cancellation of the in-person MacDiarmid Institute Symposium and Future Leaders’ Forum 2022*

Chapter 2

OPTICAL MICROMACHINES FOR BIOLOGICAL STUDIES

Studies that apply forces to samples and monitor their response can be used to determine the mechanical properties of specimens, and in the life sciences they can be used to investigate the relationship between force and biological processes. This can be seen on a population-wide level in studies examining the response of bacterial biofilms to anti-microbial treatments [17], and in studies measuring the responses of cancer cell tissue to compression, for example. The observation of the smaller components of a larger subject enables a more comprehensive understanding of the subject, particularly as collective behaviour may differ significantly from what is exhibited by individual components in complex systems [18, 19]. Additionally, for dynamic processes such as those involved in spermatogenesis, multiple different molecules have to interact to perform all the steps involved, meaning that single-cell and single-molecule studies allow researchers to more sensitively monitor the details of processes as they occur [20]. As biology is a field rife with so-called complex systems [21], including heterogeneous and dynamic environments, a combination of population and single-member studies must be carried out to understand how differences in molecules, sub-cellular organelles, cells and tissues consequently influence organismic behaviour.

Examining biological samples on a sub-cellular level has enabled the identification of mechanical force as a regulator for cell function. An example of this is the study of how forces enable cell organisation for adhesion [22], and another on the molecular level is the role force plays in activating the enzymes used for DNA transcription [23]. This conversion of mechanical forces experienced by cells into chemical and genetic changes (and vice versa) within the cells is known as mechanotransduction [24, 25], and single-molecule studies can assist researchers in developing better models for these processes.

Single-molecule studies of DNA have produced insight into a variety of force-regulated

processes, as well as providing a method to measure the molecule's mechanical properties, which are related to the DNA's environment and its condition. For example, single-molecule analysis of double-stranded DNA has helped to verify the worm-like chain polymer model as a description of its structure, as well as reveal the deficiencies of this model when it comes to extremely short lengths of DNA [26, 27]. This has potential for applications in the biomedical field, where developing causal models for changes in DNA leads to better understanding of how diseases cause damage to DNA. Understanding of mechanisms for damage could then lead to better therapies to mitigate this. For example, some mutagens produce phase-shift mutations through intercalation, which has an impact on the mechanical properties of DNA. How the intercalation takes place, through either major or minor groove binding, influences the mechanical changes that are observed [28], and studies involving the examination of these differences have influenced the development of cancer treatment therapies [29]. Performing force-based studies on other molecules could similarly be used to construct models for how function and structure are related. For example, force-based, single-molecule analysis of the plant cell-wall polysaccharide pectin could provide insight into structure-related gelling properties and provide a complement for current studies which rely on fragmentation of the molecule to investigate different functional groups [30]. This would be helpful in the food industry, where the gelling properties of pectin are useful for stabilising mixtures [31] and in the pharmaceutical industry, where pectin is used as a carrier.

From an engineering point of view, single molecule studies, particularly of well-studied and modelled molecules such as DNA, offer an exciting opportunity in the use of molecules as a metrology standard [32]. Just as polymerase chain reaction (PCR) methods have enabled tiny amounts of DNA to be amplified for genomic analysis applications [33], PCR can be used to create thousands of identical DNA strands from specific fragments. This means that DNA could be used as an extraordinarily reproducible tool for force and displacement calibration, allowing for the comparison of many different technologies. As research interest in nano and microscale systems increases, such a calibration standard will become more and more valuable, as more researchers develop custom tools and methodologies for nano and microscale manipulation. Therefore, researchers working on the nanoscale- even those with very little interest in biology or the fundamental physics of molecules- would do well to consider including DNA stretching in their work.

2.0.1 DECLARATION

This chapter centres around a literature review published in the MDPI journal *Micro-machine* with co-authors Dr Ebubekir Avci and Prof. Martin A. K. Williams. Dr Avci and Prof. Williams supervised the project and acquired funding. I wrote the original

draft, and all authors edited the final paper. Supported by the Marsden Fund Council from Government funding, managed by Royal Society Te Aparangi (MAU1714). The review article is reproduced and expanded upon here under the terms of the Creative Commons CC BY license that the original work was published under.

2.1 OPTICAL MICROMACHINES FOR BIOLOGICAL STUDIES

2.1.1 INTRODUCTION

Improvements in tools for the visualisation of objects at the micro- and nano- scale have given researchers the ability to investigate materials and processes previously out of reach. The dominant forces and phenomena that can be accessed at these small scales often differ greatly from those observed at the macroscopic scale. This can lead to challenges, such as adhesion between objects in micro-manipulation experiments [34, 35], but also to opportunities, where forces which would be unnoticeable at the macroscale can be used to great effect on micro and -nanoscale objects; such as in the atomic force microscope and optical and magnetic tweezers [16]. Of these technologies, optical tweezers have shown themselves to be particularly flexible tools for the investigation of structures, systems and processes covering the mesoscale. This has led to optical tweezers being used as a tool in the vast fields of biomedical research, material science and soft-matter studies, where they can be used to apply and measure forces that range from 10^{-14} to 10^{-10} Newtons. Optical tweezers were invented by Nobel laureate Arthur Ashkin and colleagues and were first officially introduced in a 1986 paper [36] following more than a decade of experiments with what was termed the radiant pressure force [37, 38, 39, 40, 41, 42]. These experiments were themselves inspired by earlier work by researchers in the early-to-mid 1900s [43, 44, 45], who had experimentally shown what James Clerk Maxwell had theorised: that light carries momentum. However, these earlier researchers had been severely limited by the range of forces that could be applied, and these experiments relied on observation of extremely slight perturbations. This restriction was removed with the invention of the laser [46, 47, 48], which allowed for experiments with high intensity beams of coherent light. The potential for applications other than simple manipulation of dielectric spheres was soon realised, with a paper by Ashkin and Dziedzic demonstrating the ability to manipulate viruses and bacteria shortly after the influential paper that introduced single-beam optical traps [49]. This led to rapid uptake of the technology by researchers interested in probing the properties of biological subjects. In particular, the relationship between force and biological behaviours has been a subject of enduring research interest, as researchers took note of the ability to investigate intra-cellular phenomena non-invasively

[50]. A particularly interesting subset of optical tweezers research is the emerging field of optical microrobotics. Optical microrobotics has been demonstrated to have applications in optical scanning-force microscopy [51], cell manipulation [52, 53, 54] and cell analysis [55]. The behaviour of optical micromachines has also been used to validate the use of classical mechanical models at the microscale [56, 57] as well as providing insight into how material properties may be affected by scale [58]. However, optical micromachines have been under-utilised thus far in biological studies, making this area one with tremendous potential for researchers. In order to place the opportunities for micromachines in context, this review covers a brief introduction to optical tweezers and the impact of optical trapping in biological studies, as well as exploring the concerns associated with optical trapping of biological specimens. The potential for optical micromachines in this area is then explored through an evaluation of the achievements and challenges associated with optical micromachines, considerations for microrobot design and the choice of optical tweezers for manipulation of optical microrobots. Finally, the review finishes with a speculative view of the future, briefly exploring a few possibilities for the use of optical microrobots in biological studies.

2.1.2 AN INTRODUCTION TO THE THEORY OF OPTICAL TWEEZERS

Although the theory of optical tweezers is not a central feature of this review, an introduction to the optical force is helpful. Many papers have been written about the theory involved in modelling optical tweezers [59, 60, 61], and this summary does not hope to offer more than a basic introduction, with the reader encouraged to follow the references for more thorough explanations. While the effect of the sun on direction of comet tails prompted Johannes Kepler’s theories about the mechanical effects of light, the real impact and potential of radiation pressure are most clearly observed on the micro- and -nano-scale, where the intensity afforded by lasers makes the forces originating from changes in the momentum of light significant. The main feature of an optical tweezers setup is a laser focussed through a high numerical aperture (NA) objective, which turns the force associated with the laser into a useful tool. The high NA objective serves to tightly focus the laser beam to a narrow region of space, resulting in an extremely steep gradient of the laser’s electromagnetic field at this point. This is shown in Figure 2.1. The force associated with the focussed laser beam is treated in two parts in the theory of optical tweezers: a gradient force that “pulls” objects in towards the focus, and a scattering force which acts like water in a “hosepipe” of photons, bombarding the object [62].

Calculations of the gradient and scattering forces can then be performed according to different equations depending on whether the object being trapped can be said to

belong to the ray optics regime (particle diameter $d \gg$ trapping wavelength λ) or the Rayleigh regime ($d \ll \lambda$). The ray optics explanation assumes that the objects are sufficiently large that they act as lenses, and relies on the understanding that the collimated laser beam is comprised of many single rays of light. The intense focus of the laser beams used for optical trapping means that there is a higher density of rays at the focus. Each ray carries momentum and experiences a change in this momentum when refracted through the microsphere. This change in momentum corresponds to an equal and opposite change in the momentum of the trapped object, acting to move the object. The moment provided by the beam is calculated by decomposing the incident light beam into a series of rays with appropriate intensity, direction and polarisation, and each ray is understood to be a plane wave which changes direction upon interaction with the object's surface. Diffraction is ignored in this regime, and the gradient (\mathbf{F}_{grad}) and scattering (\mathbf{F}_{scat}) force can be calculated using Equations (2.1) and (2.2), respectively [47, 63].

$$\mathbf{F}_{grad} = \frac{n_1 P}{c} R \sin(2\theta) - \frac{T^2 [\sin(2\theta - 2r) + R \sin(2\theta)]}{1 + R^2 + 2R \cos(2r)} \quad (2.1)$$

$$\mathbf{F}_{scat} = \frac{n_1 P}{c} 1 + R \cos(2\theta) - \frac{T^2 [\cos(2\theta - 2r) + R \cos(2\theta)]}{1 + R^2 + 2R \cos(2r)}. \quad (2.2)$$

In these equations the incident momentum is given by $\frac{(n_1 P)}{c}$ where n_1 is the refractive index of the trapping medium, P is the power of the ray, and c is the speed of light. The angle of incidence is given by θ and the angle of refraction by r . The terms R and T refer to the Fresnel coefficients for reflection and transmission due to the interface of the medium and target object, which are dependent on the polarisation of the beam [64]. For the case where the light is unpolarised, equal amounts transverse-magnetic (P polarized, R_p , T_p) and transverse-electric (S polarized, R_s , T_s) are used. The Fresnel coefficients for transverse-magnetic and transverse-electric waves are given by Equations (2.3)–(2.6).

$$R_p = \left| \frac{(n_1 \sqrt{1 - (\frac{n_1}{n_2} \sin(\theta_i))^2} - n_2 \cos(\theta_i))}{(n_1 \sqrt{1 - (\frac{n_1}{n_2} \sin(\theta_i))^2} + n_2 \cos(\theta_i))} \right|^2 \quad (2.3)$$

$$R_s = \left| \frac{(n_1 \cos(\theta_i) - n_2 \sqrt{1 - (\frac{n_1}{n_2} \sin(\theta_i))^2})}{(n_1 \cos(\theta_i) + n_2 \sqrt{1 - (\frac{n_1}{n_2} \sin(\theta_i))^2})} \right|^2 \quad (2.4)$$

$$T_p = 1 - R_p \quad (2.5)$$

$$T_s = 1 - R_s \quad (2.6)$$

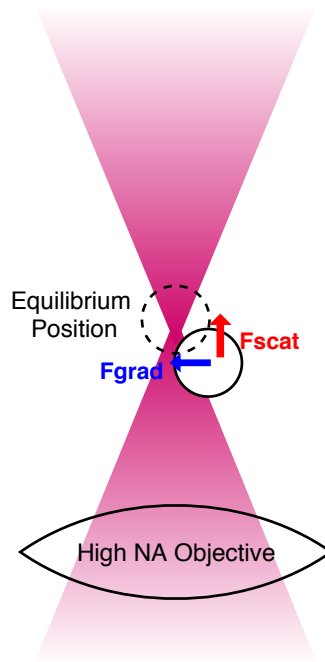


Figure 2.1: Optical tweezer theory treats the force associated with the focussed laser beam as two components, which can be visualised as resulting from the intense focussing of the light.

If the ray optics regime can be thought of as treating objects as lenses, then objects meeting the size requirements to be considered as Rayleigh scatterers can be thought of as particles that become polarised in response to the changing electromagnetic field. The interaction of the induced dipoles with the steep gradient of the electromagnetic field associated with the tightly focussed laser results in the object being pulled towards the waist of the beam [65]. The scattering force can then be understood as being produced because the intensely focussed field is not static, and thus it induces a magnetic field around the dipoles, resulting in the particles being “pushed” [60].

In this regime the equations for the gradient and the scattering forces are given by 2.7 and 2.8 [66, 67], where n_1 is the refractive index of the medium, c is the speed of light, a is the radius of the object being trapped, m is the ratio of the refractive indices of the object and medium ($m = \frac{n_2}{n_1}$, where n_2 is the refractive index of the object), I is the intensity, r is the object’s position (x, y, z) and k is the wave number ($k = \frac{2\pi}{\lambda}$). The intensity of the laser is related to the electromagnetic field E by Equation 2.9. These equations provide reasonable approximations of the forces acting on spheres ranging from a few nanometres to a few hundred nanometres, but become unreliable as the size of the object of interest approaches the wavelength of the trapping laser [66].

$$\mathbf{F}_{grad}(\mathbf{r}, t) = \frac{2\pi n_1 a^3}{c} \left(\frac{m^2 - 1}{m^2 + 2} \right) \nabla I(\mathbf{r}, t) \quad (2.7)$$

$$\mathbf{F}_{scat}(\mathbf{r}, t) = \frac{8\pi n_1 k^4 a^6}{c} \left(\frac{m^2 - 1}{m^2 + 2} \right) I(\mathbf{r}, t) \quad (2.8)$$

$$I(\mathbf{r}, t) = \frac{\epsilon_0 c E(\mathbf{r}, t)^2}{2}. \quad (2.9)$$

Unfortunately, most of the objects that researchers are interested in trapping have characteristic dimensions that lie between these two basic regimes, in the intermediate range close to the trapping wavelength. Theoretically, for a small, spherical object in a vacuum, Maxwell's stress tensor provides a solution for the force imparted by an electromagnetic wave, but it assumes complete knowledge of the field, and is impractical for experimental applications. In the case of spherical objects, Mie theory can be used for an exact solution to the problem of scattering [68, 69], but it assumes a plane wave, and this makes it inapplicable to the focused beams used for optical tweezers. However, early experiments with laser light validated the use of Mie theory for objects in the intermediate range, with Mie scattering patterns analysed for non-homogeneous, sphere-within-a-sphere particles [70]. This provided valuable information about how this type of particle interacted with the laser light, and provided some evidence that this theory would hold for experiments with biological cells, which cannot always be assumed to be spherical, isotropic or homogeneous structures. Modern use of Lorenz-Mie theory has seen it adapted to cope with arbitrary illumination [71, 72], and in this form it is known as Generalised Lorenz-Mie theory (GLMT). GLMT has been combined with other theories of light propagation to more accurately model particular set-ups; such as the Debye-Wolf theory in order to model the forces from holographic optical tweezers [73]. The main limitation of GLMT is that it is applicable to homogeneous, isotropic spheres, rather than complex shapes. Therefore, further generalisation of the theory to extend it to arbitrarily shaped particles was necessary, resulting in the development of T-matrix theory.

First proposed by Waterman in 1965 [74], the T matrix method is useful for calculating the forces on an object in a dynamic optical tweezers set-up, as the matrix depends on the shape, size, refractive index and position of the scattering object, rather than the incident or outgoing fields of light. Additionally, the matrix simplifies for objects with some degree of symmetry, with a sphere being the simplest shape. This greatly reduces the computational effort. The T-matrix method has been reviewed and utilised by many researchers since Waterman's introduction of the method for solving scattering problems, with different methods for calculating the matrix used [75, 76], including the extended boundary condition method (EBCM) [75] and the point-matching method [77, 78]. A comprehensive overview of the T matrix method specifically for optical tweezers has been written by Nieminen et al. [79] and a thorough explanation of

T-matrix and generalised Lorenz-Mie theory has also been produced by Gouesbet [80].

While these methods provide a way to calculate the forces associated with optical tweezers, researchers can reduce difficulty by modelling optical tweezers as a Hookean spring [81]. The Hookean spring model is based on the understanding of an optical trap made from a Gaussian beam as being a “harmonic potential well”, with a defined equilibrium point, and a characteristic stiffness constant. Using the separation of the scattering and gradient components of the force as a starting point, in a stable trapping scenario the gradient force will dominate, meaning that the particle will remain at an equilibrium position in a trap, notwithstanding Brownian motion. Then, the stiffness coefficient of the optical trap can be estimated by measuring the root mean square displacement of the particle from the centre of the trap induced by thermal fluctuations and using the equipartition theorem [82, 83]. Other calibration methods for measurement of trap stiffness have been developed [84], and are popularly based on balancing a viscous drag imposed on the particle in the trap [85] or by performing power spectrum analysis [86]. The simplicity of the Hookean spring approximation, and the wealth of different methods for calibration hints at a limitation of this method: the effective spring constant is affected by fluctuations in experimental parameters such as viscosity and temperature, and so may require recalibration during long-running experiments. For researchers looking to bypass this issue, a method of force measurement arising from first principles has been successfully demonstrated in both dual-beam, counter-propagating optical traps [87] and single beam traps [88]. This method involves the measurement of the change in momentum of light before and after interaction with the sample, and requires the collection of scattered light in order to extract the change in momentum from the resulting intensity pattern using a position-sensitive detector. A drawback of this method is that it requires precise alignment of all the components required, and it is not feasible to collect all of the scattered light in a single-beam set-up. However, the results from Reference [88] indicate that the “lost” backward-scattered light contributes very little to the overall calculations, and this could be a useful method for researchers working with non-spherical or non-homogeneous objects, as it does not require experiment-specific calibration.

2.1.3 FIRST APPLICATIONS AND IMPACT ON FIELDS

While experiments with the radiant pressure force were initially intended for atomic cooling applications [41, 62], their potential for use in biological research was quickly realised [89, 49, 90]. Ashkin’s own experiments with trapping viruses and bacteria [49] sparked further interest in optical tweezers as a non-invasive technique for probing the material properties of biological subjects [91] and for investigating force-related phenomena [92]. In the past few decades this research has included applications

that have ranged from investigating the mechanisms behind cell stiffening due to high blood pressure [93] to examining the impact of chemical binding on DNA's mechanical properties [94, 28, 95]. In fact, stretching of single-molecules such as DNA has proven to be a topic that has benefited greatly from the development of optical tweezers.

While the pioneering DNA stretching experiment was conducted using magnetic tweezers [96], the spatial resolution of optical tweezers, which, even in the 1990s, allowed displacements of only a few nanometres to be affected [97], proved particularly attractive to researchers for single molecule studies. Additionally, the range of forces that can be applied cover a range from 10^{-14} – 10^{-10} N, which means that several different force regimes can be investigated [98], from those where thermal fluctuations provide restoring forces, to those where high-forces that can impart conformational changes in constituents of the chain [85]. The popularity of DNA stretching studies has meant that there is ample data available for researchers wanting to develop improved models for the molecule's structure and behaviour [99]. In this way, theoretical models for single-molecule structure and behaviour can be readily evaluated, and their limitations found. An example of this is the breakdown of the freely-jointed model for single DNA molecules and the subsequent validation of the worm-like chain model [99, 100, 101, 26].

Early optical tweezers-based DNA stretches featured molecules that were fixed to a coverslip at one end, with a free-moving end attached to a functionalised microbead. This microbead was then held in the optical trap and the coverslip was translated in order to create a stretch on the molecule [102]. However, this meant that the stretch was affected by disturbances to the translating equipment, due to mechanical coupling of the stage to the rest of the set-up. Additionally, tethering the DNA to the coverslip meant that the stretches could not be truly uni-directional, with an orthogonal component that could not be determined with a level of accuracy comparable to the in-plane displacement. Another popular method for fixing one end of the DNA tether was attaching the corresponding functionalised microbead to a micropipette, which likewise introduces the possibility of unwanted mechanical coupling. A potential fix for the problem of mechanical coupling can be found in the introduction of steerable traps. Steerable traps allow for the manipulation of both ends of a free-floating DNA molecule, decoupling the process from the rest of the apparatus. In the resulting "dumbbell assay", functionalised beads are attached to DNA molecules that have been modified to feature bead-binding compounds (typically biotin and digoxigenin) at the ends. Each bead is then confined to a separate optical trap, with one trap being stepped away from the other, which is held in a constant position, in order to stretch the molecule [103]. The change in the distance between the beads is taken as the extension of the DNA tether, allowing for the use of the Hookean spring model of optical tweezers. These three

different methods for forming a DNA tether for stretching can be seen in Figure 2.2, which has been reproduced from Heller et al.'s review of the use of optical tweezers for analysing DNA-protein complexes [1].

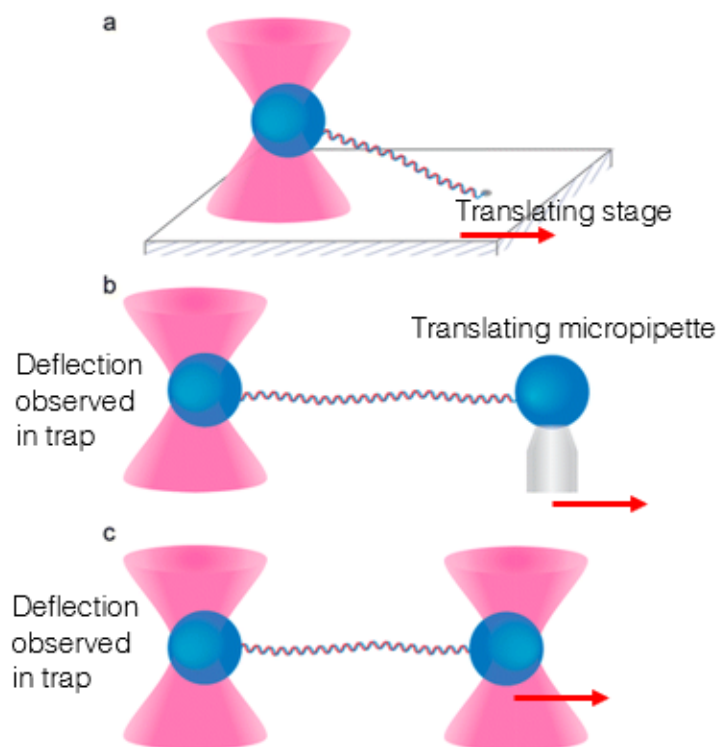


Figure 2.2: Three different methods for stretching a DNA tether with optical tweezers can be seen in this figure: the translating slide method (a), using an anchoring micropipette (b) and using two separate optical traps (c). Reproduced with permission from Reference [1]. ©2014 American Chemical Society.

While the introduction of a second optical trap in DNA stretching studies decoupled the experiment from vibrations of the apparatus, it also introduced another source of intense laser light. It is accepted that laser irradiation has a negative impact on trapped biological samples, but it is not known how much the laser light affects the DNA molecule, as it is not being directly trapped. However, this leads to an important topic; concerns for biological research involving optical tweezers.

2.1.4 OPTICAL TRAPPING: CONCERNS FOR BIOLOGICAL RESEARCH

The negative effects of laser radiation on biological samples were discovered just as quickly as the potential for optical tweezers in biological studies [49], necessitating the development of strategies for minimising damage to biological samples during assays

with optical tweezers. The first consideration for making the trapping beam less damaging to samples was the beam wavelength, with the beam changed from visible radiation to infrared in order to reduce absorption [49]. Infrared lasers commonly produce light in the near-infrared range from 700 nm to around 1200 nm. Even within this range there are significant differences in the damage observed in biological samples, depending on the wavelength used [104, 105]. Interestingly, while 740–760 nm have been found to be the most damaging, the commonly used 1064 nm wavelength was found to reduce clonability of CHO cells to below 20% of the control group within five minutes of laser exposure [105]. 990 nm, on the other hand, was found by the same study to only reduce clonability to around 70% after a full 20 minutes of exposure, at the same laser power. However, when the damage caused to cellular DNA after exposure for 30s is compared, 1064 nm is clearly less damaging than wavelengths in the range of 700–900 nm [104]. Therefore, the wavelength used for trapping can be clearly seen to be one of the key considerations when trapping biological samples.

In another study, the presence of oxygen was considered as a factor influencing damage, with the motility of *E. coli* examined to quantify damage [106]. A range of wavelengths from 830 nm to 1064 nm were used, and the wavelength-dependent damage observed appeared to agree closely with that from Liang et al. [105]. When free oxygen was removed from the system, either through introduction of a scavenging species, or by growing and trapping cells in an anaerobic environment, the damage was found to decrease to levels comparable with the control group, which was not exposed to the laser. Other studies have been performed that also seem to corroborate the hypothesis that oxygenation of the sample is a main cause of damage induced during optical trapping [107, 108]. However, there is not yet a clear consensus on the exact mechanism for this damage, and other effects related to laser proximity have also been found to induce damage, such as localised heating [109, 110]. Research into parameters influencing the damage inflicted by optical trapping has revealed that the trapping medium affects the temperature increase the laser generates, with glycerol producing much higher temperature variation than water [110].

Not all experiments with biological matter can be adapted to remove oxygen, change the trapping medium, or cope with the introduction of a scavenging species. Therefore, other methods for reducing damage as much as possible must be considered. The laser beam itself has been identified as a potential hazard to biological samples, simply due to the high intensity needed to produce an optical trap. As the electromagnetic field varies sharply, with the intensity dropping rapidly with respect to the distance from the waist of the beam, it has been proposed that some of this damage can be avoided simply by spatially separating the optical traps from the object being examined. An example of this theory can be found in the use of functionalised microbeads for DNA

stretching, where the DNA itself is not trapped [99] but rather it is chemically bonded to microbeads which act as trapping points for the molecule. The use of these beads is also necessary to enable DNA stretching at all, as the size of the molecule is below the diffraction limit; a limiting factor for optical tweezers until recently [111]. This also has additional advantages, one of which is that the size of the beads can be adjusted to a size that is advantageous for optical trapping with the set-up being used, ensuring a high trap stiffness. The process can also be better visualised with the help of these beads, with the behaviour of the microbeads informing the researcher about the behaviour of the molecule being stretched between them. If direct trapping of the DNA molecule was to be attempted, then the use of a dye would be required, in order to determine the location of the molecule. Use of such dyes can change the mechanical properties of the DNA molecule, depending on the binding mechanism [92], and labelled molecules can be affected by photobleaching, severely limiting experiment times [112]. While using quantum dots as fluorescent markers may solve the issue of photobleaching, there are concerns about toxicity, although this is not considered a drawback for *in vitro* studies [113].

Larger biological samples such as cells and their organelles can be directly trapped without difficulty [51], but it is desirable to find strategies for mitigating the damage that high intensity laser traps can inflict [114]. As in the case of single-molecule studies, the effect of the wavelength of light used has been considered, with near-infrared traps preferred because of low endogenous absorption at wavelengths between 700 and 1200 nm [115]. Additionally, the use of non-Gaussian traps has been explored as a possible method for stable trapping of living cells. This includes the creation of “optical funnels” using ring-shaped optical fibres to create a funnel of light, in which objects with a lower refractive index than the trapping medium can be stably trapped [116]. Annular traps have also been constructed using axicons, and used to trap living sperm cells, with the added benefit of exposing the spermatozoa to less intense light [117]. Annular traps constructed using axicons have the added benefit of propagating for long distances within the sample, unlike traps constructed using Gaussian beams which are limited to a small distance from the objective. This means that the working distance in the *z*-direction can be much greater in a ring-shaped trap [118]. The use of two lenses to create the Bessel beams required also means that the size of the resulting ring-shaped beam can be adjusted by moving one of the lenses, changing the focal length and thus the ring’s diameter, which has potential for studies involving objects of different sizes [119]. However, while some experimental success has been demonstrated using axicons for trapping cells and atoms [120], the use of axicon traps is less straightforward than the theory suggests [121], as the lower intensity of the light consequently means that the optical forces produced are lower than in Gaussian-beam traps. This limits

the applications of these traps, as they cannot produce the high forces required for applications such as investigating the mechanical properties of cells [122]. This means that alternative solutions that are not reliant on changing the power or intensity of the trapping beam are desirable for applications that require high forces.

A possible method for retaining the effective power of optical traps, while reducing damage to the subject is using other optically trapped objects as intermediates, effectively using them as end-effectors to manipulate delicate biological subjects. The use of functionalised beads for DNA stretching can be regarded as pioneering work in indirect optical trapping, with functionalised rigid-body structures made from SU-8 also used to manipulate cells in a system with six degrees of freedom [52]. Indirect optical manipulation of cells has also been demonstrated using non-functionalised end-effectors [53], indicating that non-specific bonding due to physical adhesion forces can be sufficient for such studies. This indicates that intermediate optically trapped objects may have potential for a variety of applications where orientation of the cell is important, such as cell aspiration and nucleus extraction. Additionally, experiments using trapped objects as “force probes” indicate that optical end-effectors can be designed to retain the sensitivity of force application that optical tweezers are known for [123, 124]. This is important, as the range and resolution of force that can be applied by optical tweezers are distinguishing features of the technology when compared to conventional mechanical manipulation, where limited resolution of force and displacement can limit the use of these methods for high-precision tasks [125].

2.1.5 OPTICAL MICROROBOTS

2.1.5.1 POTENTIAL TOOLS FOR BIOLOGICAL STUDIES

While researchers have not yet reached a consensus on the exact mechanisms for damage incurred during optical trapping, it is widely agreed that exposure to intense light is a problem. As previously mentioned, it is not always possible to adapt experiments for lower trapping powers, and it is not always practical for researchers to have multiple custom optical trapping set-ups for different samples. Therefore, using microrobots to reduce specimen contact with the trap’s focus, while still enabling application of optical trapping forces, would be a conceptually simple solution for the problem of optically inflicted damage. As already noted, the use of optically trapped objects as scanning probes, for DNA stretching, and as tools for simple cell rotation can be thought of as pioneering work in the field of optical microrobotics. It follows that the use of more complex, articulated robots may be the solution to reducing exposure to laser light, and potentially they may also be the answer to overcoming the limitations of optical tweezers, such as limited force and difficulty performing truly 3D manipulation.

While the potential for optical microrobotics in biological research is clear, there

are still relatively few examples of the technology used in this field. This could be partially attributed to historical difficulties in manufacturing optical microrobots. Micro-manufacturing methods have traditionally been iterative processes based off those used for semi-conductor applications, limiting the resolution and shapes that can be achieved. While there is some scope for the use of these iterative-process methods in the development of microrobots [126], they are limited due to their two-dimensional nature. In the case of the paper by Mittas et al., the difficulty of using traditional silicon micromanufacturing techniques can be seen due to the need of precise alignment of the different patterning stages. Additionally, the use of etching for high aspect-ratio features is problematic as it is a time dependent process, which means that the etchant generally spreads in an undesirable manner, leading to feature-undercut. However, this undercutting has been purposefully used to produce three-dimensional micromachine elements, when etchant has been used to remove patterned elements from silicon wafers to produce independent components for use with optical tweezers [127]. In situations where repeatable manufacturing and high feature resolution ($<1 \mu\text{m}$) are required, relying on etching to produce the desired outcome becomes impractical. Similarly, photore-sist patterning using mask aligners can be used to good effect to produce reasonably complex structures [128], but this is an arduous task that is prone to error due to the need for extremely precise alignment of subsequent layers, and only allows for 2.5 dimensions, with extrusion of a planar pattern occurring in one direction. Additionally, making multi-component robots from these methods is complex, due to the requirement for assembly, although the components themselves can be produced [129]. Fortunately, the development of three-dimensional photolithography, based on two-photon absorption polymerisation, has enabled the manufacture of complex structures with $<100 \text{ nm}$ resolution. The use of this laser-based 3D printing technology is well-established, with the first patent for 3D stereolithography granted in 1986 [130], and examples of complex structures present in literature since the early 2000s [131].

Although two-photon absorption was first theoretically suggested by Nobel laureate Maria Göppert-Mayer in her doctoral thesis [132], like many light-based phenomena it was only experimentally demonstrated after the invention of the laser. Two-photon absorption involves the simultaneous absorption of two photons- that can be of the same or different energies- to bridge the energy gap between electronic states of a molecule and bring it into a higher energy electronic state. The fact that two photons must be absorbed for the process to occur means that it is non-linear, with the rate of absorption (R) being given by 2.10, where δ is the two-photon absorption cross-section and I is the intensity of the light.

$$R = \delta I^2. \quad (2.10)$$

This phenomenon is the cause of two-photon absorption polymerisation (TPAP),

which occurs when two-photon absorption occurs in a matrix of monomers or oligomers and a photoacid-generator [133]. This initiates polymerisation of the material in the regions of the material where the required energy threshold is met [134]. A highly focussed, femto-second pulsed laser beam is used to provide the necessary light for the reaction, and due to the narrow region of focus, high aspect ratio features with feature resolution of less than 100 nm is possible, as the region of polymerisation can be finely controlled [135, 136]. This has enabled the printing of complex structures with fine detail, with functional 3D-printed helical springs being evidence of what the technology can achieve [55, 137]. This technology is especially promising for creating optical micro-robots for use in biological studies, as several commercial resists are biocompatible, with SU-8 being a common example. Additionally, conceptually any resin can be used, so long as it has sufficient absorption of the wavelength of the laser used to induce TPAP, and a high enough proportion of photoacid in the matrix. This allows researchers to create custom resins with the properties that they require, a feature that has already been exploited by researchers creating cell-scaffolds from hydrogels [138]. While in principle two-photon absorption polymerisation simply requires a high-speed pulsed laser, the invention of the Nanoscribe, a commercial solution developed by researchers at Karlsruhe Institute of Technology, has led to more user-friendly TPAP-based 3D printing. The availability of commercial solutions such as this means that 3D laser printing has become accessible to researchers from different backgrounds, widening the scope of applications.

2.1.5.2 ACHIEVEMENTS TO DATE AND CHALLENGES

It has been established that complex shapes can be printed using TPAP, and there has been some work performed using optically trapped objects as end-effectors for studies involving the manipulation of biological subjects [139]. This positions optically driven micromachines as a promising technology for researchers looking to reduce exposure to intense laser traps. However, there are also several challenges that need to be addressed before the technology can be adopted for regular use, rather than as a novelty.

Optically-driven microrobots have been successfully used to amplify forces from optical tweezers [56, 57], and to transform planar input-motion to out-of-plane rotation [140]. It has also been demonstrated that trapped microspheres, arranged in groups of three, create an attractive pocket that approximates a weak optical funnel; which could be used to indirectly trap biological objects [141]. This is similar to what can be achieved using the “doughnut” shaped beams used for dark trapping [116], and demonstrates the potential for optical microrobots as an alternative and more flexible solution to altering the beam used for optical trapping. Additionally, the impressive resolution and dimensions that can be achieved using TPAP has enabled the printing

of nano-springs. These nano-springs have been used as more than just examples of what TPAP can achieve, they have also been used to measure force amplification [56], and to investigate the impacts of post-curing UV exposure on photoresins [142], using optical tweezers. The use of levers and articulated microrobots to amplify force and produce out-of-plane movement shows that micromachines can be used to improve upon the abilities of optical tweezers, which are currently rather limited in these areas. Additionally, by demonstrating that classical models of springs hold at the microscale [56, 58], researchers have shown that springs could potentially be used to directly measure the forces applied with optical tweezers. However, this approach requires extensive knowledge of the polymer used to fabricate the springs and precise control of printing parameters, as non-uniformity could lead to large differences from expected results [143]. This has become less of a problem as laser-based 3D printing technology has advanced, and as more research has been performed to ascertain the effects that laser printing parameters have on mechanical properties of printed objects [144], but it is still an issue worth considering.

While these examples show what can be achieved in optical microrobotics, the authors also make note of the challenges involved in producing and actuating them. Particular difficulties are caused by adhesion forces between discrete moving parts [56, 140] and the tolerance of pin joints when optical trapping is performed. Adhesion forces in particular form a barrier when it comes to developing articulated optical microrobots, as more complex machines offer more opportunities for seizure due to links and joints bonding to each other through physical interactions such as van der Waals forces. Additionally, this poses a particular barrier for the use of microrobots in biological research, where studies are often carried out in particular fluids which are intended to mimic *in vivo* conditions. Some of these fluids, such as the tris-buffered saline used for DNA stretching [145], have relatively high salt concentrations, leading to a shortening of the Debye length and thus a decreasing importance of any stabilising electrostatic interactions [146]. Methods for reducing adhesion forces in microrobotics are based around reducing contact area between objects [140, 147]. The reason for this can be easily appreciated when one considers the equations for the van der Waals force between a sphere and a plane (2.11) [148]—a key contributor to adhesion forces.

$$F_{vdW} = \frac{H}{6} \frac{d}{2z} + \frac{d}{2(z+d)^2} - \frac{1}{z} + \ln\left(\frac{1}{z+d}\right). \quad (2.11)$$

In Equation (2.11), H represents the Hamaker constant of the material [149], d is the diameter of the microsphere and z is the separation between the sphere and the plane. This equation assumes the same material for the plane and the microsphere, and that the plane is extremely large compared to the microsphere, and so has some

limitations, but it clearly illustrates the effects of separation distance and size of the objects on the van der Waals forces between them. Therefore, it can be deduced that adhesion forces can be limited by increasing separation between moving parts of the nanomachines, and by minimising the contact area between parts, which is supported by results from the literature. While equation 2.11 does not explicitly refer to contact area- due to the assumption of perfect tangential contact between sphere- if we consider that overlapping area is comprised of multiple single contact-points then the implication is clear.

Another challenge in creating multi-component optical microrobotics is being able to use non-spherical objects. Relatively small ($d \approx \lambda$) spherical shapes are the easiest objects to trap with single Gaussian traps, as they are isotropic and the curved surface leads to lower reflection and so to lower scattering forces when compared to flatter objects. Additionally, as already mentioned, they are also the easiest shape to model. Conversely, objects with high aspect ratios, such as cylinders, tend to orient themselves with the axis of the optical trap [150], a tendency first discovered when Ashkin and Dziedzic trapped cylindrical viruses [49], which can lead to difficulty in manipulating such objects as desired. A method for getting around this problem is to add spherical features as trapping “handles” [151], similar to the use of functionalised beads in DNA stretching. This strategy has been adopted by many researchers, and spherical parts feature in many optical microrobot designs [54, 56, 57, 140, 152]. Another strategy is to use several optical traps, positioned so that the forces are balanced when manipulation takes place, regardless of the shape of the “handles”. Examples of this can be found in the use of cylindrical trapping points in the development of an optical scanning probe [153], where spheres are used as tracking points rather than trapping handles, and in the use of flat discs as handles for structures produced using 2D deposition and etching methods [127].

While the gradient force is most commonly used to control the movement of optical microrobots, optical tweezers can also actuate micromachines through the scattering force, or through thermal effects. The use of the scattering force to trap objects has perhaps most successfully been used in the case of the counter-propagating optical trap, where two aligned, counter-propagating laser beams work together to create a balanced trap based on the scattering force produced by each laser [154, 155]. This configuration, while complex compared to single-beam optical tweezers, allows for lower intensity light to be used, and so does not require the high NA objectives used for a gradient trap. The use of a lower NA objective also allows for longer working distances than optical tweezers, which are generally limited to a working distance of less than a millimetre from the objective. On the other hand, an example of the use of thermal effects from optical tweezers to actuate microtools is the creation of a “micro-syringe”, where the

inclusion of a thin metal layer inside a 3D printed chamber creates thermally-induced flow in response to the laser light, moving silica and polystyrene microspheres in the process [2]. The process of pulling in a microsphere to later be ejected can be seen in Figure 2.3.

As discussed previously, the force resulting from the interaction of the laser beam with the object of interest is commonly split into two parts, and F_{grad} & F_{scat} is commonly accepted to be the condition necessary for stable trapping. However, the scattering force can also be used to actuate microrobots, and can be used for applications involving a rotating part which can be “pushed” by the light, rather than being dragged into place [20, 156]. In-plane rotation of a twin-rotor micropump has been demonstrated, by focusing a Gaussian beam on the sides of flat-lobed “wings” [157]. Out of plane rotation has also been demonstrated using an optical “paddle wheel”. In this case two micro-spherical features were used as “trapping handles” to hold the object in place, while the central “paddle” was driven by the scattering force of another trap, creating out-of-plane rotation [3]. A schematic of this microrobot, as well as stills taken from a video of it moving, can be seen in Figure 2.4.

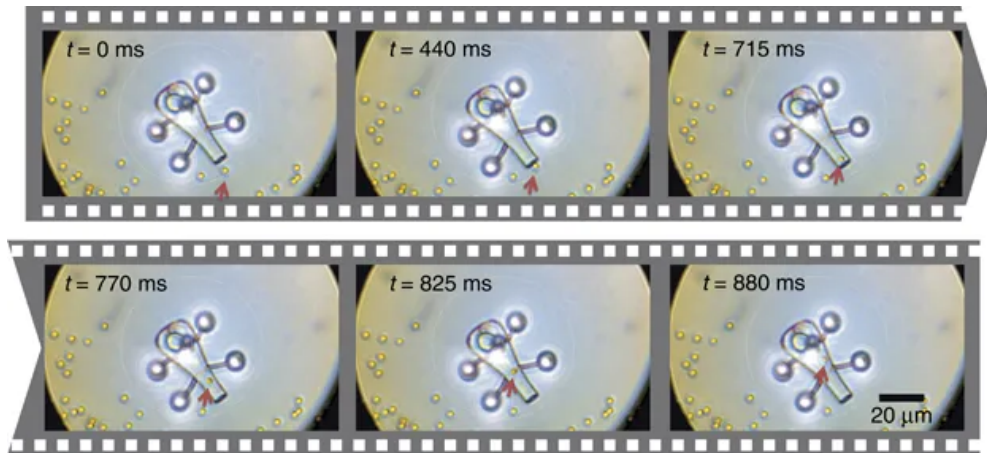


Figure 2.3: The inclusion of a thin metallic layer inside a 3D printed chamber leads to the movement of silica and polystyrene payload particles through convection. Reproduced from Villangca et al. [2], under Creative Commons license NC ND 4.0.

Optical forces have also been utilised to rotate chiral objects, where the design of the object means that the incoming momentum is unbalanced and creates an optical torque around the beam’s trapping axis [158]. This has been utilised by researchers to produce micropumps, through the rotation of self-orienting Archimedes screws [159], and through the use of rotors with tilted “blades”, similar to a waterwheel [160]. Anisotropic quartz particles have been used to apply and measure torque from Gaussian, single-beam optical tweezers, due to the birefringence of quartz resulting in non-uniform response to linearly polarised light [161]. Another paper by the same group demonstrated

the influence of changing the beam polarisation on the particle's resulting torque, showing that the torque obtained depends on the polarisation rotation rate, allowing for the use of a trapped particle as a passive constant-torque wrench [162]. In the case of optical rotors, it is generally true that the rate of rotation is governed by the power of the laser used, and these could be used for micropump applications such as cell-sorting or as mechanisms for exerting mechanical force on objects such as cells, to investigate mechano-transduction processes.

Control of articulated optical microrobotics is commonly achieved by manually moving them using an optical trap. Therefore, the development of automated control strategies presents a gap in the research, although some examples exist for simple microrobotics set-ups involving rigid bodies [163, 164]. Improving the control strategies available for articulated optical micromachines, particularly ones that allow for parallelising and automating, would help to move them from research curiosities to useful tools for non-experts. The ability to do this is strongly linked to the ability to repeatedly produce micromachines, as tiny differences in structure can have large effects at the microscale, which could impact functionality. This was noted in Reference [140], where success rates of different designs were tracked in order to determine a reliable microrobot design. The ability to model the behaviour of microrobots in response to the beam is also important for control system design, and repeatable experimental results are integral to building reliable models. However, a major difficulty that researchers face is the fact that all parts of an optical microrobot are affected by the presence of an optical trap. This means that there is difficulty controlling the movement of multi-component microrobots, as the different components are all attracted to a single point, the optical trap. Therefore the shape of the micromachine's components, and the mechanical coupling of the different parts is key to ensuring the micromachine operates as required. Additionally, as covered earlier in this review, the number of optical traps that can be used, and the ability to control them separately should be considered.

2.1.5.3 EFFECTS OF MICROROBOT SHAPE

As previously touched on in this review, the simplest shape for optical trapping is the homogeneous sphere. However, obviously this is not an ideal shape for multi-body microrobots, for tasks involving gripping, or for tasks where movement around a fixed axis is the desired outcome. Therefore, the shape of the microrobot must be decided according to the same principles as any other engineering challenge: namely, the task at hand and equipment restrictions with respect to manufacturing and controlling the resulting machine.

The production of simple, classical machines involving lever arms, springs and even

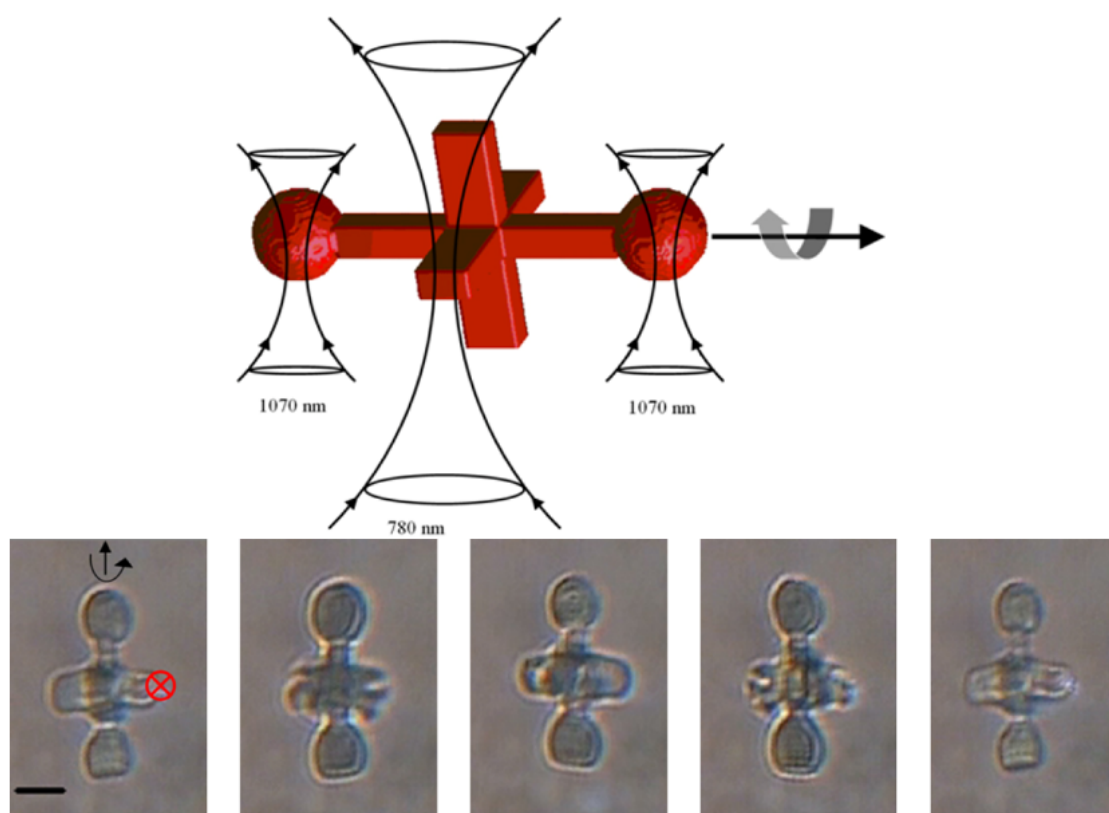


Figure 2.4: Asavei et al. produced an optical “paddle wheel” held in place using two 1070 nm optical traps and driven with a separate 780 nm beam. Reproduced from “Optically trapped and driven paddle-wheel”, [3], under Creative Commons license CC BY 3.0. (**Top**): Schematic of the device. (**Bottom**): Stills taken from a video of the device in action, where the position of the 780 nm beam is shown with a red x.

Archimedes screws has been achieved using TPAP, and functionality has been demonstrated by using optical tweezers to actuate movement. The shape of these microrobots is highly relevant when it comes to their functionality. In the case of an optically controlled lever arm [56], the long arm, if unconstrained by the pin-joint, would naturally orient itself with the trapping beam. The fixed axis, which is attached to the substrate, prevents this from occurring to some extent, but the effect has been noted as a restriction of micro-scale pin joints, as it increases undesirable, out-of-plane movement [57]. The inclusion of spherical features which act as “trapping handles” serves to reduce undesirable motion, as these points are more strongly drawn into the optical trap than relatively flat surfaces.

While this review has already covered some of the situations in which the scattering force is useful for actuating a microrobot, the shape of micromachines that are intended to be actuated in this way also deserves some attention. For instance, the angle of interaction of the optical tweezers with the surface of the screw is vitally important for producing rotation in the desired direction. This has been demonstrated in the creation of the wheel with tilted blades referenced earlier [160], where the direction of rotation was changed by moving the optical tweezers to different points of the wheel. This effect was exploited in the creation of a twin-rotor using a similar design by different researchers [165]. This can be simply explained according to the refraction and reflection of light in an asymmetric shape leading to the resultant forces being directed off-centre and leading to an optical torque [158]. This concept also explains the positive impact of adding spherical “trapping handles” to micromachines, as the curved surface means that the refractive (gradient) and reflective (scattering) components of force from the optical tweezers are directed through the centre of the sphere.

While spherical handles work well for optical tweezers utilising Gaussian beams, where the refractive index of the micromachine is higher than that of the surrounding medium, this is not the case for situations where the refractive index of the object is the lower value of the two. In this case, in fact, the opposite becomes true, and doughnut-shaped objects have been stably trapped using Gaussian optical tweezers, utilising the interaction of the gradient force on the inner walls of the doughnut [4, 166]. A diagram of this can be seen in Figure 2.5, where the case of a spherical particle (a) is compared with ring-shaped particles (b) and (c), and the impact of the beam waist position in the Z-axis is evaluated. The demonstration of stable optical trapping of low-refractive index particles further increases the options for optical trapping studies by increasing the range of mediums that can be used, and it is possible that ring-shaped objects could be used as “trap handles” for micromachines in these scenarios.

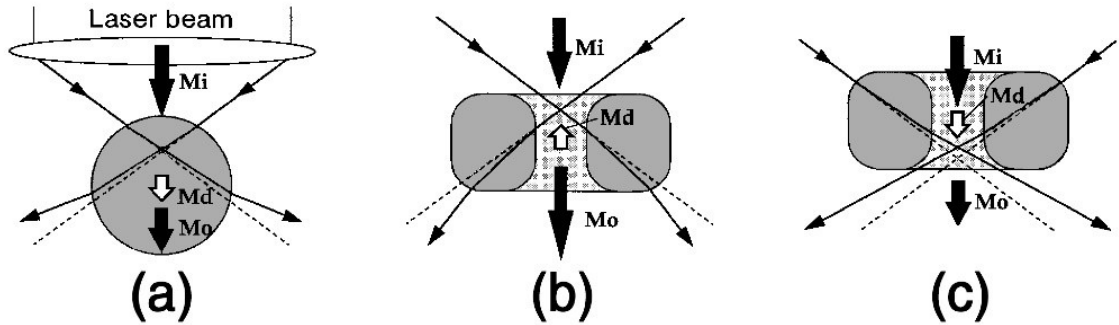


Figure 2.5: Illustration of the interaction of the optical tweezers with differently shaped low-refractive index particles, and the impact of the position of the beam waist. In (a) and (c) the object shape and the beam waist position act to push the object out of the trap, whereas in (b) the incident forces are balanced on the inner walls of the ring, and the position of the beam waist in the Z direction acts to pull the object towards the waist, producing a stable trap. M_i is the incident momentum, M_o is the outgoing momentum and M_d is the momentum transferred from the light to the object. Reproduced with permission from Reference [4] ©The Optical Society.

2.1.6 CHOICE OF OPTICAL TWEEZERS FOR MICROROBOTICS

It can be seen that the ability to create multiple optical traps is extremely useful in microrobotics. This is particularly true in the case of free-floating micromachines with moving parts [3], when the overall position of the microrobot must be controlled as well as its relative motion. Using several different laser beams would be both expensive and greatly increase the space required for an optical trapping set-up. Luckily, several solutions have been developed for the creation of multiple traps from a single focused laser beam. These can be divided into space-sharing and time-sharing set-ups, with holographic optical tweezers [167] being an example of the first type and fast-switching acousto-optic deflectors [168] being an example of the latter. Holographic optical tweezers (HOT) utilise spatial light modulators (SLM) to split an incoming beam into several different beams, which are then directed through the microscope aperture, as shown in Figure 2.6. This technique is particularly flexible in terms of the number of traps that can be created, and the range of movement that is allowed, as it relies only on the pattern imposed on the SLM. Work regarding the calibration of HOT using the power spectrum analysis has also revealed that trap stiffness does not vary significantly during trap movement, and that trap placement is controllable with single-nanometer resolution [169]. These capabilities identify HOT as a useful and versatile tool for force application and measurement in biophysical experiments. However, the real-time use of the technique is limited, due to the calculations required to determine the required pattern of orientations of liquid crystalline pixels across the

device in order to create the desired trap positions. Several different methods for performing this calculation are presented in the literature, including the high-performance yet low-speed Gerchberg-Saxton algorithm [170] and the low-precision yet high-speed direct superposition method [171]. Therefore, when calculating holograms for optical tweezers or other laser-based applications, a trade-off must be made in terms of either speed or accuracy [172], with attempts made to adapt these existing algorithms to produce high speed, high performance alternatives [173, 174].

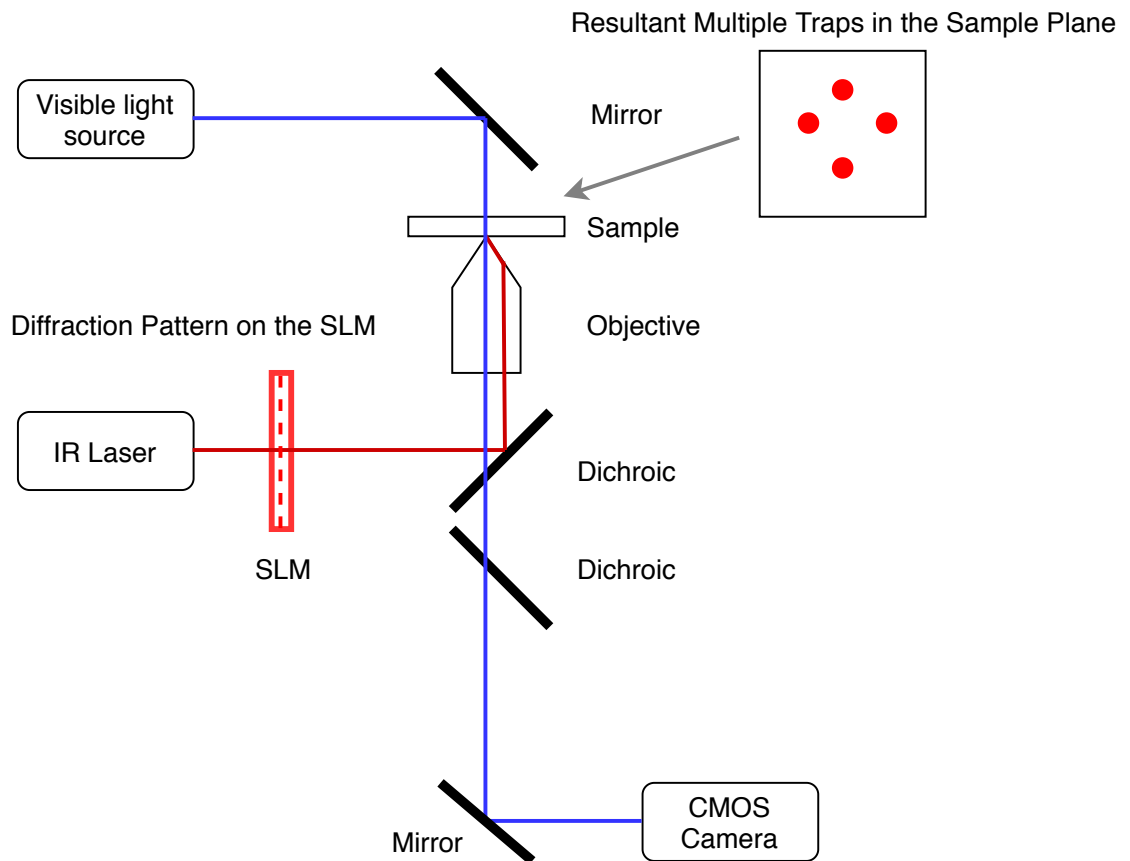


Figure 2.6: Simple schematic of holographic optical tweezers, based on the authors' laboratory set-up.

Time-sharing set-ups for optical tweezers are based on rapid movement of the beam and typically use acousto-optic (AOD) or electro-optic deflectors (EOD), which deflect the beam by a certain angle, controlled by the frequency of an input signal [175, 176]. The calculations involved in this type of dynamic optical tweezers are less time-intensive than those for HOT, but time-sharing optical tweezers are limited in the displacement of traps that can be achieved. This limitation has been tackled through the introduction of additional deflectors [177], and through careful selection of the transducer used to convert the signal that controls the deflector position, which can affect both resolution

and range of frequencies that can be used [178]. As HOT and time-sharing dynamic optical tweezers both have their shortcomings, and both have been used successfully in optical microrobotics applications, the decision to use one or the other is largely based on hardware restrictions, with the introduction of an SLM into an existing general optical tweezers set-up potentially much simpler than the creation of a beam-deflecting system. Additionally, commercial options are available for both HOT and AOD-based optical tweezers, but in laboratories where a small range of specific experiments are performed then it may be preferable to build a custom optical trapping set-up according to specific requirements, and researcher expertise. Additionally, many advances have been made in the development of novel optical tweezers setups, and while they are not a central part of this review it is worth mentioning the counter-propagating optical trap [127, 155], and the optical fibre tweezers [179]. The latter allows for light to be precisely directed into a sample by use of optical fibres which are pig-tailed to the laser diode, focusing the light using the tapered end of the fibres. Optical fibre tweezers offer the opportunity to precisely trap objects in crowded samples, and so could be considered for situations where trapping is to take place in a complex environment. A review of optical fibre tweezers that covers the use of the technology for a range of optical trapping applications is provided by Zhao and colleagues, including a theoretical explanation of both dual and single fibre setups [180].

2.1.7 LOOKING TO THE FUTURE

There is potential for the use of micromachines in almost any discipline where optical tweezers are used to perform tasks, rather than as a laser-physics demonstration. Also, as previously mentioned, the improved and simplified ability to produce optical microrobots without post-manufacture assembly means that researchers from a variety of backgrounds can make use of the opportunities that optical microrobots offer. However, the achievements in microrobotics to date appear to have a bent towards biological research, where the dexterity and precision of optical microrobotics could make activities such as polar-body biopsy or cell enucleation swifter and easier. One of the main reasons that microrobotics have such potential in these areas is the potential for parallelising experiments. For instance, cell aspiration is typically performed using a very thin micropipette, which makes it a delicate task that is susceptible to any disruption to the apparatus [181]. Using a micro-machine that features a sharp point, similar to the nanowire used for temperature measurement in Reference [55] to probe cell stiffness could improve experiment success rates by reducing equipment breakage and decoupling the aspiration set-up from outside vibration, and this concept is shown very simply in Figure 2.7. Using multiple micromachines controlled by multiple optical traps could increase the speed of such experiments, with many aspirations taking place

in parallel with one another. Additionally, the highly customisable and controllable nature of optically controlled microrobots in terms of output force and object displacement means that experiments adapted for optical tweezers using optically controlled microrobots could have lower intrinsic uncertainty than conventional, non-optically actuated methods. A potential example could be single-cell surgery, where the exact force required to breach the cell membrane without causing undesirable damage could be carefully applied with optical microrobots every time. As well as this, the potential that optical microrobots have for reducing laser-induced damage during optical tweezer assays further cements their probable application in biological research in the future, as these assays get adapted to the technology. An example of this could be micro-machine assisted DNA stretching, by adapting the protocol that already makes use of functionalised microbeads, as discussed earlier in this review.

The methods developed to control optical microrobotic systems could also indirectly benefit research using optical tweezers. For example, the work done to determine position and orientation in a 3D workspace [182], or to control the position of holographic optical traps in real-time [164, 183] has applications in optical tweezer-based cell sorting. Therefore, it is fair to say that research into optical microrobotics will offer both direct and indirect benefits to the scientific community, moving forward.

2.1.8 CONCLUSIONS

The use of optical tweezers in biological studies has allowed for the investigation of processes and subjects which would otherwise have remained out of reach, due to the resolution of force and displacement possible. However, as has been outlined in this review, the negative effects of optical tweezers are well-known. The common methods for reducing optical damage, such as altering trapping wavelength or introducing radical scavenging species do not allow for flexibility in the experiments that can be performed, and may require completely changing the trapping set-up. This means that such methods are unsuitable for retrofitting to existing trapping set-ups, and are not suitable for general trapping set-ups which may be used for a variety of applications where wavelengths that are more damaging to biological samples are completely acceptable. Reducing the power of the laser is also often less than ideal, as this lessens the forces that can be applied, which limits the ability to research high-force phenomena such as DNA overstretching. Optical micromachines present a flexible solution to these problems, as they can be used to limit direct exposure of the subject to the laser, which has been theorised to be one of the main ways to reduce optically induced damage, through direct sample heating, photobleaching and generation of free radicals in close vicinity to the sample. While indirect manipulation through microrobotics will not remove the risk of damage due to free-radical damage, it would move the origin

further away from sensitive biological matter, such as DNA, resulting in more time before their diffusion to the polymer. Additionally, optical micromachines show potential to be used to extend the capabilities in biological studies, with proof of concept demonstrated for force amplification and direct force measurement. The printing resolution that can be achieved through two-photon absorption polymerisation, along with the ability to print articulated machines also means that many different micromachine designs are possible. This not only means that the technology is extremely flexible and can be adapted for many different applications, but it also means that there could one day be solutions for many of the challenges associated with the technology, such as the dominance of adhesion forces. However, there is still much work to be done in making micromachines attractive to non-roboticists, such as in automating manipulation and improving repeatability. Overall, optical micromachines present many opportunities for biological studies, as well as interesting engineering challenges, and will likely be a subject of research interest for years to come.

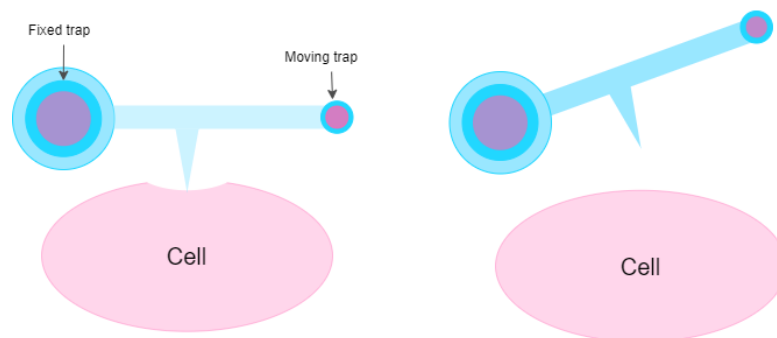
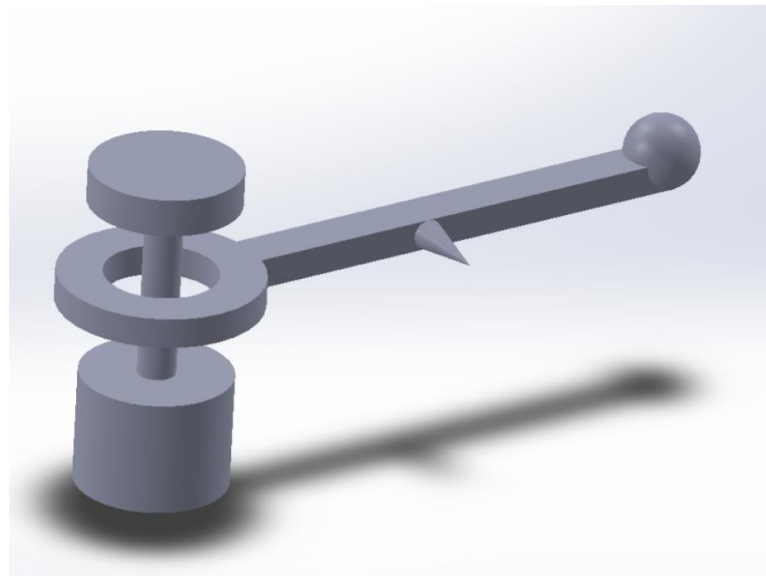


Figure 2.7: A free-floating microrobot, such as this lever, equipped with a sharp tip, could be used to apply amplified forces for measuring cell membrane stiffness. At least two traps are necessary for this, one fixed trap to hold the microlever in place near the cell and another to move the lever arm.

Chapter 3

FUNCTIONAL OPTICAL MICROMACHINES

This chapter is centred around a published article regarding the development of optical micromachines for use in challenging, salty environments. The written article necessitated keeping to a strict page limit, but the published work represented only a small part of the work performed in the design process for creating functional micromachines. Therefore, this chapter expands on the work presented in that article, originally published in the proceedings of IEEE/ASME international conference on Advanced Intelligent Mechatronics 2020 [184]. As a result, this chapter includes: a short introduction explaining the premise of the work; an overview of two-photon absorption polymerisation (TPAP) and the Nanoscribe printing system; an overview of the optical tweezers used for the work; and the initial design work performed; as well as the published article.

3.1 PREMISE

The over-arching goal of this project was to produce nanomachines that could extend the capabilities of optical tweezers; helping to address traditional weaknesses of optical tweezer studies such as low force limits and the possibility of radiation-induced damage. In order to overcome these problems associated with optical tweezers, it was determined that the optical nanomachines should meet the following criteria:

- Be easily oriented and controlled by holographic optical tweezers.
- Have a mechanism for force multiplication.
- Function in the environment required for molecular studies.

The desired application for the nanomachines is in molecule studies, specifically DNA stretching. Gathering reliable results from DNA stretching requires dozens of stretch repetitions, meaning that using nanomachines to assist in such studies would require repeatable and precise movement of the machines. This, combined with the desired mechanism for force multiplication, led to the concept of using multi-body nanomachines for the project: specifically nano-levers. Traditionally, producing such machines has been a serious obstacle to progress in nanoscale manipulation, due to the challenges of assembling nano-sized parts. This is largely because of the prevalence of surface forces over volumetric ones, which makes manipulation of micron and sub-micron sized objects an exercise in frustration due to parts adhering to each other as well as to the manipulating tool [148]. In Chapter 2 we saw that Equation (2.11), relies on the separation between parts, as well as the size of microscopic objects. This means that the van der Waals forces are influenced by a single-dimension length-based measurement.

$$\mathbf{F}_g = \rho V g \quad (3.1)$$

Conversely, (3.1) demonstrates that the force resulting from gravity is proportional to the mass of the object, which is given as the product of density (ρ) and volume (V). This notation emphasises the dimensional component of the equation. As volume decreases more dramatically than length and area as objects become smaller, the force acting on an object due to gravity is quickly overshadowed by so-called surface forces, such as the van der Waals forces. For example, a silica microbead with a diameter of 2 μm and Hamaker constant of 6.7×10^{-20} [185], separated from a silica plane by 10 nm, would experience an attractive van der Waals force of approximately 1.11 pN. The same bead would experience a force due to gravity of 0.11 pN, about ten times smaller than the van der Waals force. This is why non-contact manipulation [186] and carefully designed tools have become popular strategies for tasks requiring micromanipulation.

Despite the challenges that surface forces pose, researchers have made progress in assembly of more complex structures from simple micro-objects, sometimes using optical tweezers to guide the components [187]. Additionally, self-assembling colloidal structures- which use molecular and chemical bonds to form shapes with unique properties- have been used in applications such as drug delivery [188]. However, these approaches do not solve the problem of miniaturising classical mechanisms such as levers and wheels. Two-photon absorption polymerisation (TPAP), on the other hand, all but does away with the problem of assembly, as it allows for the printing of separate, yet intersecting parts which cannot be made using traditional micro-manipulation using pick-and-place or aspiration strategies, nor yet through the exciting “from the ground up” colloidal assembly strategies being explored currently [189]. Additionally,

the negative photoresists suitable for TPAP are necessarily transparent to infrared light, making them highly suitable for optical trapping, which has typically used infrared wavelengths for biological studies since Ashkin's discovery of the destructive effects of visible wavelengths, which are still used for non-biological studies [89, 49].

3.2 TWO PHOTON ABSORPTION POLYMERISATION (TPAP)

TPAP's suitability for assembly-free printing of multi-body, nanoscale machines can be attributed to two things: the high resolution achievable, and the fact that the unpolymerised resist supports the printed voxels during the process, preventing the shapes from collapsing as they print. In TPAP, unlike standard lithography, the rapid (simultaneous) absorption of two lower energy photons is required, rather than absorption of one high energy photon. The speed of absorption is crucial: both photons must be absorbed before the interacting electron returns from its excited state to its base state. TPAP is a non-linear process, just as two-photon absorption itself is, and the probability of absorption is proportional to the square of the intensity of light. Therefore, highly focused pico or femtosecond pulsed infrared lasers are used for TPAP systems, rather than more conventional ultraviolet light sources. The use of high intensity infrared light as the photon source is what enables truly three-dimensional "printing" from TPAP, compared to the 2.5D printing enabled by traditional one-photon polymerisation. This is because the intensity is only high enough for two-photon absorption to occur in a tiny volume of resin in the direction of propagation, as well as being restricted in the other Cartesian directions due to being focused through a high numerical aperture objective. When UV light is used as a source for photopolymerisation, the high energy of the light means that absorption of single photons is sufficient to reach the threshold for polymerisation. This means that greater volumes of resist are exposed, particularly in the Z-direction, as the region of the laser beam that meets the threshold for polymerisation extends over the Rayleigh length of the laser. On the other hand, the much lower energy of each photon in an infrared beam means that the volume of the beam that reaches the threshold required for two-photon absorption is much more restricted. Using extremely short pulses of the laser also acts to restrict polymerisation by time-limiting the laser dose. This restricts the polymerisation that occurs due to diffusion of free radicals through the photoresist. Fig. 3.1 illustrates the process of TPAP using infrared lasers, showing schematically how polymerisation continues until a stable polymer forms.

By changing the position of the laser focus in the resin, many voxels of resin can be joined together, and low absorption of the infrared light by the photoresin means that

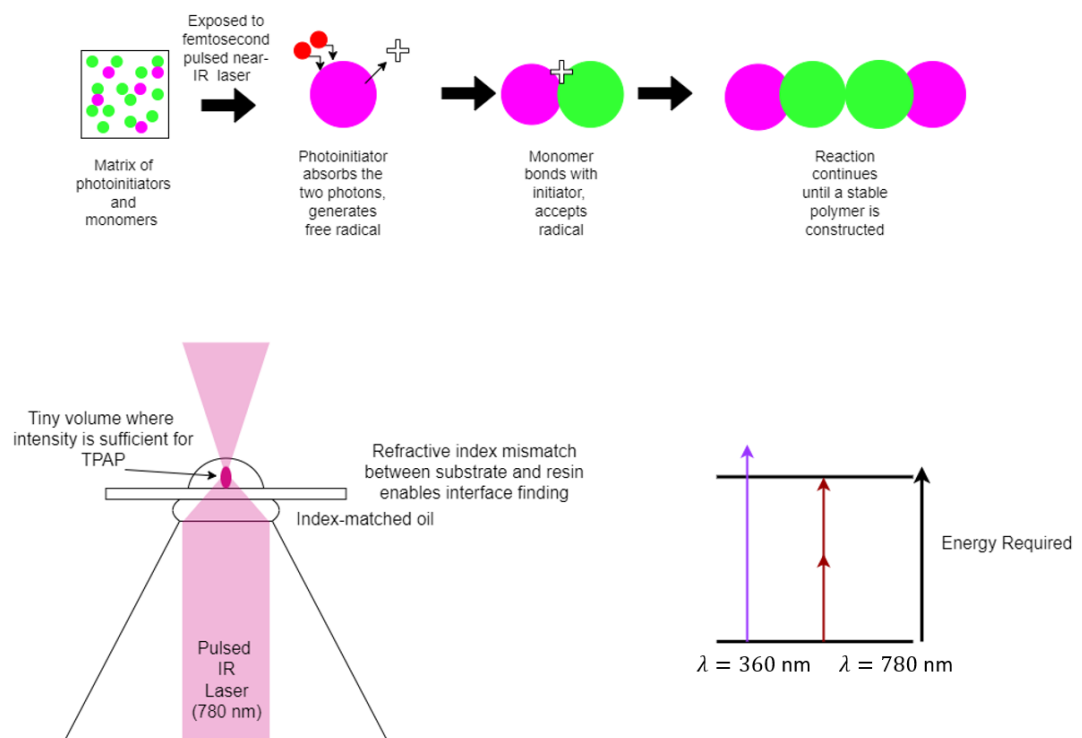


Figure 3.1: The highly focused, pulsed infrared lasers used for TPAP allow for the polymerisation of tiny voxels of resin at a time, in contrast with the 360 nm ultraviolet sources commonly used for conventional, 2D photolithography.

the intensity of the laser will remain relatively consistent, maintaining the voxel size as it prints. This enables the reliable printing of mechanical elements such as wheels on axles through TPAP, where the dimensions of parts need to be consistent for the micromachine to be functional. Due to the tendency for micro-sized objects to adhere to one another, and van der Waals forces being dependent on overlapping area between objects, it becomes easy to conceptualise the problematic effects of a wheel printed with a slightly different thickness along its arc, particularly if it is to turn. The problem becomes even easier to imagine when the driving force for such a machine is to be provided using optical tweezers, which are generally limited to a range between a few femto-Newtons and a maximum of hundreds of pico-Newtons. In such a case, adhesion of the order of 10 pN between parts could mean the difference between a useful machine and a stationary object.

3.2.1 THE NANOSCRIBE PHOTONIC PROFESSIONAL GT2

The Photonic Professional GT2 (PPGT2), from Nanoscribe GmbH provides a commercial solution for TPAP, which centres around a femto-second pulsed (pulse length 100-200fs), 780 nm laser focused through an objective in order to provide the necessary intensity of light for polymerisation. Several interchangeable objectives are available for use with the set-up; each one suited for different scales of design. These include both air and immersion objectives, as the range of applications for TPAP expands, and different feature scales are required. However, as this work is focused on the use of TPAP for nano and microscale printing, only the objectives suitable for the highest resolution features have been described in Table 3.1.

Table 3.1: Key Features of the objectives used for high resolution direct laser writing with the PPTG2

Magnification	Numerical Aperture	Immersion	Print Configuration	Resolution
63x	1.4	Oil/resin	Conventional/DiLL	<200 nm
25x	0.8	Oil/resin	Conventional/DiLL	<600 nm
20x	0.5	Air	DiLL	<800 nm

The 25x objective is used for intermediate “micro-to-mesoscale” prints, with a print volume of up to 1 mm³, the 20x air objective is used for prints on reflective or opaque substrates, such as those coated with indium tin oxide, and for similarly sized features as the 25x objective. The 63x immersion lens delivers the finest resolution and smallest print volumes, being appropriate for jobs with nano-microscale features. The user can define a trajectory of points for laser-writing, electing to expose these “point by point” or to use the “ConnectPoints” command to let the PPGT2 define a series of

interpolated way-points to also be polymerised. However, of potentially more interest when printing miniaturised conventional machines, Nanoscribe also have their own software, DeScribe, which converts .stl files to Nanoscribe’s proprietary GWL (General Writing Language) for direct laser writing. This conversion process allows the user to define a recipe for the print job. The “Recipe” system represents a great advantage of the Nanoscribe setup: it presents users with a workflow that largely follows the standard for conventional 3D printing. In the recipe for the print job, the user can define the slicing and hatching distances, as well as the hatch angle and whether the object will be printed with constant or varying laser power- helpful for creating shell objects. This has made the attractive features of TPAP accessible to researchers outside of specialised laser laboratories, and generally improved reproducibility of micromachines printed using TPAP. As the same base design and recipe can be followed each time, it also enables simpler design iteration processes, as changes to various parameters can be made easily. This can be seen in Fig. 3.2, where a simple DeScribe workflow is described.

The conversion process produces several files, one of which, the job file, can be opened in DeScribe and edited using NanoScribe’s simple, human-understandable programming language, to define printing parameters that are not set in the recipe. One such parameter is the writing power, which defines the laser power used to print the design as a percentage of the total available laser power. The laser power is set as a percentage of the laser power measured in the focal plane of the instrument, which is generally measured to be 50 mW for the PPTG2. The power scaling factor (PSF) is also set in the job file, at a default value of 1.0. The PSF can be used to increase the power past the theoretical “full power” value of 50 mW, as the combination of PSF and laser power as a percentage sets the writing power, as shown in (3.2).

$$\%LaserPower \times PSF \times \frac{50mW}{100} = ActualPower \quad (3.2)$$

The job file automatically includes instructions to print the imported design, but Nanoscribe’s programming language allows the user to write scripts to make the printing process less laborious. For example, defining FOR loops to print arrays of objects makes it simple to vary printing parameters, or even designs, throughout a sample, according to the object’s place in the array. This allows the user to combine several .stl parts into one print job, which can be useful for complex objects and structures. DeScribe also offers the option of “advanced .stl processing”, which allows the user to simply perform a parameter sweep, systematically varying print parameters across a matrix of printed objects. This is an excellent way to understand how the different parameters combine to produce a specific result. One such parameter is the scanning speed, which can be varied dramatically depending on the printing mode, with speeds of dozens of mm/s

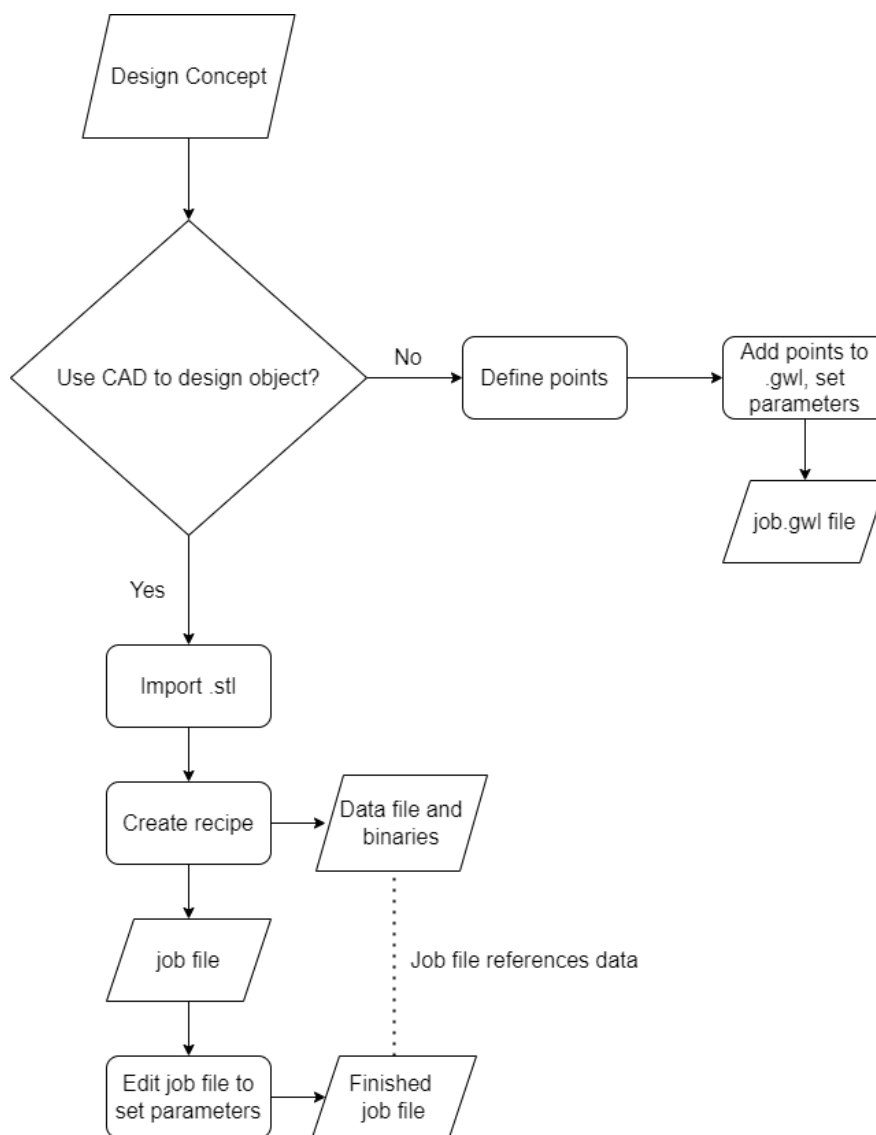


Figure 3.2: Nanoscribe's PPGT2 allows the user to define points for polymerisation directly (point by point) or use DeScribe's import wizard to define a recipe for an already designed .stl file.

possible. While laser power is the primary parameter affecting the laser dose received by the photopolymer, the scanning speed also influences it, with the proportional influence of these parameters shown in (3.3).

$$Dose \propto \frac{LaserPower^2}{ScanSpeed} \quad (3.3)$$

Nanoscribe recently released a series of “default workflows” for prints suited to different design outcomes: defining default print parameters depending on the approximate feature size. These default recipes are named accordingly, and are known as the small, medium, large and extra large feature sets. Nanoscribe’s aim in releasing these default recipes is to provide a recommended starting point for the print parameters and laser dose for jobs, based on averages for jobs with roughly similar dimensions. Such a starting point is expected to be particularly useful for cases where users are applications focused, and have little theoretical or practical knowledge of TPAP. However, the user still needs to spend time refining the parameters according to their own tests and experimentation, as the default recipes are of course highly generalised. A 2021 paper by Bunea et al. illustrates the importance of performing such tests by printing and characterising high resolution designs and publishing the suggested parameters for achieving similar results [190]. The process for defining these parameters is discussed in Appendix A.

3.3 THE OPTICAL TWEEZERS SETUP

One of the key limitations, and indeed one of the sources of motivation for this project, was the low forces that can be applied with optical tweezers. While some optical tweezers are capable of providing hundreds of pico-Newtons of force, the optical tweezers available for this work were far weaker. The tweezers consisted of a holographic optical tweezers (HOT) system which was capable of exerting a maximum force of approximately 10 pN, and a separate pair of traps created using a 1030 nm laser. The latter which were capable of exerting at least 70 pN and had been previously used for DNA overstretch experiments by colleagues [145]. The tweezers are created by focusing the lasers through a 1.2 numerical aperture, 60x magnification Nikon plan APO water-immersion lens. A 1.5x secondary objective is used to further increase magnification for imaging experiments.

The 1030 nm trap set-up (referred to as the HP, or high power trap from here) splits the beam one fixed trap, which was located in the centre of the viewing plane, and a steerable trap, which could be moved approximately +/- 40 μm in the X and the Y directions. The steerable trap is manoeuvred in the XY plane by adjusting the position of a mirror using linear piezo-actuators controlled by a New Focus Picomotor

controller. The addition of the positioning mirror means that the path of the steered trap is longer than that of the fixed trap, resulting in an offset in the Z direction between the traps. Additionally, losses associated with the mirror position result in changing trap stiffness depending on position, with the strongest differences seen near the maximum displacement of the trap. This further limits the range over which the trap can be moved, with 30 μm being suggested as the maximum displacement in order to reduce losses in trap stiffness.

Holographic optical traps are created, as the name suggests, by generating holograms using a diffractive optical element (DOE), creating a diffraction pattern which determines the position and features of resulting optical traps. Liquid crystal spatial light modulators (SLMs) are often used to create HOT, as pixels on the SLM can be addressed by computer control, allowing for dynamic hologram generation. Spatial light modulators can control both the intensity and the phase of the light, with amplitude-modulating SLMs being used in projector technology. However, in optical trapping it is generally desirable to maximise the intensity of the laser light, and so phase-only SLMs are often used to generate holograms for optical trapping. The phase modulation imposed by the SLM passes on the information about the desired beam pattern- how many traps and where they are positioned. Phase modifications can not only control the position of the laser within plane, but can also adjust the depth (Z-position) and shape of optical traps. This allows the user to create interesting traps such as doughnut-shaped Laguerre-Gaussian beams or line traps from a Gaussian input [191].

While this flexibility makes HOT very attractive for research, there are inherent limitations to the technology. These include hardware limitations, such as discretisation effects due to the limited number of pixels on the SLM and the refresh rate, as well as time limitations caused by how long it takes to calculate and apply the desired phase modulation. When calculating the light field for holographic traps there is a trade-off between the speed of the calculation, and the quality of the resulting traps and there are two methods which represent the extremes. These are the accurate yet slow Gerchberg-Saxton algorithm [170], which was adapted from X-Ray crystallography calculations to calculate the required phase modulation for optical traps, and the much faster but lower precision direct superposition method [192]. The latter is computed by calculating the complex sum of all the beams required to produce the desired diffraction pattern, disregarding the amplitude variation and keeping the resulting phase. Despite the lower precision afforded by the direct superposition method; which results in wildly varying intensities in different traps and a number of ghost traps; it can be improved by finding the phase shift for each pixel that reduces the intensity variation for all of the traps [171].

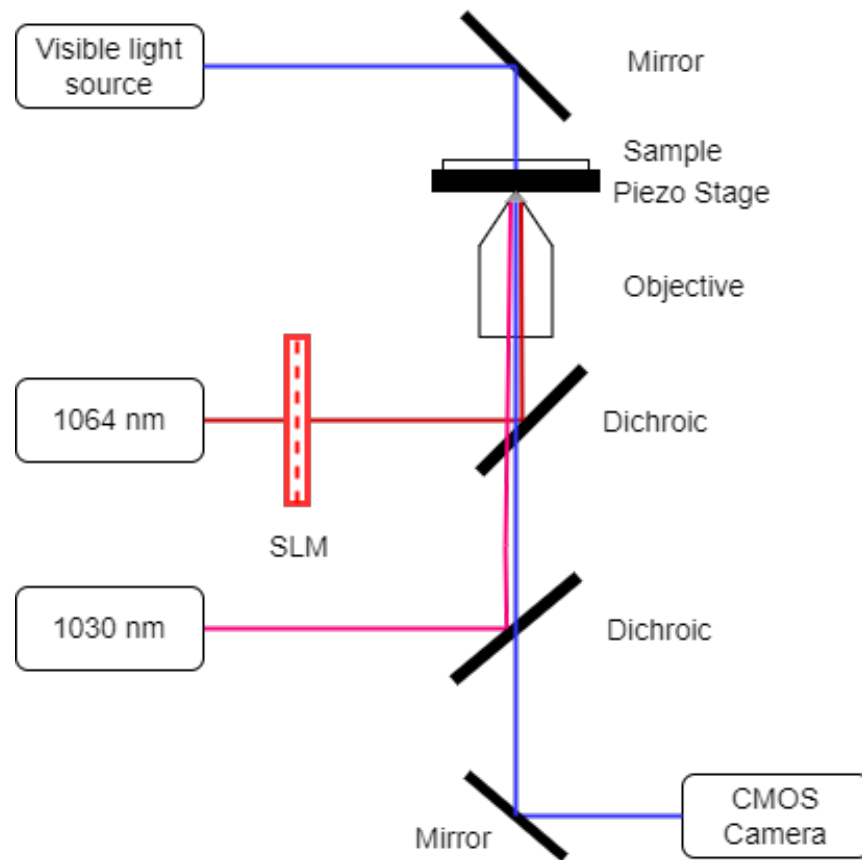


Figure 3.3: The optical tweezers setup used for this work included both HOT and a pair of higher power traps, one of which was fixed in place and the other which could be steered by positioning a mirror using a piezo controller.

The hologram calculation for the HOT used in this work relied on Bowman et al.'s Red Tweezers software [174], which uses an algorithm based on the direct superposition method, with additional terms to balance calculation time and trap quality. The Red Tweezers software uses a shader language to render the computer hologram, allowing fast updates to the optical traps. While the hologram generation is indeed very fast, making this useful for optical nanorobotics, and the parameters added to the superposition calculation theoretically allow the user to individually control the trap intensities, the trap stiffness varies depending on where the trap is placed. This is dealt with by performing position-specific trap calibration when using the HOT. Additionally, there is a “dead zone” where traps cannot be generated, directly in the centre of the viewing plane, and it is speculated that this is due to some feature of the SLM used, where interference in the hologram results in loss of the trap. However, this “dead zone” coincides almost exactly with the position of the fixed HP trap, meaning that when the HOT and HP traps are used together this feature is actually quite useful for “passing” objects into the HP trap.

Despite the varying trap stiffness and “dead zone”, the HOT could be used to place traps throughout the viewing plane, rather than having the restrictions of placement that the steered HP trap had. This made the holographic trapping system a great deal more flexible than the high power traps. Additionally, the HOT system allows for adjusting the Z position of the trap, as well as the position in the XY plane, meaning that the Z-position of the HOT could be matched to that of the fixed HP trap if the two were used together. Another useful feature of the HOT is that several optical traps could be generated at once. These traps could also be grouped and manipulated simultaneously, for example rotating around a shared centroid. A diagram of the optical tweezers set-up can be seen in Fig. 3.3.

In summary, the optical tweezers available for this work were relatively low force, but could be used in a variety of configurations. The HP and HOT traps can be used simultaneously, with the HOT being especially useful for “passing” particles to both the fixed and steered HP traps. The optical tweezers have been primarily used for soft matter studies: with micro-rheology, cell-studies, emulsion droplet interactions and molecule stretching all being performed. These applications require high force sensitivity and can be performed at low forces, while optical nanorobotics work is commonly performed using very high force optical tweezers. This work was the first optical robotics work performed in the research group, and the potential for using optical robotics to assist in soft-matter studies was a source of great interest. Of the examples mentioned, DNA stretching- specifically over-stretching- has the highest force requirements. The characteristic DNA overstretch transition happens at 65 pN, and the fact that overstretching could be performed using the HP tweezers not only provides

a high force value for the tweezers, but also indicates that the steered and fixed traps have approximately the same capabilities for force application. The low forces that can be applied using the HOT emphasise the importance of careful design for the optical nanomachines, as the HOT provided the most trapping flexibility and would likely be the primary optical trapping system used in this project. Additionally, being able to use the HOT to “pass” nanorobots to the HP traps relied on the HOT trap providing suitable force to move said nanorobots.

3.3.1 HOOKEAN SPRING MODEL OF OPTICAL TWEEZERS

As mentioned in the review contained in Chapter 2, there are several models used for calculating the forces that can be applied with optical tweezers. The two most basic, the ray optics and Rayleigh models are only valid for very large and very small particles respectively, and techniques that work well for intermediate particles tend to be computationally intensive and limited in their accuracy. In addition, due to possible inconsistencies in the optical trapping system used, the calculated force can be extremely different to the experimental results reported. However, the Gaussian distribution of laser intensity for conventional optical tweezers creates a parabola-shaped potential well, meaning that optical tweezers can be modelled as a harmonic oscillator. This means that the energy of the potential well in one dimension can be described using the classic model shown in (3.4).

$$E_{potential} = \frac{1}{2}kx^2 \quad (3.4)$$

This is very helpful when it comes to experimentally determining optical forces, as it means that the force required to move the particle in the trap can be given by the familiar Hookean spring force equation given by (3.5). Where k is the “spring constant” of the optical trap

$$\mathbf{F}(\mathbf{x}) = kx \quad (3.5)$$

There are two main simple methods for experimentally determining the stiffness of an optical trap, and both lead to very similar results when compared [193]. The first is to apply a fluid flow to the trapped particle, which can be simply done by applying an oscillation to the sample chamber via piezomotor stage. This creates drag that displaces the trapped particle from the centre of the trap. At sufficiently high fluid velocity, the drag force on the particle will be high enough to escape the trap. This is known as the escape drag and allows for the calculation of the optical spring constant by equating the harmonic restoring force to the Stokes drag, as shown in (3.6). In this equation a is the particle radius, η is the dynamic viscosity of the trapping fluid and v_x is the escape velocity.

$$F(\mathbf{x}) = kx = 6\pi\eta av_x \quad (3.6)$$

The second method for determining the stiffness constant comes from understanding that the optical trap restricts the Brownian motion of a trapped particle. At thermal equilibrium a harmonic oscillator such as optical tweezers has the average energy shown in (3.7). Here k_B is the Boltzmann constant and T is the temperature in Kelvin.

$$\langle E \rangle = \langle E_{kinetic} \rangle + \langle E_{potential} \rangle = \frac{1}{2}k_B T + \frac{1}{2}k_B T = k_B T \quad (3.7)$$

By monitoring the position of the particle within the optical trap, the trap stiffness can then be found by using the equipartition theorem, which is shown in (3.8), where $\langle x^2 \rangle$ is the variance of the particle's position in the relevant dimension.

$$k_x = \frac{k_B T}{\langle x^2 \rangle} \quad (3.8)$$

This latter method was the one used throughout the work contained in this thesis, with the position of the trapped particle extracted from high-speed video recordings of 10 000 frames. Exposure times for the videos were kept to 0.05 ms and the frame rate was high (generally 500 fps) in order to represent the trap stiffness as accurately as possible. It is also common to make use of a quadrant photodiode (QPD) in order to determine position with greater bandwidth than can be achieved with a camera. In cases when a QPD is used, power spectrum analysis of the resulting signal is used to determine the trap stiffness. A thorough explanation of this method is given in a paper by Berg-Sørensen and Flyvbjerg [86].

The trap stiffness was calculated for each experiment using calibration measurements taken *in situ* for that experiment. Trap stiffness varies depending on the properties of the trapped particle, which may appear contrary to other harmonic systems, but makes sense when one remembers that the optical trap is not the laser beam itself, but rather refers to the interaction between beam and particle. In addition, the variation in trap stiffness is in keeping with the ray optics and Rayleigh models where it is shown that refractive index and particle size influence the optical force.

3.4 PRELIMINARY DESIGN WORK AND RESULTS

Successfully producing functional nanomachines was identified as the first milestone of the project. However, as the scope of the project was defined to include molecule stretching, awareness of the later goals of the project influenced the initial design process. Therefore, the first major design consideration was to avoid direct, or close ($< 5\mu\text{m}$ distance) contact with the sample, when the nanomachine was being manipulated by

optical tweezers. Using a micro-lever to transfer force from the optical tweezers also had the advantage of being conceptually simple to adjust for our force amplification goals; as amplifying the force would theoretically just involve small changes to the lever, while the overall design remained similar. The very first levers were printed by Dr Daniel Fan, at the time a postdoctoral researcher with the Precision and Micro-Engineering Department in the Faculty of Mechanical, Maritime and Material Engineering at the Technische Universiteit Delft. This marked the beginning of the collaboration with TU Delft.

Three basic designs were decided on: two pin-jointed and one elastic cantilever. This was based on a survey of the literature, which revealed that both pin and elastic jointed structures had been successfully fabricated using TPAP. These base designs can be seen in Fig. 3.4.

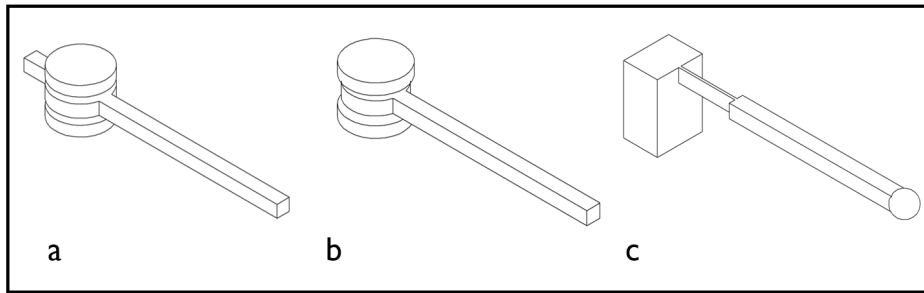


Figure 3.4: The three initial levers: (a) a first-class pin-jointed lever, (b) a second-class pin-jointed lever and (c) a simple cantilever.

The initial lever designs were all $20\ \mu\text{m}$ long, a fairly arbitrary size that was decided based on being able to manipulate $20\ \mu\text{m}$ microbeads with the HOT, as well as the much lower maximum forces available in our trapping setup compared to those in the literature. For example, Lin et al. produced a $60\ \mu\text{m}$ long pin-jointed lever [56], which was used with $280\ \text{pN}$ tweezers. Additionally, the lever used in that work was printed with an H-shaped cross-section, to improve rigidity while reducing weight, due to the challenges of printing and manipulating high-aspect ratio shapes. The motivation for the initial lever designs was to determine, at the most basic level, whether microlevers could be manipulated with the optical tweezers setup, and so the beams were kept square. The lever beams were designed to have a $1.2\ \mu\text{m} \times 1.2\ \mu\text{m}$ cross-section, as this was identified in the literature as a suitable value to preserve the rigidity of a printed beam [140, 57], as well as being close to the wavelength of the optical tweezers, resulting in strong optical trapping. The spherical handle on the cantilever beam was $2\ \mu\text{m}$ in diameter, while neither of the pin-jointed levers were originally designed with handles, in order to focus on just printing unsupported levers. The pin-jointed levers were designed to have a $20\ \mu\text{m}$ “effort” length and a $5\ \mu\text{m}$ “output” length, while the

cantilevers were simply designed to see if they would bend, although the length of the elastic joint was also $5\ \mu\text{m}$. One of these cantilevers can be seen in Fig. 3.5

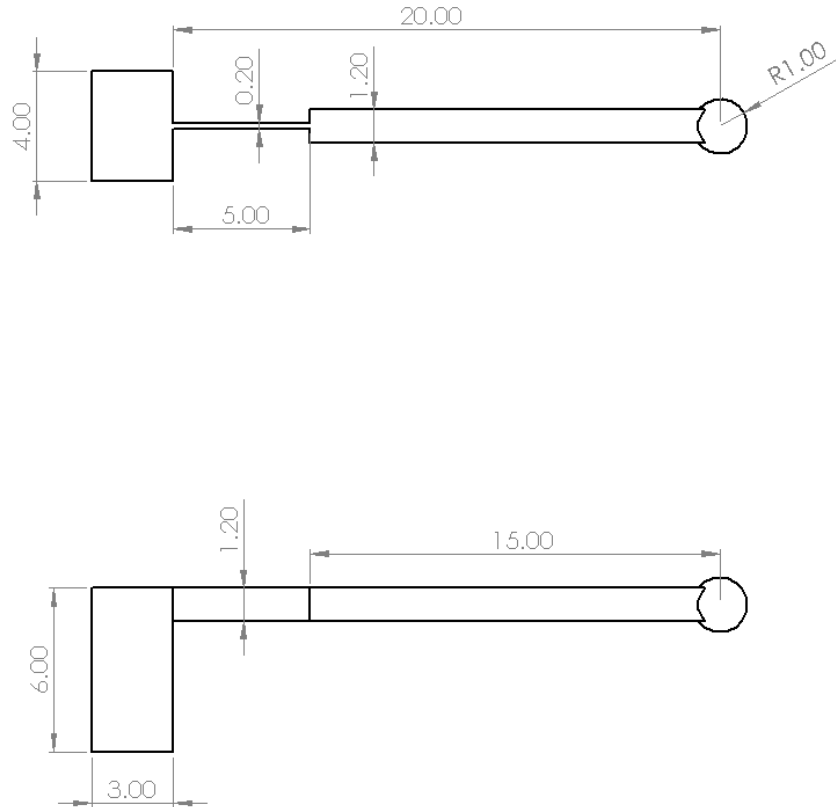


Figure 3.5: The initial concept for a simple cantilever, with a much thinner segment of the beam acting as an elastic joint. All measurements are in micrometres.

While the elastic-jointed structure used in Jeong et al. [57] was successfully used to amplify forces from optical tweezers, the optical tweezers used provided a great deal more force than the ones available for this work. The trapping force used for the displacement of elastic beams in the cited work was 13 nN, several orders of magnitude higher than most optical tweezers. Therefore, in order to investigate the potential for using cantilevers and elasticated joints in this work, using much lower driving forces, a simulation was performed. The simulation was performed using SolidWorks, with 65 pN used as the driving force, acting on the spherical handle at the end of the lever. According to Nanoscribe's provided specifications for their proprietary resists, IP-L 780 has a far lower elastic modulus than IP-Dip: 3.4 GPa rather than 5.1 GPa. Therefore, IP-L 780 was the material simulated. A value for the Poisson's ratio of IP-L 780 was not available at the time, and it was understood that this, as well as the Young's modulus

would vary according to polymerisation. Therefore, the Poisson's ratio was estimated to be similar to SU-8- a widely used photoresin- and a Poisson's value of 0.22 was used [194]. The finest SolidWorks mesh was used, in order to give reasonable results given the extremely small part and applied force and the maximum displacement produced was 34.75 nm, a screenshot of the simulation results is given in Fig. 3.6. This displacement would be measurable, but not useful for our desired application, and so the decision was made to proceed with pin-jointed levers.

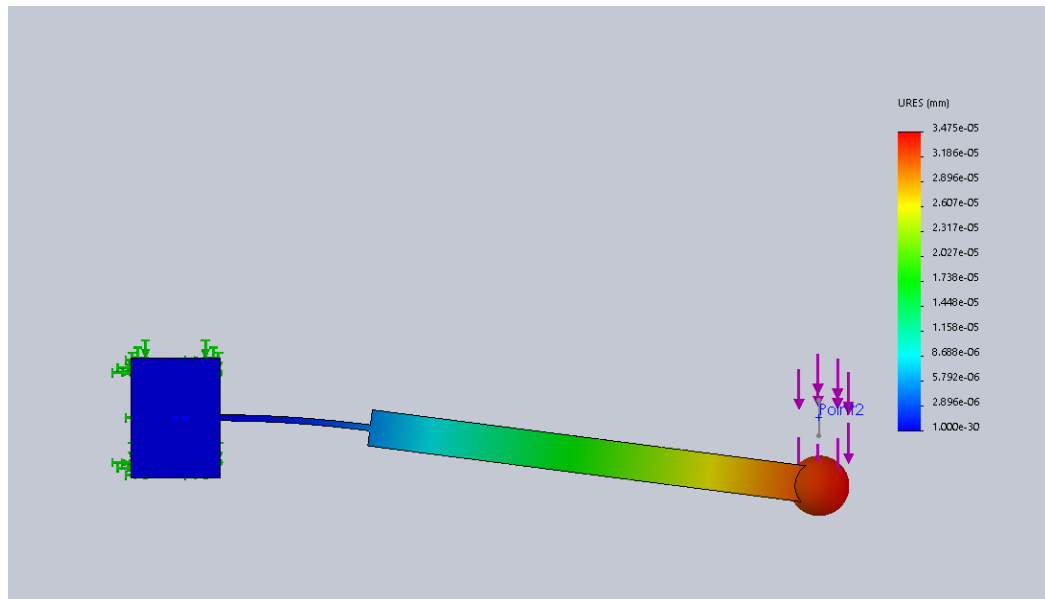


Figure 3.6: The results of SolidWorks simulation indicated that forces near the limit of the HP trap's powers would be insufficient to usefully bend the cantilevers (despite the dramatic looking bend that the simulation animation produces).

3.4.1 SAMPLE PREPARATION AND OPTICAL TRAPPING CONFIGURATION

While the levers were supported by either unpolymerised resist or solvent during the printing and development processes, once they were dried the unsupported levers rest on the centre pin and substrate. The contact between the parts can create relatively strong adhesive bonds, which had to be broken before the levers could be manipulated using optical tweezers. Additionally, the supported levers were anchored to the substrate by the supports, and the support-substrate bond likewise had to be broken before the levers were able to turn. Therefore, the levers were turned using a borosilicate microprobe which was pulled to create a point with a tip radius $< 1\mu\text{m}$ using a capillary puller (PC100, Narishige). This was part of a chopstick-like micromanipulation set-up consisting of two such microprobes mounted to a series of precise stepper-motor stages

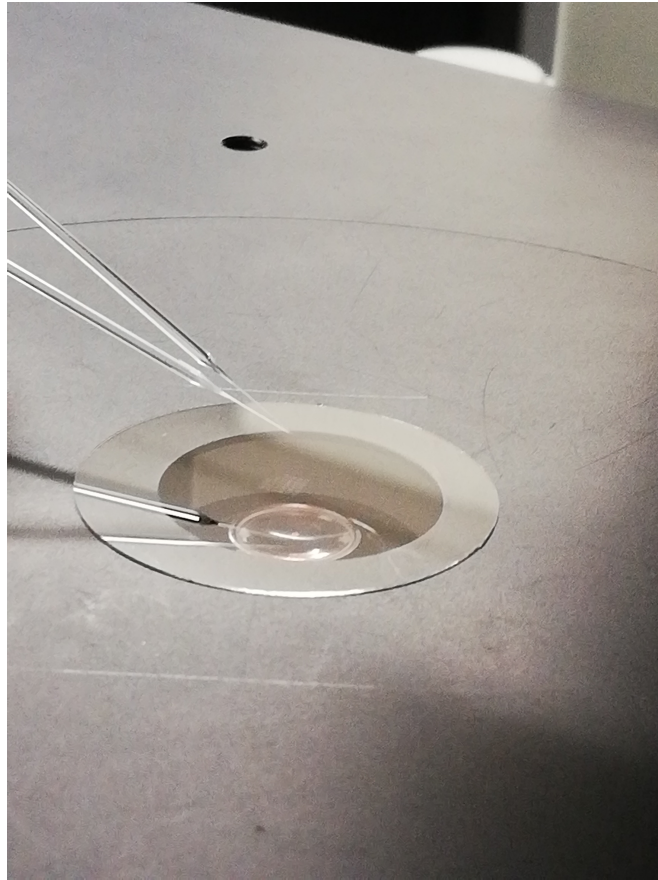


Figure 3.7: The borosilicate microprobes pictured above a sample populated with levers printed using IP-L 780.

for coarse (OSMS80 and HPS80, Sigma-Koki) and fine (TAMM40-10C and OSMS60-5ZF, Sigma-Koki) movement. The stages were controlled through two Sigma-Koki SHOT-304GS 3-axis stage controllers, with commands passed via serial port. This micromanipulator set-up was connected to an Olympus IX-71 inverted microscope, and a manual stage was used to move the sample relative to the microprobes when preparing samples printed with large numbers of levers. The microprobes can be seen in Fig. 3.7, positioned above a sample, before the turn test. The levers themselves can actually be seen with the naked eye, due to the pattern created as they scatter the light.

The goal for this sample preparation was to turn the levers, but leave the centre pin securely fixed to the substrates they had been printed on. This would allow the IP-L 780 levers to be trapped “right side up”, through the coverslips they were printed on, while the IP-Dip sample would need to be sealed with a coverslip and then inverted for trapping. The requirement for trapping through a thin coverslip comes from the working distance of the objective used for the optical tweezers ($270\ \mu\text{m}$), which meant

that the traps could not have been placed above the $700\ \mu\text{m}$ thick substrates used for the IP-Dip.

A very brief investigation into the possibility of using Bessel beams for trapping instead of the standard Gaussian traps was performed, to see if this would be a feasible option for optical trapping through the silica substrates. Creating doughnut traps, which do not have the same depth restriction on trap intensity as Gaussian traps, would involve using axicon lenses to create the beam shape required. However, introducing axicons into the trapping setup would take significant rearranging of the existing path of the optical tweezers, due to needing to account for the focal length of a pair of axicons. It was also unclear whether the force required to move the levers would be available using doughnut traps, as these generally provide lower power when compared to Gaussian trap, which is seen as a positive when trapping living organisms but is not ideal for optical nanorobotics. Therefore, it was determined that different sample orientations would be used for the IP-L 780 and IP-Dip levers instead. A diagram showing these trapping configurations can be seen in Fig. 3.8.

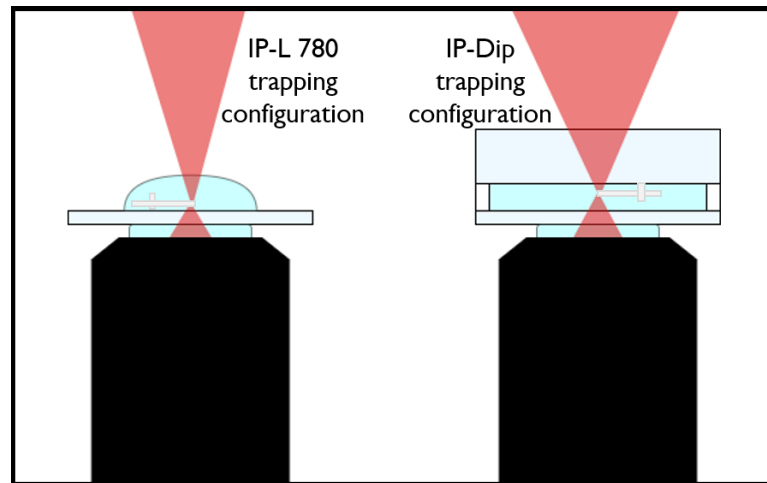


Figure 3.8: The depth limitations of the optical traps required different orientations for the levers printed with IP-Dip and IP-L 780.

After dry turn tests, milliQ water was added to the sample and the levers were turned again. Levers were then transported to the optical tweezers laboratory where the HOT was used to attempt to rotate the levers. If the levers could not rotate in response to the HOT, then the HP trap and the piezomotor stage were used to try to move the levers by trying to trap the lever, and creating relative motion with the stage. Levers were graded qualitatively according to how they performed during each testing stage, with an ideally functioning lever being able to complete full turns at all stages.

3.4.2 FIRST LEVER RESULTS

Pin-jointed levers were successfully printed with IP-L 780 and IP-Dip. However, the microlevers printed with IP-Dip detached from the substrate when turning was attempted. This meant that the levers were unable to turn, as the forces anchoring the centre pin to the substrate were apparently lower than the adhesive forces between the lever arm and the centre pin. This followed the pattern seen in Lemma et al. [144], where the force on the IP-Dip pillars had to be limited during the bending tests, as the pillars would otherwise detach. This may have been due to the DiLL printing creating weaker adhesion between the substrate and the resin, which may be useful for applications where printed objects should be entirely removed from the substrate, but it was not desirable for this work. The fact that the levers detached before turning meant that optical manipulation of detached levers could not take place, as the lever arm would not be able to move separately from the pin, and the only result would be movement of the entire lever, assuming that it could be trapped stably.

Several iterations of the first and second class levers were printed in order to find a combination of design features and PPGT2 printing parameters that would produce successfully rotating levers. The results from the initial experiments, and the layouts of the samples can be found in Appendix B.1. The most important parameters for successful printing of functional levers were found to be the vertical and lateral gap between the lever arm and the centre pin and the height of the base of the centre pin, although varying the printing parameters such as scanning speed and slicing and hatching distance also affected the results. Levers were also printed without supports, with single supports at the end of the lever arm, or with multiple supports along the arm. The supports were introduced to avoid sagging of the resin, which was a persistent problem in the first few lever prints, an example of which can be seen in Fig. 3.9.

The first successfully turning levers were first class levers printed with the features and settings shown in Table 3.2 and the DeScribe screenshot shown in Fig. 3.10. Only one lever out of a field of 49 with these parameters could be turned fully using the HOT- although it was rotated through 360° multiple times. Therefore, the decision was made to take these parameters to represent the minimum requirements for functional optical levers.

Table 3.2: The features of the first successfully rotating microlever.

Vertical Gap (μm)	Base Height (μm)	Lateral Gap (μm)	Supports Number/ Placement	Slicing Distance (nm)	Hatching Distance (nm)	Hatching Angle ($^\circ$)	Laser Power (%)
1.4	3.0	0.9	⁴ Along Arm	100	100	Auto	30

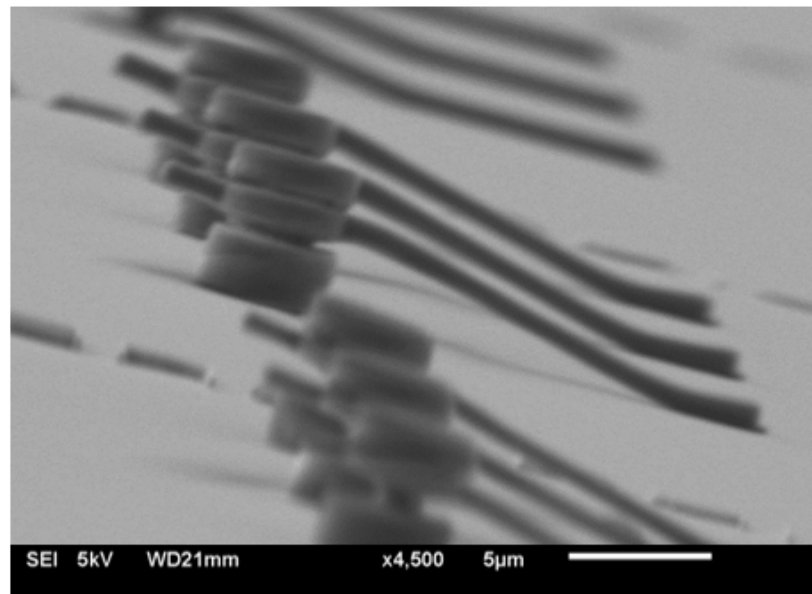


Figure 3.9: Lowering the laser power used for polymerisation resulted in a well-defined vertical gap, but sagging lever arms. Additionally, this SEM image seems to show resin sagging in the lever ring, as well as along the arm. Image by Dr Daniel Fan, 2018.

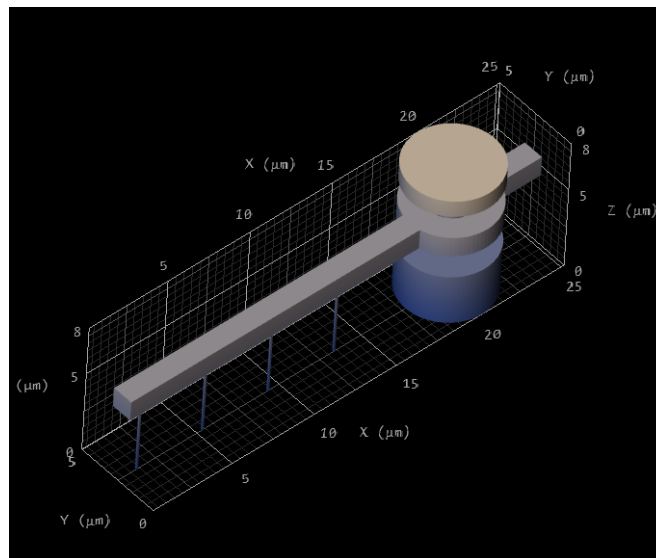


Figure 3.10: The design that produced the first successfully rotating levers was supported with four long, thin pillars of resin. These were easily detached from the substrate, but not easily removed from the levers.

The reason for printing these initial levers was to determine the basic starting parameters for nanomachines with the PPGT2 and the optical tweezers set-up available. Therefore, none of the first lever iterations were printed with the spherical handles which are necessary for stable optical trapping. The result of this was that the first lever that successfully rotated was pushed around by the HOT, rather than stably following the position of the trap, a phenomenon that can be seen in the screen recording stills shown in Fig. 3.11. This immediately showed that spherical handles would have to be included for stable position control with the optical tweezers.

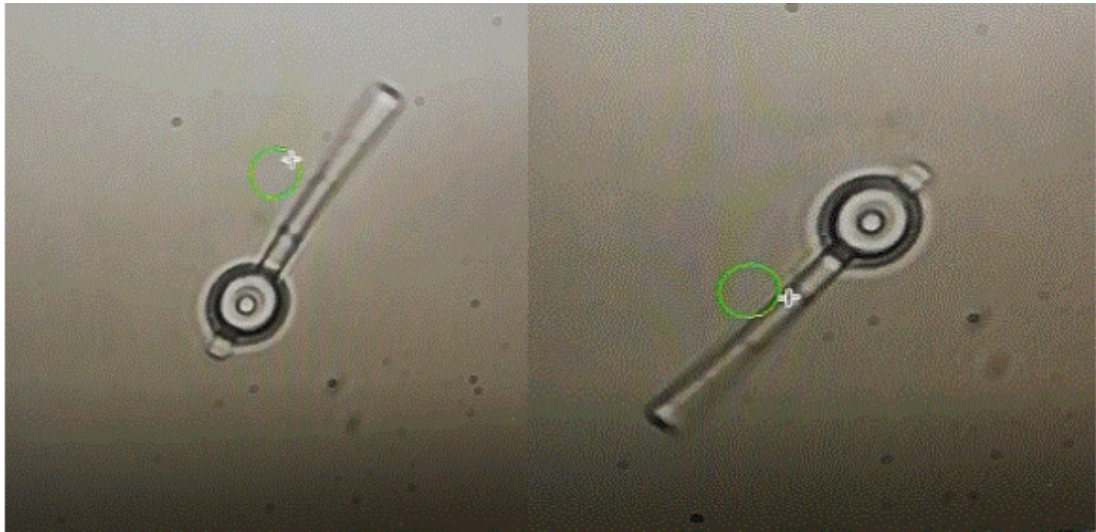


Figure 3.11: Stills from a screen recording of the first successfully optically manipulated lever. It seemed that the trap (shown in green) was pushing the lever around, rather than actually trapping the lever, potentially due to scattering effects from the flat surfaces of the lever.

3.4.3 SECOND ITERATION OF LEVER DESIGNS

Following the results of the first lever tests, it was decided that the lever arm should have equal length on either side of the pivot, to make rotating the levers with the microprobe easier and to move towards force transfer. While a goal of the project was to amplify forces, the unamplified transfer of force across the pivot was seen as a necessary way-point, rather than jumping straight to magnifying forces. Additionally, the question of reducing overlapping area and improving part separation came into play. Therefore, new levers were created with varying vertical and lateral separation between pin and lever arm, and with two different pins. One of the pins had an angled base, with the goal of reducing contact between the pin and lever arm while maintaining strong adhesion between the base and the substrate after printing. The levers were also printed with three trapping handles and a pocket at the end of the lever. The

idea was to attach functionalised micro-beads to the levers utilising this pocket, which would make the levers suitable for experiments requiring chemical interactions between the end of the lever and the subject. The lever arm and two base types can be seen in Fig. 3.12.

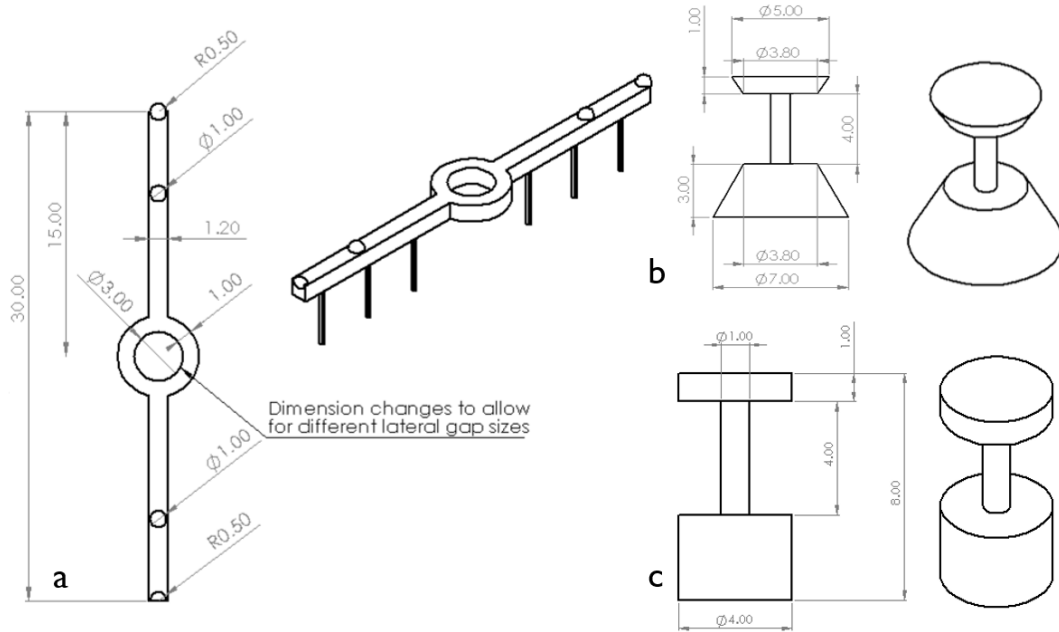


Figure 3.12: The second group of levers were designed to have lever arms with equal length on either side of the pivot. There were $30\ \mu\text{m}$ long from end-to-end, with dimensions shown in (a). The two types of pins used were the “A” (angled) pins, marked (b) in this figure and the “B” (flat) pins, marked (c) here.

The first trapping handles were $1\ \mu\text{m}$ in diameter. This meant that the entire sphere did not actually protrude from the levers, instead being hemispheres “on top” of the levers. Despite this deficiency, it seemed that they still worked as handles sufficiently well to allow more stable trapping. Speculatively, this may have been due to the spherical shape in the model affecting the polymerisation of the resist, and still forming a preferable path for the optical trap at these handle locations. The levers were divided into two main sub-types, according to whether they had an “angled” (Group A) or a “flat” (Group B) centre pin, and then further divided depending on the lateral and vertical gaps as shown in Table 3.3. Levers were printed with 20, 25 and 30% laser power, following a change in the slicing method from “fixed” to “adaptive” mode, described previously, with a specified range of 50 to 100 nm. The smaller distances between sliced layers due to this meant a slight increase in the laser dose received by the resin. This made 25% laser power the appropriate choice: 30% laser power produced burning and bubbling resin, while 20% meant that the levers were too soft

and sticky to turn. While this demonstration of the effect of slicing distance on laser dose and resin polymerisation was qualitatively interesting, it could not be used as a definitive answer to the optimum set power to use. This is due to the fact that the power of the PPGT2 drifts over time, and requires annual calibration, meaning that further dose testing would be needed throughout the course of the project. Indeed, advice from Nanoscribe is to conduct a dose test for each new print, which marks a problem for researchers wanting to produce identical repetitions of their designs.

Table 3.3: Variations of the second iteration of levers, and the code used to label them.

		Vertical Gap (μm)			
Lateral Gap (μm)		1.4	1.6	1.8	2.0
1.0		1i	2i	3i	4i
1.2		1ii	2ii	3ii	4ii
1.4		1iii	2iii	3iii	4iii

The levers were rotated in dry conditions and in milliQ water using the borosilicate microprobes, and then tested with the optical tweezers in milliQ water to assess their basic functionality. During the microprobe turn-tests and the optical tweezer rotation tests it was noticed that levers that turned in response to the drag produced by the microprobe's movement- rather than requiring direct contact to turn- were more likely to be successfully manipulated using the optical tweezers. As the microprobe was moved at a speed of $10 \mu\text{m/s}$ and we assume the droplet of liquid is a low-Reynold's number environment, the drag on the microprobe can be estimated to be $< 1 \text{ nN}$, within reasonable range of the hundreds of pN that strong optical tweezers can exert. In Fig. 3.13, the results from the Group A levers show that while the response to microprobe drag is a good indicator of lever performance, the optical tweezers are still noticeably less powerful. Additionally, it seemed that there was no clear trend in functionality with increase in gap. However, the sample size was extremely small, with only 10 levers in each group to begin with, and several removed accidentally over the course of the experiment- with the lowest number of levers in a subgroup being A1iii, which only had 5. Therefore, no real conclusions could be drawn from these tests. Nevertheless, when the results were compared with those of the Group B levers, shown in Fig. 3.14, far more of the Group A levers were able to turn. This seemed to indicate that the overlapping area between components should be the main consideration for optical microrobotics, as the overlap between centre pin and lever was smaller for Group A than it was for Group B, due to the centre pin design.

Following the functionality tests in milliQ water, attention turned to testing the capabilities of the levers in solutions with higher ionic strength. This is a challenge due

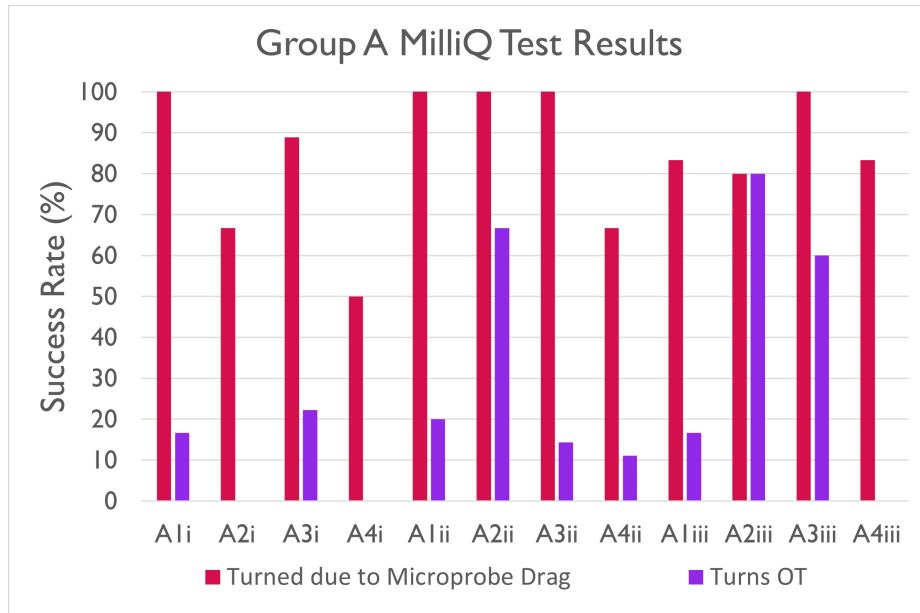


Figure 3.13: Test results from the Group A microlevers, for the milliQ water manual turn test (with the microprobe) and with the optical tweezers.

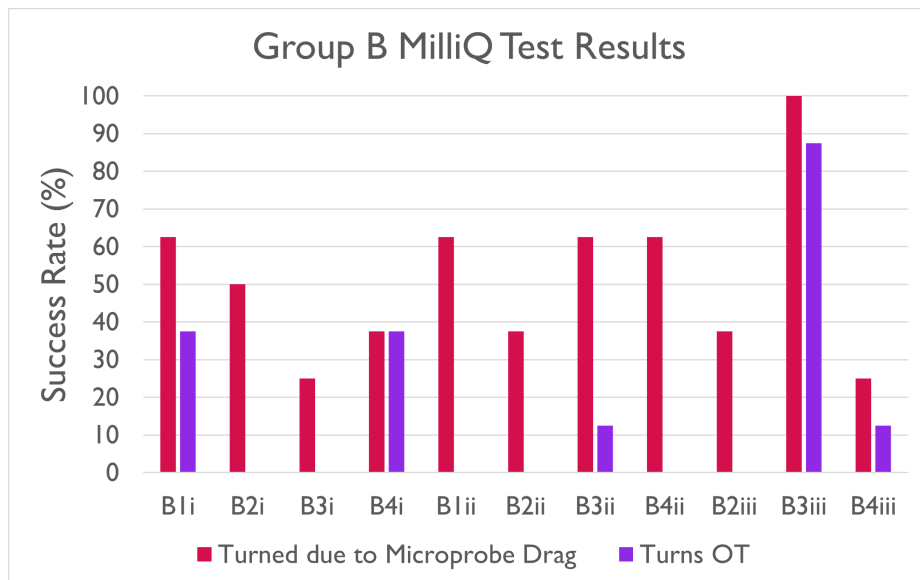


Figure 3.14: Test results from the Group B microlevers, for the milliQ water manual turn test (with the microprobe) and with the optical tweezers.

to the screening of repulsive electrostatic forces between objects of the same material when said objects are immersed in a salty solution. Screening of these forces allows the objects to come into closer contact, within the range over which van der Waals and other attractive forces start to dominate interactions. Of all the levers tested, only one was able to turn in tris-buffered saline (abbreviated as TBS or TSB: 50 mM Tris, 150 mM NaCl, 1 mM EDTA, pH 7.6, the solution in which previous single-molecule DNA stretching experiments had been conducted). This lever was from group B4iii, which had the largest lateral and vertical gaps. While this was once again, too little information to make strong design decisions, it indicated that microlevers for use in high ionic strength environments can be produced by careful selection of key design features. Additionally, attachment of a streptavidin coated polystyrene microbead ($r = 500$ nm) to the levers, was attempted. The microbead was guided into the pocket printed at the end of the lever, using the optical trap, but failed to properly adhere. Additionally, the lever appeared to produce some unwanted interference with the trap, meaning that the microbead escaped the trap on several attempts. It was expected that the microbead would have easily attached to the microlever, due to the high-salt environment provided by the TSB, but the failure to attach implied that further work would be needed to achieve the desired “in-pocket” attachment. An unsuccessful attempt can be seen in Fig. 3.15, where the streptavidin-coated bead appears attached when the optical trap holds it in place, only to disappear when the trap is switched off. Rod-shaped bacteria can also be seen in the micrographs, a consequence of using the same sample for multiple experiments in non-sterile liquid environments, at room temperature. Pipette tips were autoclaved and liquids were kept in refrigerated or frozen storage and filtered ($0.2 \mu\text{m}$ pore size) before the experiments in order to try to reduce bacterial colonisation of the samples, which helped to prolong their useful lifetimes.

3.4.4 FURTHER CHANGES TO LEVER DESIGNS

Following the failure to attach the streptavidin beads to the optical microlevers, the decision was made to increase the size of the pocket radius to $1 \mu\text{m}$, and to attempt to attach a larger bead, coated with anti-digoxigenin ($r = 1.06 \mu\text{m}$, again from the requirements for previously successfully carried out DNA stretching experiments). This change was made due to many reasons, one of them being the proportionally-greater effects of Brownian motion on the smaller, streptavidin-coated microbeads when compared with larger beads. It is thought that this led to a greater chance of the smaller microbeads moving away from the lever once the trap was switched off, rather than staying near the lever and becoming attached due to proximity increasing the likelihood of adhesion. Additionally, increasing the size of the “cut-out” on the end of the lever

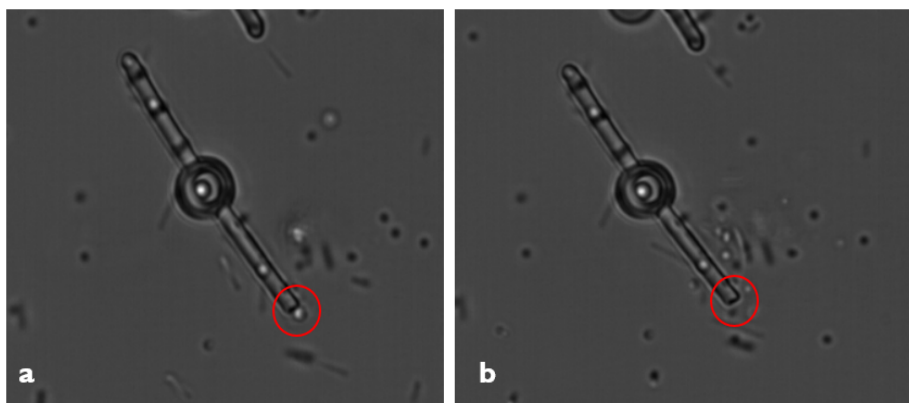


Figure 3.15: The first attempt at attaching a functionalised microbead to the especially printed pocket at the end of the lever. (a) The microbead appeared to be attached when the optical trap was holding it in place, seemingly against the lever. (b) However, when the trap was switched off the bead was shown to not be attached. Additionally, the micrographs shown here illustrate one of the problems with using the same sample for multiple experiments in liquid environments: namely the colonisation of the sample by bacteria.

would decrease the interference of the lever with the optical trap when the bead is being guided into place. This helped to spark the realisation that the spherical handles on the lever should also be enlarged, as similar interference with the flat underside of the lever was likely occurring, and disrupting the stability of the trap. Therefore, the size of the spherical trapping handles was increased to $2\ \mu\text{m}$ in diameter. Increasing the size of the pocket, and using a $2\ \mu\text{m}$ functionalised bead, enabled the attachment of the bead to the lever pocket. This was first achieved using the borosilicate microprobes, and was a laborious, picky process. However, it was achieved with optical tweezers at salt concentrations higher than $7.5\ \text{mM}$, when the bead was held to the pocket for up to 60s before switching off the trap.

3.4.4.1 KEY FEATURES OF MICROLEVERS

At this point, it is useful to emphasise the key features of the microlevers, and the purpose of these features as they relate to the original requirements for functional optical microlevers, which were given in 3.1. The key feature of the levers are shown in Fig. 3.16, along with a repetition of the three main requirements for the levers to be considered fit for the purpose of this project. While many different lever types and iterations were trialled throughout this project, and extra features such as supports were added, these same main features were always present.

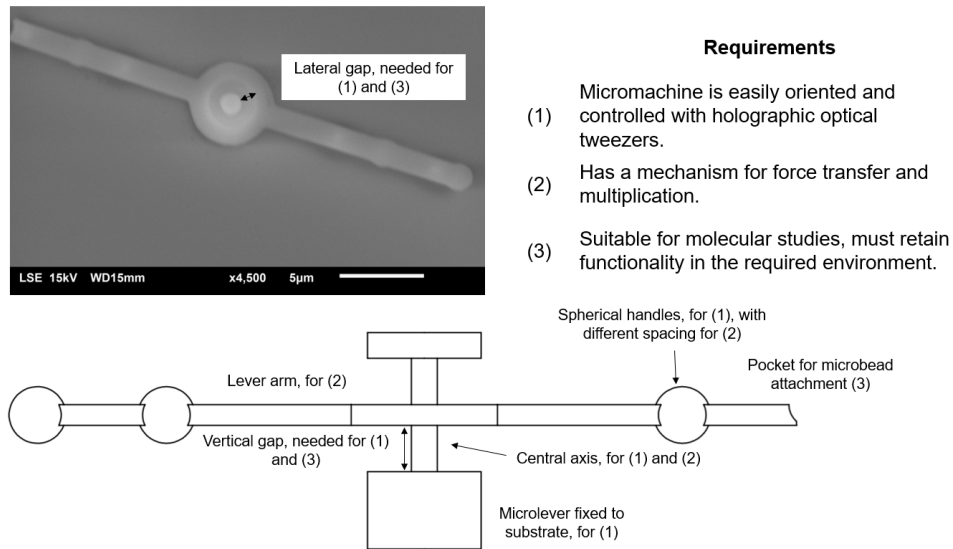


Figure 3.16: While changes were made to the levers to improve their functionality, the key features were chosen specifically for the goals of this project. In this diagram, the explanation for these key features is given. The SEM image in the inset shows an excellent view of the lateral gap between lever arm and axle, due to removal of the top of the pin.

3.4.4.2 SUPPORTED AND UNSUPPORTED MICROLEVERS

The first successful levers were all supported using narrow, cylindrical supports, around 300 nm in diameter. These proved difficult to break off, with levers most often being used with the supports still intact, and simply bent to the side. One such lever is shown in Fig. 3.17, where most of the supports are fully intact. Over time, as the levers settled downwards, these supports would become stuck to the substrate, reducing the functionality of the levers. However, the supports prevented the levers from settling onto the base of the centre pin, and so it was not certain whether unsupported or supported levers would work better. Additionally, the original printing tests had shown the difficulty of printing straight, unsupported levers. This led to an investigation into whether different support shapes and types, or even unsupported levers, would improve lever functionality.

Initial interest in supports was limited to ensuring that printing and development happened correctly, and removing the supports after printing was the original goal. Therefore, the first variations on the support shape were intended to reduce the connection between the supports and the lever arm proper. One strategy explored was the creation of a gap between the top of the supports and the lever arm. The idea was that this would allow the supports to be more easily removed, with the gap only filled by expansion of the resin, creating a weak bond between supports and lever arm. Another

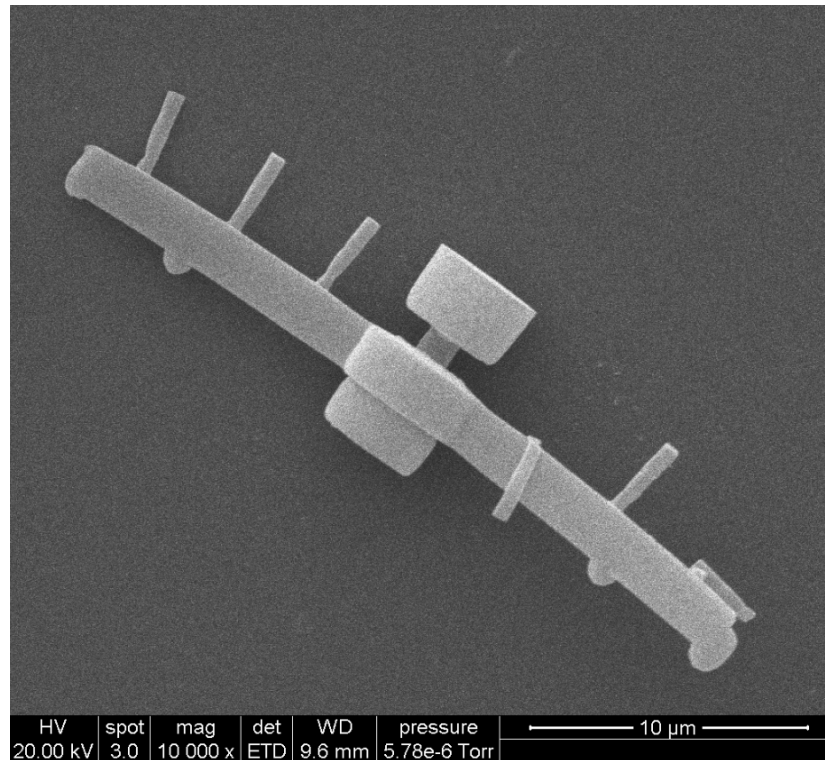


Figure 3.17: Attempts to remove supports using the borosilicate microprobe were largely unsuccessful, with the supports instead being detached from the substrate, and then bent out of the way.

strategy was to increase the base area of the supports, in order to increase the bond with the substrate, rather than with the lever arm. These strategies were unsuccessful. Several different gap sizes were trialled: 200 nm, 400 nm, 600 nm and 800 nm, and none of these produced supports which were easier to cleanly remove, although some apparent difference in shape at the top of the supports was visible, in the case of the 800 nm gap. Additionally, decreasing the support length to introduce gaps between the supports and the levers meant that when the resin filled the gap between them, it had the effect of “pulling” the lever into a curved shape rather than a straight lever arm. This effect can be seen in Figs 3.18 and 3.19.

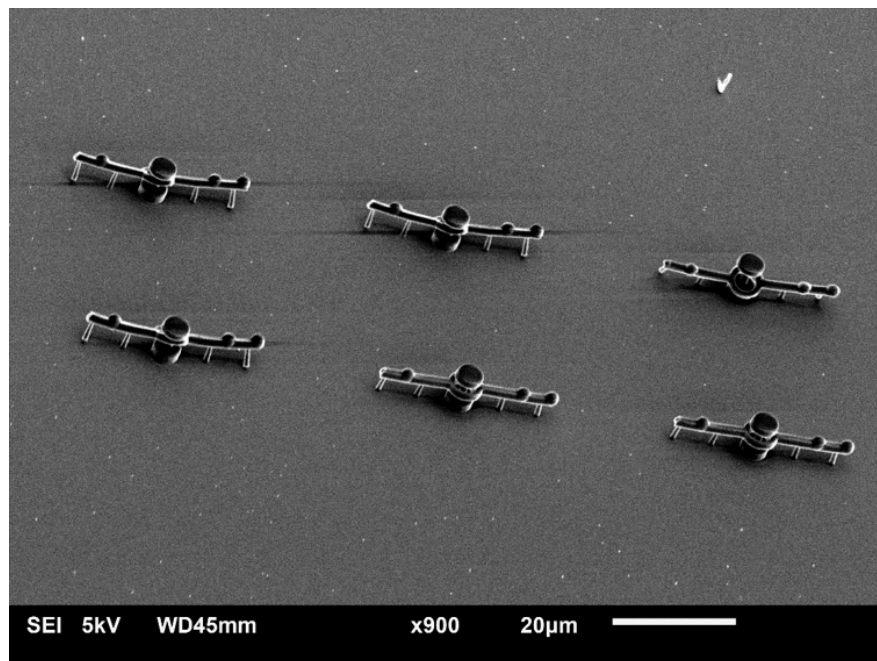


Figure 3.18: Attempting to print levers with gaps between the supports and the lever arm did not yield promising results, with some distortion of the lever visible.

As the supports could not be removed from the levers using the borosilicate probes, and the bases were relatively wide (500 nm in diameter) the levers that were printed with such supports settled and stuck to the substrate relatively quickly during experiments, typically settling within 10 minutes. Therefore, this design was abandoned and attention turned to printing levers with low-adhesion supports, and entirely unsupported levers.

3.4.4.3 IMPROVING MICROLEVER FUNCTIONALITY

The relationship between power and voxel size is generally agreed upon: higher laser power produces larger features. This relationship has been demonstrated in the literature in various ways, including the printing of grid-like [195] or complex mandala

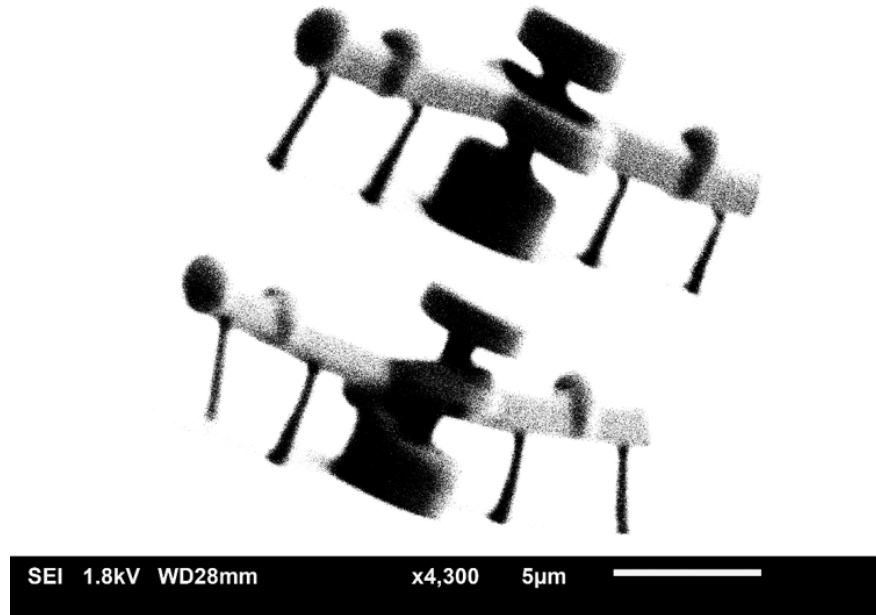


Figure 3.19: A designed gap of 800 nm was not sufficient to create more easily removed supports, but did have the effect of deforming the levers printed.

Table 3.4: Printing parameters used for levers in Fig. 3.20 and Fig. 3.21.

Slicing (nm)	Hatching (nm)	Hatch Angle (degree)	Hatch Offset (degree)	Speed (mm/s)	Contour	Resin
100	100	30	30	10	None	IP-L 780

structures [190]. Similarly, levers printed using the same .stl file and hatching and slicing parameters demonstrate different levels of functionality depending on the laser power used to print them. Specifically, levers with larger lateral gaps could be rotated with optical tweezers (in milliQ water) over a larger range of laser power, while levers with smaller gaps required lower laser powers, and were functional over a narrower range of laser power. As an example of this, Fig. 3.20 presents the results for three different lever designs, where the lateral gap size- and consequently the overlapping area between lever arm and centre pin- was varied between 1.0 and 1.4 μm . The printing parameters used for these microlevers can be seen in Table 3.4. A more dramatic representation of the same phenomenon can be seen in Fig. 3.21, which shows an SEM image of levers with 1.0 μm and 1.2 μm lateral gaps printed with 31 – 38% laser power.

The decision to use a 30° hatch angle and offset was made based on the observation that 90° and 0° angles produced interesting effects on the straightness of the lever arm. While a 90° angle and offset is recommended by Nanoscribe for symmetric and spherical

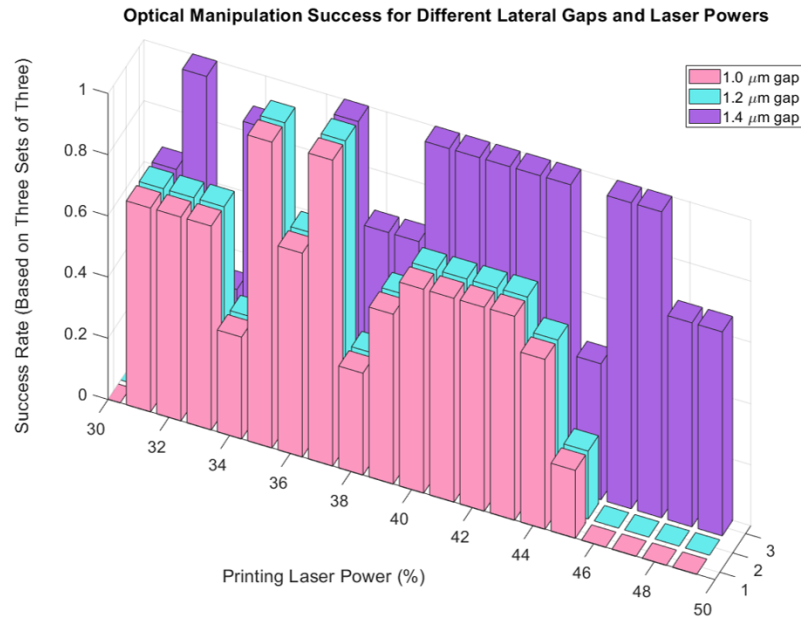


Figure 3.20: The relationship between laser dose and voxel size in TPAP means that different ranges of laser power produce the most effective results for different geometries. Here this manifests as a difference in range of power required to produce functional microlevers. The data shown on the graph are the combined averages taken from three samples with three levers printed at each laser power.

objects, the lever arms tended to warp when using these settings. It is possible that this was due to the combination of other parameters with this hatch angle and offset, rather than the angle settings themselves. Likewise, attempting 0° hatching angle and offset-somewhat predictably- also caused warping of the levers. This is potentially due to the fact that the oil immersion lithography method involves the laser repeatedly passing through already polymerised regions of resist, leading to unequal polymerisation of one side compared to the other. Additionally, the 0° angle seemed to produce notably worse spherical handles at the same laser powers. Images of lever warping can be seen in Fig. 3.22 and Fig. 3.23. These levers were printed using two contours, which somewhat helped to improve the apparent smoothness of the print.

With the relationship between laser dose and lever functionality noted, it was then worth exploring the parameters required to create levers with the best optical resolutions: specifically those with the best apparent smoothness and well-printed features. Examples of key features include the spherical handles, and the pockets where microbeads should be attached. SEM images taken of the samples printed with the fixed hatching and slicing distance used in Table 3.4 seemed to show that using the fixed slicing and hatching distance was not sufficient to produce smooth features. Additionally, this seemed insufficient to produce well-shaped spherical handles and pockets, as

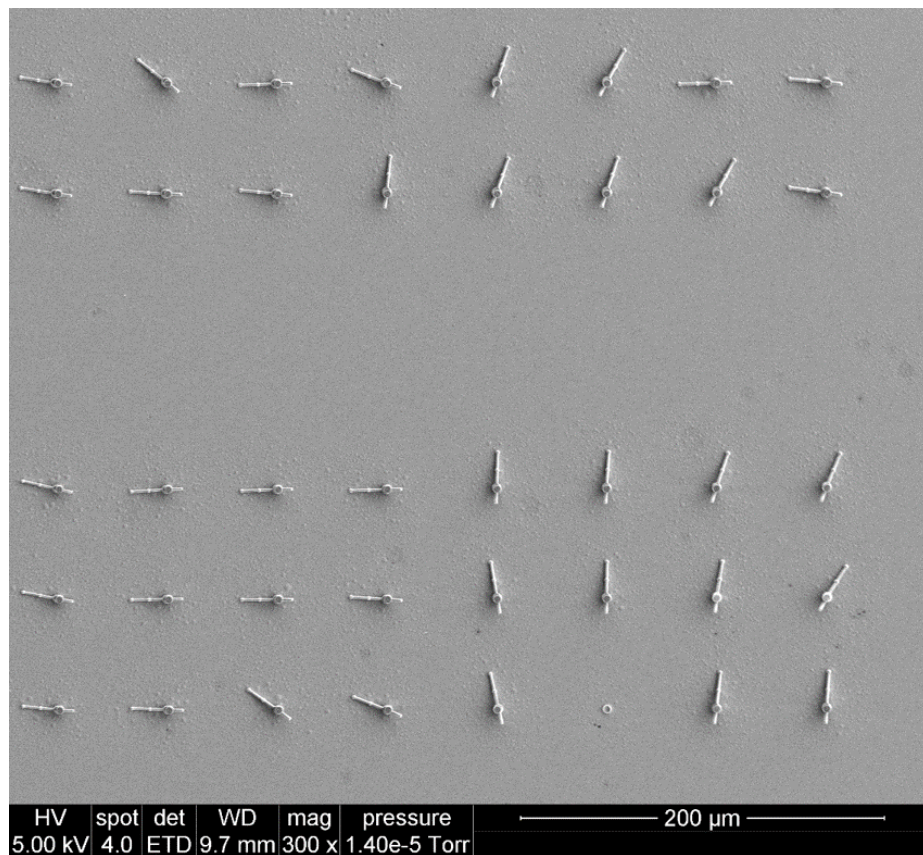


Figure 3.21: In this SEM image, the narrow window of laser power for optimum functionality can be seen, as some of the levers have rotated without requiring manipulation after printing. This can be seen as a difference in orientation, from the 0° printing direction to almost 90° . The upper group, which was printed with a $1.0 \mu\text{m}$ lateral gap, also appears to show a decrease in functionality at around 37% laser power, indicating that the separation between parts may be compromised by increased voxel size at this laser power.

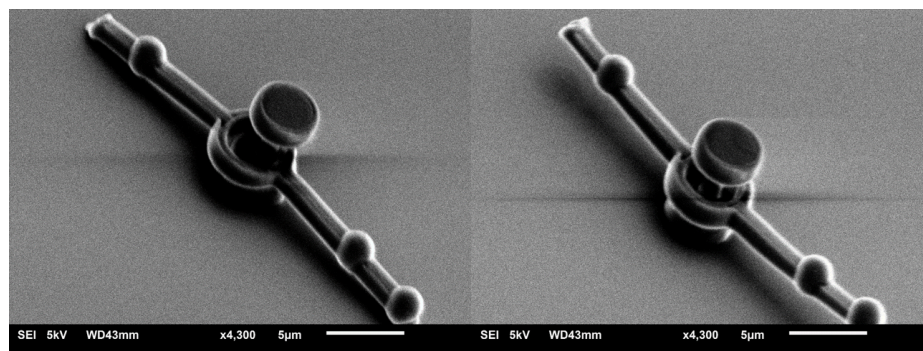


Figure 3.22: Lever sagging and hogging seen when using 90° hatch angle and offset.

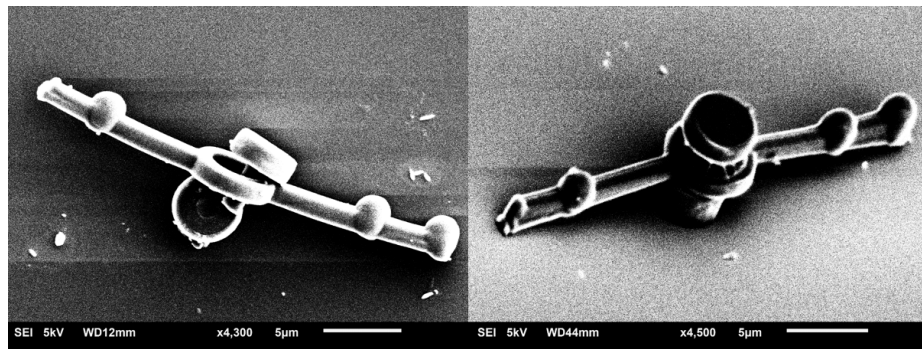


Figure 3.23: Lever deformity seen when using 0° hatch angle and offset. The poor sphere shape was of particular concern.

can be seen in the SEM images shown in Fig. 3.24 and 3.25.

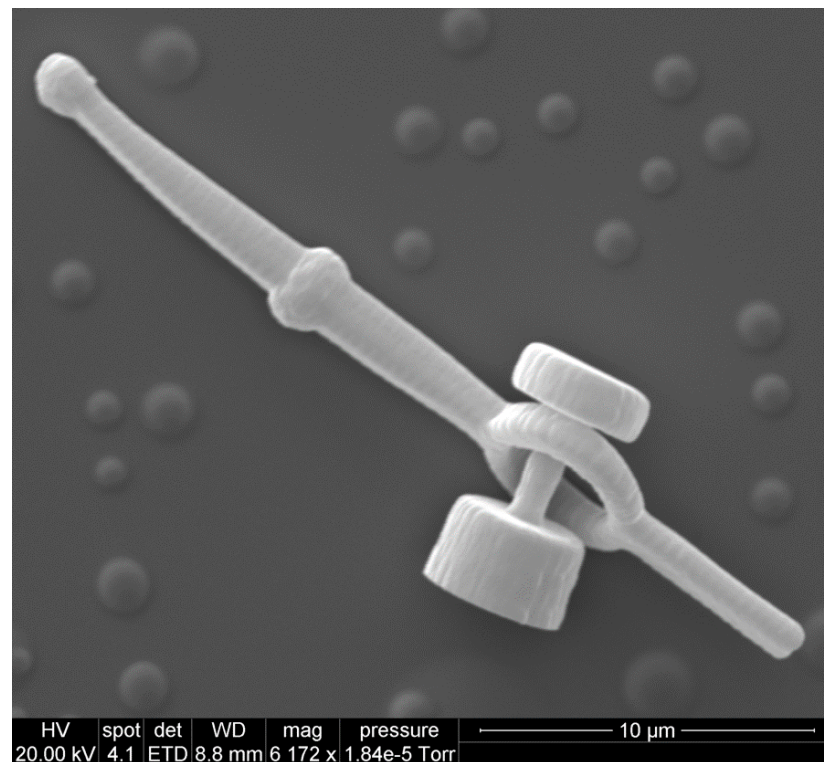


Figure 3.24: The printing parameters outlined in Table 3.4 seemed to be insufficient for producing levers with high quality surface finish, although the overall lever shape was good.

Introducing two contour layers to the print, as well as changing the slicing method from “fixed” to “adaptive” helped to improve the optical smoothness of the lever, and improved the appearance of the handles and pockets. An example of this improvement can be seen in Fig. 3.26. The adaptive slicing parameters can be seen in Table 3.4.4.3,

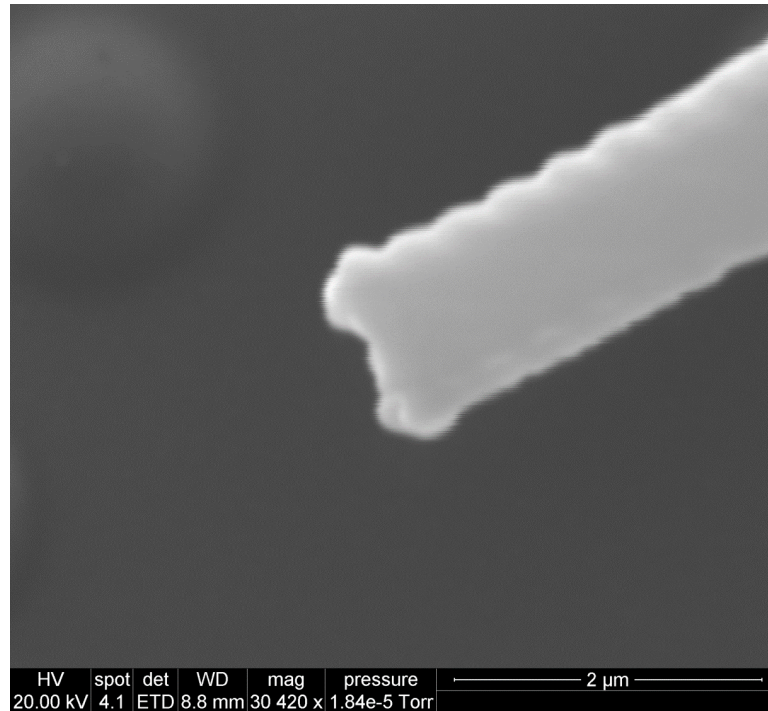


Figure 3.25: A high magnification image of a lever’s pocket seems to show the effect of the fixed hatching and slicing distance, as well as the lack of contour.

where the minimum slicing distance was set at an extremely small value to ensure voxel overlap, in order to improve sphere appearance. Changing the slicing method meant that another laser power dose test had to be performed, as the voxel overlap leads to higher exposure of the resin for the same laser power compared to the fixed slicing distance. In this case, the appropriate laser power was approximately 26–30%, compared with the 38–43% range that produced functional levers with a $1.4\ \mu\text{m}$ lateral gap in Fig. 3.20. This was in line with what was found when printing the second iteration of microlevers, discussed in the previous section.

Table 3.5: Adaptive slicing mode parameters used to produce smooth levers.

Minimum Slice (nm)	Maximum Slice (nm)	Slope Evaluation	Surface Normals
20	100	Maximum	Flat

A study on untethered microrobots, which were used to perform out-of-plane rotation in response to in-plane optical manipulation, used the exceptionally high resolution of TPAP to print microrobots with features that reduced the overlapping area between parts [140]. The study found that using thin ridges to reduce contact around a pin in

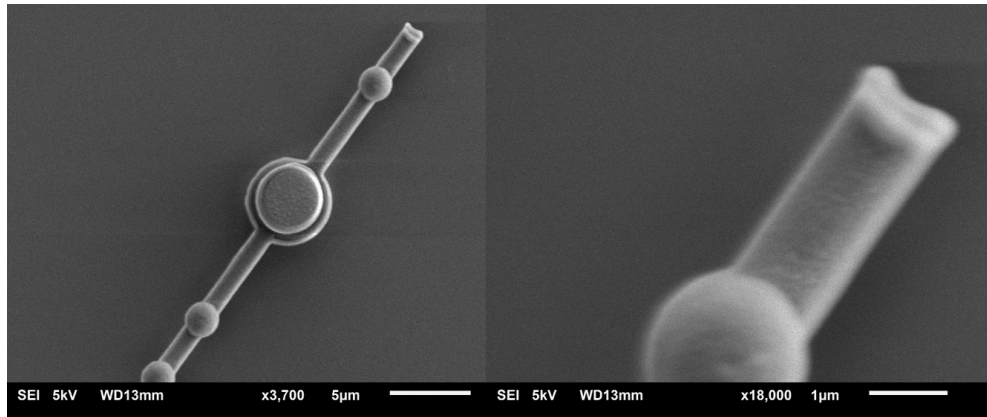


Figure 3.26: Changing the slicing mode from fixed to adaptive, and introducing two contours in the printing settings resulted in vastly improved lever smoothness and pocket quality, as shown in this image.

a rotational joint substantially increased the rates of successful optical manipulation of the objects. The apparent success of this approach made the addition of such features to the microlevers highly attractive, and so the repeatability of such features was investigated. As levers had been successfully printed at thicknesses of 800 nm and 1.2 μm , 200 nm was thought to be a suitable size for an area-reducing ridge.

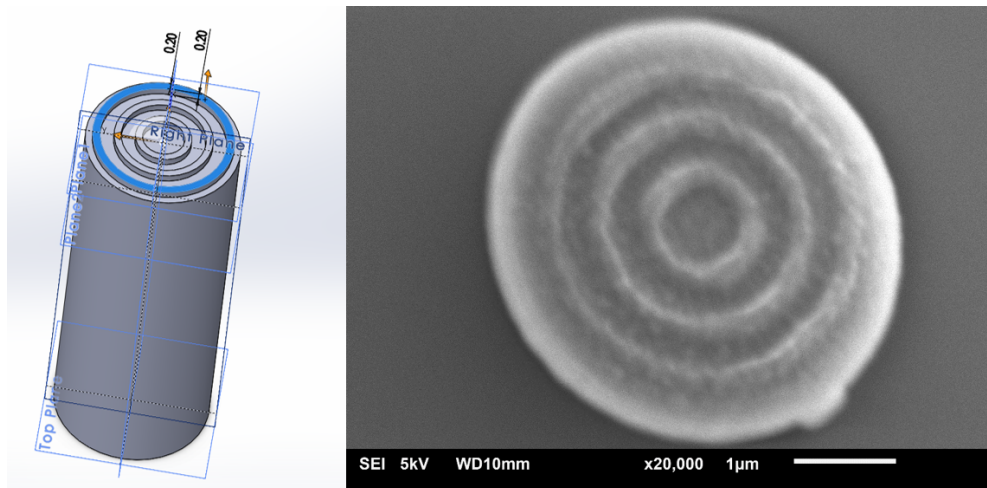


Figure 3.27: Ridges were printed on the tops of pillars in order to determine repeatability when printing thin ridges, as well as how this varied when the printing laser power was adjusted.

Pillars were printed with “crop circles” on top of them, in order to measure the resulting thickness of the ridges, which were designed to be 200 nm in width and height. The adaptive slicing parameters in Table 3.4.4.3 were used, along with 100 nm hatching, and 30° hatch angle and offset in order to approximate the situation where

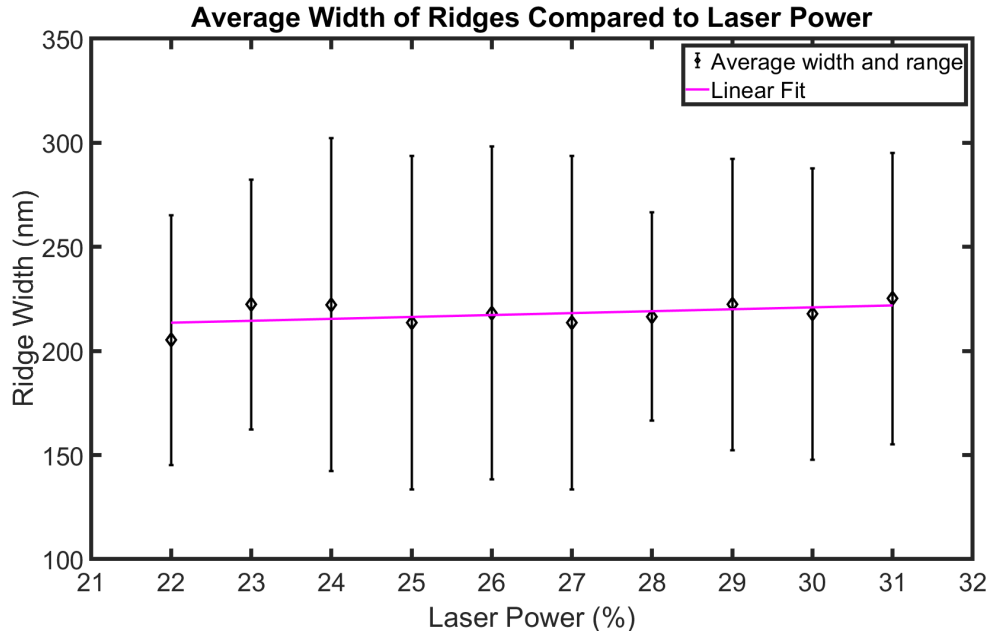


Figure 3.28: Evaluation of the thickness of the different ridges with respect to the laser power used to print them revealed that the average thickness varied only slightly, with high variability within the samples that used the same power. The average size of the features remained roughly consistent at just over 200 nm.

such ridges would be printed on microlevers. Laser power was varied between 22 and 30%, in increments of 1% to evaluate the effect of laser power on the ridges. Fig. 3.27 shows a screenshot of the SolidWorks model of the pillars, as well as an SEM of one such pillar printed with 23% laser power. SEM images of the ridges were analysed using ImageJ [196]; and the thickness of the three rings were averaged to produce a value for each laser power. Two pillars were printed for each laser power used in order to increase confidence in the measurements. The results can be seen in Fig. 3.28, where it is clear that there is a huge spread of values for each laser power used, and while there is a slight increase in average ridge size as the laser power increases, the overall trend is not severe. This seems to indicate that ridges with a thickness of approximately 200 nm are achievable with the laser powers that have also been used to print levers with well-shaped pockets and spherical handles.

3.5 DESIGN OF OPTICAL MICROMACHINES FOR USE IN BIOLOGICALLY RELEVANT ENVIRONMENTS

The following section discusses design changes made to ensure that the levers stayed functional in high ionic-strength (biologically relevant) solutions as these are required for DNA stretching, and also mentions the usefulness of salt in ensuring microbead attachment. The article was originally published in the proceedings of the 2020 IEEE/ASME International Conference on Advanced Intelligent Mechatronics (AIM), with coauthors Dr Daniel Fan (Nanoscribe training and assistance with lever printing), Matthew Lofroth (assistance with sample preparation), Dr Allan Raudsepp (assistance with experiment design), Prof.dr. Urs Staufer, Prof. Martin A. K. “Bill” Williams and Dr Ebubekir Avci (supervision and grant application), with Dr Avci also performing some sample preparation.

3.5.1 DECLARATION

The IEEE (Institute of Electrical and Electronics Engineers) does not require individuals working on a thesis to obtain a formal reuse license. However, the following copyright notice should be displayed: ©2020 IEEE. Reprinted, with permission, from Philippa-Kate Andrew, Daniel Fan, Allan Raudsepp, Matthew Lofroth, Urs Staufer, Martin A. K. Williams and Ebubekir Avci, “Design of Optical Micromachines for Use in Biologically Relevant Environments”, *2020 IEEE/ASME International Conference on Advanced Intelligent Mechatronics (AIM)*, July 2020. The following article has been reproduced from the accepted version of the paper.

3.5.2 INTRODUCTION

The pervasiveness of adhesion forces at the micro and nanoscale has presented a challenge to researchers interested in micromanipulation. In the area of optical micromanipulation, these adhesion forces hinder the actuation of multi-component optical microrobots, due to the low forces provided by optical tweezers (10^{-14} – 10^{-10} Newtons) [98]. Despite the restriction on force magnitude, the associated resolution of displacement and force makes optical manipulation an attractive option for life-science research [197, 169, 92, 198]. However, optical tweezers also present serious drawbacks, namely the potential for damaging biological objects under study [199, 200]. While the exact mechanisms for this damage are not agreed upon, studies have identified several possible pathways including localised heating [201, 202], photogenerated free radicals [107] and photobleaching [203]. Optical micromachines present an exciting opportunity

for reducing damage to biological subjects, as well as the potential for extending optical tweezers to new uses [5]. However, the propensity for surface forces to dominate has meant that researchers are faced with challenges when it comes to designing multi-component micromachines that work reliably. While optical tweezers have been used to perform micromanipulation in air [204], traditionally, optical micromanipulation is performed in a liquid medium. Trapping objects submerged in a liquid allows researchers to neglect inertial terms in analysis of an object's movement in a trap [205], and reduces electrostatic and capillary forces. The reduction of these forces theoretically reduces the adhesion forces between surfaces, which is vitally important for the successful actuation of multi-component micromanipulators. This is demonstrated in the literature in the cases of levers [56], micromanipulators that transform an in-plane translation to an out of plane rotation [140], and micro-gears [206]. In these studies, trapping took place in milliQ water- ultra pure water deionised until it has a resistivity of 18.2 M Ω cm- and a surfactant was added to lower adhesion forces between components, improving the chance of success. However, in order to use optical micromanipulators as tools for research in the life sciences, rather than as research curiosities, micromanipulators must be functional in cellular conditions. Hence, rather than milliQ water, the micromanipulators need to be tested in biologically relevant salt concentrations. This is important as the ionic strength of the surrounding medium has been demonstrated to affect the properties of biological samples; for instance the elasticity of DNA is affected by the amount of salt in the medium [207]. Salts screen repulsive electrostatic interactions between objects due to reduction of the Debye length [208], thus, adhesion between parts of multi-component micromanipulators becomes more of an issue as salt increases. This work aims to determine the geometry required for levers with equal-length arms to function in tris-buffered saline (TBS), which has a molarity of 150 mMol sodium chloride (NaCl), and contains 45 mMol of Tris and hydrochloric acid in order to maintain a slightly alkaline pH of 7.5. The use of salty buffers such as TBS, has two functions in biological studies, with one being to maintain an environment with biological ionic strength, and the other being to inhibit undesirable enzymatic functions, so that biological molecules and processes can be observed without undesirable changes taking place during the experiment. This selectivity has allowed researchers to directly observe enzyme behaviour in highly controlled conditions [209]. These kinds of interactions cannot be studied in milliQ water, and so optical micromachines that are functional in different mediums are required.

Previous works regarding the problem of adhesion for microrobotics have identified surface forces as problems for pick-and-place tasks [210, 211], as attractive forces between the micromachine and target object make precise placement and release difficult. However, in this study the focus is on the effects of attractive forces on the

functionality of multi-part micromachines. In the case of multi-part micromachines, non-contact attractive forces between parts are of particular concern, as the parts must be separate, and in the case of pin-jointed structures, must retain their axis of rotation. In this work, structural variations of a 1:1 first-class microlever were tested in a series of different TBS solutions, ranging in strength from 1% to 50% TBS. The performance of different designs was then evaluated with respect to overall success rate, and the way in which the levers moved. This study covers the theory associated with screened electrostatic interactions briefly, before detailing the design and manufacture of optical micromachines and discussing the results of trialling the levers in different concentrations of Tris-buffered saline solutions. As an extension, anti-digoxigenin coated microbeads were attached to the microlevers, to demonstrate their potential use as a tool for biological studies.

3.5.3 METHODS

3.5.3.1 THEORY

Traditional models for attractive force between micro-objects in liquids are based on DLVO theory [212], which was developed to describe the stability of aqueous dispersions. This theory describes the stability of systems as being determined by two groups of forces, the van der Waals and electrostatic forces, which govern the dispersion and aggregation of particles in the system. The total contribution to the forces that exist between particles can then be expressed as:

$$F_{DLVO} = F_{vdW} + F_{el} \quad (3.9)$$

Where F_{vdW} is the contribution provided by van der Waals interactions between the objects, and F_{el} is the contribution from electrostatic forces. As the attractive van der Waals forces are significant only at very small displacements, the repulsive electrostatic interactions generally dominate the interaction. However, as levers move the distance between parts may become small enough for van der Waals forces to temporarily overcome electrostatic repulsion and lead to contact and adhesion between parts. This effect is facilitated further by lower electrostatic repulsion when the Debye length shortens.

Electrostatic interactions between particles in an electrolyte solution are caused by the surface charging of the particles, due to adsorption of ions within the solution and resultant ionising reactions with the material of the particle [213]. Both parts of the micromachine are made from the same material, and immersed in the same fluid, and so it is assumed that the charge on the surfaces will be similar, and consequently repulsive. The expression for this interaction relies on the Debye length [208], as can be seen in 3.10, which gives the electrostatic force between two identical spheres, positioned a

distance x apart, where $x < 2R$. In this equation R is the diameter of the particles, Z is the surface charge, κ^{-1} is the Debye length, ϵ_0 is the permittivity of free space, ϵ_r is the relative permittivity and e_c is the elementary charge.

$$F(x) = (e_c^2 Z^2 / (8\pi\epsilon_0\epsilon_r R^3)) \kappa^{-1} e^{-\kappa x} \quad (3.10)$$

The Debye length, which is given by κ^{-1} , is in turn influenced by the concentration of salt in the solution, as shown in 3.11. In this empirical expression the Debye length is taken to be completely dependent on the concentration of cations, n_c , and anions, n_s in the bulk.

$$\kappa^{-1} = 0.304 / \sqrt[4]{n_s n_c} \quad (3.11)$$

Given that adding salt reduces the Debye length, consequently reducing the stabilising electrostatic repulsion, there is good theoretical basis to investigate the effect that geometry has on the functionality of multi-component micromachines in high-salt environments. While this equation is for the case of two spheres, it provides a clear illustration of how electrostatic forces in aqueous solutions are affected by the addition of salt, as well as an indication of the dependence of the force on object separation.

Seven different concentrations of TBS were used in this study, and it was approached from a simplistic perspective where the shortening of the Debye length would lead to a higher chance of component adhesion. Therefore, the dependence of successful lever turning on salt concentration should produce a results graph with a similar shape to the one illustrating the change in Debye length with increasing TBS concentration (Fig. 3.29).

3.5.3.2 DESIGN AND MANUFACTURE

This work was done as part of a project geared towards developing micromachines for use in biological experiments using optical tweezers. Therefore, levers were designed with this objective in mind. This led to the concept of a 1:1 first class lever, which can be used to transfer force over its fixed central axis to the target. Levers have been successfully utilised in the literature for force-multiplication [56, 57], which implies that the force applied on one side of the equal-armed lever can be transferred over the joint to be applied elsewhere. The levers all featured three spherical trapping handles and a pocket on one end (Fig. 3.30). This pocket is intended for the optional attachment of a functionalised microbead which can then be used to probe biological subjects, or for direct attachment to a target object such as a red blood cell. The spheres located part-way along the lever arms allow for the use of two balanced optical traps to rotate the levers, rather than just using one trap on the end of the lever, although this is

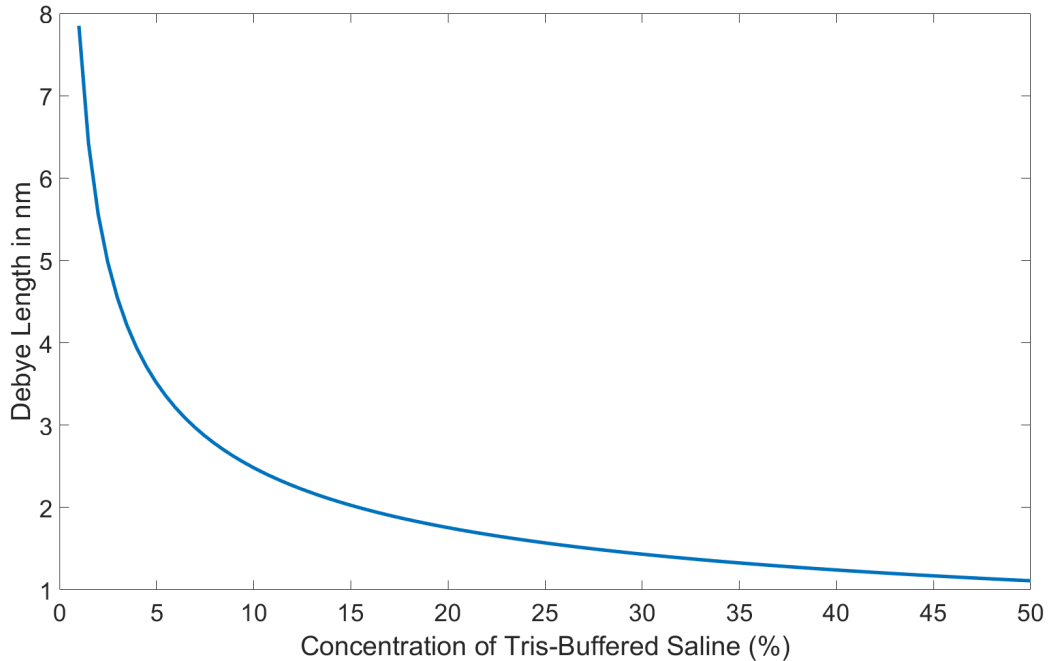


Figure 3.29: The dependence of the Debye length on the concentration of TBS, according to (3).

also an option for equal force transfer. From this basic first design several different iterations were produced, with this study focusing on variations of this design featuring three different kinds of support structures, varying overlapping surface area and slight changes in part separation. Five variations of the design were trialled in this work, with 20 levers in each batch, and the features of these designs are detailed in Fig. 3.31 and Table 3.6, where the features of the different designs can be compared. The lateral separation between the pin and the lever arm was kept at $1.6 \mu\text{m}$ for all designs in order to minimise contact area with the pin. Additionally, initial trials of lever functionality in milliQ water showed that this dimension allowed for centred rotation around the pin, while smaller separation distances led to increased likelihood of stiction.

Levers were manufactured using the Nanoscribe GmbH Photonic Professional, a laser-based 3D printer capable of producing objects with 50 nm resolution using the technique of two-photon absorption polymerisation (TPAP) [214]. The photoresist used was Nanoscribe's proprietary IP-L 780 resist. Levers were designed using SolidWorks and printed from .stl files, similar to conventional macro-scale 3D printing. The choice of laser power for printing was made following several trials, and it was found that 13 mW consistently produced levers with the resolution required, with minimal instances of printing errors caused by resin bubbling. An SEM image of one of the levers can be seen in Fig. 3.32.

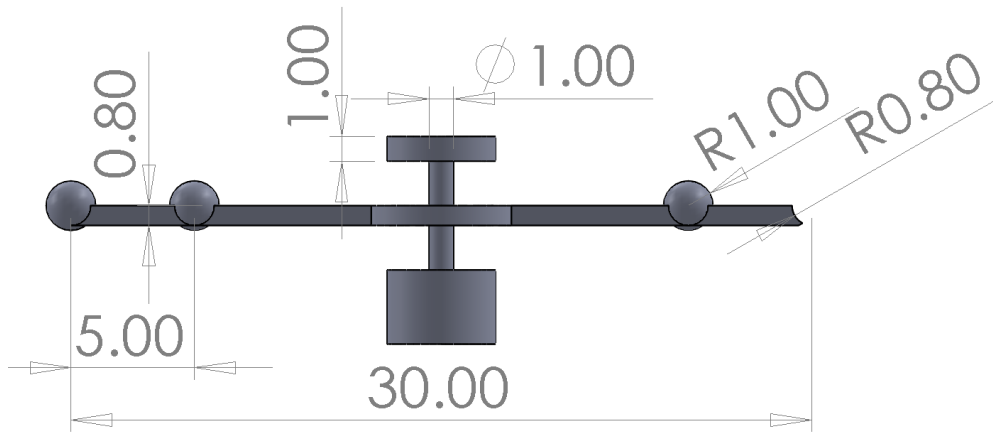


Figure 3.30: The basic design was a first-class lever, with equal length arms. Three spherical features are positioned as trapping handles, and a pocket is positioned at the end of the lever. All measurements are in micrometres.

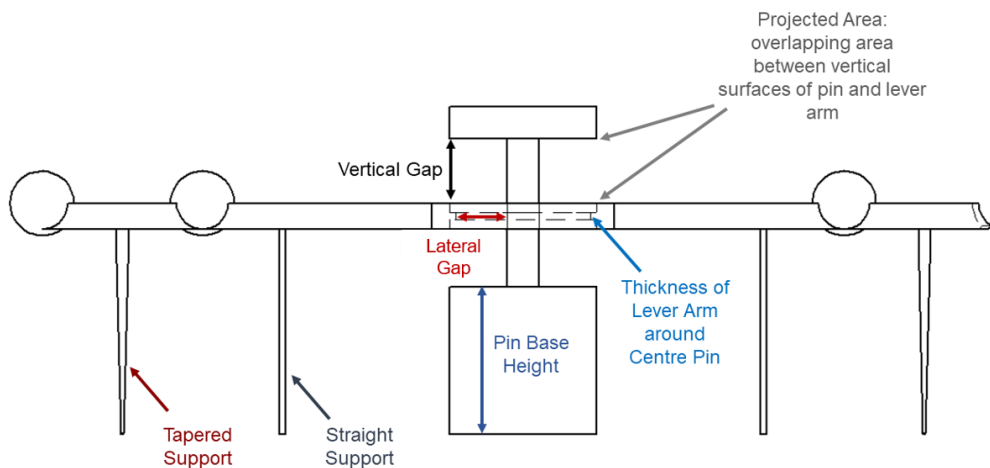


Figure 3.31: Five variations of the basic 1:1 lever were used in this study. Two of these designs featured no supporting structures, while the other three were supported using either straight or tapered supports. Additionally, centre-pin height, vertical gap size and lever arm thickness varied between designs.

Table 3.6: Features of levers used in this study.

Sample	Support Style	Overlapping Area (Vertical Projection) (μm^2)	Lever Arm Thickness (Around Centre Pin) (nm)	Lateral Gap (μm)	Vertical Gap (μm)	Pin Base Height (μm)
Straight Supports	Straight	1.35	800	1.6	2.0	3.0
Cone Supports, Low Contact	Tapered	1.35	200	1.6	1.8	3.0
Cone Supports, Low Contact 2	Tapered	1.41	200	1.6	2.1	4.8
No Supports	None	1.35	800	1.6	1.8	3.0
No Supports, High Pin	None	1.35	800	1.6	2.0	4.6

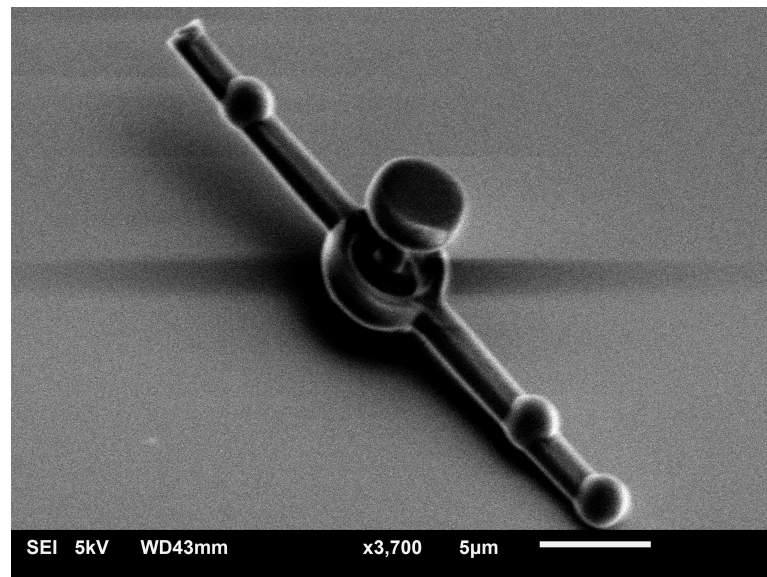


Figure 3.32: The “No Supports” type lever under SEM.

3.5.3.3 EXPERIMENTAL

Levers were kept on the original substrate that they were printed on, and a borosilicate microprobe with a tip-radius of approximately $1\ \mu\text{m}$ was used to detach support material in dry condition, and turn the levers to ensure functionality. Following this initial step, the levers were turned 360° in milliQ water, which took place to ensure all levers were in a freely moving state. Levers were kept attached to the substrate by the bases of the centre pins in order to provide a stable rotation point. A lever was considered ready for optical trapping when it rotated in response to the drag force of the microprobe, as this is approximately the same magnitude as the force supplied by optical tweezers, in the high tens of pico-Newtons.

Following preparation using the microprobe, samples were taken to the optical trapping apparatus. Holographic optical tweezers were used for this work, and the setup consisted of a Nikon Eclipse TE2000 inverted microscope, Arryx Holographic Optical Tweezers and Basler Ace ac2040-uc CMOS and Andor Neo sCMOS cameras for imaging, all isolated from vibration. The HOT was comprised of a 2W 1064 nm infrared laser and a Boulder Nonlinear Systems phase-only spatial light modulator (SLM); with a 1.2 numerical aperture, 60x magnification Nikon plan APO water-immersion lens used to focus the beam. A 1.5x secondary objective was used to further increase the image magnification to 90x. The Arryx Labryx software was used to control power to the laser, while the Red Tweezers software developed by Bowman et al. was used to position optical traps [174]. A diagram of the setup is shown in Fig. 3.33.

Trapping was performed at maximum power, and the trap was positioned as shown in Fig. 3.34a for a stable trap. The trap was then moved in order to rotate the lever a full 360° , which was regarded as a success. If the lever did not make the full 360° turn with one trap, or if the lever was pulled out of focus, then two traps would be used, as shown in Fig. 3.34b. The first experiment with each set of levers was trapping performed in high purity milliQ water. Trapping was performed with the laser passing through the substrate that the levers were printed on, and the samples were not sealed, due to the need to change the trapping liquid, and to manipulate the levers with the borosilicate microprobe. This meant that evaporation of the medium was an issue, but liquid was added to the substrate as required during the experiment, with $80\ \mu\text{l}$ added at the start of the microprobe step, and a further $40\ \mu\text{l}$ added before optical trapping. While open-substrate trapping is not common, it is useful in circumstances when contact manipulation of micro-objects is required in between optical trapping [215]. After trapping was conducted in milliQ water, the liquid was wicked away using a Kim Wipe. This was performed with the aid of the Olympus IX71 inverted microscope, at a magnification of 16x, in order to ensure that the levers were not accidentally removed in the process and that the liquid was properly removed. Optical trapping

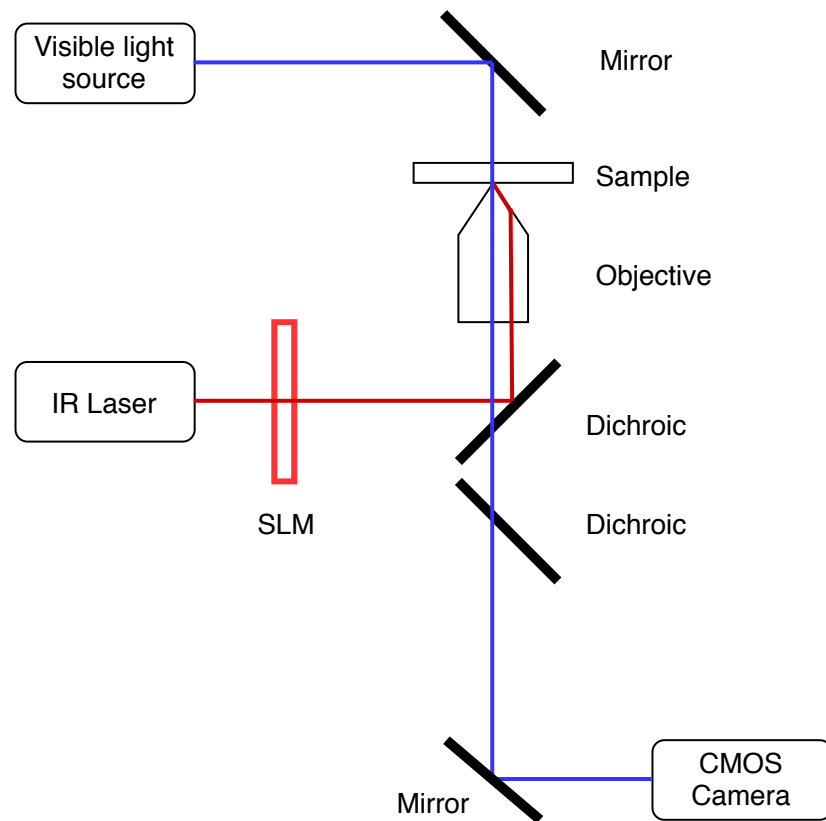


Figure 3.33: The optical trapping set-up used for the work. This diagram was previously published in [5].

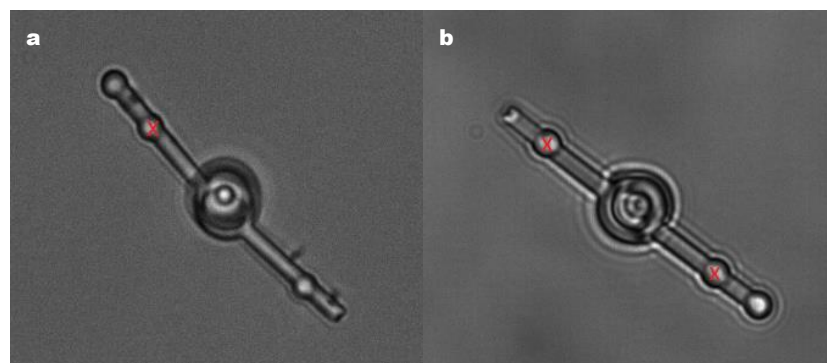


Figure 3.34: Trapping was performed using a holographic optical trap, placed on one of the “inner” trapping handles, as shown here with the red “x” in (a). If a full turn was not possible in this configuration, or if the lever moved out of focus due to the unbalanced force, then two traps were used, as shown in (b).

Table 3.7: Tris-Buffered Saline Concentrations Used for Trapping

Experiment Run	TBS Concentration (%)
Run 1	0 (milliQ water)
Run 2	1
Run 3	2
Run 4	5
Run 5	10
Run 6	20
Run 7	50

was carried out in six different concentrations of TBS, as well as in milliQ water, which provided the baseline results for each group of levers. The order of experiments is shown in Table 3.7. The decision was made to only use concentrations of up to 50% TBS due to the likelihood of excess salt being present on the substrate due to the method of adding and removing the solution throughout the experiment. This means that the actual concentration of TBS that remained on the sample could be close to double the expected amount. However, the lowest amounts that could possibly be present have been quoted here; i.e. the concentration of TBS added to the sample in each experiment.

The Andor Neo sCMOS camera was used to video the trapping experiments, collecting video at a frame rate of 100fps. These videos were then analysed using ImageJ [196] for information about how the levers responded to the traps.

3.5.4 RESULTS AND DISCUSSION

The first subject of interest for this work was the success rate of lever operation. This was defined as the percentage of levers out of a batch that turned at every concentration of TBS used. Levers were then defined as either successfully rotating; exhibiting a limited response to the optical trap; or having no response to the trap. These results can be seen in Fig. 3.35. Only one group of levers demonstrated successful 360° turning in each medium. This group was the Conical Support, Low Contact (CSLC) sample, where levers had a 1.6 μm separation between the inside of the lever arm and the centre pin, a 1.8 μm separation between the lever arm and the base of the centre pin and tapered supports which served to decrease the surface area in contact with the substrate, while also maintaining the vertical separation between lever arm and pin and reducing out of plane motion. The next-best performing designs were the unsupported ones: labelled No Support (NS) and No Support, High Pin (NSHP). There was little difference between these two designs, indicating that the effect of increasing vertical

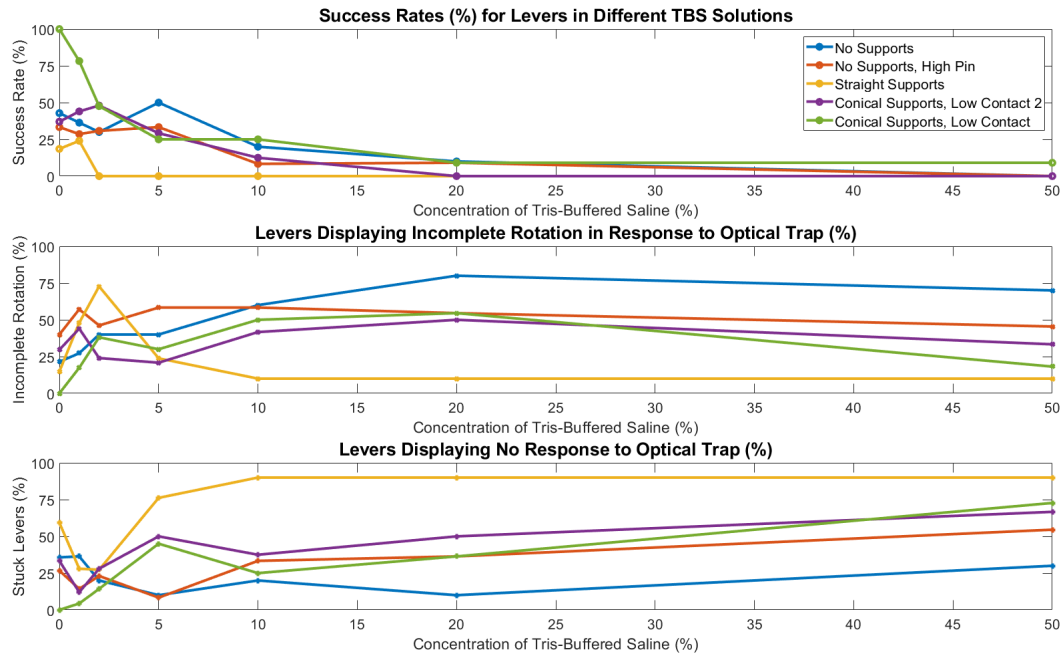


Figure 3.35: Lever performance was simply grouped into three categories: successful, multiple 360° turns (top); response to the optical trap but no full turns, where out-of-plane movement and limited rotation are counted (middle); and stuck levers (bottom).

separation between lever arm and pin and between the lever and the substrate had minimal impact. The worst performing group of levers was the Straight Supports (SS) sample. This was unsurprising as this group featured both the thickest lever arm; with respect to projected thickness onto the centre pin; and supports with more surface area in contact with the substrate when compared to the tapered kind.

Initially, it had been expected that the performance of Conical Supports, Low Contact 2 (CSLC2) would be very similar, or potentially better than CSLC. However, while the thin ridges added to the centre pin increased the gap between the thin ridge on the lever arm and the centre pin, these ridges also led to the likelihood of the lever arm “cupping” the centre pin when they moved off-centre, or if the levers settled downwards. Freely-moving, and hence trappable, levers move off-centre due to thermal fluctuations, and so this became a major source of poor performance for this lever group. The relevant dimensions can be seen in Fig. 3.36. Theoretically, the presence of the supports should have stopped this “cupping” from happening, but the sample-preparation using the microprobe can be damaging, leading to bending and deformation of supports. The thinness of the supports also means that they bend in response to even very low forces, as can be seen in the two video stills in Fig. 3.37, where the supports flex against the turning of the lever. Additionally, the slightly larger projected vertical area would also have contributed to increased attractive force between the two components. While



Figure 3.36: The ridges added to the centre-pin served to keep overlapping area small, and increase vertical separation. However, the size of the outer cut-out on the lever arm was the same diameter as the outside of the pin, meaning that “cupping” of the centre pin during settling would actually increase the contact area between parts.

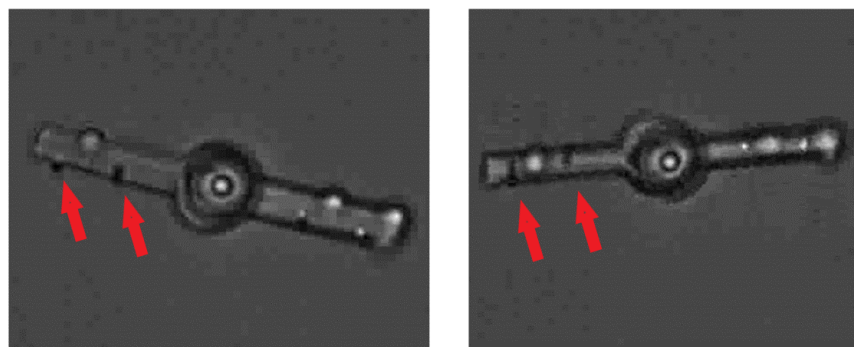


Figure 3.37: In this case it is possible to see the support structures flexing against the lever turning. Due to the strength of adhesion between the substrate and the supports, a full turn was impossible, but the supports were flexible enough to allow slight twisting and rotation around the axis. The red arrows point to two of the supports, showing a slight change in position and angle.

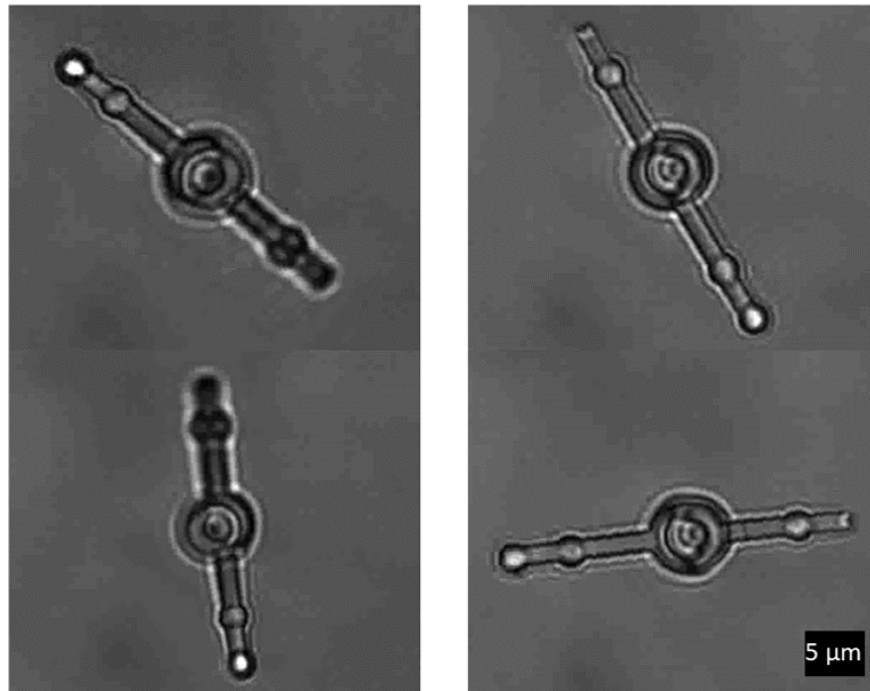


Figure 3.38: Unsupported levers required two traps to ensure planar rotation. In these stills from the trapping videos for NS levers in milliQ water the difference between trapping using a single trap (left) and symmetric rotating traps (right) can be clearly seen.

the levers without supports performed relatively well, out-of-plane rotation increased severely compared to the supported levers when using a single trap. Therefore, using two traps and rotating them around the axis became the method of choice. The difference in out-of-plane motion when using one trap versus using two can be seen in the set of stills shown in Fig. 3.38. While all lever groups largely complied with the predicted effects of increased TBS concentration, the results from the CSLC group matched the shape of the Debye curve very closely. This could be due to the fact that the supports and geometry of the lever arm enabled relatively consistent projected area and separation throughout the experiment, whereas levers with higher contact area ceased to move at much lower concentrations (SS, CSLC2) and the supportless levers demonstrated more out-of-plane motion, and so less consistent part separation. This demonstrates the inherent difficulty in predicting behaviour of optical micromachines, which has motivated studies by other researchers, including one regarding pose estimation from video, due to the difficulty calculating this from conventional forward dynamics [216]. The lack of predictability could be put down to small changes in surface roughness and individual differences between levers in a batch. The relatively small sample size of 20 levers in each sample also means that these results are statistically limited, and it is possible that larger sample sizes and more gradually varying

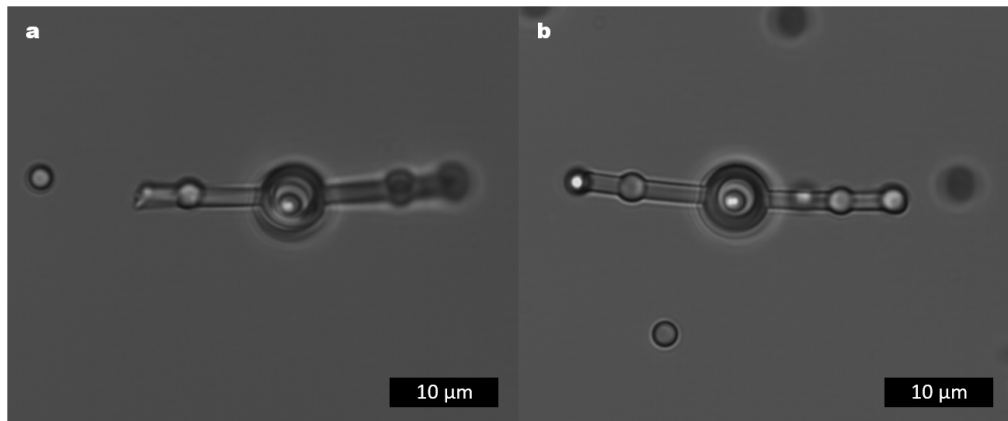


Figure 3.39: Microbeads could be successfully attached to functional levers at 5% TBS. Before attachment (a) and after (b).

concentrations of TBS would result in graphs that better followed the expected shape. Additionally, while the TBS solutions were kept chilled before use, and experiments with each sample took place over the course of a single day, colonisation of samples by bacteria, and build up of dust was an issue that could have introduced differences in sample environment. Future experiments could take place in a sealed chamber. However, different samples would need to be used due to the inability to change the fluid or prepare samples using the microprobe, which would introduce further variation in samples.

Grouping all non-360° responses to optical trapping as “limited response” means that a true comparison of lever performance is difficult to gauge. Therefore, the non-360° responses for each sample were compared, as well as the mechanisms which caused sticking. From Fig. 3.35, it is clear that the supported styles have more instances of “no rotation” responses to the optical traps. This is due to the fact that the reason for loss of functionality for these levers tended to be the support structures sticking to the substrate. This was in direct contrast with the unsupported levers, which tended to start to stick around the axle, and tended to more gradually lose the ability to turn, which is potentially due to progressively stronger attraction to the axle as the Debye length decreases.

A separate experiment was performed with a batch of ten levers of the NS style. This involved slowly adding TBS to the sample to increase the concentration of the solution used as the trapping medium, while using the optical tweezers to guide 2.12 μm diameter anti-digoxigenin coated microbeads into the pockets at the ends of the levers. Ten attempts were made at each concentration, with no successful adhesion of the bead with the lever observed until the concentration reached 5% TBS, when all ten attempts were successful. This is significant as the Debye length is predicted to have

dramatically shortened at 5% TBS compared to lower concentrations, and this is also where four out of five samples showed a sizeable decrease in success rate. A before-and-after of the attachment process can be seen in Fig. 3.39. The use of these beads in DNA-stretching protocols makes the ability to securely attach them to the levers an important step forward in demonstrating the potential for optical machine-assisted biological studies.

3.5.5 CONCLUSIONS

The experiments performed demonstrate that geometry of optical micromachines is vitally important for functionality when the ionic strength of the trapping medium is increased from minimal levels. The data gained from the comparison of these levers show that small, nanoscale differences in design make a large difference in functionality, and that taking a considered approach to this may save many research hours of trial and error. The introduction of support structures as a method for reducing out-of-plane motion is one that has not been seen elsewhere in the literature, and the results from this study demonstrate that this is not only viable, but that this design outperforms more conventional unsupported designs, when other design features are also carefully considered. Additionally, the successful attachment of microbeads at 5% TBS corroborates the other findings regarding the effects of increased molarity on Debye length. The results from this work, which are congruent with a very basic model of electrostatic attraction between surfaces, will serve as a baseline for further work in modelling micromachine behaviour in different environments.

Chapter 4

DNA STRETCHING

4.1 DNA AS A MECHANICAL OBJECT

DNA is an important bio-polymer that consists of thousands of repeating units- or nucleotides- comprised of nucleobases, deoxyribose and phosphates. The nucleobases pair- adenine to thymine, and guanine to cytosine- to form the characteristic double-helix structure. As DNA can be readily synthesised into identical strands it makes an ideal candidate for a molecular force metrology standard, [32]. As a polymer, the mechanical behaviour of DNA can be approximated by making use of models that break it down into a series of segments, with these segments being the maximum length that can be treated as a single unit. The two models described in this section do this in slightly different ways, with the freely-jointed (or ideal) chain model being the basis for the more specific worm-like chain model.

4.1.1 THE FREELY-JOINTED CHAIN

The simplest model for modelling a polymer such as DNA is the freely-jointed chain model (FJC), which approximates polymer structure as a series of rigid links- called Kuhn segments [217]. These links are entirely free to rotate, and the rotations are completely uncorrelated between segments. This freedom of movement means that interactions between linked segments are completely disregarded, and that two or more segments could theoretically occupy the exact same space. A very simple diagram showing this concept is seen in Fig. 4.1

At equilibrium, and with no force applied to the molecule, the entropy is high and the configurations the molecule can take are many. The variance of the end-to-end vector, given by (4.2), helps us understand this, showing a high number of possible configurations considering the “actual” length of the polymer is given by (4.1), where N is the number of Kuhn segments and b is the Kuhn length.

Freely Jointed Chain

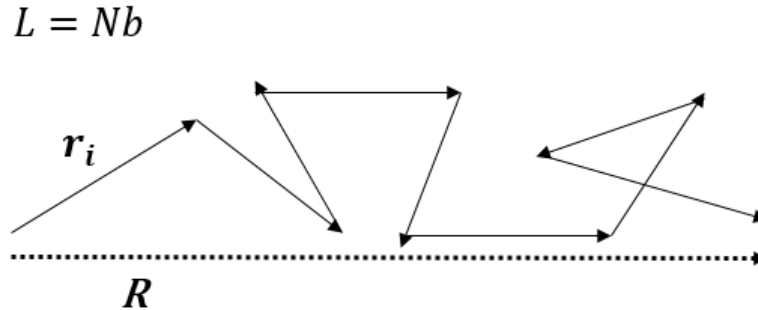


Figure 4.1: The FJC breaks a polymer of length L into N equal-length segments of length b . The end-to-end vector for the entire polymer is R and the vector for each segment is represented by r_i , where $i = 1, 2, \dots, N$.

$$L = Nb \quad (4.1)$$

$$\langle R^2 \rangle = Nb^2 \quad (4.2)$$

If the ends of the chain are pinned at set points that are close together compared to the actual length of the chain, then it can inhabit many possible states, as shown in Fig. 4.2. The mean force exerted by the chain pulling along its length between these set points is given by (4.3), where T is the absolute temperature and k_B is the Boltzmann constant. In the situation described by this equation, entropic fluctuations are enough for the configuration of the molecule to change.

$$\langle f \rangle = -k_B T \frac{3R}{Nb^2} \quad (4.3)$$

As the extension of the molecule increases- i.e. as the end-to-end displacement approaches the length of the polymer- the number of available states decreases. Essentially, forces applied serve to straighten the molecule out until it fits its conformation length, and as the separation distance between the ends approaches the overall length of the polymer chain, certain configurations become less probable. The relationship between end-to-end distance and force is given by (4.4) [96].

$$R = L \left(\coth \frac{Fb}{k_B T} - \frac{k_B T}{F} \right) \quad (4.4)$$

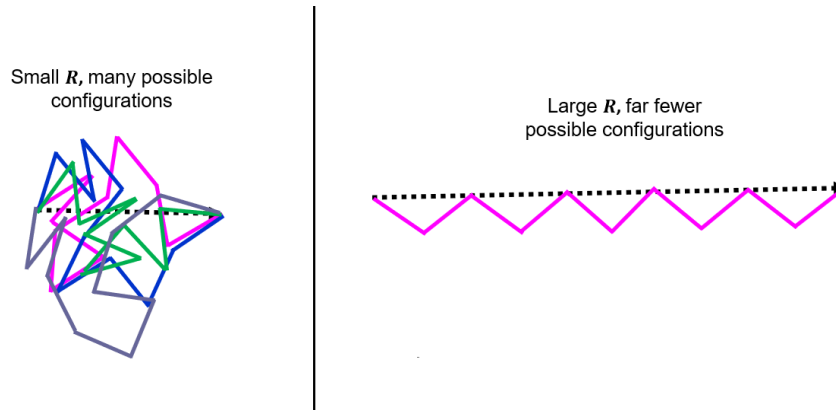


Figure 4.2: The possible configurations of DNA are many at the equilibrium state, but the probability distribution of these changes as the polymer is extended. Stretching DNA thus allows researchers to determine characteristic properties of the molecule, even when using simple models such as the FJC.

4.1.2 THE WORM-LIKE CHAIN MODEL

As seen from the FJC model, the force-extension behaviour of dsDNA can be parameterised according to its contour length and stiffness, which in the FJC is accounted for by the length of the Kuhn segments, b . Notably, this is only true of extension in the low to intermediate force regime, as after a certain point the bonds holding the two strands of DNA together will be pulled apart [218], leading the DNA to “melt” and unzip, similar to permanent deformation occurring after a material’s yield point. While the FJC provides a fairly good approximation of the mechanical behaviour of dsDNA at low forces, DNA is obviously not a series of rigid links. An alternative model is the worm-like chain (WLC), first introduced by Kratky and Porod in 1949 [219], which models polymers as single rods made up of curved sections. The improvement over the FJC may not be immediately apparent from this description, but rather than modelling the chain as a series of rigid links, each set at an arbitrary angle and being completely separate from its neighbours, the worm-like chain defines stiffness according to the persistence length. For two points that are very close together—perhaps a few picometres—a tangent to the curve at each of these points will point in a very similar direction. At some point the two tangents will become uncorrelated, and this distance is what defines the persistence length. The diagram in Fig. 4.3 illustrates this concept.

The other important “length” measurement in the WLC is the contour length. This term refers to the physical length of the molecule in metres measured along its phosphate backbone. The same entropic effects are still accounted for in the WLC, as the same thermal fluctuations will lead to different configurations at room temperature, and the equation for parameterising the force-extension behaviour of dsDNA at low to intermediate forces is given by (4.5). Here force, (F) is described in terms of the

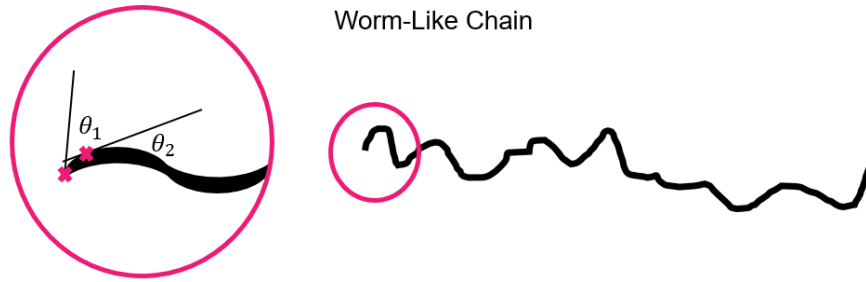


Figure 4.3: The persistence length is defined as the distance between points at which the tangent angles are no longer correlated. The zoomed in view in the magenta circle shows the persistence length as the distance between the two points marked by crosses, with the tangent angles indicated by θ_1 and θ_2 .

persistence and contour lengths of the DNA (l_p and l_c), as well as the separation between the the ends of the molecule (d).

$$F = \frac{k_B T}{l_p} \left(\frac{1}{4} \left(1 - \frac{d}{l_c} \right)^{-2} - \frac{1}{4} + \frac{d}{l_c} \right) \quad (4.5)$$

The persistence length of dsDNA is affected by the ionic strength of the environment the molecule is in. This is unsurprising, as electrostatic interactions between bases are a well known feature of DNA [220]. High quantities of ions in the medium act to screen repulsive electrostatic forces between bases on the DNA backbone [221, 207], and causing the persistence length to be shorter than it is in low-ion environments.

4.2 TRADITIONAL DNA STRETCHING PROTOCOL

The lever-assisted DNA stretching component of this work followed on from the dual-trap stretching protocol used by the Massey University biophysics and soft-matter group. Dual-trap stretching can be performed in two main ways using the optical tweezers apparatus available:

- Using two holographic traps, and stretching in the low-force domain (< 10 pN).
- Using the high power traps to perform high-force stretches (< 100 pN).

DNA stretching is performed using double-stranded DNA, which exhibits a characteristic overstretch at 65 pN, behaviour which has been used to detect the effect of structural changes to the DNA [145]. The particular DNA used for this work was λ -phage DNA, with a length of 10 000 base-pairs, resulting in a relatively long physical length of approximately 3 μm . The DNA was modified to have chemical handles on either end: biotin on one side and digoxigenin on the other, which enabled attachment of

the DNA strands to functionalised microbeads. The microbeads were purchased from Spherotech, already functionalised with coatings of streptavidin or anti-digoxigenin, which bind strongly to the biotinylated and digoxigenated ends of the DNA. This forms a “DNA dumbbell”, which allows each end to be trapped by optical tweezers. In this work the streptavidin beads had a diameter of $1.26\ \mu\text{m}$ and the anti-digoxigenin beads were $2.12\ \mu\text{m}$ in diameter. The differently sized microbeads were used in order to easily differentiate between the functionalised beads, as the streptavidin-coated beads are incubated with the DNA before being added to the sample and are hence pre-coated with DNA, whereas the anti-digoxigenin-digoxigenin bond has to be created *in situ* with a naked bead when performing the experiment.

The protocol for DNA stretching involved the preparation of a 0.025% w/v suspension of streptavidin beads in TSB (1 μl 1% w/v streptavidin beads in 39 μl of TSB), which was sonicated briefly in order to ensure that the streptavidin beads were dispersed evenly in the solution, and to reduce the formation of dimers. One μl of 120 ng/ μl DNA suspension was added to the streptavidin beads, and then incubated for an hour at 25°C on a temperature-controlled mixer (Eppendorf ThermoMixer), which stirred the suspension at 400 rpm. A 0.0375% w/v (15 μl 0.1% w/v beads in 25 μl TSB) suspension of anti-digoxigenin microbeads was then prepared, and also sonicated to ensure free-floating particles. One μl of each suspension was then added to TSB in a well of a microscope slide (18 mm diameter well) and the sample was sealed using a standard 22x22 mm (size 1, 120 μm thick) cover-slip and clear nail polish. The slightly higher concentration of anti-digoxigenin beads was purposeful, as the larger beads settle out of the suspension more rapidly than the streptavidin-coated microbeads, and using a higher number of them helps to compensate for this.

When using the holographic optical tweezers to stretch DNA, a streptavidin bead is held in one holographic trap while an anti-digoxigenin bead is trapped separately and brought towards the streptavidin bead so that the two appear to be touching in the camera view. This can be done easily using teleoperation in the Red Tweezers interface, where traps can be clicked and dragged into position. Alternatively, the trap position can be controlled by altering the “trap position” array in the interface, or by using the arrow keys. The microbeads are held together for a few seconds to allow a DNA tether to form, before altering the position of the anti-digoxigenin bead to initiate a stretch. Due to the Hookean spring model used to model optical tweezers, the trap stiffness is usually measured in the standard Cartesian 3D coordinates. Therefore, it is easiest to measure the stretch in one direction, and the microbead should only be moved in this direction to make the measurements accurate to the stretch that is happening.

Alternatively, if a high-power stretch is to be attempted, the microbeads have to be “passed” into the high power traps using the holographic traps. This is relatively easy,

as the HP traps are much more powerful, and as a result are more attractive to the microbeads. However, the high trap stiffness of the fixed trap, can prove problematic when the beads have to come close together, as at the start of the stretch, in order to form tethers, as it can pull both beads into the trap. This is also a risk with the lower strength holographic traps, but happens less frequently. A more pressing risk with the HOT set-up for DNA stretching is that the beads may stick together. In general, DNA stretching is a process that requires skill and patience.

4.2.1 MODIFYING THE DUAL-TRAP PROTOCOL

As discussed in Chapter 3, the microlevers have limited mobility in high ionic strength solutions. Therefore, the first adaptation to the DNA stretching protocol was to reduce the concentration of the TSB, and see whether DNA stretches could still be performed in the usual dual-trap configuration, using the holographic optical tweezers.

A sample was prepared using the same concentrations of DNA and microbeads as outlined in the previous paragraphs, but in a solution that was comprised of TSB diluted in milliQ water to a concentration of 10%. The sample was once again prepared in a well slide and sealed with a coverslip and nail polish. The sample was then mounted on a piezomotor stage (Physik Instrumente) to allow fine positioning, which is useful when performing trapping studies as ideally only one pair of beads will be imaged at a time. The HOT power was set to 2 W and a streptavidin bead was selected and isolated from the other beads by moving the stage. An antidigoxigenin bead was then selected and moved to the same focal plane, before being moved into contact with the streptavidin bead. The streptavidin bead was moved away to create a stretch in the X-direction, as shown in Fig. 4.4. While this method of moving the traps was not ideal in terms of creating a single-direction stretch, due to the imprecision associated with teleoperation, it was sufficient to produce data that could be analysed and fitted to the worm-like chain model. The stiffness of the optical trap on the antidigoxigenin bead was measured to be $9.30 \text{ pN}/\mu\text{m}$ in this configuration, using the restricted thermal fluctuations of the microbead and the equipartition theorem to measure the stiffness in this position, as explained in 3.3.1. The trap stiffness can then be multiplied by the displacement of the antidigoxigenin bead from the trap centre to calculate the forces during a stretch. The results of four stretches with a single pair of microbeads can be seen in Fig. 4.5, where fitting to the WLC produced a persistence length of $67.2 \pm 2.1 \text{ nm}$, and a contour length of $3.35 \mu\text{m}$, which is a relatively good fit for 10 000 kbp DNA, assuming a length of 0.34 nm per base pair. The persistence length produced from this fit was longer than that from previous work in full strength TSB, where it was reported to be 59.1 nm [94], as expected due to the lower ionic strength. The main aim of these stretches was to determine that the standard double-trap protocol for low

force stretching could be directly adapted to perform DNA stretching in a lower salt buffer to ameliorate the problem of adhesion to some extent, and the results seemed to show that this was possible.

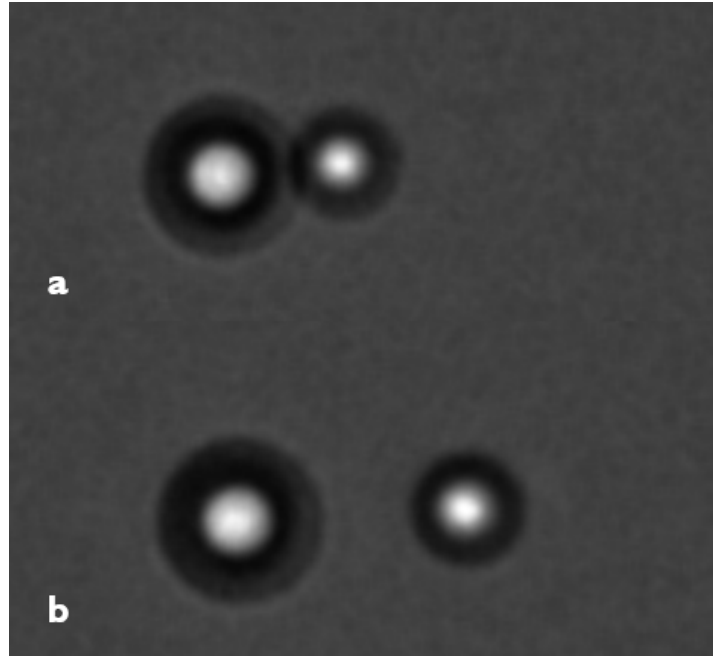


Figure 4.4: The HOT system was used to stretch dsDNA in a low-power dual trap assay in a 10% TSB solution, and the results were fit to the WLC model to test whether stretches could be performed in such a solution. (a) The beads are brought close together to allow a tether to form before one is pulled away to create a stretch. (b) When a stretch is created, the bead in the stationary trap moves out of the trap centre, which allows the force-extension to be measured.

Following the successful performance of dual-trap DNA stretches in a low salt buffer, attention turned to the introduction of microlevers into this protocol. The addition of microlevers complicates the situation due to the requirement that microbeads be attached to the microlevers, and preferably specifically attached to the especially printed pocket. DNA-stretching is generally time-limited, with it being anecdotally observed that stretching becomes harder to achieve after a few hours under the microscope. This, combined with the fact that the levers are prone to settling faster in salty environments, compared to their behaviour in milliQ water, means that there is a requirement for the microbeads to be attached to the levers and “ready to go” when the DNA-streptavidin suspension is added to the sample. The need to prepare the levers and attach microbeads before adding the DNA means that the sample had to be left open and unsealed, meaning that the liquid level has to be monitored, and more milliQ water added as necessary to avoid a rapid increase in salt concentration as the sample dried out.

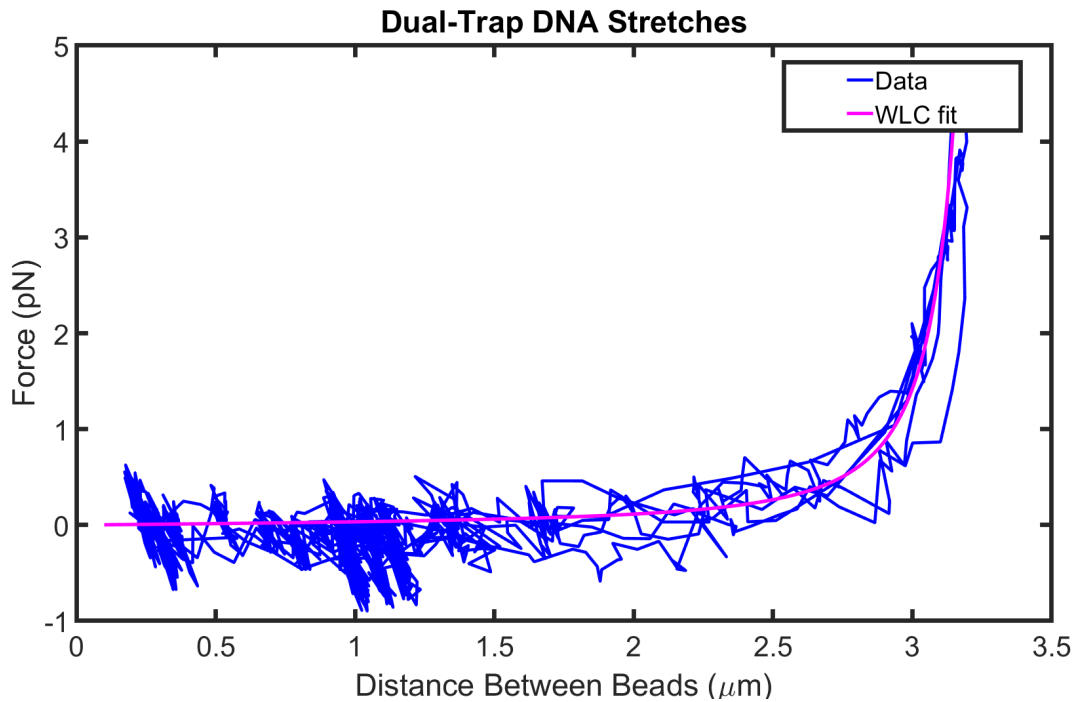


Figure 4.5: A short series of low-force DNA stretches were performed using the dual-trap configuration with the HOT, and a 10% TSB solution, in order to evaluate the possibility of performing DNA stretches in a low-ionic strength environment.

At first a droplet of 10% TSB solution was added to a sample of microlevers, which had been rotated per the description in Chapter 3. Both supported and unsupported microlevers were used, as it was uncertain whether any noticeable performance gains were made in using either, following the work performed in designing functional levers. One μl of a 0.0375% antidigoxigenin (AD) bead suspension- also made using a 10% dilution of TSB- was then added to the sample, but adding a small volume of a fairly high concentration of beads meant that it was difficult to locate beads to attach to the microlevers. The volume of AD bead suspension was increased to 5 μl , but it very quickly became apparent that this was far too high a quantity of microbeads, and they covered the substrate as they settled out of suspension, blocking movement of the levers. Additionally, as the microlevers form the only features on the glass substrate, the microbeads are drawn to the levers, particularly as the sample dries, as shown in the micrograph of a dried sample shown in Fig. 4.6. The concentration of beads in the suspension was decreased by diluting it to 1/10th of the starting concentration using 10% TSB, and 10 μl of the resulting suspension was then added to a sample of levers. This produced a good number of microbeads, as the samples were typically populated with between 10 and 30 microlevers, and so relatively few microbeads were required. Microbeads were then selected and guided into the pockets on the ends of microlevers

using the HOT, and held in place until they seemed to be attached. This process could take several minutes for a single microlever, slowing down the entire experiment. Additionally, sometimes the microbeads were only extremely weakly attached to the pocket, resulting in loss of the AD bead when the lever turned. This prompted the inclusion of a “rotation” step after microbead attachment; where the borosilicate microprobe was used to rotate the levers to check whether beads were adequately attached. This step also served to unsettle any levers that had settled during attachment of the microbead, making them trappable with optical tweezers.

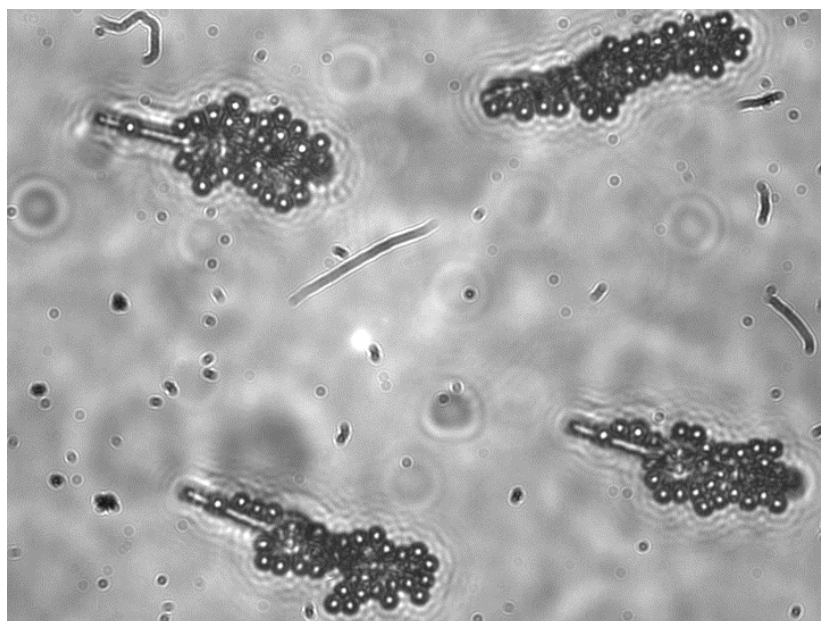


Figure 4.6: Initial attempts at adding AD beads to the samples used higher concentrations than were required, resulting in the levers becoming covered in microbeads.

The time that it took to attach AD microbeads to the microlevers was of concern, as it became difficult to prepare multiple microlevers before the microbeads settled out of suspension. It was discovered that suspensions of AD beads prepared in full-strength TSB could be more easily attached to the microlevers, even when a droplet of this suspension was introduced to an otherwise milliQ water environment. As the microbeads tend to become more strongly attached over time- provided they have been properly attached to the microlevers- this was seen as a useful way to make up the 10% TSB concentration that had been tested for DNA stretching, based on the assumption that the ions would diffuse through the droplet on the sample.

Aside from the attachment of the AD microbeads, another important aspect of lever-assisted DNA stretching was the mobility of the microlevers. To test mobility of microlevers in 10% TSB the HOT and the piezomotor stage were used in conjunction to set a chosen microlever up so that the non-pocket end of the lever was in the fixed

HP optical trap. The steerable component of the HP trap was blocked off in order to prevent it from interfering with the experiment, which is possible due to the separate optical path used to steer this trap, and the HP trap was supplied with 1 W of power. This high laser power was used in order to ensure that the trapped end of the microlever was firmly held in place, and capable of resisting the motion of the piezomotor stage. Various waveforms were applied to levers using the piezomotor stage to ensure that the lever was held fixed in the optical trap while the stage was moved, and the movement was recorded at 50 fps using an Andor Neo high-speed CMOS camera. This was also used to determine an appropriate waveform amplitude for producing rotation without translating the entire lever out of the stable trapped position.

Five points along the levers were tracked using the Hough transform for circle detection to locate the printed “handles” along the length of the lever, and centre-of-mass tracking, to ensure that the levers were both trapped stably and able to move back and forth for multiple cycles. These five points are shown in Fig. 4.7, with the Hough circle transform used to label the points in (a). In ideal cases, the lever remained stably trapped for multiple cycles, while in others a change in behaviour revealed that the lever was either becoming progressively stuck, or had experienced a scattering event that caused a disruption to the trap. An example of the latter can be seen in Fig. 4.8(b), where the trap was suddenly disrupted due to a microbead “flying in” to the trap used to hold the lever. In this case, the lever remained trapped over all, but its movement changed, whereas in the case shown in Fig. 4.8(a) the lever displayed the same motion consistently.

DNA stretches were performed by co-locating DNA-incubated streptavidin beads to the AD beads in the pockets of the microlever, and then applying a triangular waveform to the piezomotor stage, stretching the tethered DNA as the lever moved away from the trapped microbead. The protocol used to perform DNA-stretching with the microlevers was further adjusted, and the final results were presented in the Optics Express article reproduced in the following section.

4.3 OPTICAL MICROLEVER-ASSISTED DNA STRETCHING

Optical microrobotics is an emerging field that has the potential to improve upon current optical tweezer studies through avenues such as limiting the exposure of biological molecules of interest to laser radiation and overcoming the current limitations of low forces and unwanted interactions between nearby optical traps. However, optical microrobotics has been historically limited to rigid, single-body end-effectors rather than even simple machines, limiting the tasks that can be performed. Additionally, while multi-body machines such as microlevers exist in the literature, they have not yet been successfully demonstrated as tools for biological studies, such as molecule stretching. In this work we have taken a step towards moving the field forward, by developing two types of microlever, produced using two-photon absorption polymerisation, to perform the first lever-assisted stretches of double-stranded DNA. The aim of the work is to provide proof of concept for using optical micromachines for single molecule studies. Both styles of microlevers were successfully used to stretch single duplexes of DNA,

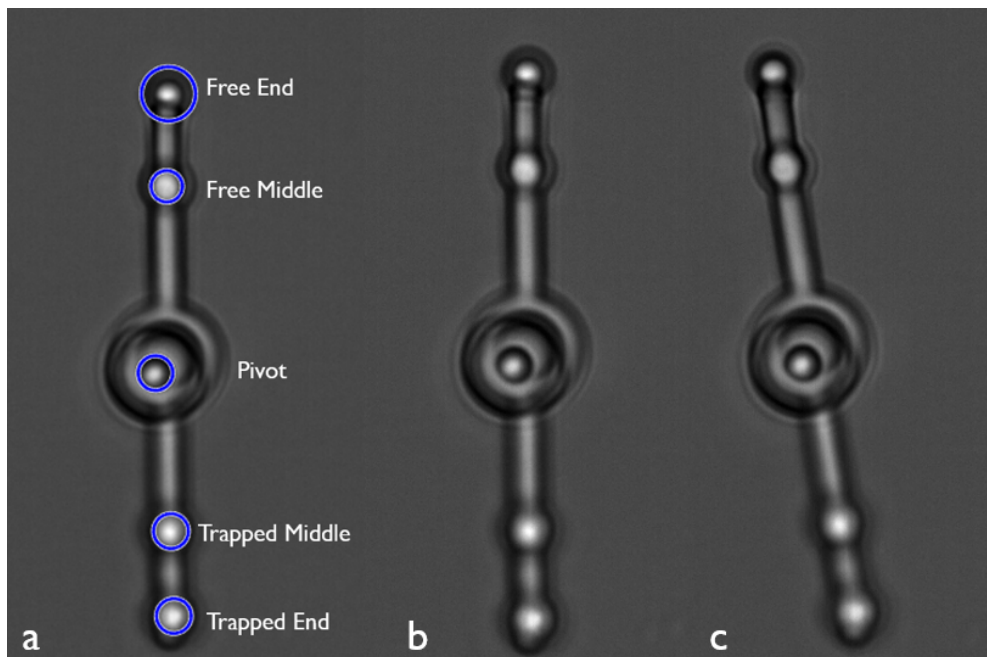


Figure 4.7: (a) The Hough circle transform was used to detect circles at the start of a sequence of images, and centre-of-mass tracking was then used to monitor the movement of these points over the course of the sequence. (b) A lever at the start of a sequence of oscillations, where the entire lever appears to be in focus. (c) A lever at the peak of oscillations, the lever still appears to be in focus and the trapped end remains in the optical trap, indicating that the lever is not sticking as it moves around the pivot.

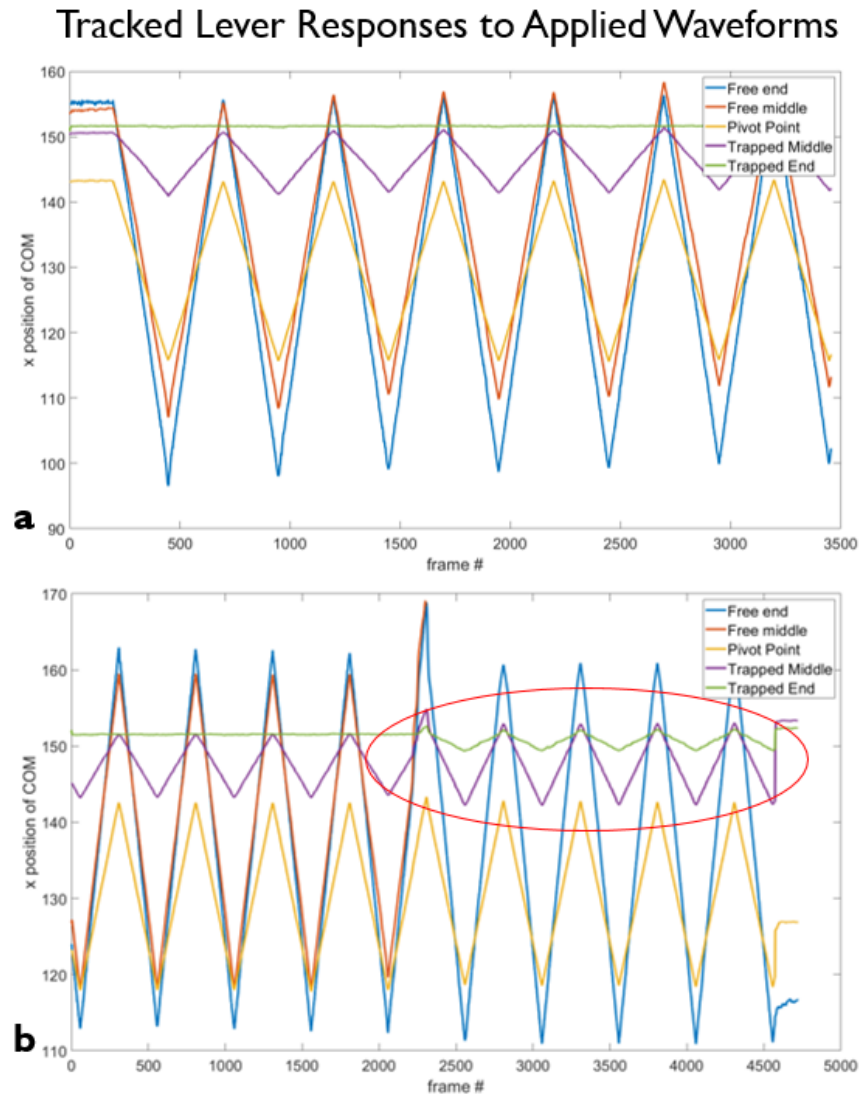


Figure 4.8: (a) In the ideal case microlevers remained trapped over multiple waveform cycles, and displayed the same motion. Here it can be noted that the Free End (where the AD bead is attached using the pocket) demonstrates motion with 2x the amplitude of the input waveform (measured using the motion of the pivot). (b) Events that disrupt the trap, such as a free microbead flying into the trap, in this case, cause noticeable differences to the levers' movement. Of particular note is the disruption to the position of the trapped handle, circled in red.

and the results were analysed with the worm-like chain model to show that they were in good agreement.

4.3.1 DECLARATION

An OSA-formatted open access journal article PDF may be governed by the OSA Open Access Publishing Agreement signed by the author and any applicable copyright laws. Authors and readers may use, reuse, and build upon the article, or use it for text or data mining without asking prior permission from the publisher or the Author(s), as long as the purpose is non-commercial and appropriate attribution is maintained.

This article was coauthored with Dr Allan Raudsepp (DNA stretching assistance and help with interpreting results); Dr Daniel Fan (Nanoscribe PPGT2 training); and Prof.dr. Urs Staufer, Prof. Martin A. K. “Bill” Williams and Dr Ebubekir Avci (supervision and funding). It was published in *Optics Express*, an Optica journal (rebranded from OSA: Optical Society of America), and the full reference can be found in the bibliography of this thesis [222].

4.3.2 INTRODUCTION

Optical tweezers (OT) have been used to perform biological studies since 1987, when Ashkin and Dziedzic performed optical trapping of bacteria and viruses [49]. This experiment also exposed an enduring problem with the use of optical tweezers for biological studies: the damage the intense laser light can cause. The mechanisms for this damage have been the subject of several papers [108], with local heating [114, 202], photobleaching [112] and oxidation due to photogenerated free radicals [107] all being considered. As a result, several different approaches to reducing damage have been suggested, including minimising laser power, using lasers of specific wavelength [89], and performing experiments in an anaerobic environment. However, each of these is subject to limitations. For example, the maximum force that can be applied with optical tweezers is related to the power of the laser [223]. Therefore, limiting laser power effectively prevents researchers from investigating phenomena at high forces. Restricting experiments to anaerobic environments is likewise limiting in terms of the scope of research that can be performed. The suggested use of certain wavelengths necessitates the build of an entirely new set-up, in cases where the original laser is inappropriate, which is inconvenient and expensive. Therefore, all of these potential solutions can be described as either limiting experiments, or requiring a full overhaul of the system. However, an alternative solution- indirect manipulation of biological material using optical microtools- has been recently proposed [5]. The great advantage of using optical microtools, when compared with the other suggested strategies, is that they can theoretically be introduced into any OT set-up. Indirect optical manipulation has been demonstrated using single-body optical microtools made through two-photon absorption polymerisation (TPAP) [224], and examples can be found in the literature for yeast cells [225, 226], and for rotating and translating filamentous cells [54]. Additionally,

researchers have recently used a single-body optical microtool made using TPAP to measure the elasticity of human microvascular cerebral endothelial cells (hCMEC/D3) [227], further validating the use of microtools for biological studies at a cellular level. However, the potential of optical micromachines for single molecule studies- such as DNA stretching- is yet to be realised. This paper introduces a modified version of the well-known “dumbbell assay” for DNA stretching that uses a microlever made through TPAP to facilitate a stretch. The comparison between the conventional assay and the microlever-assisted method can be seen in Fig. 4.9.

Working optical microlevers have been demonstrated in the literature [56, 57, 184], and great interest has recently been shown in developing strategies for successfully using optical tools in biologically relevant environments, [184, 228]. However, there is still a lack of work demonstrating the successful use of multi-body optical micromachines as tools, meaning that the field is largely limited to single-body microtools. The few multi-body tools in the literature have been demonstrated to be able to perform tasks such as controlled out-of-plane rotation [140], which is typically extremely challenging for optical microrobotics. Stretching double stranded (ds) DNA, which has a well-characterised force-extension curve, using a simple experimental setup, presents an ideal starting point for proof-of-concept of the potential uses of optical micromachines. In this work we describe the adaptation of the dumbbell assay to include a microlever.

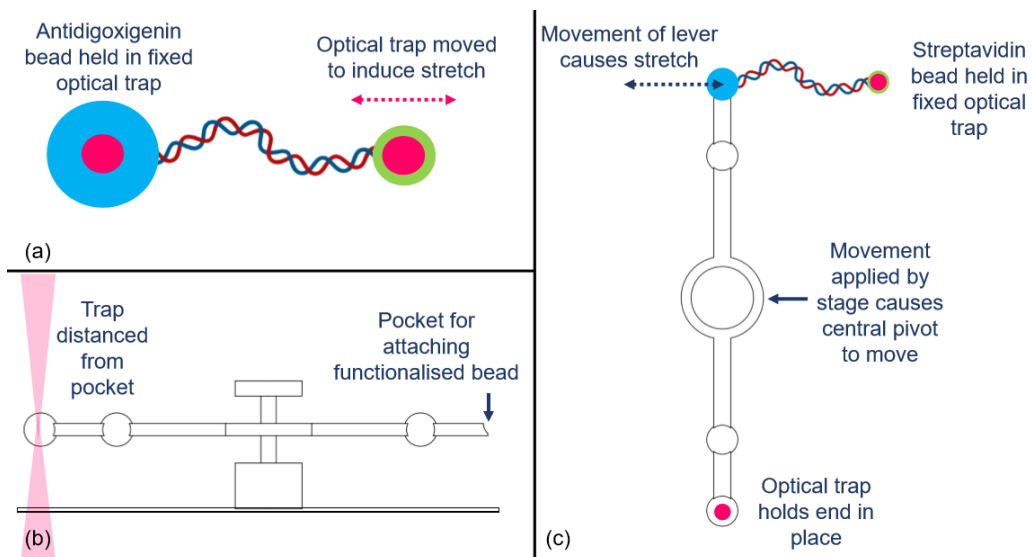


Figure 4.9: (a) The familiar dumbbell assay moves functionalised microbeads apart, using optical tweezers to stretch DNA. (b) The microlevers used for this work have a pocket for attaching a microbead, and offer a simple mechanism for distancing the trap from the target. (c) The modified assay, using a microlever to distance one of the traps.

4.3.3 DESIGN OF MICROLEVERS

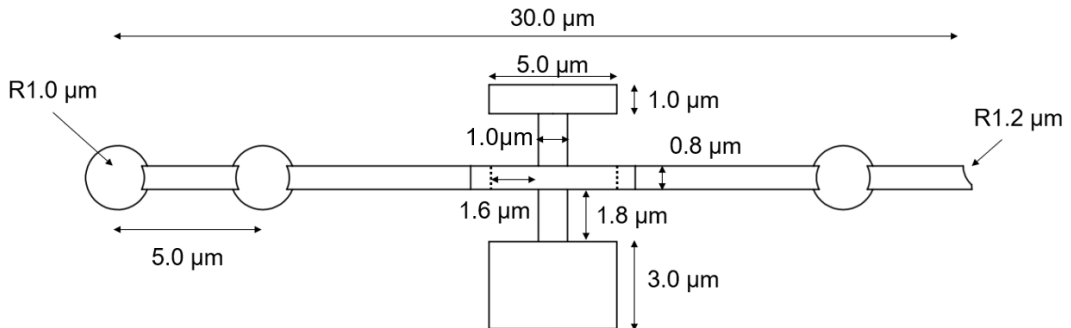


Figure 4.10: The levers used for the DNA stretching were made with the dimensions shown.

The microlevers were designed specifically with the task of molecule stretching in mind. Therefore, the starting point for the design was a fixed pivot point, known as the centre pin, about which a lever arm would rotate. The idea behind this was that a centred lever arm would allow for force transfer from the optical trap to the DNA. The next key consideration was the attachment of DNA to the levers. The dumbbell assay being adapted uses $1.25 \mu\text{m}$ diameter streptavidin coated beads and $2.12 \mu\text{m}$ diameter antidigoxigenin coated beads, which attach to biotin and digoxigenin handles on the termini of the DNA, respectively, creating handles that can be manipulated with optical tweezers. Therefore, a pocket was printed at one end of the lever arm, to allow for the attachment of the antidigoxigenin microbead. The other end of the arm featured a spherical “handle” for trapping, in order to replace the direct trap on the antidigoxigenin bead with a distanced trap, with the motivation of limiting the exposure of the DNA to laser radiation. Two other spherical handles were also printed partway down the lever and these were previously also used as trapping handles [5]. However, in this work they served as a way to easily check whether the lever was in focus, and to track the movement of the lever, rather than being used as a trap handle. Following our previous work, two variations of the lever design were used, one which was supported by conical posts and the other which was unsupported. The supported levers also featured a thin ridge on the lever arm, where it encircled the centre pin, in order to reduce the overlapping area between the two components. Dimensions of the basic lever design can be seen in Fig. 4.10, and diagrams and SEM images of the supported and unsupported levers can be seen in Fig. 4.11.

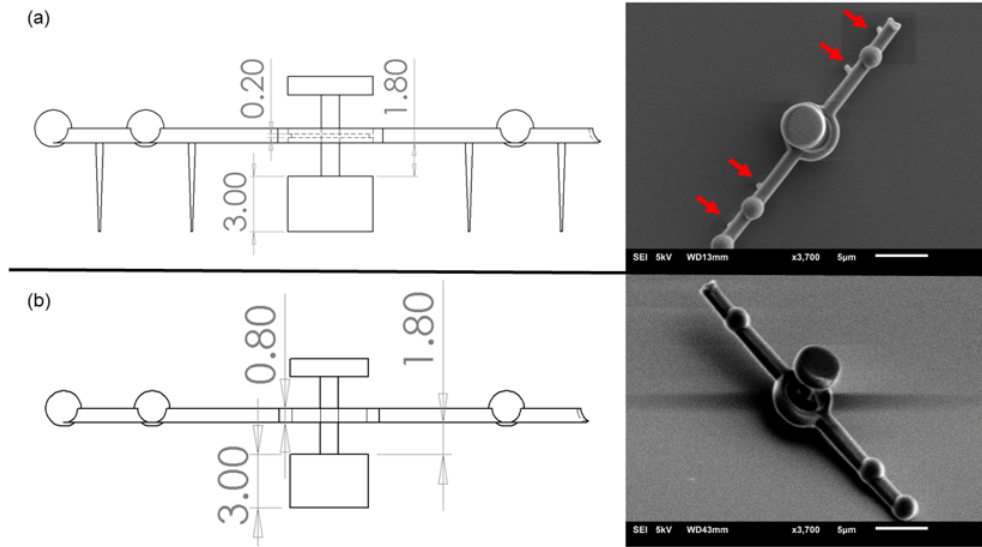


Figure 4.11: (a) The supported levers used for DNA stretching had tapered supports that narrowed at the bottom, but otherwise shared the same dimensions as the unsupported levers shown in (b). The supports in the SEM image are pointed out by red arrows in the diagram.

4.3.4 EXPERIMENTAL METHOD AND MATERIALS

4.3.4.1 OPTICAL TWEEZERS SET-UP

A Nikon Eclipse TE2000-U inverted microscope was used as the major component of both the imaging and trapping setup. A 2 W 1064 nm laser and a 5 W 1030 nm laser were routed through a 60x, 1.2 NA plan apo water immersion objective (Nikon) to create two separate optical traps. A Boulder Nonlinear Systems spatial light modulator (SLM) was used in conjunction with the Red Tweezers software [174] and the 1064 nm laser in order to create a steerable trap, while the 1030 nm trap was treated as fixed, and aligned with the centre of the microscope's field of view. Rather than manoeuvring the 1030 nm trap, a piezomotor stage (Physik Instrumente) was used to finely position the substrate on the microscope. Experiments were conducted in bright field conditions and were imaged using a high speed CMOS camera (Andor Neo). The microscope and associated peripherals were mounted on a vibration isolation table in order to reduce the effects of mechanical noise. A diagram of the setup can be seen in Fig. 4.12.

As the experiment relies on the levers being free to rotate, a borosilicate microprobe was used to free the levers before experiments; separating the lever arm from the centre pin. The microprobe had a tip radius of $<1 \mu\text{m}$ and was mounted on three stepper motor stages (TAMM40-10C and OSMS60-5ZF, Sigma-Koki), which were in turn mounted to the isolation table. This set-up allowed the microprobe to be controlled with three degrees of freedom, with a resolution of $1 \mu\text{m}$ in the x and y directions and

0.5 μm in the z direction.

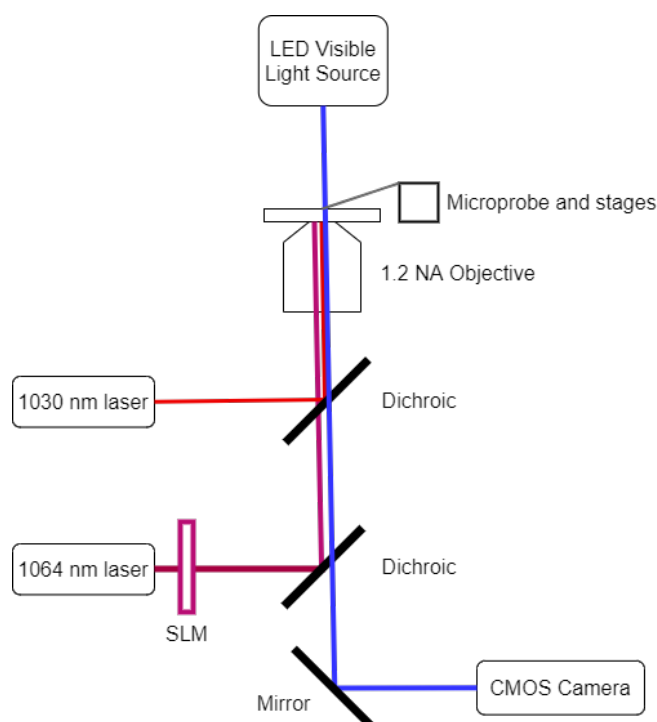


Figure 4.12: The optical tweezers setup used for this study consisted of two separate lasers, with dichroic mirrors used to reflect the beams into the objective.

4.3.4.2 LEVER PRINTING

The levers were printed directly onto 170 μm thick coverslips, using the conventional oil-immersion writing method, and remained on this substrate throughout the experiment. The coverslips were cleaned with isopropanol and a brief oxygen plasma was performed to improve adhesion of the microlever devices to the coverslips before printing. The levers were printed using the Nanoscribe GmbH Photonic Professional set at 14 mW laser power and the proprietary IP-L 780 resist. Levers were developed in PGMEA for 30 minutes, followed by a five minute rinse with isopropanol. The sample was then blow-dried using compressed air. Printing the levers to the coverslip meant that the levers had a fixed rotating point, and so only the relative position of the lever arm needed to be controlled, rather than the pose of the entire microlever. The relatively close proximity of the microlever arm to the substrate also meant that there was little chance of additional beads being trapped during the experiment, as can sometimes happen in dual-trap experiments when beads “fly-in” to the trap from below.

After printing and developing, the levers were inspected in dry conditions, using the borosilicate microprobe to rotate them 360°. This step was performed to ensure

that the levers were printed correctly, and were capable of rotating, as this is difficult to ascertain through visual observation under microscope alone.

4.3.4.3 SAMPLE PREPARATION

The double-stranded DNA used for the experiment was 10 kilobase-pairs (kbp) long and synthesized using PCR and modified primers to have biotin and digoxigenin present at the end of each strand. Anti-digoxigenin and streptavidin coated microbeads could then be attached to the DNA termini, forming a tether. In traditional dumbbell assays, the microbeads are then used as trap handles for stretching, as previously explained. However, in this work, the anti-digoxigenin beads were attached to the levers, using the pockets printed for this purpose. In order to do this the anti-digoxigenin beads were kept in a tris-saline buffer (TSB, 50 mM Tris, 150 mM NaCl, 1 mM EDTA) at a concentration of 0.01% w/v, and then added to filtered milliQ water on the lever substrate in order to produce a droplet of dilute microbead suspension containing approximately 10% TSB (approximately 5 mM Tris, 15 mM NaCl, 100 μ M EDTA). The quantities used for this study were 20 μ l of the microbead suspension into 180 μ l mQ water. The anti-digoxigenin beads were then guided into the lever pockets using the 1064 nm SLM trap, and held in place until the beads were firmly adhered. Images of this can be seen in Fig. 4.13(a) and (b). A suspension of streptavidin beads was prepared concurrently, at a concentration of 0.04% w/v, and 1 μ l 1/10 diluted biotin-digoxigenin functionalised DNA (lambda DNA, 10kbp) was added to the suspension. The streptavidin-DNA suspension was then incubated for an hour at 25°C, while being stirred at 400 rpm, after which 1 μ l of the incubated mixture was introduced to the lever substrate. Later, a sample of 1/100 diluted DNA was used, in response to results that showed multiple DNA strands tethering when using the higher concentration of DNA. The concentration of DNA in the 1/10 dilution was 120 ng/ μ l and the concentration of the 1/100 dilution was 12 ng/ μ l. Other than changing the DNA dilution, the sample preparation method remained the same.

4.3.4.4 DNA STRETCHING PROTOCOL

Once the microbeads were introduced to the trapping medium, a target lever was selected and manoeuvred using the piezo-electric microscope stage so that its trapping end was in the path of the fixed optical trap. The lever was then turned with the borosilicate microprobe in order to release any adhesion between the centre pin and the lever arm, meaning that the lever arm would be free to rotate when moved relative to the trap. Fig. 4.13c shows the microprobe setup on the microscope, and Fig. 4.13d shows the probe being used to turn the lever. Turning the lever in this way also tested the adhesion between the anti-digoxigenin bead and the lever, as a weakly adhered bead

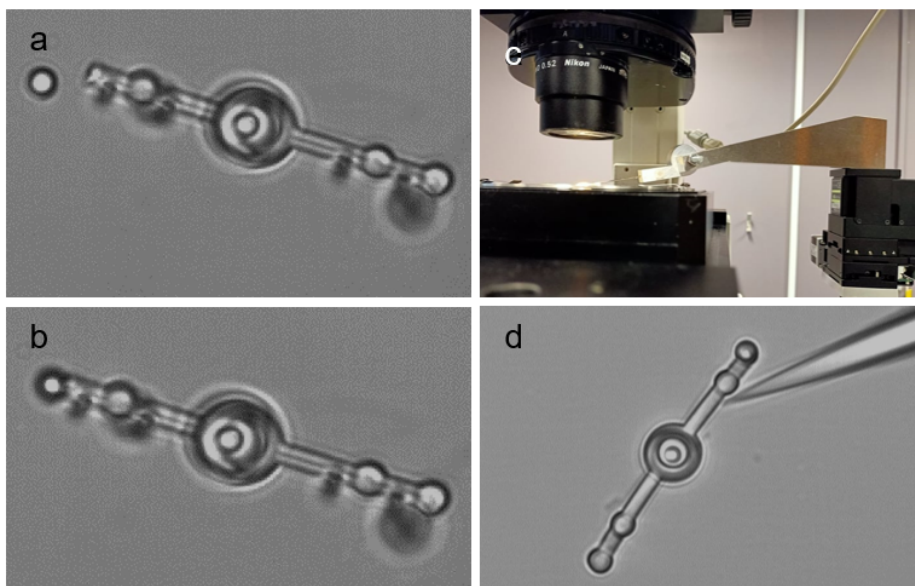


Figure 4.13: (a) and (b) show an anti-digoxigenin coated bead being guided into the pocket of a lever. (c) shows the borosilicate microprobe setup on the microscope, and (d) shows the borosilicate probe being used to turn a microlever with a bead in its pocket. This process was useful for testing how firmly the beads were attached, as well as freeing seized levers.

would be lost during the turning process. A streptavidin-DNA bead was then trapped using the SLM-based optical tweezers, set at 2 W (full power), and brought near the anti-digoxigenin coated microbead positioned in the pocket of the microlever. The streptavidin bead was held in this position, almost touching the anti-digoxigenin bead, for a few seconds to allow for a DNA tether to form between the two microbeads. A triangular waveform then was applied using the microscope stage, creating a rotation of the lever due to its trapped end, and consequently stretching the DNA tethered between the two microbeads. The frequency and amplitude of the triangular wave was varied during the experiment, but it became clear that the amplitude had to be limited to $2.0 \mu\text{m}$ to keep the stretch within the limits of the SLM trap and the contour length of the DNA (estimated at $3.35 \mu\text{m}$), due to the lever amplifying the motion applied. The amplitude also had to be kept above $1.2 \mu\text{m}$ to create a clear stretch. Therefore, the majority of the stretches reported in this work were performed with $2.0 \mu\text{m}$, 0.1 Hz triangle waves. Stretching was repeated with the same lever for as long as the streptavidin bead remained in the SLM trap, and the extension of the DNA was inferred from the displacement of the bead from the trap centre. This method was used to perform DNA stretches with several different levers- both supported and unsupported. The process of anti-digoxigenin attachment, lever turning and DNA stretching can be seen in Visualisation 1, in the supplementary material.

4.3.5 RESULTS AND DISCUSSION

4.3.5.1 LEVER-ASSISTED STRETCHES

Lever-assisted DNA stretches were successfully performed with both supported and unsupported lever types. Ten supported levers were used to perform 42 DNA stretches and nine unsupported levers were used to perform 26 DNA stretches. The forces applied were calculated using the stiffness constant of the SLM trap and the displacement of the streptavidin bead from the centre of the trap. The trap stiffness was calculated using Eq. (1), where k_x is the trap stiffness, k_B is Boltzmann's constant, T is the room temperature in Kelvin (293 K) and $\langle X^2 \rangle$ is the variance of a streptavidin bead's restricted Brownian motion in the trap. This calculation produced a stiffness of 8.14 pN/ μ m in the x direction, sufficient for performing low force stretches.

$$k_x = \frac{k_B T}{\langle X^2 \rangle} \quad (4.6)$$

The force-extension data was then fitted to the worm-like chain (WLC) model [99], which is parameterised to produce l_c , the contour length of the DNA, and l_p , the persistence length. The WLC is given by Eq. (2), where d is the distance between the two microbeads tethered by the DNA.

$$F = \frac{k_B T}{l_p} \left(\frac{1}{4} \left(1 - \frac{d}{l_c} \right)^{-2} + \frac{d}{l_c} - \frac{1}{4} \right) \quad (4.7)$$

The supported levers were tested first, as it was expected that the supports on the design would assist in keeping the levers plane, which is key to facilitating the straightforward analysis of a stretch. However, when the levers were positioned in the 1030 nm optical trap, there was a chance that scattering due to "folded" supports that had been damaged during sample preparation would cause the lever to be "pushed up" out of the trap, causing the lever to tilt down on the other side of the pivot, which can be seen in Fig. 4.14a. In several cases this caused the supports to stick to the substrate, stopping the lever from turning. Even when the lever remained able to turn, the unfocused trapped end meant that the motion of the lever could not be reliably tracked. As a result, the DNA stretches reported in Fig. 4.15 were all carried out with levers that had their supports purposefully bent sideways, so as not to impede lever rotation. Additionally, as is shown in Fig. 4.14b, some levers would spontaneously rotate slightly in the trap, which resulted in the entire lever being slightly angled, and leaving the supports completely visible.

In both the supported and unsupported cases the main challenge in the experiments was to continue stretching only a single duplex over many stretches, as more DNA tethers could be formed between the streptavidin and anti-digoxigenin beads as the

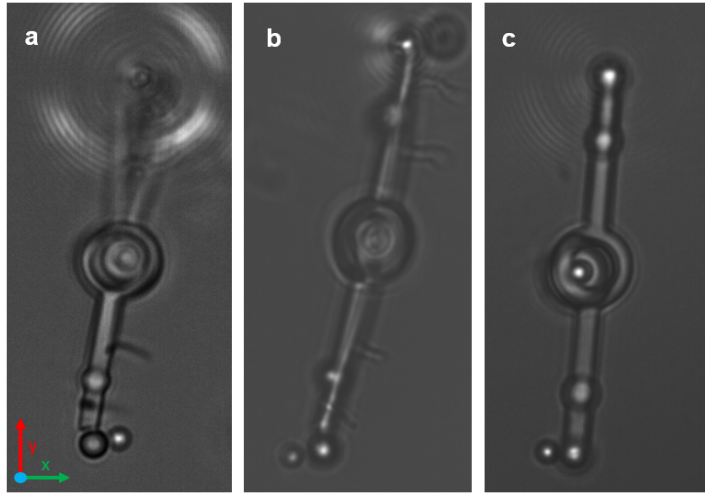


Figure 4.14: Scattering interactions of bent supports occasionally led to levers being “pushed up” out of the plane, as in (a). (b) shows a supported lever spontaneously reorientating in the optical trap, resulting in the entire lever being slightly angled around the y (long) axis, rather than being flat in the x - y plane. (c) shows an unsupported lever, appearing to be well focused and flat in plane. Comparisons such as this validated the use of unsupported levers for this work.

lever rotated and the beads came into close contact. Several DNA strands building up over multiple repetitions can be seen in Fig. 4.15.

The concentration of DNA used in the supported-lever experiments was actually a 1/10 dilution, 10x higher than that described in our methods. This meant that it was highly likely that each streptavidin bead had several attached DNA duplexes, and as the lever swung back and forth, repeatedly bringing the microbeads close together, more DNA became tethered. This effect can be seen in Fig. 4.15, with the force-extension data appearing to curl up and away from the curve with repeated stretches. Traditionally, researchers discard the stretches involving multiple duplexes as in the AFM data reported in this reference [229], but they have been presented here as they dominate the stretches performed with the supported levers at the DNA concentration used. It is plain to see that once the concentration of DNA was reduced sufficiently, as it was for the unsupported levers, it becomes much easier to perform stretches with single duplexes. This can be seen in Fig. 4.16, where the vast majority of the data conforms well to the worm-like chain (WLC) model. Using the WLC to fit the stretches produced a persistence length value of 63.8 nm (± 1 nm) and a contour length of 3.35 μm (± 0.01 μm). This persistence length is longer than the 59.1 nm previously reported for this DNA [94] but is in agreement with the higher electrostatic repulsion between DNA segments, due to the lower ionic strength of the trapping medium [230]. Specifically, in the 2015 study TSB was used, whereas in this study the ionic strength of the trapping

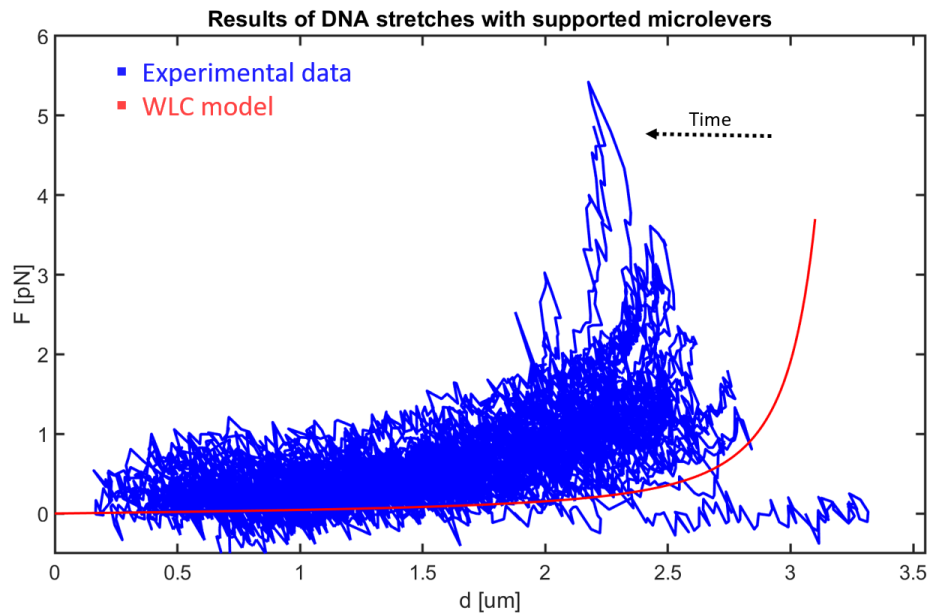


Figure 4.15: Compilation of stretches performed using supported levers. These stretches demonstrated the difficulty of repeating a stretch with a single DNA duplex, as often over the course of the experiment more DNA attaches, leading to a narrowing of the force-extension curve.

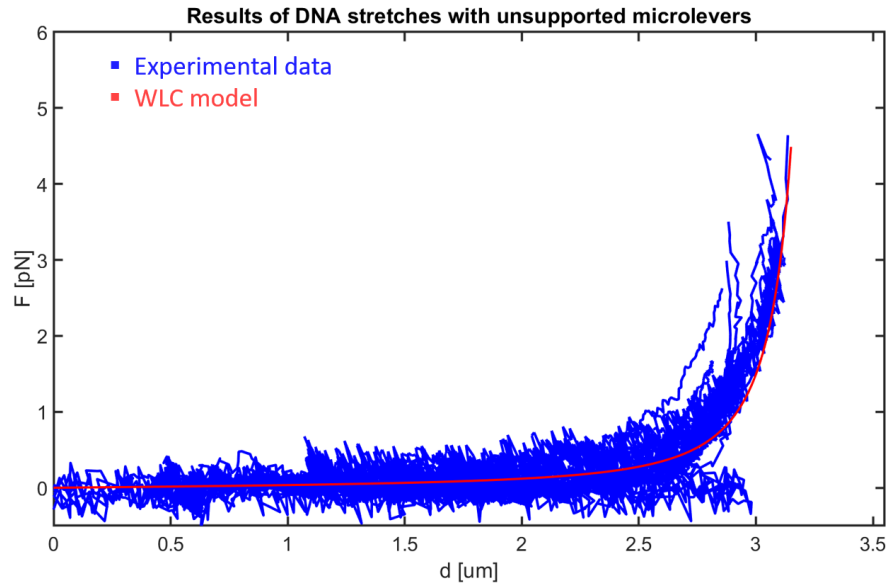


Figure 4.16: Compilation of stretches performed using unsupported levers. These stretches were performed with a 10x lower concentration of DNA, indicating that the problem of multiple strands attaching could be overcome for DNA-assisted stretches.

medium was approximately 10x lower. The low ionic strength medium was used to reduce the likelihood of levers seizing during the experiment, which is related to the

screening of electrostatic forces in high ionic strength environments [5]. While direct comparison of the lever-assisted stretches cannot be performed, due to the different DNA concentrations used, the fact that the supports added no discernible improvement to the levers' ability to stay in plane during stretches means that unsupported levers should be used for future work.

4.3.5.2 TRACKING LEVER MOVEMENT

The movement of levers was tracked during several of the DNA stretches, as well as in several cases where no DNA was present. In the latter case, it was far easier to track lever movement for multiple cycles, as during DNA stretches large movement of the lever would often entirely displace the streptavidin bead from the SLM trap during the stretches, meaning that experiments were often stopped early, or even after a single stretch. However, the results of tracking one of the levers used in a particularly successful stretching run are shown in Fig. 4.17, for the sake of interest. Tracking the spheres on the levers during the experiments revealed subtle differences in how some of the levers were trapped, with fluctuations in the position of the trapped handle possibly due to slight differences in printing or inexact positioning of the lever, an example of this can be seen in the supplemental document. However, in each case the movement of the trapped end was minor compared to the amplitude of the waveform applied, which is given by the movement of the fixed centre pin. When the lever was free to rotate clear amplification of motion was demonstrated.

4.3.5.3 STRETCHES USING TWO BEADS

In order to evaluate the general performance of the lever-assisted method, we used the same dsDNA to perform traditional microbead-based DNA stretches. This was done by fixing a large microbead to a coverslip and performing stretches by applying a waveform and measuring displacement from the SLM trap, with the laser once again set to 2 W. Much larger ($4.37 \mu\text{m}$ diameter) anti-digoxigenin beads were used to perform these stretches, to reduce the chance of DNA strands becoming mechanically tethered to the substrate rather than attaching via the digoxigenin on the termini. The results of these stretches can be seen in Fig. 4.18. In these stretches, just as in the lever-assisted stretches, multiple strands of DNA appear to build up over the course of several repetitions. Applying the WLC model to the data gathered from the fixed-bead stretches resulted in a persistence length value of $63.0 \text{ nm} (\pm 2 \text{ nm})$ and a contour length of $3.35 \mu\text{m} (\pm 0.02 \mu\text{m})$, which is in agreement with the results from the lever-assisted stretches.

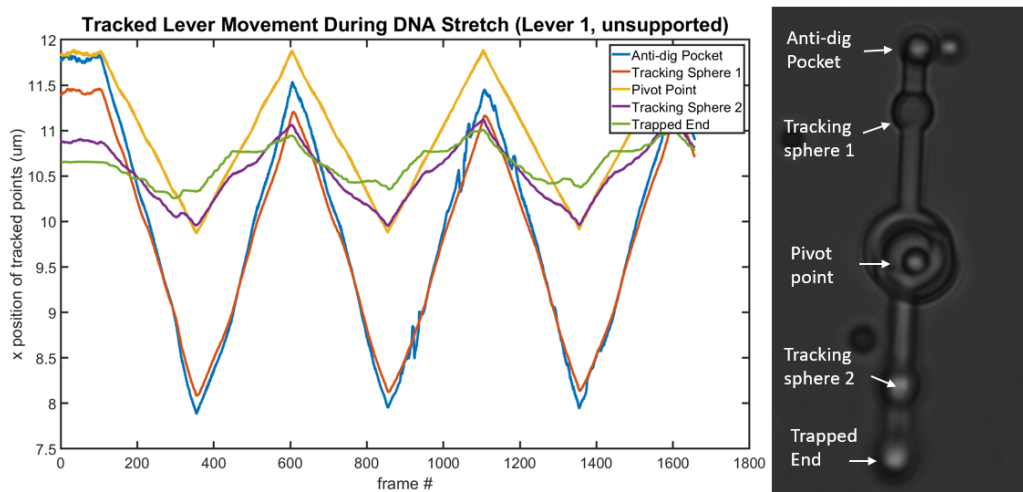


Figure 4.17: It was difficult to perform multiple stretch repetitions with the levers, due to the difficulty of restricting the stretches to a regime that would not pull the streptavidin bead out of the trap, and the possibility of the lever seizing during the stretch. Here a particularly successful lever was tracked, which resulted in three stretch repetitions. A $2.0 \mu\text{m}$, 0.1 Hz triangle wave was applied and data were recorded at 50 fps .

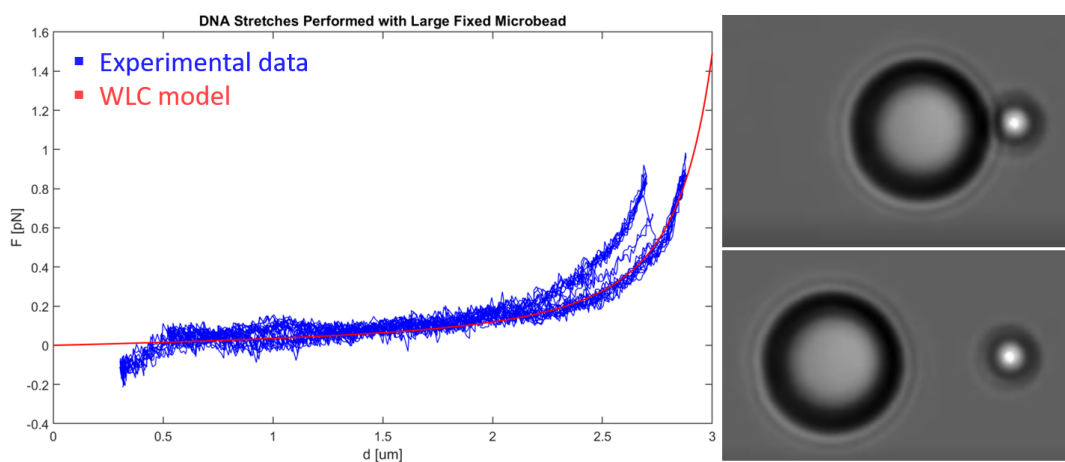


Figure 4.18: Performing DNA stretches with microbeads allowed for a comparison of lever-assisted stretches with a more traditional method, here results are shown for 12 stretches performed using the fixed bead method. The stretches performed using this method show the same kind of multiple-strand behaviour seen in the supported lever results.

4.3.5.4 DISCUSSION OF THE LEVER-ASSISTED METHOD

While this work represents a step forward in the use of micromachines in biological studies there are currently still some limitations and drawbacks to be overcome. Primary among these is that the method is relatively complex and involves multiple steps.

This makes the lever-assisted method currently more difficult than single-trap methods. However, the distinct shape of the lever offers multiple tracking points for image analysis and makes this method a good candidate for automation, which would eliminate a good deal of the set-up difficulty. The simplicity of conventional single-trap stretching methods, such as surface tethering and using micropipettes to actuate stretching are also not without cost, as they mean that the experiment is vulnerable to mechanical drift and noise [1]. However, dual trap methods have been implicated in increasing the risk of damage to the sample, due to the proximity of two traps to the DNA [107, 1]. Our lever-assisted method retains the ability to separate the DNA from the surface, and likewise to isolate it from some of the noise of the mechanical assembly. The end of the dsDNA that is distanced from the trap is also the handle that relies on the weaker antidigoxigenin-digoxigenin (antidig-dig) bond [231], while the microbead that provides the stronger streptavidin-biotin handle remains directly trapped. This could help to mitigate a mechanism for damage based on the irradiation of the antidig-dig bond, although this has not been investigated further.

Like most tools generally used for optical tweezer assays of DNA, the levers are currently one-shot devices. While the microbeads can be removed through sonication, the likelihood of contamination of the lever surface is considered too high for them to be used multiple times for different experiments. However, the small size of the lever, along with the capabilities of the Nanoscribe Photonic Professional, means that several hundred levers can be printed on a single substrate, and these could be pre-functionalised ahead of time, potentially following a process similar to that performed in Aekbote et al. [232]. Functionalisation during manufacture would make them specialised for a certain task rather than the general device that we have presented here, but it would reduce set-up time and researcher effort.

Stretches performed with dsDNA and the protocols used here do also have a limited experimental lifetime. In common with conventional dual-trap assays it is well known that after several hours, it becomes progressively harder to successfully stretch the DNA. However, by introducing the microlevers, another time window during which the experiments have to be completed, also of the order of hours is introduced, during which the levers turn freely before seizing. At the low ionic strengths used in this paper this is not a grievous problem, but the seizing time becomes more problematic at higher salt concentrations.

4.3.6 CONCLUSIONS

In this work we have developed functional microlevers and demonstrated that microlevers have the potential to become a key tool in the development of complex optical microrobotics systems. We developed both supported and unsupported levers for the

task, and both types were successfully used to stretch dsDNA strands. The results were analysed and fit to the WLC, indicating that multi-body micromachines can be used to remotely apply forces with a high degree of sensitivity. Levers are a fundamental machine, and as limiting the exposure of biological subjects to laser light is a key concern, they represent an opportunity to address such concerns in a way that can theoretically be adapted to any optical tweezer setup. Both supported and unsupported levers were used to stretch DNA, but supports carried the risk of producing undesirable scattering effects, leading to less stable trapping and more out of plane movement, while unsupported levers had the advantage of a simpler shape. Additionally, it was shown that the problem of multiple DNA stretches building up could be simply dealt with by lowering the concentration of DNA used, meaning that the potential for this to occur is not a serious drawback of the method. When the results of more traditional microbead stretches were analysed, it became clear that the build up of multiple strands is also present when one of the beads is fixed to the substrate, meaning that it is not unique to the lever-based method. This work can serve as a proof-of-concept for more complex optical microrobotics studies, such as fully-remote, lever-assisted DNA stretches, as well as studies involving force amplification.

4.4 FURTHER WORK

4.4.1 DOUBLE LEVER ASSISTED STRETCHES

Following the success of the lever-assisted DNA stretching method, where one trap was distanced from the DNA by a microlever, it was only logical to attempt what might be called “fully microlever-distanced DNA stretching”. Several attempts were made on this goal, using the optical tweezers system. The initial idea was to simply print two microlevers near each other, in order to facilitate the matching up of the two pocket-ends. Fig. 4.19 shows a DeScribe screenshot of a print job of 20 pairs of such microlevers, while Fig. 4.20(a) shows a close view of such a pair. The microlevers were printed with an offset of $30 \mu\text{m}$ in the Y direction and a $4 \mu\text{m}$ offset in the X direction, to enable the turning of each lever without collisions, as well as allowing the levers to come into contact with each other when microbeads were attached to the pockets, and one lever slightly rotated. The idea was to use the same general protocol as for the single-lever-assisted DNA stretches to perform stretches with levers in this configuration, with the streptavidin beads also attached to a lever. A schematic of the considered set-up is shown in Fig. 4.20(b).

The first problem became apparent when it came to attaching the streptavidin-coated (strep) microbeads to the levers. The shape of the pockets, shown in Fig. 4.21,

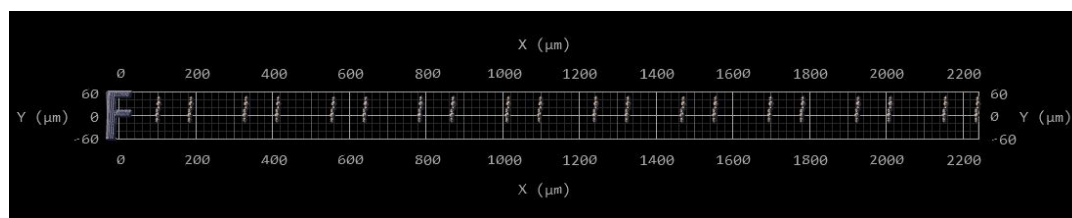


Figure 4.19: In previous work regarding the functionality of microlevers in challenging, salty environments, only a fraction of levers worked well. Therefore, samples were printed with 20 pairs of microlevers to increase the chances that both levers would be able to turn, which is necessary for lever-assisted DNA stretching. A large “F” was printed on all samples over the course of this project, for ease of locating the levers for SEM imaging, and to provide orientation information, as “F” has no rotational symmetry.

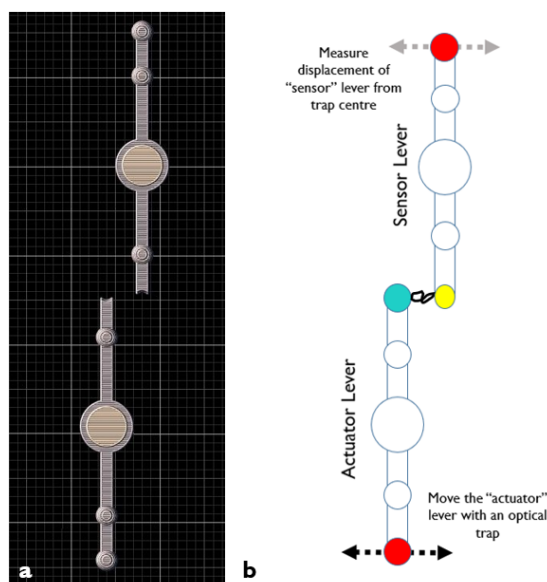


Figure 4.20: (a) Levers were printed with a slight offset ($4 \mu\text{m}$) in the X direction, in order to allow for contact between microbeads when they were attached to the printed pockets. (b) The first concept for double lever-assisted DNA stretches involved trapping the microlevers at the handle furthest from the pockets.

caused there to be significant interference to the trap when guiding the small strep microbeads into the pocket. This resulted in many microbeads being lost when attempting to attach them to the microlevers. Using $2 \mu\text{m}$ diameter strep beads instead seemed to work well, and beads could be attached to both microlevers. This was once again done with a salt concentration of 10% TSB. Stills from successfully moving microlevers with microbeads attached can be seen in Fig. 4.22, showing that this technique seemed to be promising. However, attempts to stretch DNA using this configuration soon showed that the time to perform an experiment was extremely restricted, as both levers needed

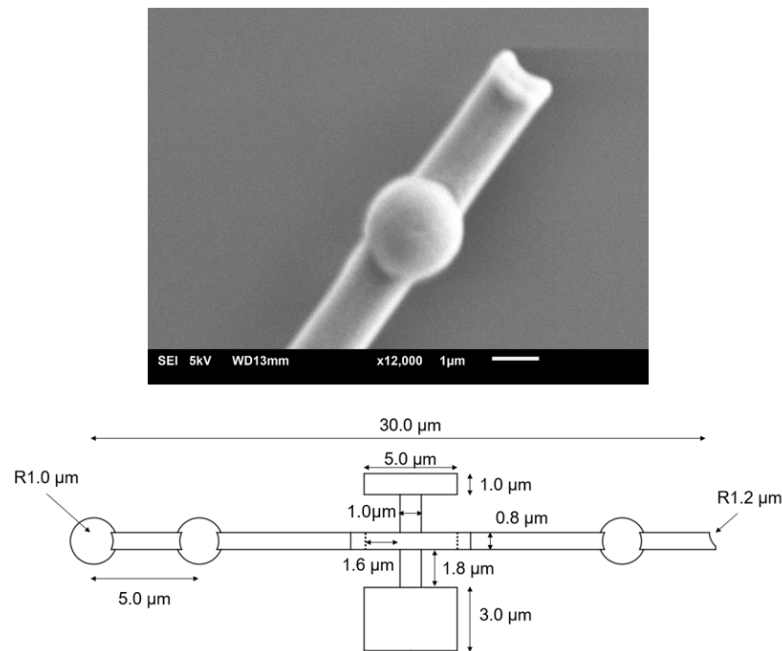


Figure 4.21: Attaching the $1.26 \mu\text{m}$ diameter streptavidin beads to the levers proved problematic due to interference to the optical traps, likely due to the shape of the pockets on the microlevers.

to be free to rotate in order to actuate and register stretches. Additionally, when the microbeads became adhered to each other, connecting the microlevers, it became apparent that the tolerance about the pin-joint, as well as the long distance separating the sensing trap from the “action” meant that little perceptible displacement was registered at the sensor trap. This is shown in Fig. 4.22(d) and (e), and would be particularly problematic when stretching DNA, due to the flexibility of the polymer and the low forces used to stretch it.

Following this discovery, and due to the difficulties posed by using two relatively large and quick-to-settle microlevers, the decision was made to redesign the experiment to incorporate a “half-lever” as a sensor. Additionally, it was thought that using the high powered optical tweezers would help to extend the time it took for the levers to become immobile, as higher forces could be applied ($> 65 \text{ pN}$ compared to the 10 pN that can be applied with the HOT). The steered and fixed elements of the high power trap would then be used to control the levers and to measure the stretch. This would require the steered trap to be manoeuvred at a distance of at least $30 \mu\text{m}$ from the fixed trap, in either the X or the Y direction, relatively close to the extent of the trap’s range of movement. At such a high displacement from its “neutral” position close to the fixed trap, the steerable trap is weaker than it is at the centre of the field of view, and so there was a slight possibility that it would not be possible to sense a stretch using

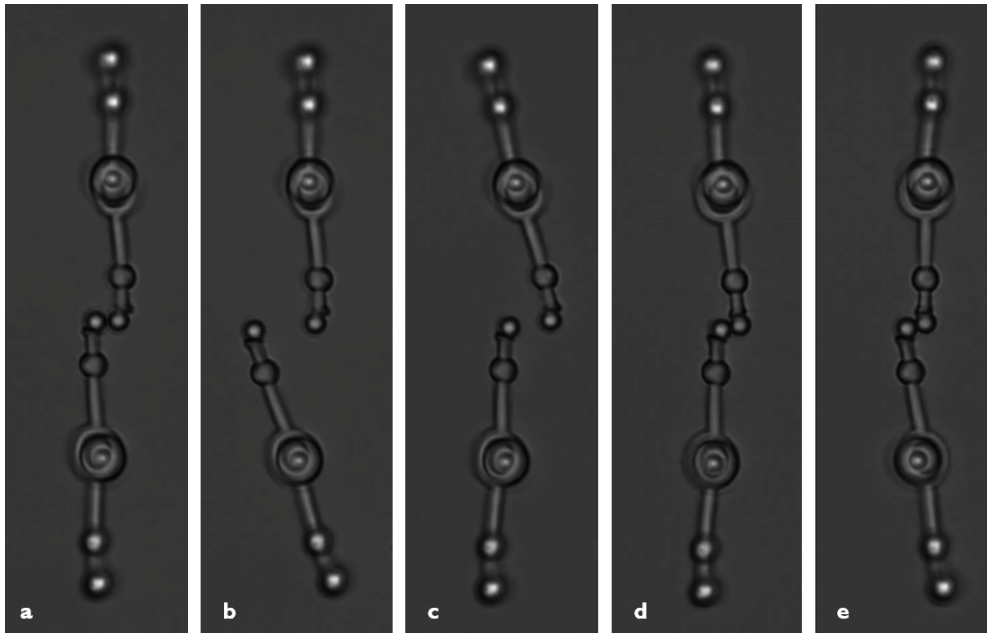


Figure 4.22: Stills taken from a montage of attempted DNA stretching with a double microlever configuration revealed problems with the concept. (a), (b) and (c) demonstrate lever mobility in response to movement of the top (a and b) and bottom (c) traps. (d) and (e) show the microbeads becoming stuck together, an occurrence that revealed the sensor trap’s lack of sensitivity in this configuration.

the fixed trap. Therefore, the design of the “actuator” lever was altered, to create the possibility of force amplification, should that be necessary to register a stretch with the fixed component of the HP trap. The pocket at the ends of the levers was also redesigned to reduce interactions between the pocket and the optical trap when guiding beads into the pockets. Additionally, as the tolerance in the pin joint had been found to be problematic for registering force applied over a long distance, the gap between the inner radius of the lever arm and the centre pin was reduced to $1 \mu\text{m}$ from the $1.6 \mu\text{m}$ previously used, and an area-reducing ridge was introduced to make up for the expected increase in adhesion. The revised design for the sensor and actuator levers can be seen in Fig. 4.23, and an SEM image of a pair of such microlevers can be seen in Fig. 4.24(a). Fig. 4.24(b) also shows the revised stretch concept, which would make use of a “step-up, step-down” force application and measurement configuration. Ideally, the force from the steered trap, shown in violet, would be doubled, and then the effect of this would be easily picked up as a displacement from the distanced fixed trap, shown in red, which would be placed in a mechanically disadvantaged position. Assuming ideal behaviour, this would allow for direct measurement of the forces applied.

Despite the elegance of the idea, it remained to be seen whether the set-up could practically work, and whether the mechanical amplification of forces was indeed so

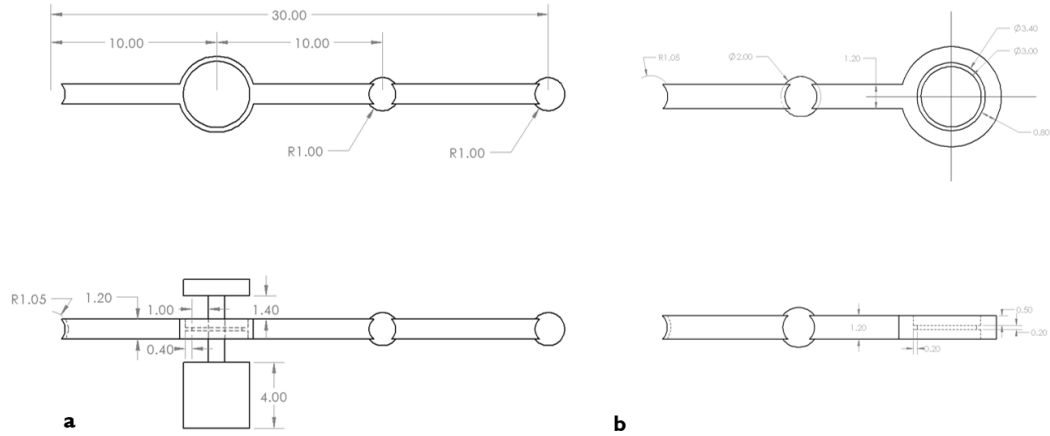


Figure 4.23: (a) The actuator lever was changed to be asymmetric, allowing for the possibility of force-amplification, a thin ridge around the inner radius of the lever arm was added to try to increase the time that the lever remained functional for, and the lateral and vertical gaps were decreased in order to try to reduce tolerance in the pin joint. (b) The sensor lever was changed to a “half lever” with the same lateral gap as the actuator lever, as well as an area reducing ridge. Both the actuator and sensor levers were printed with “centred” pockets, in the hope that this would make bead attachment quicker and easier.

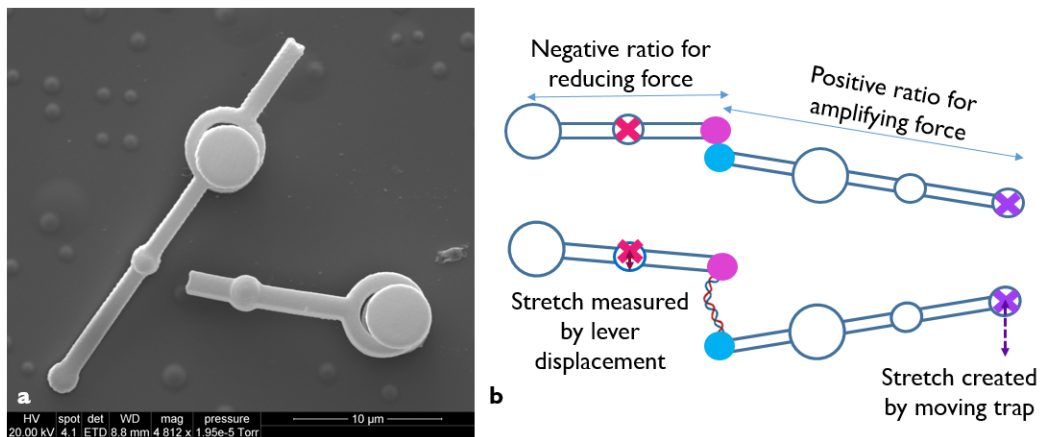


Figure 4.24: (a) An SEM image of the new paired levers for attempted double-lever-assisted DNA stretching. The clear radius of the pockets was especially good to see. (b) The concept for the stretch included making use of the ratios between the distance between the force application points (the microbeads) and the trap positions from the lever axes.

straightforward. The differently shaped pockets made the attachment of microbeads easier, potentially due to less interference with the optical trap, but the beads appeared to be less strongly adhered. This made setting the levers up to attempt a stretch somewhat difficult, especially because, in order to avoid confusion between the similarly sized strep and AD microbeads used ($2\ \mu\text{m}$ and $2.12\ \mu\text{m}$ diameter respectively), the beads were added at different times. The addition of microbeads disturbed the droplet of liquid, which occasionally caused microbeads to detach from the levers, and this was also a problem when additional liquid was added to compensate for evaporation. The issues with microbead adhesion led to the decision to increase the ionic strength of the medium from 10% to 20%, in the hope that this would improve bead adhesion to the pockets. The weaker adhesion between the microbeads and pockets was likely due to the smaller overlapping area in the new pockets, compared to previous iterations. Additionally, the centering of the pockets meant that as the “sensor” lever settled to the substrate, it was more likely that the microbead would become stuck to the substrate, and then lost, and this was a common occurrence over 11 samples, each printed with 20 pairs of levers. While it was possible to set the levers up in the configuration required to perform DNA stretches, using the high powered traps meant that there was far less flexibility when attempting to set up the experiment, which resulted in non-ideal starting configurations, as shown in Fig. 4.25. Additionally, despite successful set up in four cases (out of 220 lever pairs), no successful DNA stretches were recorded. It is possible that this could have been due to confusion between the strep and AD beads, and if such a mix-up occurred then it was possible that there was no DNA to form tethers between microbeads. Nonetheless, it may be possible that this technique can be adapted to produce successful stretches in the future. Additionally, the recent work of Dr Allan Raudsepp in determining a system for fitting stretches involving multiple DNA strands to an adapted WLC model means that even non-ideal results, such as those seen in the supported-microlever stretches from the article “Optical Microlever-Assisted DNA Stretching”, could be compared with conventional stretching techniques [233]. Such comparisons would allow for easier interpretation of the multi-molecule, non-ideal stretches that are likely to result from double-lever-assisted DNA stretching, making it more worthwhile for researchers to pursue remote DNA stretching methods.

4.4.2 MEASURING FORCE AMPLIFICATION USING DNA STRETCHING

As has been previously mentioned, the use of PCR to synthesise and copy specific lengths of DNA, and robust models for its force-extension behaviour, make DNA a useful molecule for metrology on the micro-nanoscale [32], as identical molecules can be reliably produced. Therefore, following the failure of the double-lever DNA stretches,

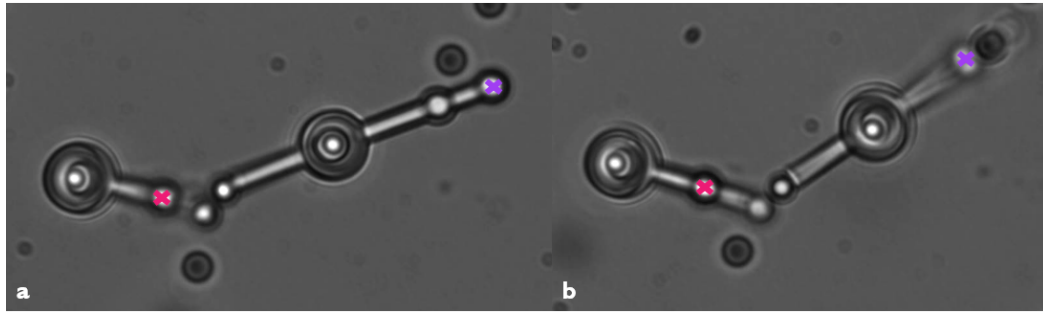


Figure 4.25: The comparative lack of flexibility of the high power optical tweezers, compared with the holographic optical tweezers, meant that the levers started in non-ideal positions (compared to the horizontal starting point imagined in Fig. 4.24. Fixed trap position is shown in red, while the steered trap is shown in violet. (a) The difference between the Z position of the fixed and steered components of the trap means that when the steered position is aligned with the camera focus, the fixed trap is out of focus. Here the bead attached to the sensor lever was actually stuck to the underside of the lever rather than perfectly in the pocket, meaning it remained somewhat in focus. (b) In this image the handle mid-way along the lever is being used to control the position of the sensor lever, which seems to allow for better matching of the microbeads in the lever pockets. However, it results in more out-of-plane movement of the microlever overall.

an attempt was made to measure amplified forces using the extension of DNA to validate amplification. The set-up was similar to that used to produce the original lever-assisted DNA stretches, with a $1.26 \mu\text{m}$ DNA-incubated streptavidin microbead held in a fixed optical trap, and the microlever swung to produce a stretch. However, rather than using the piezomotor stage to swing the microlever, or even using the steered component of the high powered trap, the holographic optical trap was used to move the microlever to try to create a stretch. The concept was that, with an unamplified force, such as that applied at the “intermediate” handle, the force from the holographic trap would be insufficient to pull the strep bead out of the high power trap, and instead a deflection of the microlever out of the HOT trap would be seen. However, if amplification was successful, then it could be possible to create deflection from the high powered trap, and measure the stretch from this deflection. A diagram of this concept is shown in Fig. 4.26, where the holographic trap is shown in violet, and the HP trap is shown in red.

Two more samples were printed with the pairs of levers that had been intended for double-lever stretching, and the sensor levers were removed during turn-testing, using a borosilicate microprobe. The leftover levers, with a 2:1 lever arm ratio for force amplification, were then loaded with antidigoxigenin coated beads ($2.12 \mu\text{m}$ diameter) and $1.26 \mu\text{m}$ streptavidin beads were incubated with DNA using the same method described for the previous lever-assisted stretches. The steered part of the high power

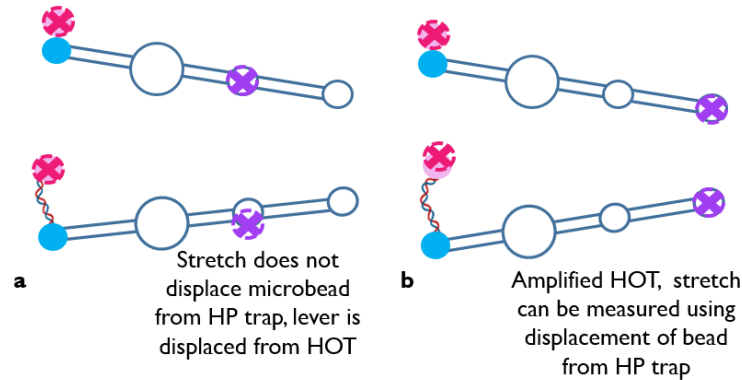


Figure 4.26: Single-lever DNA stretching, with the option for force amplification was seen as one way to investigate the use of DNA as a metrology standard, and to test the amplification abilities of the microlevers. (a) The expected scenario with an unamplified HOP trap: the force is too low to displace the strep bead from the HP trap, and a low-force stretch, as well as displacement of the lever, is the result. (b) Moving the HOP trap so that it has a mechanical advantage against the HP trap was thought of as a method to amplify forces, hopefully allowing for force measurement based on displacement from the HP trap.

trap was blocked off, and the HOP trap was used to pass a streptavidin bead into the high powered trap, after the levers had been manoeuvred into place using the HOP trap and the piezomotor stage. However, the experiments did not go further, as the strength of the high power trap consistently pulled the levers into the trap when the pocket containing the AD bead was moved towards the strep bead in the trap to try to form a tether. This can be seen in Fig. 4.27, along with another problem associated with the high power trap: the tendency for more than one strep bead to be trapped at a time, resulting in what looks like an out-of focus trap, due to the formation of a dimer. The lowest power that could be supplied to the high power trap in its current configuration was 0.5 W, which still resulted in an extremely high trap stiffness- dozens of $\text{pN}/\mu\text{m}$ - when compared to that of the HOP trap, and this was most likely the reason that this occurred. At such a high trap stiffness, the method for measuring stiffness by monitoring the restricted Brownian motion of a trapped bead becomes unreliable [145], and the stiffness of the trap made it unlikely that any amplification of the HOP trap would actually be measured. Therefore, it was decided to abandon this experiment for the time being, and to focus purely on measuring force amplification with the microlevers, in order to better understand the process.

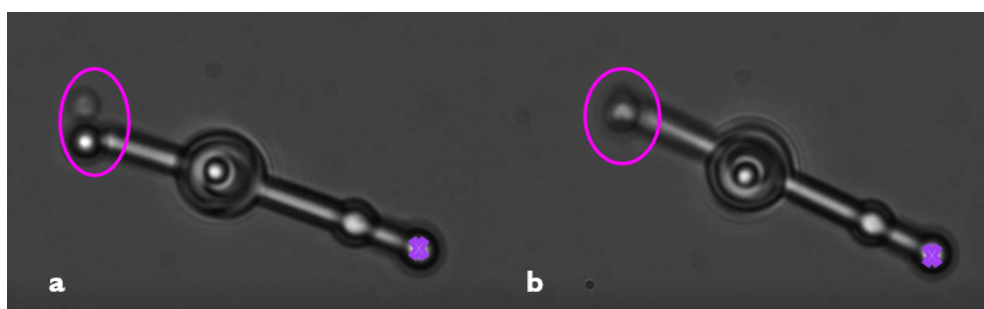


Figure 4.27: Attempting to perform DNA stretches using the HOT to move the microlever, and the high power tweezers to trap a free streptavidin bead did not work well. (a) The high power of the optical trap resulted in multiple beads being trapped at once, leading to the seemingly out-of-focus trap seen here, and making alignment with the levers difficult (circled in magenta). (b) Like free microbeads, the levers themselves were pulled into the high powered trap when alignment with the trapped strep beads was attempted (circled in magenta). Position of the holographic trap is marked by a violet “x”.

Chapter 5

GIVING OPTICAL TWEEZERS A MECHANICAL ADVANTAGE

Following the decision to abandon attempts at double-lever and lever-amplified DNA stretching, which were discussed in Chapter 4, focus shifted to showing that force could be amplified using a simple microlever. Force amplification in the literature relied upon high power optical tweezers, which could be used to compress 3D printed elastic joints and springs over micrometres [57, 56]. Such results would not be possible with the optical tweezers used for this project, as discussed in Chapter 3, when the possibility of printing elastic joints was examined. Additionally, while DNA could be thought of as a spring, and stretching would produce results which could be measured with the optical tweezers, the previous chapter demonstrated that performing such stretches was a considerable challenge. One of the major issues with attempting to measure force amplification through DNA stretching with the optical tweezers used for this project was the extreme differences in force that can be produced by the holographic and high power traps. It was apparent that the high power trap would need to be attenuated to lower forces, so that amplification of the holographic forces could be demonstrated. Additionally, the separate optical paths of the holographic and high power optical tweezers allowed for the attenuation of the high power laser, separate from the holographic tweezers, allowing the HOT traps to operate at full strength while the HP traps were weakened. Therefore, a Schott glass neutral density filter (OD 0.6, ThorLabs, Chicago) was placed in the optical path of the high power trap, in order to reduce the power of the fixed optical trap.

The 2:1 lever arm ratio of the microlevers to be used for force amplification meant that the microlevers tended to settle unevenly after development, with the longer side

resting on the substrate. In some cases, particularly when using flattened or misshapen spheres as potential trapping handles (as a result of low laser powers being investigated in the printing process) stable trapping of the microlevers was difficult to achieve, and shifts in focus were noticeable over time. While the problem of flattened spheres could be dealt with during printing by using the “adaptive” slicing method ($0.02\ \mu\text{m} - 0.1\ \mu\text{m}$), adding a contour and using appropriate laser power, this led to an investigation into the effects of optical trap handle shape for the microlevers. This investigation formed part of the following paper, which was accepted for publication as part of the proceedings of MARSS 2022 (International Conference on Manipulation, Automation and Robotics at Small Scales). I was primarily responsible for the conceptualisation, planning, experimental work and analysis, as well as for writing the main draft. Allan Raudsepp assisted with the conceptualisation and with the experiment set-up, while Daniel Fan also assisted with conceptualisation. Volker Nock produced some of the nanolevers used for this study, and Urs Staufer, M. A. K. Williams and Ebu Avci were responsible for supervision.

5.1 DEVELOPING AN OPTICAL MICROLEVER FOR STABLE AND UNSUPPORTED FORCE AMPLIFICATION

Optical micromachines have the potential to improve the capabilities of optical tweezers by amplifying forces and allowing for indirect handling and probing of specimens. However, systematic design and testing of micromachine performance is still an emerging field. In this work we have designed and tested an unsupported microlever, suitable for general-purpose optical tweezer studies, that demonstrates stable trapping performance and repeatable doubling of applied forces. Stable trapping was ensured by analysing images to monitor focus shift when levers oscillated repeatedly, before the best-performing design was selected for force amplification. This study also shows that direct measurement of trap stiffness using the equipartition theorem appears to be a valid method for measuring applied forces on the spherical handles of microlevers.

5.1.1 DECLARATION

©2022 IEEE. The following is the accepted version of the article written for MARSS 2022, which will be published in the official conference proceedings. This article was coauthored with Dr Allan Raudsepp (assistance with optical tweezers setup and experimental conceptualisation); Dr Volker Nock (access to the Nanoscribe PPGT2 and SEM, as well as printing some of the microlevers used for this study); Dr Daniel Fan (help with the initial microlever design); and Prof.dr. Urs Staufer, Prof. Martin A. K.

“Bill” Williams and Dr Ebubekir Avci (supervision and funding), with assistance in interpreting results from Dr Avci and Prof. Williams.

5.1.2 INTRODUCTION

Optical tweezers have proven to be a useful technology for investigating the effects of minuscule forces on biological specimens [92]. Investigating mechanical changes in cancer cells [234], examining enzyme activity [235], and stretching single molecules [236] are just a few of the studies that have been enabled by optical tweezers. However, there are two major drawbacks to optical tweezers: the potential for damage to biological samples, due to the intensely focused laser used to create the traps; and the low limit to forces that can be applied (tens of femto-Newtons to hundreds of pico-Newtons) [98].

There are several strategies that have been proposed to reduce damage caused by optical tweezers. These traditionally include the introduction of scavenging species to deal with free radicals generated during trapping [108], careful selection of the laser wavelength to limit absorption [237, 199], and limiting the laser power to reduce overall exposure. Indirect manipulation has also been utilised, which has the added bonus of allowing researchers to examine specimens that cannot be trapped with traditional Gaussian beams, such as DNA, which is below the diffraction limit [236], large, flat objects that scatter the beam [238] and complex biological cells with varied refractive indices [232].

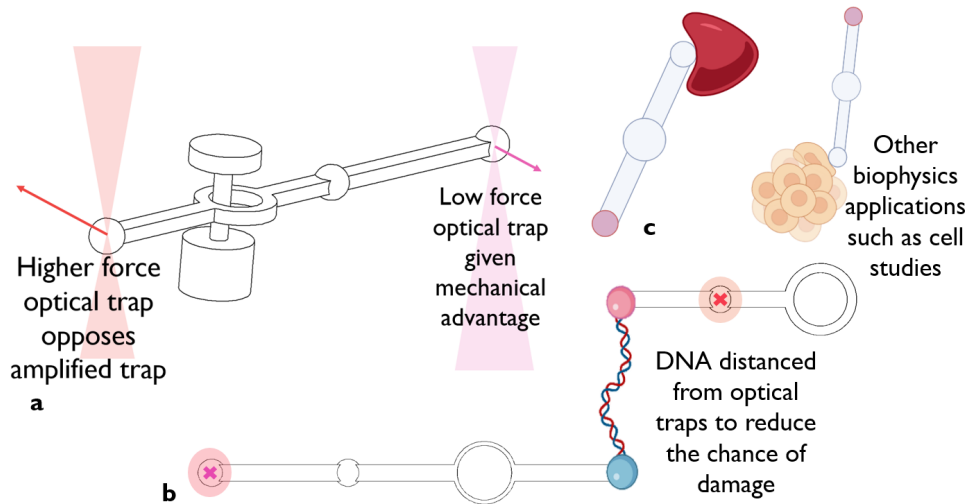


Figure 5.1: Our experiment uses a two-trap set-up to test and quantify optical force amplification (a), with the hope that such levers could become useful tools in areas such as molecule stretching (b) and cell studies (c).

The past 20 years have brought advances in micro-manufacturing for optical micromachines, particularly the use of two-photon absorption polymerisation (TPAP) to

facilitate laser-based, nanoscale 3D printing [239]. This has allowed the tools for indirect manipulation of biological specimens to advance beyond microbeads to more complex shapes [227] and even multi-body micromachines [222]. Using micromachines as end-effectors for optical tweezer studies also introduces the opportunity to tackle the problem of limited forces, as well as the damage associated with trap proximity [5], through giving optical traps the mechanical advantage [56, 57]. In Fig. 5.1 we have illustrated our method to test force amplification of unsupported levers using two optical traps of different strengths, as well as some applications where distancing the optical traps, and potentially amplifying force, would be useful.

While the multiplication of optical force has been demonstrated, and optical micromachines have been used to perform a few tasks, systematic analysis of optical microrobots is still in its infancy. Analytical models of optical trapping forces are known to be relatively simple when the trapped particles fit in the dipole [66] or ray optics regimes [63]. Even so, these models require exact knowledge of the optical trapping set up, which may not be available to every user, and the majority of strongly-trapped (and therefore useful) objects are of intermediate size, similar to the trapping wavelength. Likewise, forces on spheres which fall within the intermediate size range can be calculated using Mie theory, but producing a quantitative result is non-trivial, and complexity increases for non-spherical objects [240].

One popular way to calculate forces on non-spherical objects is to define a transformation matrix (T-matrix) that describes how an object scatters the incoming electromagnetic wave, in order to extract forces by comparing incoming and scattered waves [241], and computational toolboxes have been developed for this method [242]. However, for scientists undertaking inter-disciplinary research, a more practical method is to accept a Hookean spring model of optical tweezers. This allows the researcher to simply take calibration measurements of trap stiffness and forces based on restricted thermal diffusion of trapped particles [243] or of forces generated in competition with known Stokes drag forces through monitoring particle velocity [193]. This gives good results for spherical objects, and can be used to determine the relationship between laser power and optical tweezers force. Comparison of the stiffness measurement and drag force methods also show that they are in good agreement with each other, leaving the choice of method up to the researcher [193].

In previous works involving micromachines, calibration on spherical particles has been used to find a relationship between optical force and supplied laser power. It has then been assumed that this relationship between power and force is exactly maintained when a spherical handle on a lever, rather than a single particle, is trapped [56, 244, 245]. Some studies, such as one involving 3D printed optical gears, do not attempt to quantify

the forces used at all, and instead use successful movement of the machine as proof-of-principle that amplification of optical forces can occur in this way [246]. Several lever-based studies have used a spring, fabricated through TPAP to measure the resulting forces after amplification [56, 57]. While this is an excellent way to demonstrate both the amplification of force and the capabilities of TPAP, it means that only amplification of high powered optical tweezers can be demonstrated, as lower power optical tweezers lack the stiffness required to compress the polymer. Such springs also act to restrict the motion of the lever, ensuring motion remains in the plane of force application, but restricts direct application of such tools. Removing the spring to create a general-purpose lever means that stable optical trapping of the tool becomes crucial.

In this article we cover the design and characterisation of levers to be used for force amplification, using the Nanoscribe Photonic Professional GT2 (PPGT2) (Nanoscribe GmbH, Karlsruhe, Germany) and the IP-L 780 photoresin, also from Nanoscribe. These levers were used to demonstrate force amplification using two optical traps: an adjustable holographic optical tweezers (HOT) trap, controlled using the Red Tweezers software from Bowman et al. [174] and a fixed trap, capable of applying much higher forces. In contrast to earlier studies, our levers are completely unsupported, and the pivot point is created by mechanical contact between the central pin and the lever arm, rather than the lever being held in place by a spring. In addition, we have compared the trapping stability offered by differently shaped “handles” on the levers, as well as the impact of reducing separation between components, by analysing changes in image quality over cycles of lever oscillation. This work shows the capability of well-designed optical micro-levers to amplify even low forces, in contrast with previous studies, which used extremely high-powered optical tweezers to actuate micromachines. As TPAP is an extremely versatile technique, which can be used to create complex geometries, a general purpose lever such as this can be easily adapted for different biological studies. An example of such an adaptation can be found in our previous work [222], where a pocket was printed at one end of the lever, for the attachment of a functionalised microbead.

5.1.3 LEVER DESIGN

The lever is a classic machine for amplifying mechanical forces, and examples can be found everywhere in engineering and in nature. To amplify forces, there needs to be a greater distance between effort and pivot compared to that between the pivot and the output force. Therefore, the first step of this work was to design a basic lever that rotates around a central pin, with one side of the arm twice as long as the other. This should allow for a doubling of the input force, assuming no losses, and a drawing of the basic lever is shown in Fig. 5.2, where dimensions are shown in micrometres.

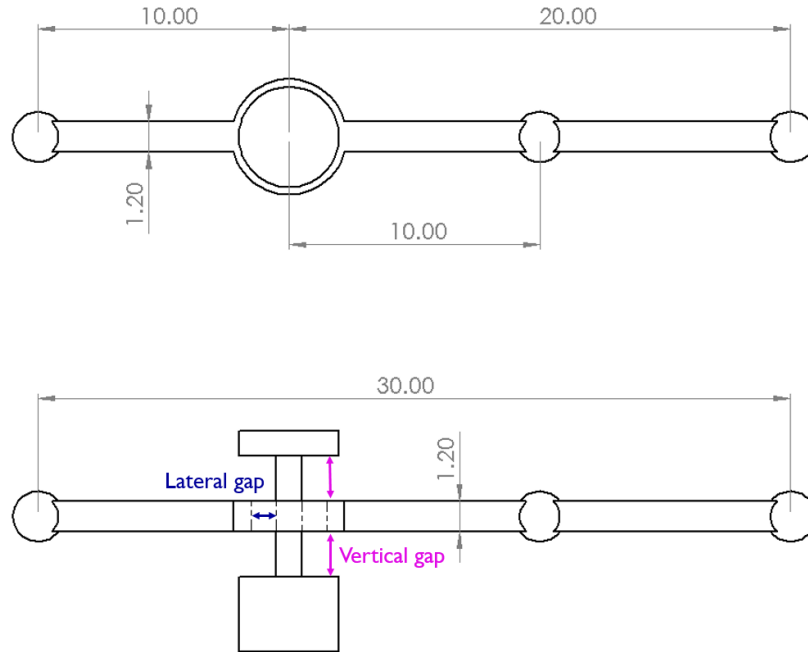


Figure 5.2: The basic design for levers in this work featured an “effort arm” twice as long as the shorter “output arm”. The longer side also featured two spherical handles, to be used for optical trapping, to allow for comparison between force applied with an equal lever arm ratio and a force applied using the 2:1 arm ratio. The lateral and vertical gaps, shown in dark blue and magenta respectively, are important for the functionality of the lever, as inadequate separation between parts leads to a greater likelihood of adhesion between parts.

While this is an extremely simple concept, the prevalence of surface forces contributing to adhesion at the microscale means that even ensuring the lever will rotate is a relatively difficult task. Attractive forces on the microscale are associated with small separation distance and large overlapping area between objects, so introducing large gaps between parts, and minimising the overlapping area both seem like appropriate first steps when creating functional micromachines [140, 184]. However, in this case, the goal is to demonstrate effective multiplication of force, which requires some contact between the pin and the lever arm. Therefore, the tolerance around the pin joint, which is required to ensure the clean printing of two parts, and to increase the likelihood of turning, poses a challenge to force multiplication. In short, the joint needs to have enough tolerance to print correctly, enough contact to multiply force, and low enough friction so that it does not prevent the lever from turning. In previous studies [56, 245] the problem of pin-joint tolerance and internal friction was dealt with by introducing a spring, which held the lever at an appropriate pivot point and showed force amplification through its compression and extension. In our work, joint tolerance has been improved by limiting the gap around the centre pin to $1.0 \mu\text{m}$, which was

the smallest lateral gap that led to 100% of the levers in a printed batch being able to rotate in milliQ water.

The choice to use a small lateral gap contrasts with our earlier work [184], where a gap of $1.6 \mu\text{m}$ was used, in order to increase the chances of rotation in high ionic strength environments. However, in that work the primary motivator for such a large gap was to decrease the overlapping area between the pin and the lever arm. A short test using a very large centre pin and levers with four different lateral gap sizes was used to validate that the previous success of designs with large lateral gaps was likely due to reduction in overlapping area rather than the increase in part separation, as shown in Fig. 5.3. Decreasing the diameter of the centre pin to $4.0 \mu\text{m}$ from the $6.0 \mu\text{m}$ diameter used for this test was then sufficient to improve rotation success to 100%. While the parameters used for this study were sufficient to produce 100% successful levers in each test batch of 10 levers, fabrication windows for the PPGT2 may change over time, requiring dose-testing and adjustment.

The levers have a very high aspect ratio (a length:width/thickness value of 25 for the lever arm) meaning that stable optical trapping is a challenge, due to the tendency of optically trapped objects to align their longest dimension with the axis of the trap. This is partially addressed by leaving the centre pin of the lever fixed to the substrate, rather than entirely detaching it. However, some movement of the lever out of the trap centre will still be seen, and it is our wish to mitigate this as much as possible. One method is to change the size and shape of the printed handles, using the intuitive understanding that flatter surfaces lead to more scattering interactions with the trap, which decreases the apparent strength of the gradient force. By making the handles larger, the difference in geometry between the spheres and the rest of the lever arm becomes more pronounced, which is also true if we elongate the handles, making them spheroids rather than spheres by design. Therefore, in this work we have produced levers with $2 \mu\text{m}$ and $3 \mu\text{m}$ diameter spherical handles, as well as levers with elongated spheroidal handles, which have a long axis of $3 \mu\text{m}$, and a short axis of $2 \mu\text{m}$. These different lever handles are shown in Fig. 5.4.

Additionally, a reduction in the vertical gap between the centre pin and the lever arm was explored. Similar to the lateral gap size, the decision was made to produce some levers with a vertical gap size of $1.4 \mu\text{m}$, compared to the larger gap of $1.8 \mu\text{m}$, as this was found to be the smallest vertical gap at which 100% rotating, 10-lever batches could be produced. The varying features of the chosen lever designs are explained in Table 5.1. All levers had a vertical projected area of $5.5 \mu\text{m}^2$ and a 200 nm thick ridge on the inside radius of the lever arm, in order to reduce the area in contact with the centre pin.

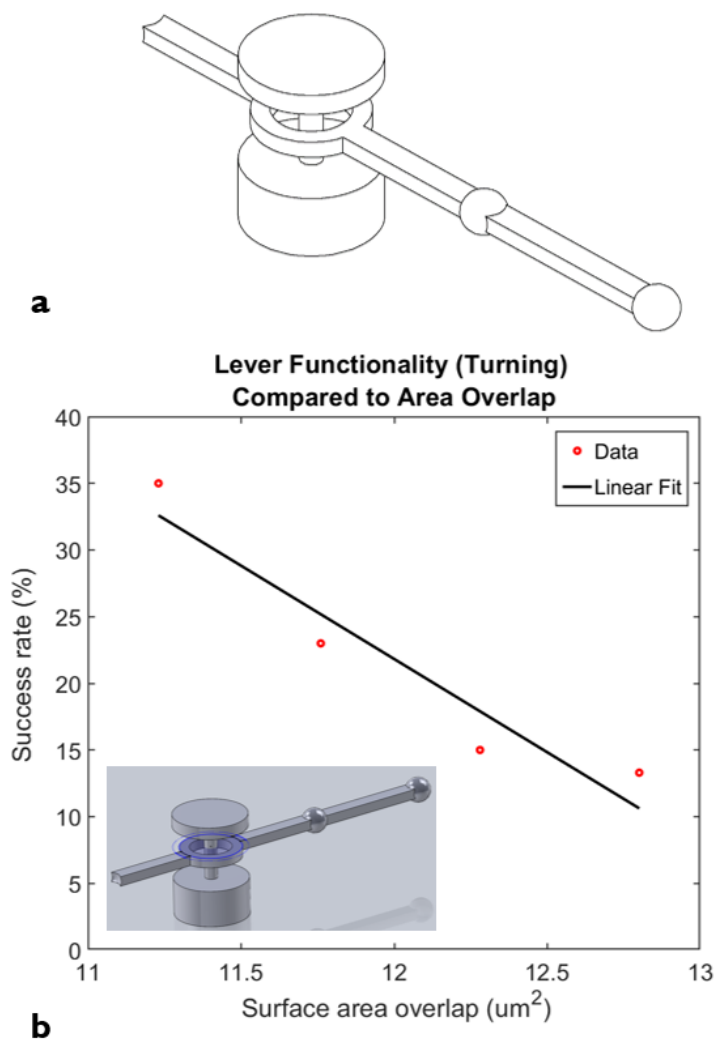


Figure 5.3: A short test using a series of levers with outsize centre pins (concept shown in a) showed a decrease in success rate with increasing area (b), despite the levers with larger area also having larger lateral gaps. Gap size was incremented by $0.2 \mu\text{m}$, from 1.0 to $1.6 \mu\text{m}$. Overlapping area was calculated per the shaded area shown in (b, inset), based on the projected vertical area of the lever arm on the pin, when in a perfectly centred position.

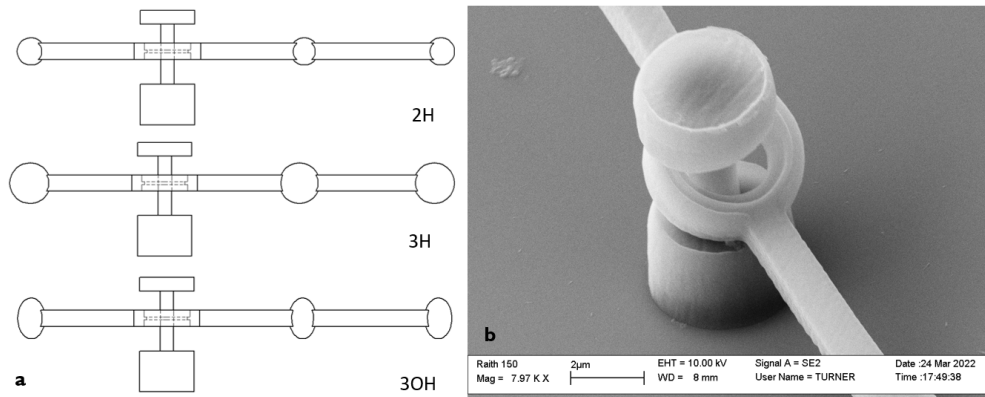


Figure 5.4: (a) The levers used for this study had different handle shapes, which were referenced by 2H, 3H or 3OH in the naming convention used. (b) an SEM image showing the successful printing of the ridge that was used to reduce contact between the centre axis and the inner radius of the lever arm.

Table 5.1: Variable features of the levers used in this work.

Lever Name	Vertical Gap (μm)	Handle Shape	Handle Diameter (μm)
1014 2H	1.4	Spherical	2.0
1014 3H	1.4	Spherical	3.0
1014 3OH	1.4	Elongated Spheroid	3.0/2.0
1018 2H	1.8	Spherical	2.0
1018 3H	1.8	Spherical	3.0
1018 3OH	1.8	Elongated Spheroid	3.0/2.0

5.1.4 OPTICAL TWEEZERS SET-UP

The experiments for quantifying out of plane movement and amplifying force were both based around a Nikon Eclipse TE2000-U inverted microscope, mounted to a vibration isolation table. The microscope was equipped with a 1064 nm, 2 W maximum power laser for creating holographic optical tweezers (Arryx, Chicago, USA) and a 1030 nm, 5 W maximum power laser for creating a single, fixed trap in the centre of the imaging plane (Arryx, Chicago, USA). These lasers were focused through a 60x, 1.2 NA plan apo water immersion objective (Nikon) to create optical tweezers.

The fixed optical trap provides much higher optical forces than the holographic optical trap- approximately 6x higher [222, 145]. The power of the fixed trap was attenuated using a neutral density filter (OD 0.6), in order to measure the force amplification by limiting the force to approximately twice as high as that which can be achieved with the HOT. Without attenuating the fixed trap, it would be too stiff to measure force amplification at the 2:1 mechanical advantage trialled here. The holograms for the HOT were created using a Boulder Nonlinear Systems spatial light modulator, and

placed using the Red Tweezers software. A piezo-motor stage (Physik Instrumente, Karlsruhe, Germany) was used to position the sample relative to the 1030 nm trap. Experiments were performed in bright field conditions, and images were captured using a high speed sCMOS camera (CC215MU, ThorLabs, USA). The microlevers were rotated using a borosilicate microprobe mounted on stepper-motor stages (TAMM40-10C and OSMS60-5ZF, Sigma-Koki, Japan), prior to the experiments, to ensure the levers were free-floating and able to rotate. A diagram of the set-up is shown in Fig. 5.5.

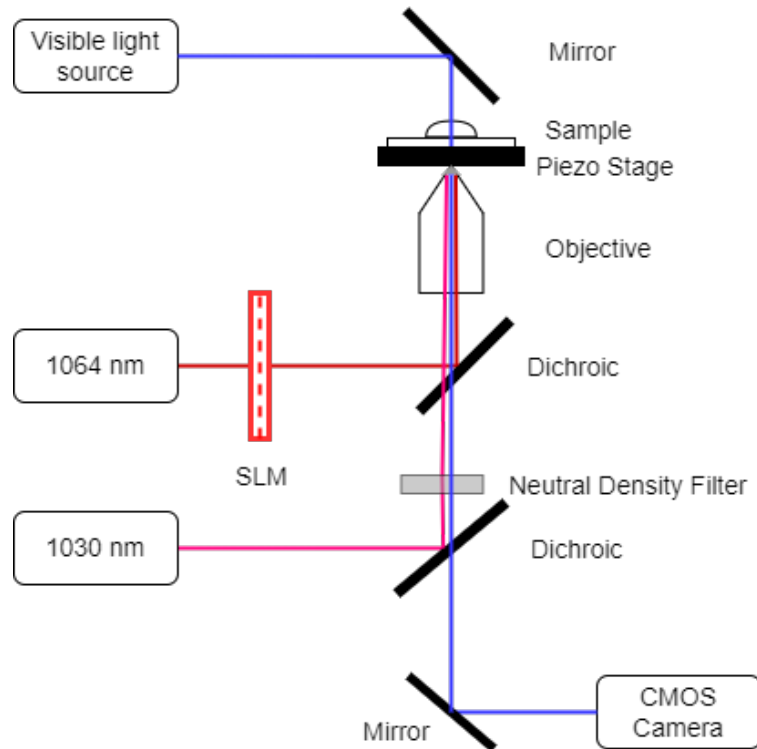


Figure 5.5: The setup was equipped with two lasers for creating separate optical traps. This forms two optical tweezers: one holographic and dynamic and the other fixed. The fixed trap was attenuated using a neutral density filter.

5.1.5 EXPERIMENTATION AND RESULTS

5.1.5.1 QUANTIFYING OUT OF PLANE MOVEMENT

Confidence in the results from force-related experiments performed using optical tweezers can be improved if the motion used to apply the force is restricted to the x-y plane, where it can be directly observed using a conventional microscope. This is relatively simple when using microbeads to apply force, as the focus of the optical tweezers can be adjusted to coincide with the focus of the camera used to image the experiment. In our system, despite the use of two separate traps, the matching focus is created by

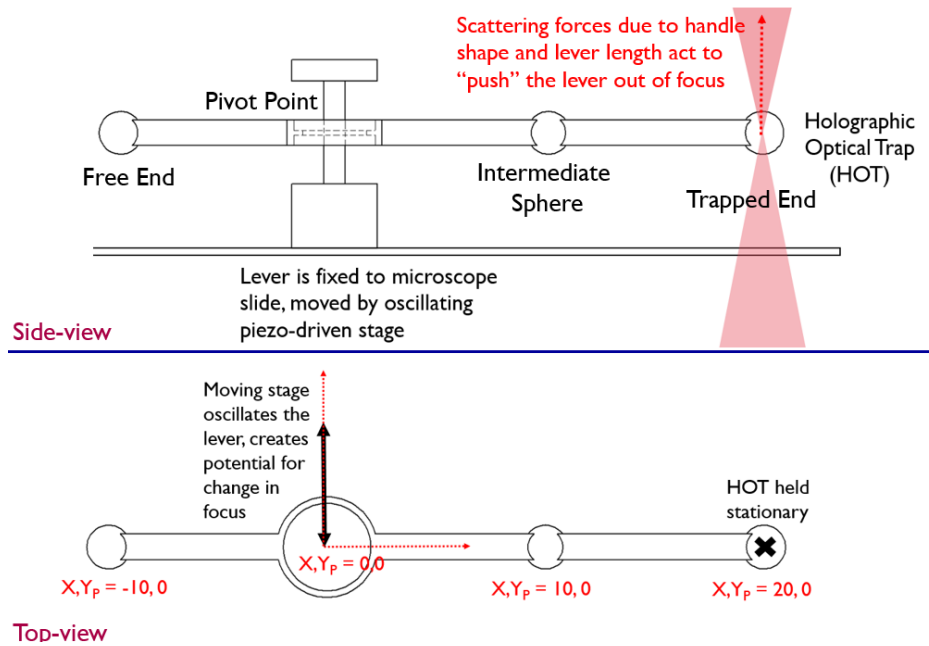


Figure 5.6: The levers were oscillated in the Y-direction, for 10 cycles using the piezo stage, with the goal of monitoring out-of-plane movement over the course of these oscillation.

adjusting the height of the sample using a piezo stage, and the height of the HOT, while the position of the 1030 nm trap is fixed. However, despite the careful adjustment of focus, maintaining in-plane motion over the course of an experiment is a challenge.

In order to quantify the out-of-plane movement of the different lever types, the levers were oscillated using a sin-wave applied via the piezo-stage (frequency = 0.2 Hz, amplitude = 2.0 μm), while trapped by the HOT as shown in Fig. 5.6. The experiment imaged at 100 fps using the ThorLabs CC215MU camera and it was assumed that a change in Z-position of any part of the lever would result in a change in focus, which could be detected using changes in pixel intensity values. Obviously, a change in position of the lever in-plane also results in a change in intensity values, and so images in the sequence are compared with others showing the same lever position. Two positions were chosen: the stationary “flat” lever at the start of an oscillation, and the “rotated” lever at the peak of the oscillation. The frames were easily selected by tracking movement of the lever’s centre pin, or pivot point, over the course of the experiment, as shown in Fig. 5.7 and selecting frames at the peaks and the troughs of the resulting wave.

Once frames were selected, evenly spaced rows of pixels were compared with those in the other frames corresponding to the same lever position. The Image Quality Method described in [247] was used to quantify the focus shift between frames, namely by calculating the Pearson correlation of the vectors of Fourier power spectra corresponding

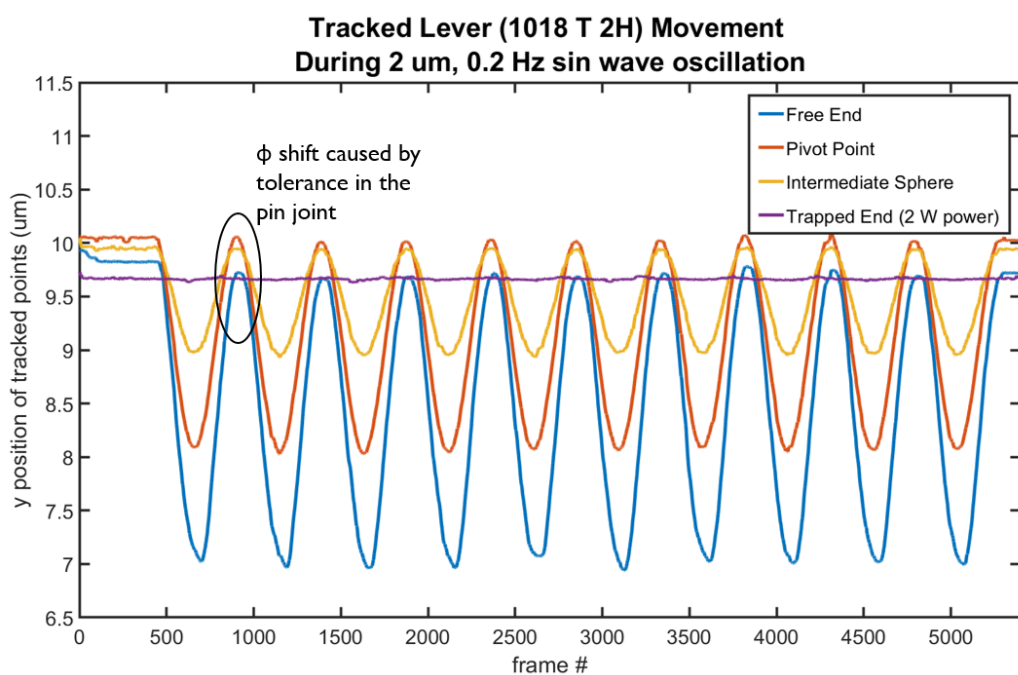


Figure 5.7: Tracking the movement of the lever over the course of the experiment provided an easy method for selecting frames to compare to each other. In this case 100 frames were selected from the peaks and the troughs of the pivot's movement, respectively. This plot also shows the inconsistent phase shift between the free end of the lever and the oscillating pivot, which is attributed to the tolerance of the pin joint.

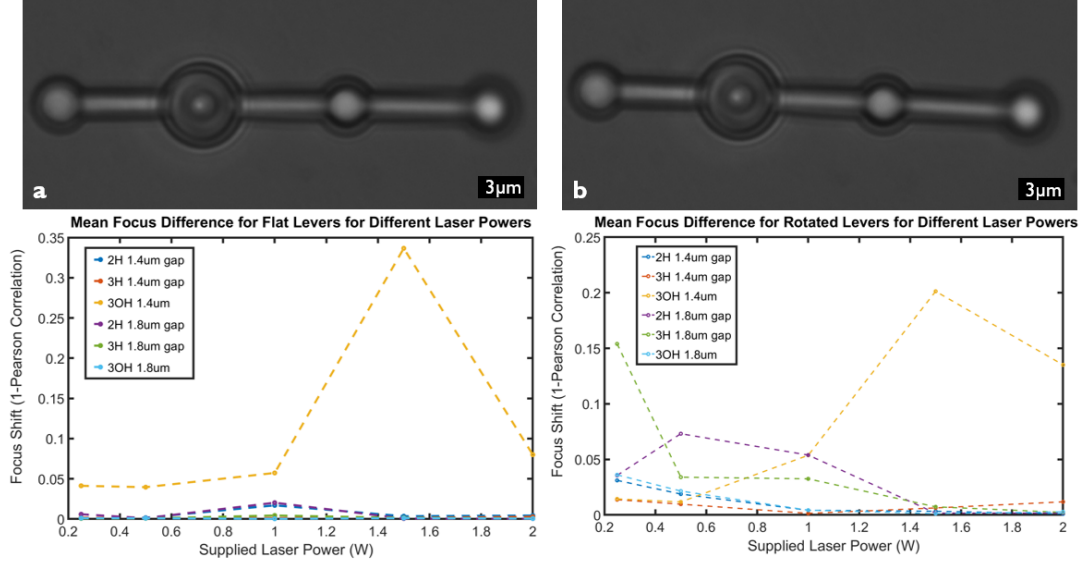


Figure 5.8: Strips across the image were used to quantify a change in focus as the levers were moved back and forth to test trap stability. Correlation of the Fourier power spectra of these strips was calculated for the “flat” (a) and “rotated” (b) cases, which corresponded with the beginning and peak of oscillations respectively.

to the different images. It was assumed that the best focused frames of the image sequences would be those at the start of the oscillations, and so the correlation was calculated using (5.1), where η is the length of the Fourier power spectrum vector, X is the power spectrum vector of the first image and Y is the power spectrum vector of the image being compared.

$$r_k = \frac{\eta \Sigma XY - \Sigma X \Sigma Y}{\sqrt{(\eta \Sigma X^2 - (\Sigma X)^2)(\eta \Sigma Y^2 - (\Sigma Y)^2)}} \quad (5.1)$$

As the lever is oscillated in the Y-direction, a large amount of pixel variation in this direction can be expected. Therefore, the intensity was sampled using ten evenly spaced rows of pixels, rather than the evenly spaced columns used in the cited paper. The mean focus shift over the course of the levers’ oscillations for different supplied trapping powers is presented in Fig. 5.8, where lever design 1014 3OH, which had spheroidal handles and a 1.4 μm vertical gap, was shown to perform most poorly. Interestingly, lever design 1018 3OH performed well, perhaps indicating that interaction between the vertical pin and lever arm, rather than the trapping handle shape, caused the issue. Most of the levers showed more out of plane movement when rotated at lower laser powers, as levers are more likely to move out of a weak trap.

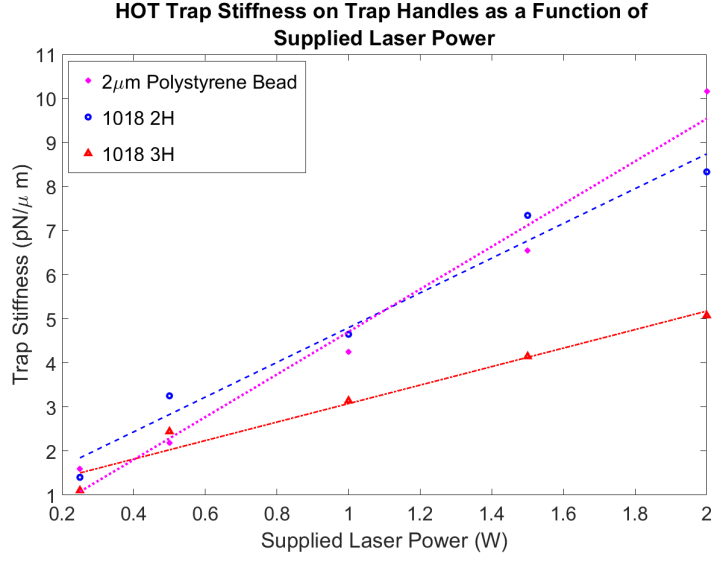


Figure 5.9: The calculated trap stiffness for the 3 μm trap handles was much lower than for the 2 μm handles at the same trapping powers, while the values for the 2 μm handles were comparable to values for 2 μm polystyrene beads.

5.1.5.2 AMPLIFYING FORCE

The levers selected for the force amplification task were from the 1018 2H and 1018 3H design groups, as these had the lowest average focus shift at 2 W trapping power. The trap stiffness of the HOTA acting on the lever handles was calculated using the equipartition theorem, (5.2), where $\langle Y^2 \rangle$ is the position variance of a trapped sphere in the Y direction, k_B is the Boltzmann constant and T is the temperature in K. The resulting relationship between supplied laser power and the trap stiffness can be seen for the two handle sizes in Fig. 5.9, where the stiffness measurements for a trapped free polystyrene bead (diameter = 2 μm) are also shown. The fair agreement between the values for the microbeads and those for 1018 2H adds confidence to the use of this method for measuring forces on the levers. The slightly lower maximum for 1018 2H can possibly be attributed to the IP-L 780 resin having a lower refractive index than polystyrene [248].

$$k_y = \frac{k_B T}{\langle Y^2 \rangle} \quad (5.2)$$

The trap stiffness on the handles for 1018 2H was almost twice as high as that on 1018 3H at 2 W. This indicates that the size of trapping handles on micromachines should be carefully chosen according to the optical trap being used, as well as what can be repeatably manufactured. As the HOTA is much weaker than the fixed trap, the highest trap stiffness was desirable for this experiment. Therefore, the decision was

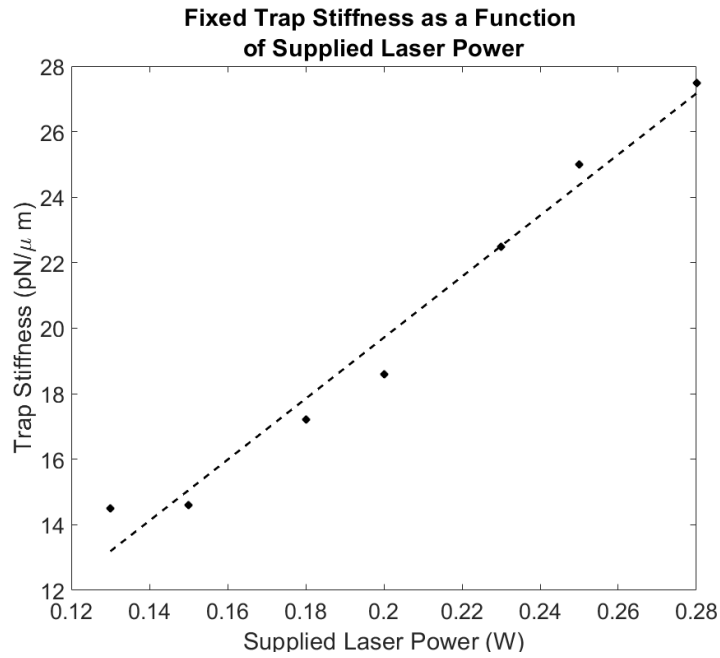


Figure 5.10: The calculated trap stiffness for the fixed high power trap was much higher than for the HOT trap, as expected.

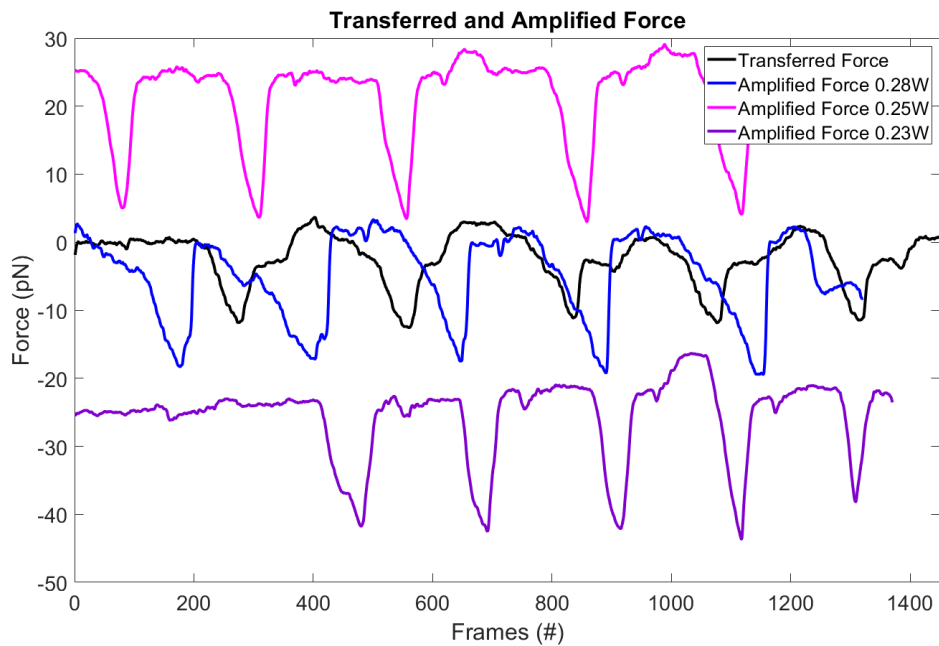


Figure 5.11: Force amplification could be measured successfully at three different laser powers, with results shown vertically offset in order to make separate lines clearer.

made to only attempt force amplification with levers from the 1018 2H group. Stiffness of the fixed trap on the 1018 2H lever handles was measured using the same method,

and the results are shown in Fig. 5.10.

The lever was positioned with the “sensor” handle in the 1030 nm fixed optical trap, and the HOT was used to move the lever, opposing the fixed trap. By using the intermediate handle, a 1:1 proportional factor was created and no force amplification occurred, resulting in small fluctuations from the fixed trap. When the end handle was used, a 2:1 proportional factor was created, and increased movement was observed. It was expected that the force provided by the HOT would be amplified by the same ratio as the proportional factor, due to balancing of moments about the central pivot. Force amplification was attempted using 2 W power for the HOT and the full range of powers used for the fixed trap stiffness calculations. However, repeatable force transfer and amplification could not be properly tested until the fixed trap was supplied with ≥ 0.23 W. This is because at lower trap powers the amplified force from the HOT was sufficient to move the lever completely out of the fixed trap, meaning that the amplification could not be quantified. Amplification was attempted five times at each of the fixed trap powers, and the force transferred by the lever was calculated using the Hookean model of optical tweezers, given by (5.3), where k is the trap stiffness and y is the fluctuation from the centre of the trap.

$$F_{trap} = -ky \quad (5.3)$$

The amplified forces can be seen in Fig. 5.11, where force transfer and amplification are shown with 0.23 W supplied to the sensing trap, as well as the amplified forces sensed with higher powers, which have been vertically offset for clearer viewing. The force transferred when the 1:1 lever arm ratio was approximately 10 pN; in line with what we expect to be the maximum that can be applied with the HOT trap at 2 W power. The amplified forces were consistently measured to be close to 20 pN, with the mean values and uncertainties shown in Table 5.2. The restricted diffusion of the trapped handle, calculated using the mean-square displacement, can be used to estimate the lowest force that can be measured by this set-up. Based on this, the estimated lowest force is of the order of a few femto-Newtons, far below that we are interested in in this study. At such low forces, Brownian motion could become noticeable in the measurements, in which case time averaging and multiple repetitions of an experiment would go some way to reducing such effects. It is likely that error from other sources, such as drift, would become problematic before Brownian motion. The fact that the amplified force was consistently slightly lower than 2x the transferred force could point to losses in the force transfer. Therefore, characterising drag and internal friction on levers in force amplification studies could be an interesting avenue for future work. As shown in Fig. 5.7, the tolerance of the lever leads to an inconsistent phase shift- varying between 0.2 and 0.6 rad- between the movement of the pivot point and the free end of

the lever, whereas a rigid lever would be in phase with this movement. This complicates the characterisation of drag and internal friction for such pin-jointed levers, but as this work demonstrates, such levers can still be used effectively for force amplification.

Table 5.2: Mean Transferred and Applied Forces

Trap Power (W)	Measured Transferred Force (pN)	Uncertainty (pN)	Measured Amplified Force (pN)	Uncertainty (pN)
0.23	10.37	0.98	16.65	2.75
0.25	10.45	0.65	20.11	1.05
0.27	11.86	0.71	21.83	1.14

5.1.6 CONCLUSIONS

Our aim in performing this study was to systematically develop and test the performance of an unsupported microlever for amplifying forces; specifically creating a lever that could be trapped stably to repeatably perform the task. We monitored drift of the levers out of focus over the course of several oscillations, which identified spherical handles as superior to elongated spheroids, particularly at high trapping powers. While 3 μm diameter spherical handles performed well in terms of maintaining focus stability, the low trap stiffness of the HOT on these handles made the 2 μm diameter handles more suitable for the task. The work we have performed demonstrates the potential that optical micromachines have for multiplying even small forces from optical tweezers, as well as the importance of handle design. Additionally, we demonstrated that using the equipartition theorem to calculate trap stiffness on a lever handle appears to give acceptable results, allowing researchers to directly measure force amplification, rather than relying on calibration performed with free-floating microbeads. Consistent doubling of the applied force was observed and measured using three different trapping powers, demonstrating the suitability of the levers for this task. There is still work to be carried out in characterising the forces on the levers: specifically the drag on the levers, as well as internal friction in the pin joint, as the force amplification indicated losses that seem likely to originate from those areas.

Chapter 6

CONCLUSIONS AND FUTURE WORK

6.1 THESIS SCOPE AND SUMMARY

The original aim of this work was to use nanoscale manufacturing, specifically two-photon absorption polymerisation, to create optical machines that could be used in optical tweezer studies. As such, the main goals for the project, as decided during the thesis proposal were: to develop functional optical nanorobots; to use these nanorobots for studies of molecules; and to use the nanorobots to improve the capabilities of optical tweezers. Each of these goals has been met, although, as the previous chapters have demonstrated, there is room for further work to be done on this subject. DNA was selected as the target molecule for this work due to the large volume of work in the literature regarding its characterisation and mechanical properties. As the work that made up this thesis was highly inter-disciplinary, and involved a steep learning curve across multiple inter-connecting subjects the decision was made to limit the molecule stretching work to DNA, in order to keep the focus on nano-micro manipulation rather than molecular chemistry. Colleagues in the biophysics group at Massey University have recently successfully concatenated two separate strands of DNA using streptavidin linkers [249], and it is possible that such a technique could be used in the future to produce DNA strands that are linked with other polymers that are more difficult to study in isolation, inserted within long DNA sections. This could enable the standard DNA stretching protocols to be extended to other molecules, and greatly broaden the utility of the work described here.

While fully-remote, double-lever-assisted DNA stretches could not be successfully performed within the time-frame of the project, it is likely that further work in this area would yield successful results, as the experimental setup appeared promising. In addition, the publication of the article on lever-assisted DNA stretching provides an

interesting and novel proof-of-concept for incorporating optical nano-micro machines into molecular studies; which achieved the stated aim of demonstrating the use of such tools.

Finally, repeatable force amplification was demonstrated using an unsupported, pin-jointed lever, something which has historically been avoided by micro-roboticists due to the uncertainty introduced by pin-joint tolerance. While the effects of pin-joint tolerance were noticed during characterisation, it did not prevent significant force amplification that allowed a weaker holographic optical trap to be played off against a higher power trap. This would seem to indicate that similar general-purpose optical microlevers could be used in biological and soft-matter studies, where force amplification might be desired. In short, the goals of this thesis have been met, and the work performed shows promise for further use of optical nano-micro tools in optical tweezers. Additionally, the systematic consideration of different design features for optical nanorobotics, particularly the effects of overlapping area, presence of supports and handle shape on optical trapping and functionality, will hopefully add to the body of work covering what Bunea et al. referred to as “Rational Design of Light-Controlled Microrobotics” [151]. Such design work has historically been difficult due to the differences between different setups, but the work performed over the course of this project seems to suggest that improved results can be obtained from centred, spherical handles compared to spheres that jut-out from the optical robots. Additionally, despite the tendency for asymmetric shapes to align with optical traps along the long axis, no improvement was seen in trapping microlevers when elongated handles were introduced, validating the preference for spherical handles in optical manipulation.

6.2 FUTURE WORK BASED ON THIS THESIS

While the goal of producing functional optical nanorobots can be said to be conclusively met, there is extensive opportunity for future applications of such tools, that build on the work performed in this thesis. The opportunities outlined here are largely based around molecular studies and force amplification, but TPAP-produced optical microtools could be used for a host of applications for material science, biological studies and even optical physics studies.

6.2.1 DOUBLE-LEVER-ASSISTED DNA STRETCHING

One of the major challenges when attempting stretching using the double-lever configuration, and indeed for microrobotics in general, was the tendency for microlevers to settle and begin to stick at the axis of rotation, and to the substrate. This led to the addition of the borosilicate microprobe alongside the optical trapping setup, so that

levers could be “freed” directly before an experiment took place, which then required the sample to be kept open, and left it vulnerable to evaporation, which exacerbated the problem of adhesion due to relative ion concentration increasing over time. The need to add the DNA-streptavidin bead suspension after the antidigoxigenin beads were attached was another reason for keeping the sample open, but this also disturbed the microlevers, sometimes leading to loss of the attached AD beads. These issues could potentially be circumvented by enclosing the sample in a pumped microfluidic chip, which would ideally provide a slow, steady flow of fluid which would stop levers from settling during setup. Another use for pumped microfluidics in this work would be the precise introduction of a suitable number of functionalised microbeads, enabling stretches to be performed one at a time. In the current protocol, the antidigoxigenin microbeads are attached to levers before adding streptavidin beads and DNA, and attaching those beads. This is partially due to the similar size of the microbeads chosen for attachment, which made alignment of the beads easier but also made it difficult to be certain that different beads were attached to the actuator and sensor levers. Pumping in beads one at a time, from different streams in a chip would make the bead type less ambiguous. Pocket design changes to enable the use of different beads, or even direct antidigoxigenin functionalisation of the levers would also be possible solutions to this particular problem, but enclosing the levers in a microfluidic chip environment would be an elegant solution to multiple issues. However, the design and manufacture of such a chip would be time intensive, and likely suitable for a Masters of even another doctoral thesis project.

6.2.2 COMPARISON OF OPTICAL TRAPPING EFFECTS ON DNA

While the lever-assisted DNA stretching performed for this project produced similar results to direct dual-trap and fixed-microbead, piezomotor actuated DNA stretches, the comparative laser exposure, and subsequent possible effects were not investigated. It is thought that remote optical manipulation, such as that which can be performed using tools like levers, can reduce the effects of laser radiation such as photobleaching or local heating of the molecule or cell being probed. One way to examine whether using tools to remotely stretch DNA assists with such issues would be to compare the longevity of fluorescent markers on the DNA, or to examine the average number of stretches that could be performed with a single molecule. The latter method would be difficult with microlevers, due to the tendency for the levers to adhere and stop actuating a stretch, but could be investigated if a solution was found for that difficulty. Introducing fluorescent markers to the DNA is theoretically straightforward, but the current need to prepare the levers in bright-field conditions could cause bleaching from

this light exposure, limiting the lifetime of the fluorophores. If the levers themselves were also fluorescent, then it could be possible to test the effects of the optical tweezers on fluorophore lifetime directly, as the trapped end would become bleached before the free end. Like the introduction of microfluidics to the lever-assisted stretching, dyeing the levers and experimenting with fluorescent imaging of the DNA would likely take considerable effort.

6.2.3 QUANTITATIVE ANALYSIS OF TPAP EFFECTS ON OPTICAL MICROROBOTS

The properties of objects printed using TPAP are highly dependent on the parameters used during printing. Some of these parameters, such as hardness and refractive index have been quantitatively examined and linked to the cross-linking of the resin [144, 248, 195], and consequently to the laser dose. However, the results shown in Chapter 3 seemed to indicate a previously unrecognised connection between lever adhesion and the laser dose used in lever printing. While the link between geometry and adhesion is well known, it is possible that changes to the mechanical properties of the polymer based on laser dose could also add to changes in the stickiness of the resulting structure. One way to examine such an effect would be to print films of photoresins over glass slides, and then probe the films using atomic force microscopy. The results of these force maps could then be compared for films created using different printing parameters. The degree of cross-linking of the resins could then also be examined by comparing the Raman spectra of these films with the spectra of the unpolymerised resin [250, 195], to examine the relationship between degree-of-conversion and attractive forces between surfaces.

6.2.4 IMPROVING MODELLING OF FORCES ON MICROLEVERS

The investigation of the effects of trap handle shape on out-of-plane movement of microlevers also revealed a varying amount of lag in the motion of the microlevers, likely caused by the tolerance of the pin joint and the internal friction of this joint. This could be investigated by examining the variation of this effect when different optical trapping power is used, and in different fluids to try and separate the contributions from the friction and drag terms. Additionally, the stiffness values that were directly measured at the handles of the optical levers could provide an initial estimate for the effects of the optical trap on the restriction of the lever's movement as a whole, which may be helpful when attempting to characterise the forces. Including measurements such as the mean squared displacement and mean squared angular deviation of the lever would provide an additional measurement to assist in developing the model, similar to

work carried out using drag and trap stiffness to calibrate forces on microbeads [193]. Additionally, observing the rotational diffusion of the levers may provide more insight into the settling process, which could help to prolong the time over which micromachines remain useable. Such analysis and modelling would be helpful for developing multi-link microrobots in liquid environments, even for non-optically-actuated systems.

Appendix A

NANOSCRIBE PRINT SETTINGS

Fig. A.1 shows a screenshot taken from the DeScribe software, where the slicing distance is being set for an imported .stl file. There are two slicing settings: fixed and adaptive, which allow the user to set the distance between laser focus distances in the Z direction. The fixed slicing mode uses the same separation throughout the print job, which makes it effective for structures that require the same resolution throughout, or have features that are all approximately the same size. Adaptive mode, on the other hand, works well when there are features of a multitude of sizes involved in the print. Slicing effectively creates layers of polymerised resist, and the overlap of these layers creates a solid structure. As TPAP is a third order process, requiring the absorption of two photons and the generation of a free radical; which is passed from the photo-initiator to the monomers in the resin; diffusion of free radicals through the resin can lead to polymerisation of resin outside of the intended voxel, depending on the laser dose. This, combined with the beam's maximum intensity region being governed by the Rayleigh length in the z-direction, which is obviously larger than the beam waist, means that the z-direction experiences the lowest print resolution, with the voxel aspect ratio being about 3.5. Therefore, careful consideration of the slicing distance, as well as the laser power, is required to actually create a printed structure with the dimensions specified in the computer-aided design (CAD) file.

The next screen, shown in Fig. A.2, prompts the user to set the hatching parameters for the print. Just as in the slicing mode, the separation of the hatching layers can be set. However, just as importantly for the shape and properties of the resulting structure, the hatching angle can also be set. Here the user can either choose to use the "automatic" hatch angle settings, or define the angle and offset themselves. The NanoScribe Small Feature set suggests using a 90deg angle and offset for small, symmetric objects, in order to preserve the shape, and the overall shape of the print

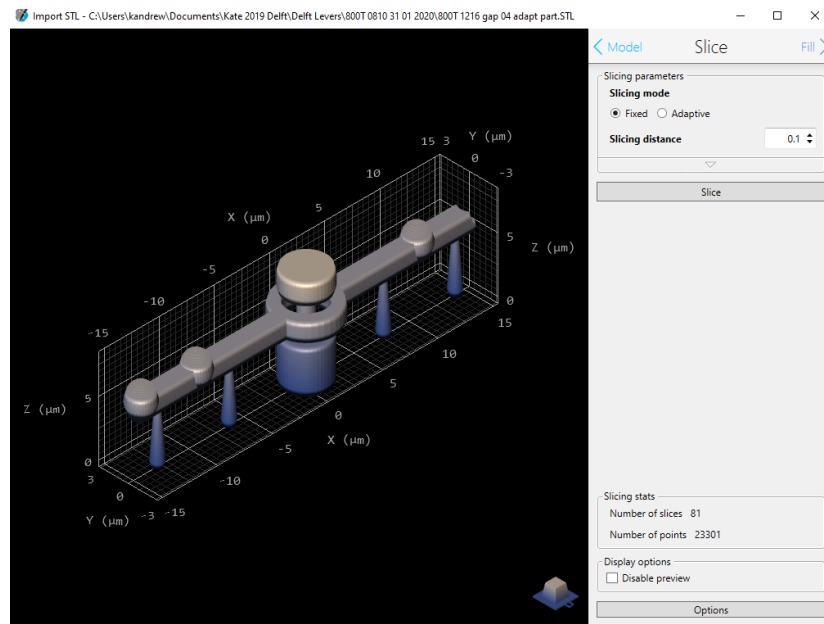


Figure A.1: Just as in conventional printing, DeScribe allows the user to set the slicing distance for a job.

job should be considered when choosing this setting. The hatching distance, just like the slicing distance, affects the laser dose used in the print and the resulting degree of conversion. The degree of conversion has been shown to effect the hardness of the resulting structure, as well as its optical properties [251], and so the hatching and slicing parameters are important for more than just ensuring the correct shape. Having smaller hatching and slicing distances essentially leads to more “lines” of laser exposure within a confined volume, increasing the total exposure relative to a structure printed with the same power and speed settings, but larger hatching and slicing separation.

The final screen of the DeScribe software is where the output file settings are finalised. The parameters set on this screen are the laser scan mode, the Z-axis control method, the direction of the hatch lines (alternating or matching direction), exposure mode, printing configuration and printing direction. These parameters can be seen in the screenshot in Fig. A.3. The “Base File Name” is also set on this page, which is the name that will identify the recipe, job, binary and data files associated with the design. If the current name for the files is already in use, then a warning shows, and the user is prompted to change the name or allow for overwriting. This feature, along with the ability to edit the job and data filenames, allows the user to easily produce and keep track of iterations of the same design with slightly varying parameters. However, as with most proprietary software, it is not possible to edit the files outside of the DeScribe environment, and any changes to the binary file- which actually contains the machine instructions for printing- can only be made by re-opening the recipe file and

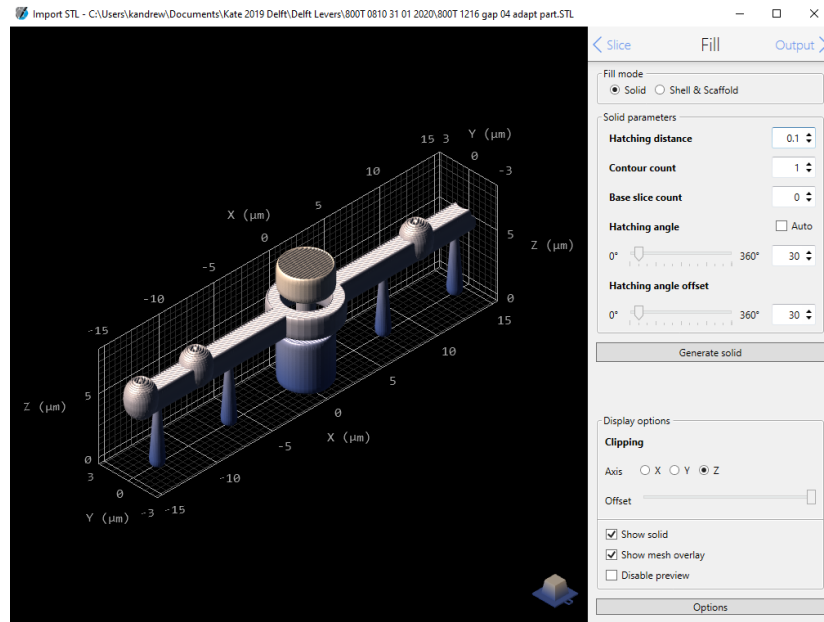


Figure A.2: The hatching configuration can be set in DeScribe, and both the angle and hatch separation are important for the overall result.

generating new files. The data.gwl file simply contains this information in a human-readable format- offering a record of the settings for the user- along with a pointer to the required binary file.

A.0.0.1 PRINTING CONFIGURATION AND DIRECTION

Of all of these settings, the choice of printing configuration is potentially most important to be certain of, when setting up the PPGT2 for a print. The two choices for configuration are the conventional “oil immersion” printing method and the dip-in laser lithography method (DiLL), which are shown in Fig. A.4. In this work the two resins that were tested were IP-Dip for DiLL and IP-L 780 for oil-immersion printing. Both of these resins are suitable for very high resolution printing, but IP-Dip has a higher refractive index than the IP-L 780 (1.552 compared to 1.519 when UV cured). There is another resist suitable for printing small, complex features with over-hanging elements: IP-G. However, this resist was not tested, as it was released by Nanoscribe after tests had already shown that IP-L 780 was suitable for our work. In both DiLL and oil-immersion printing the PPGT2 detects the interface between the resin and the substrate being printed on, which is why IP-Dip is conventionally used with fused silica rather than the borosilicate glass coverslips. Printing then begins in the printing direction defined in the job file, i.e. whether the positive Z direction defined in the model is to be printed towards or away from the objective. Generally, immersion-print

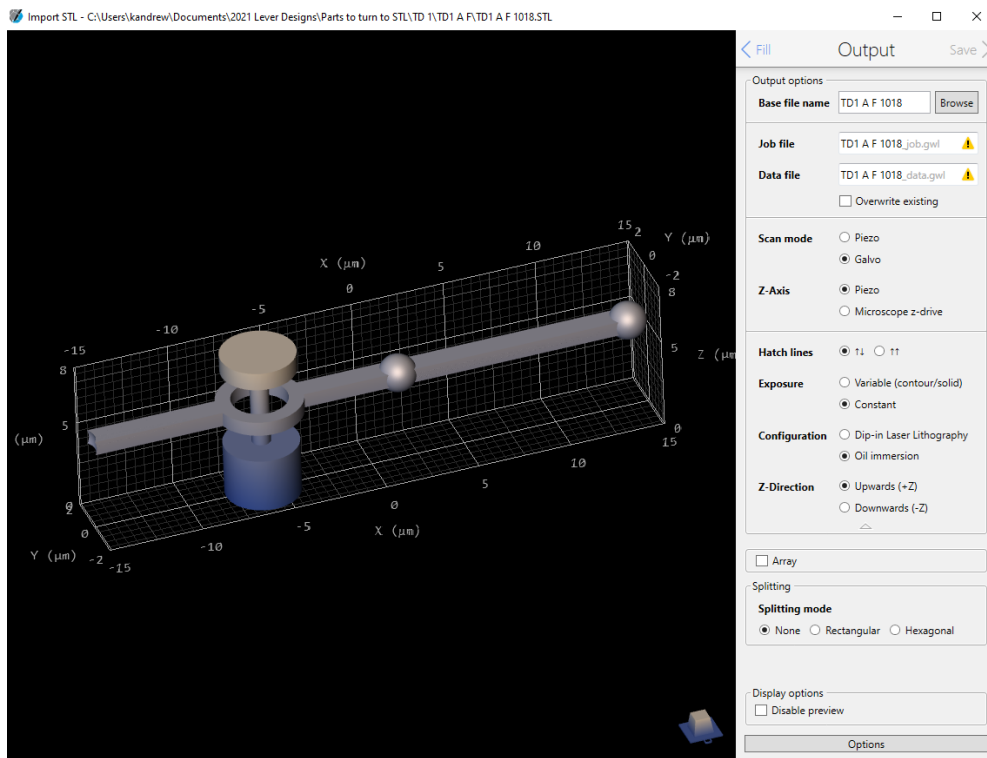


Figure A.3: The final screen of the DeScribe .stl import process allows the user to set the name that will be used to identify the associated files, as well as letting them set several printing parameters. The yellow warning symbols seen in this screenshot are displayed as job and data files already exist for this filename. In order to avoid overwriting when changing printing parameters, the data and job file names should be edited to reflect the chosen parameters, to keep track of design iterations.

jobs are printed with the Z direction set to “positive” and the DiLL jobs are printed with the Z direction set to “negative”. The fused silica substrates used for DiLL are $700\ \mu\text{m}$ thick, compared to the $170\ \mu\text{m}$ thick coverslips, as the laser does not need to focus *through* the coverslip to print.

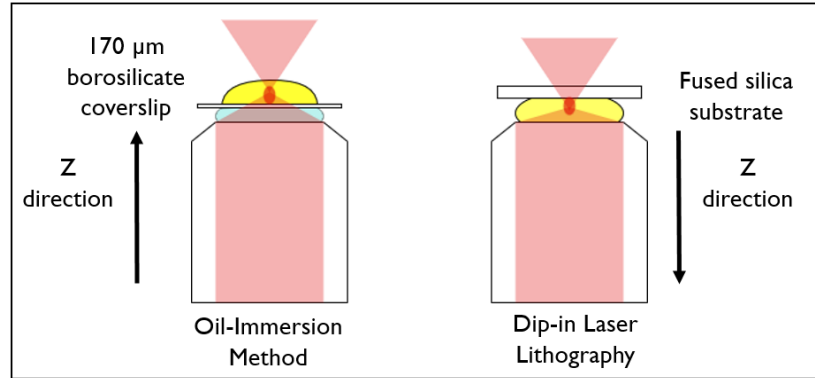


Figure A.4: The Z direction for printing is conventionally set to be “upwards” for the oil-immersion method and “downwards” for DiLL. The PPGT2 uses the refractive index mismatch between the substrate and the resin to find the interface, in both cases. In DiLL, the resin itself is used as the lens immersion media, rather than the index-matched oil used for the oil-immersion method.

A.0.0.2 LASER SCAN MODE, Z-POSITION ADJUSTMENT AND HATCHING DIRECTION

The laser scan mode parameter sets the method used for scanning the laser through the printing volume, to expose it as defined by the slicing and hatching settings. If the “galvo mode” setting is selected, then a galvanometer-based scanning mirror is used to direct the path of the laser, enabling fast, precise polymerisation. A galvanometer is a device used to measure small differences in current, by monitoring the deflection of a coil in response to these differences. Galvo mirrors use these small deflections to position mirrors with high precision, and at high speed. In contrast, when using “piezo mode” the sample is moved using piezomotors, relative to the focus of the laser. The maximum writing volume in piezo-mode is $300 \times 300 \times 300\ \mu\text{m}^3$, meaning that all of the coordinates to be reached have to lie within this space. The volume that can be accessed in Galvo mode is still more limited, with a square of $100 \times 100\ \mu\text{m}^2$ available in the XY plane, with the Z-direction limit depending on the choice of method for the Z-position control. The use of piezomotors enables extremely high accuracy, and operating in piezo mode has been used to successfully print structures such as helical springs. However, the printing is several orders of magnitude slower than galvo mode, and in many cases the precision gains from using this mode are minimal. In this work,

galvo mode was used for all but the initial test prints.

The choice of method for adjusting the Z-position can have noticeable effects on the printing resolution and quality. The two choices are “piezo” and “Microscope z-drive”. The former uses a piezomotor to move the sample vertically, just as the sample is moved in the XY plane in piezo mode printing. On the other hand, using the microscope z-drive results in much lower resolution than the piezo, which can be positioned with accuracy of a few tens of nanometres. If very tall structures are to be printed- i.e. higher than the 300 μm height that can be reached with the piezo- then the microscope z-drive has to be used. It can be used either to move the sample so that blocks of resin printed using the piezo z-drive can be stitched together, or to move the sample for polymerisation of the whole structure in layers. According to the manual for the PPGT2 it is generally preferable to use the microscope z-drive for extremely tall structures, rather than stitching together blocks that have been printed using the piezo. As the height that the microscope z-drive can reach is limited by the gap between the stage and the sample holder, structures up to 3 mm tall can theoretically be used when using dip-in laser lithography. Using the immersion method for printing such tall structures is not practical, because of aberrations in the laser focus as the printing progresses.

Like the writing mode and z-drive positioning method, the hatching direction is an important parameter for producing the desired shape in the print. Choosing alternating hatch lines means that the Nanoscribe hatches from the opposite direction for each second line, creating a kind of “zig-zag” effect. Conversely, using the single-direction hatch line setting means that the hatching will follow the same direction for each line. Research on reducing distortion of 3D-printed objects suggests that using alternating hatch lines is best for unsupported, symmetric shapes [252], such as cantilevers. However, there may be objects, such as waveguides, that benefit from a single hatching direction.

A.0.0.3 THIN-WALLED SHAPES

While the work in this thesis only concerned solid printed objects, there is also an option to create a thin-walled feature from an imported .stl. This option is enabled by selecting “Shell & Scaffold” in the “Fill” screen of DeScribe- where the hatching parameters are set. The shell is defined as being comprised of a number of contours that follow the outline of the object, while the scaffolding acts to support the shell. Using this option can dramatically reduce print time, as scaffolding can be strategically introduced in places where strictly needed while the surface quality of the object can be maintained through deciding on the appropriate number and separation of contours. Additionally, using this mode, the user can separately define the laser power used for the shell and for

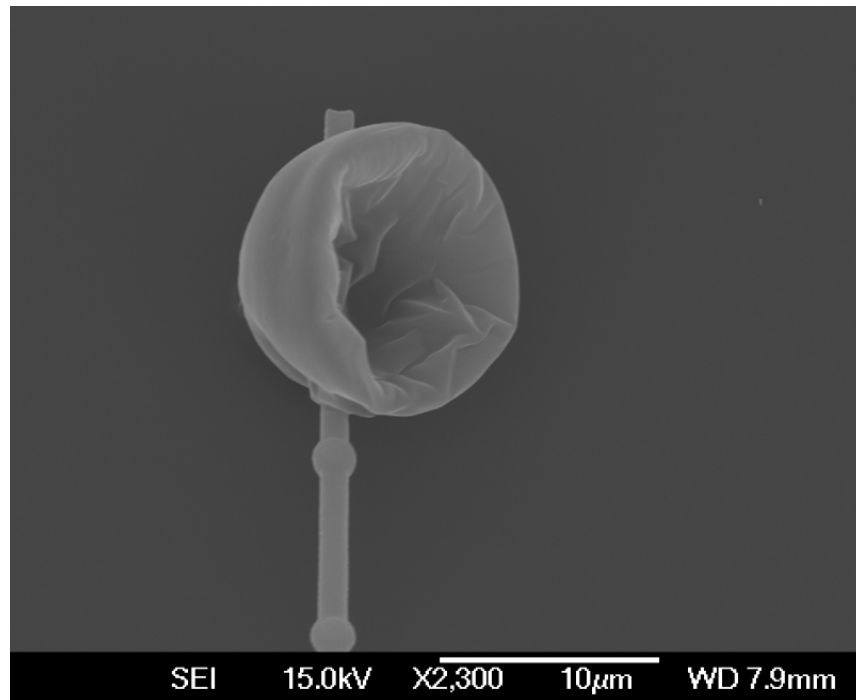


Figure A.5: Accidental bubbling of resist, caused by too-high laser dose. While such bubbling is generally considered undesirable, it can also provide interesting possibilities for creating features that are generally unprintable.

the scaffold, which might make it useful for researchers working on objects with different shell and core properties, such as refractive index. Other times that this printing mode might be useful include supporting large, curved surfaces during printing, and then ablating or otherwise removing the supports once the object has been developed [253]. One consideration to bear in mind is that it is not currently possible to repeatably print hollow, closed bodies with TPAP, as there is no way to remove the unpolymerised resist. However, some researchers have taken advantage of shrinkage of polymerised resist, as well as the fact that too-high laser dose will cause the resin to bubble, to create closed hollow spheres, although this technique will not produce perfectly controlled features. An example of accidentally bubbled resist, resulting from too-high laser dose, can be seen in Fig. A.5. If the desired effect was to produce a hollow shape from such a bubble, then the user would still need to experiment with various input shapes, in order to ensure that the bubble comes close to closing pre-shrinkage. The particular degree of shrinkage that a resin exhibits is also important for such an endeavour, and it might take a few attempts to find one which shows appropriate levels of shrinkage, as the proprietary Nanoscribe resist have been developed for low shrinkage. It should be noted that high shrinkage of polymerised materials is generally undesirable due to the differences it creates between the designed and the manufactured structure, as well

as the potential for high aspect ratio structures to collapse. Therefore, the discovery that bubbling resin could be used as a method for creating hollow shapes provides an interesting concept for taking advantage of a historically unwanted effect.

Appendix B

LAYOUT OF LARGE SAMPLES USED FOR CHAPTER 3

Table B.1: Sample layout for Sample 1A. Inner radius of the levers was 900 nm larger than the radius of the centre axle.

	A	B	C	D	E
1	Design 2 850 nm gap 36% LP 10 mm/s Tip support 1 μ m base	Design 1 850 nm gap 39% LP 16 mm/s No support 3 μ m base	Design 1 1000 nm gap 39% LP 16 mm/s No support 3 μ m base	Design 1 850 nm gap 36% LP 16 mm/s No support 3 μ m base	Design 1 850 nm gap 36% LP 10 mm/s No support 3 μ m base
2	Design 2 850 nm gap 39% LP 16 mm/s Tip support 1 μ m base	Design 1 850 nm gap 39% LP 16 mm/s Ring support 3 μ m base	Design 1 1000 nm gap 39% LP 16 mm/s Ring support 3 μ m base	Design 1 850 nm gap 36% LP 16 mm/s Ring support 3 μ m base	Design 1 850 nm gap 36% LP 10 mm/s Ring support 3 μ m base
3	Design 2 850 nm gap 36% LP 16 mm/s Tip support 1 μ m base	Design 1 850 nm gap 39% LP 16 mm/s Tip support Ring support 3 μ m base	Design 1 1000 nm gap 39% LP 16 mm/s Tip support Ring support 3 μ m base	Design 1 850 nm gap 36% LP 16 mm/s Tip support Ring support 3 μ m base	Design 1 850 nm gap 36% LP 10 mm/s Tip support Ring support 3 μ m base
4	Design 2 850 nm gap 39% LP 10 mm/s Tip support 1 μ m base	Design 1 850 nm gap 39% LP 16 mm/s No support 1 μ m base	Design 1 1000 nm gap 39% LP 16 mm/s No support 1 μ m base	Design 1 850 nm gap 36% LP 16 mm/s No support 1 μ m base	Design 1 850 nm gap 36% LP 10 mm/s No support 1 μ m base
5		Design 1 850 nm gap 39% LP 16 mm/s Ring support 1 μ m base	Design 1 1000 nm gap 39% LP 16 mm/s Ring support 1 μ m base	Design 1 850 nm gap 36% LP 16 mm/s Ring support 1 μ m base	Design 1 850 nm gap 36% LP 10 mm/s Ring support 1 μ m base
6		Design 1 850 nm gap 39% LP 16 mm/s Ring support Tip support 1 μ m base	Design 1 1000 nm gap 39% LP 16 mm/s Ring support Tip support 1 μ m base	Design 1 850 nm gap 36% LP 16 mm/s Ring support Tip support 1 μ m base	Design 1 850 nm gap 36% LP 10 mm/s Ring support Tip support 1 μ m base

Table B.2: Sample Layout for 1C (IP-L 780) and 1D (IP-Dip). All levers were printed with a scanning speed of 10 mm/s and a vertical gap of 1.4 μm .

	A	B	C
1	40% LP (beam and pin) 35% LP (ring) No support	40% LP (beam and pin) 30% LP (ring) No support	35% LP (beam and pin) 30% LP (ring) No support
2	40% LP (beam and pin) 35% LP (ring) Tip support	40% LP (beam and pin) 30% LP (ring) Tip support	35% LP (beam and pin) 30% LP (beam and pin) Tip support
3	40% LP No support	35% LP No support	30% LP No support
4	40% LP Tip support	35% LP Tip support	30% LP Tip support
5	40% LP 4 supports along beam	35% LP 4 supports along beam	30% LP 4 supports along beam

Appendix C



DRC FORMS FOR PUBLICATIONS IN THIS THESIS



GRADUATE
RESEARCH
SCHOOL

STATEMENT OF CONTRIBUTION DOCTORATE WITH PUBLICATIONS/MANUSCRIPTS

We, the candidate and the candidate's Primary Supervisor, certify that all co-authors have consented to their work being included in the thesis and they have accepted the candidate's contribution as indicated below in the *Statement of Originality*.

Name of candidate:	Philippa-Kate Andrew
Name/title of Primary Supervisor:	Dr Ebubekir Avci
In which chapter is the manuscript /published work: Chapter 2	
Please select one of the following three options:	
<input checked="" type="radio"/> The manuscript/published work is published or in press <ul style="list-style-type: none"> • Please provide the full reference of the Research Output: Andrew, P.-K.; Williams, M.A.K.; Avci, E. Optical Micromachines for Biological Studies. <i>Micromachines</i> 2020, 11, 192. https://doi.org/10.3390/mi11020192 	
<input type="radio"/> The manuscript is currently under review for publication – please indicate: <ul style="list-style-type: none"> • The name of the journal: • The percentage of the manuscript/published work that was contributed by the candidate: • Describe the contribution that the candidate has made to the manuscript/published work: 	
<input type="radio"/> It is intended that the manuscript will be published, but it has not yet been submitted to a journal	
Candidate's Signature:	
Date:	21-Jul-2022
Primary Supervisor's Signature:	
Date:	21 July 2022



This form should appear at the end of each thesis chapter/section/appendix submitted as a manuscript/publication or collected as an appendix at the end of the thesis.



GRADUATE
RESEARCH
SCHOOL

STATEMENT OF CONTRIBUTION DOCTORATE WITH PUBLICATIONS/MANUSCRIPTS

We, the candidate and the candidate's Primary Supervisor, certify that all co-authors have consented to their work being included in the thesis and they have accepted the candidate's contribution as indicated below in the *Statement of Originality*.

Name of candidate:	Philippa-Kate Andrew
Name/title of Primary Supervisor:	Dr Ebubekir Avci
In which chapter is the manuscript /published work: Chapter 3	
Please select one of the following three options:	
<input checked="" type="radio"/> The manuscript/published work is published or in press <ul style="list-style-type: none"> • Please provide the full reference of the Research Output: P. -K. Andrew et al., "Design of Optical Micromachines for Use in Biologically Relevant Environments," 2020 IEEE/ASME International Conference on Advanced Intelligent Mechatronics (AIM), 2020, pp. 2039-2045, doi: 10.1109/AIM43001.2020.9158816. 	
<input type="radio"/> The manuscript is currently under review for publication – please indicate: <ul style="list-style-type: none"> • The name of the journal: • The percentage of the manuscript/published work that was contributed by the candidate: • Describe the contribution that the candidate has made to the manuscript/published work: 	
<input type="radio"/> It is intended that the manuscript will be published, but it has not yet been submitted to a journal	
Candidate's Signature:	
Date:	21-Jul-2022
Primary Supervisor's Signature:	
Date:	21 July 2022



This form should appear at the end of each thesis chapter/section/appendix submitted as a manuscript/ publication or collected as an appendix at the end of the thesis.



GRADUATE
RESEARCH
SCHOOL

STATEMENT OF CONTRIBUTION DOCTORATE WITH PUBLICATIONS/MANUSCRIPTS

We, the candidate and the candidate's Primary Supervisor, certify that all co-authors have consented to their work being included in the thesis and they have accepted the candidate's contribution as indicated below in the *Statement of Originality*.

Name of candidate:	Philippa-Kate Andrew
Name/title of Primary Supervisor:	Dr Ebubekir Avci
In which chapter is the manuscript /published work: Chapter 4	
<p>Please select one of the following three options:</p> <p><input checked="" type="radio"/> The manuscript/published work is published or in press</p> <ul style="list-style-type: none"> • Please provide the full reference of the Research Output: P-K. Andrew, A. Raudsepp, D. Fan, U. Staufer, M. A. K. Williams, and E. Avci, "Optical microlever assisted DNA stretching," <i>Opt. Express</i> 29, 25836-25847 (2021) <p><input type="radio"/> The manuscript is currently under review for publication – please indicate:</p> <ul style="list-style-type: none"> • The name of the journal: • The percentage of the manuscript/published work that was contributed by the candidate: • Describe the contribution that the candidate has made to the manuscript/published work: <p><input type="radio"/> It is intended that the manuscript will be published, but it has not yet been submitted to a journal</p>	
Candidate's Signature:	
Date:	21-Jul-2022
Primary Supervisor's Signature:	
Date:	21 July 2022



This form should appear at the end of each thesis chapter/section/appendix submitted as a manuscript/publication or collected as an appendix at the end of the thesis.



GRADUATE
RESEARCH
SCHOOL

STATEMENT OF CONTRIBUTION DOCTORATE WITH PUBLICATIONS/MANUSCRIPTS

We, the candidate and the candidate's Primary Supervisor, certify that all co-authors have consented to their work being included in the thesis and they have accepted the candidate's contribution as indicated below in the *Statement of Originality*.

Name of candidate:	Philippa-Kate Andrew
Name/title of Primary Supervisor:	Dr Ebubekir Avci
In which chapter is the manuscript /published work: Chapter 5	
Please select one of the following three options:	
<input checked="" type="radio"/> The manuscript/published work is published or in press <ul style="list-style-type: none"> • Please provide the full reference of the Research Output: P-K. Andrew, A. Raudsepp, V. Nock, D. Fan, M. A. K. Williams, U. Stauffer, and E. Avci, "Developing an Optical Microlever for Stable and Unsupported Force Amplification", 2022 International Conference on Manipulation, Automation and Robotics at Small Scales (MARSS) 	
<input type="radio"/> The manuscript is currently under review for publication – please indicate: <ul style="list-style-type: none"> • The name of the journal: • The percentage of the manuscript/published work that was contributed by the candidate: • Describe the contribution that the candidate has made to the manuscript/published work: 	
<input type="radio"/> It is intended that the manuscript will be published, but it has not yet been submitted to a journal	
Candidate's Signature:	
Date:	21-Jul-2022
Primary Supervisor's Signature:	
Date:	21 July 2022

This form should appear at the end of each thesis chapter/section/appendix submitted as a manuscript/publication or collected as an appendix at the end of the thesis.

Bibliography

- [1] I. Heller, T. P. Hoekstra, G. A. King, E. J. G. Peterman, and G. J. L. Wuite, “Optical tweezers analysis of dna–protein complexes,” *Chemical Reviews*, vol. 114, no. 6, pp. 3087–3119, Mar 2014. [Online]. Available: <https://doi.org/10.1021/cr4003006>
- [2] M. J. Villangca, D. Palima, A. R. Bañas, and J. Glückstad, “Light-driven micro-tool equipped with a syringe function,” *Light: Science & Applications*, vol. 5, no. 9, pp. e16148–e16148, Sep 2016. [Online]. Available: <https://doi.org/10.1038/lsa.2016.148>
- [3] T. Asavei, T. A. Nieminen, V. L. Y. Loke, A. B. Stilgoe, R. Bowman, D. Preece, M. J. Padgett, N. R. Heckenberg, and H. Rubinsztein-Dunlop, “Optically trapped and driven paddle-wheel,” *New Journal of Physics*, vol. 15, no. 6, p. 063016, jun 2013. [Online]. Available: <https://doi.org/10.1088/1367-2630/15/6/063016>
- [4] E. Higurashi, O. Ohguchi, and H. Ukita, “Optical trapping of low-refractive-index microfabricated objects using radiation pressure exerted on their inner walls,” *Opt. Lett.*, vol. 20, no. 19, pp. 1931–1933, Oct 1995. [Online]. Available: <http://opg.optica.org/ol/abstract.cfm?URI=ol-20-19-1931>
- [5] P.-K. Andrew, M. A. K. Williams, and E. Avci, “Optical micromachines for biological studies,” *Micromachines*, vol. 11, no. 2, 2020.
- [6] G. Binnig and H. Rohrer, “Scanning tunneling microscopy,” *Surface Science*, vol. 126, no. 1, pp. 236–244, 1983. [Online]. Available: <https://www.sciencedirect.com/science/article/pii/0039602883907161>
- [7] G. Binnig, C. F. Quate, and C. Gerber, “Atomic force microscope,” *Phys. Rev. Lett.*, vol. 56, pp. 930–933, Mar 1986. [Online]. Available: <https://link.aps.org/doi/10.1103/PhysRevLett.56.930>
- [8] L. Möckl, D. C. Lamb, and C. Bräuchle, “Super-resolved fluorescence microscopy: Nobel prize in chemistry 2014 for Eric Betzig, Stefan

- Hell, and William E. Moerner,” *Angewandte Chemie International Edition*, vol. 53, no. 51, pp. 13972–13977, 2014. [Online]. Available: <https://onlinelibrary.wiley.com/doi/abs/10.1002/anie.201410265>
- [9] F. Sato, H. Asakawa, T. Fukuma, and S. Terada, “Semi- in situ atomic force microscopy imaging of intracellular neurofilaments under physiological conditions through the ‘sandwich’ method ,” *Microscopy*, vol. 65, no. 4, pp. 316–324, 09 2016. [Online]. Available: <https://doi.org/10.1093/jmicro/dfw006>
- [10] J. Zhu, M. Guo, Y. Liu, X. Shi, F. Fan, M. Gu, and H. Yang, “In situ tem of phosphorus-dopant-induced nanopore formation in delithiated silicon nanowires,” *ACS Applied Materials & Interfaces*, vol. 11, no. 19, pp. 17313–17320, May 2019. [Online]. Available: <https://doi.org/10.1021/acsami.8b20436>
- [11] Q. Xia, H. Xiao, Y. Pan, and L. Wang, “Microrheology, advances in methods and insights,” *Advances in Colloid and Interface Science*, vol. 257, pp. 71–85, 2018. [Online]. Available: <https://www.sciencedirect.com/science/article/pii/S000186861730475X>
- [12] K. Sablon, “Nanoelectrodes for molecular devices: A controllable fabrication,” *Nanoscale Research Letters*, vol. 3, no. 7, p. 268, Jul 2008. [Online]. Available: <https://doi.org/10.1007/s11671-008-9146-0>
- [13] X. Guo, Z. Xue, and Y. Zhang, “Manufacturing of 3d multifunctional microelectronic devices: challenges and opportunities,” *NPG Asia Materials*, vol. 11, no. 1, p. 29, Jun 2019. [Online]. Available: <https://doi.org/10.1038/s41427-019-0129-7>
- [14] Z. Wang, J. Zhang, Z. Yin, S. Wu, D. Mandler, and H. Zhang, “Fabrication of nanoelectrode ensembles by electrodeposition of au nanoparticles on single-layer graphene oxide sheets,” *Nanoscale*, vol. 4, pp. 2728–2733, 2012. [Online]. Available: <http://dx.doi.org/10.1039/C2NR30142C>
- [15] S. W. Hell, “Far-field optical nanoscopy,” *Science*, vol. 316, no. 5828, pp. 1153–1158, 2007. [Online]. Available: <https://science.sciencemag.org/content/316/5828/1153>
- [16] K. C. Neuman and A. Nagy, “Single-molecule force spectroscopy: optical tweezers, magnetic tweezers and atomic force microscopy,” *Nature Methods*, vol. 5, no. 6, pp. 491–505, Jun 2008. [Online]. Available: <https://doi.org/10.1038/nmeth.1218>

- [17] W. L. Jones, M. P. Sutton, L. McKittrick, and P. S. Stewart, "Biofouling Chemical and antimicrobial treatments change the viscoelastic properties of bacterial biofilms," *Biofouling*, vol. 27, no. 2, pp. 207–215, Feb 2011.
- [18] A. Y. Chang and W. F. Marshall, "Organelles - understanding noise and heterogeneity in cell biology at an intermediate scale," *Journal of cell science*, vol. 130, no. 5, pp. 819–826, Mar 2017, 28183729[pmid]. [Online]. Available: <https://pubmed.ncbi.nlm.nih.gov/28183729>
- [19] J. L. Caswell-Jin, C. Lorenz, and C. Curtis, "Molecular heterogeneity and evolution in breast cancer," *Annual Review of Cancer Biology*, vol. 5, no. 1, pp. 79–94, 2021. [Online]. Available: <https://doi.org/10.1146/annurev-cancerbio-060220-014137>
- [20] Y. Chen, Y. Zheng, Y. Gao, Z. Lin, S. Yang, T. Wang, Q. Wang, N. Xie, R. Hua, M. Liu, J. Sha, M. D. Griswold, J. Li, F. Tang, and M.-H. Tong, "Single-cell rna-seq uncovers dynamic processes and critical regulators in mouse spermatogenesis," *Cell Research*, vol. 28, no. 9, pp. 879–896, Sep 2018. [Online]. Available: <https://doi.org/10.1038/s41422-018-0074-y>
- [21] A. Trewavas, "A brief history of systems biology. "every object that biology studies is a system of systems." francois jacob (1974)," *The Plant cell*, vol. 18, no. 10, pp. 2420–2430, Oct 2006, 17088606[pmid]. [Online]. Available: <https://pubmed.ncbi.nlm.nih.gov/17088606>
- [22] D. Hanein and A. R. Horwitz, "The structure of cell-matrix adhesions: the new frontier," *Curr Opin Cell Biol*, vol. 24, no. 1, pp. 134–140, Feb 2012.
- [23] N. Wang, "Review of Cellular Mechanotransduction," *J Phys D Appl Phys*, vol. 50, no. 23, 06 2017.
- [24] C. Zhu, "Mechanochemistry: A molecular biomechanics view of mechanosensing," *Annals of Biomedical Engineering*, vol. 42, no. 2, pp. 388–404, Feb 2014. [Online]. Available: <https://doi.org/10.1007/s10439-013-0904-5>
- [25] E. K. Paluch, C. M. Nelson, N. Biais, B. Fabry, J. Moeller, B. L. Pruitt, C. Wollnik, G. Kudryasheva, F. Rehfeldt, and W. Federle, "Mechanotransduction: use the force(s)," *BMC Biology*, vol. 13, no. 1, p. 47, Jul 2015. [Online]. Available: <https://doi.org/10.1186/s12915-015-0150-4>
- [26] J. F. Marko and E. D. Siggia, "Stretching dna," *Macromolecules*, vol. 28, no. 26, pp. 8759–8770, Dec 1995. [Online]. Available: <https://doi.org/10.1021/ma00130a008>

- [27] J. F. Marko and S. Cocco, "The micromechanics of DNA," *Physics World*, vol. 16, no. 3, pp. 37–41, mar 2003. [Online]. Available: <https://doi.org/10.1088/2058-7058/16/3/40>
- [28] A. Sischka, K. Toensing, R. Eckel, S. D. Wilking, N. Sewald, R. Ros, and D. Anselmetti, "Molecular mechanisms and kinetics between dna and dna binding ligands," *Biophysical Journal*, vol. 88, no. 1, pp. 404–411, 2005. [Online]. Available: <https://www.sciencedirect.com/science/article/pii/S0006349505731155>
- [29] L. H. Hurley, "Dna and its associated processes as targets for cancer therapy," *Nature Reviews Cancer*, vol. 2, no. 3, pp. 188–200, Mar 2002. [Online]. Available: <https://doi.org/10.1038/nrc749>
- [30] D. Gawkowska, J. Cybulska, and A. Zdunek, "Structure-related gelling of pectins and linking with other natural compounds: A review," *Polymers*, vol. 10, no. 7, 2018. [Online]. Available: <https://www.mdpi.com/2073-4360/10/7/762>
- [31] C. Qiu, M. Zhao, and D. J. McClements, "Improving the stability of wheat protein-stabilized emulsions: Effect of pectin and xanthan gum addition," *Food Hydrocolloids*, vol. 43, pp. 377–387, 2015. [Online]. Available: <https://www.sciencedirect.com/science/article/pii/S0268005X14002392>
- [32] J. P. Rickgauer, D. N. Fuller, and D. E. Smith, "Dna as a metrology standard for length and force measurements with optical tweezers," *Biophysical Journal*, vol. 91, no. 11, pp. 4253–4257, 2006. [Online]. Available: <https://www.sciencedirect.com/science/article/pii/S0006349506721397>
- [33] E. A. Rose, "Applications of the polymerase chain reaction to genome analysis," *The FASEB Journal*, vol. 5, no. 1, pp. 46–54, 1991. [Online]. Available: <https://faseb.onlinelibrary.wiley.com/doi/abs/10.1096/fasebj.5.1.1991584>
- [34] E. Avci, H. Yabugaki, T. Hattori, K. Kamiyama, M. Kojima, Y. Mae, and T. Arai, "Dynamic releasing of biological cells at high speed using parallel mechanism to control adhesion forces," in *2014 IEEE International Conference on Robotics and Automation (ICRA)*, 2014, pp. 3789–3794.
- [35] M. Gauthier, S. Alvo, J. Dejeu, B. Tamadazte, P. Rougeot, and S. Régnier, "Analysis and specificities of adhesive forces between microscale and nanoscale," *IEEE Transactions on Automation Science and Engineering*, vol. 10, no. 3, pp. 562–570, 2013. [Online]. Available: <https://doi.org/10.1109/TASE.2013.2248150>

- [36] A. Ashkin, J. M. Dziedzic, J. E. Bjorkholm, and S. Chu, “Observation of a single-beam gradient force optical trap for dielectric particles,” *Opt. Lett.*, vol. 11, no. 5, pp. 288–290, May 1986. [Online]. Available: <http://opg.optica.org/ol/abstract.cfm?URI=ol-11-5-288>
- [37] A. Ashkin, “Acceleration and trapping of particles by radiation pressure,” *Phys. Rev. Lett.*, vol. 24, pp. 156–159, Jan 1970. [Online]. Available: <https://link.aps.org/doi/10.1103/PhysRevLett.24.156>
- [38] A. Ashkin and J. M. Dziedzic, “Optical levitation by radiation pressure,” *Applied Physics Letters*, vol. 19, no. 8, pp. 283–285, 1971.
- [39] J. P. Gordon and A. Ashkin, “Motion of atoms in a radiation trap,” *Phys. Rev. A*, vol. 21, pp. 1606–1617, May 1980. [Online]. Available: <https://link.aps.org/doi/10.1103/PhysRevA.21.1606>
- [40] A. Ashkin, “Applications of laser radiation pressure,” *Science*, vol. 210, no. 4474, pp. 1081–1088, 1980. [Online]. Available: <https://www.science.org/doi/abs/10.1126/science.210.4474.1081>
- [41] —, “Trapping of atoms by resonance radiation pressure,” *Phys. Rev. Lett.*, vol. 40, pp. 729–732, Mar 1978. [Online]. Available: <https://link.aps.org/doi/10.1103/PhysRevLett.40.729>
- [42] A. Ashkin and J. M. Dziedzic, “Optical levitation of liquid drops by radiation pressure,” *Science*, vol. 187, no. 4181, pp. 1073–1075, 1975. [Online]. Available: <https://www.science.org/doi/abs/10.1126/science.187.4181.1073>
- [43] E. F. Nichols and G. F. Hull, “A preliminary communication on the pressure of heat and light radiation,” *Phys. Rev. (Series I)*, vol. 13, pp. 307–320, Nov 1901. [Online]. Available: <https://link.aps.org/doi/10.1103/PhysRevSeriesI.13.307>
- [44] —, “The pressure due to radiation. (second paper.),” *Phys. Rev. (Series I)*, vol. 17, pp. 26–50, Jul 1903. [Online]. Available: <https://link.aps.org/doi/10.1103/PhysRevSeriesI.17.26>
- [45] R. V. Jones and J. C. S. Richards, “The pressure of radiation in a refracting medium,” *Proceedings of the Royal Society of London. Series A, Mathematical and Physical Sciences*, vol. 221, no. 1147, pp. 480–498, 1954. [Online]. Available: <http://www.jstor.org/stable/100774>
- [46] A. L. Schawlow and C. H. Townes, “Infrared and optical masers,” *Phys. Rev.*, vol. 112, pp. 1940–1949, Dec 1958. [Online]. Available: <https://link.aps.org/doi/10.1103/PhysRev.112.1940>

- [47] H. Kogelnik and T. Li, "Laser beams and resonators," *Appl. Opt.*, vol. 5, no. 10, pp. 1550–1567, Oct 1966.
- [48] D. Draegert, "Single-diode end-pumped nd:yag laser," *IEEE J. Quantum Electron.*, vol. 9, pp. 1146–1149, 1973.
- [49] A. Ashkin and J. M. Dziedzic, "Optical trapping and manipulation of viruses and bacteria," *Science*, vol. 235, no. 4795, pp. 1517–1520, 1987. [Online]. Available: <https://www.science.org/doi/abs/10.1126/science.3547653>
- [50] A. Ashkin, K. Schütze, J. M. Dziedzic, U. Euteneuer, and M. Schliwa, "Force generation of organelle transport measured in vivo by an infrared laser trap," *Nature*, vol. 348, no. 6299, pp. 346–348, Nov 1990. [Online]. Available: <https://doi.org/10.1038/348346a0>
- [51] L. Ikin, D. M. Carberry, G. M. Gibson, M. J. Padgett, and M. J. Miles, "Assembly and force measurement with SPM-like probes in holographic optical tweezers," *New Journal of Physics*, vol. 11, no. 2, p. 023012, feb 2009. [Online]. Available: <https://doi.org/10.1088/1367-2630/11/2/023012>
- [52] M. Xie, S. Chen, J. K. Mills, Y. Wang, Y. Liu, and D. Sun, "Cell out-of-plane rotation control using a cell surgery robotic system equipped with optical tweezers manipulators," in *2016 IEEE International Conference on Information and Automation (ICIA)*, 2016, pp. 103–108.
- [53] B. L. Aekbote, T. Fekete, J. Jacak, G. Vizsnyiczai, P. Ormos, and L. Kelemen, "Surface-modified complex su-8 microstructures for indirect optical manipulation of single cells," *Biomedical optics express*, vol. 7, no. 1, pp. 45–56, Dec 2015, 26819816[pmid].
- [54] S. Hu, R. Hu, X. Dong, T. Wei, S. Chen, and D. Sun, "Translational and rotational manipulation of filamentous cells using optically driven microrobots," *Opt. Express*, vol. 27, no. 12, pp. 16 475–16 482, Jun 2019. [Online]. Available: <http://opg.optica.org/oe/abstract.cfm?URI=oe-27-12-16475>
- [55] S. Fukada, H. Maruyama, T. Masuda, and F. Arai, "3d fabrication and manipulation of hybrid nanorobots by laser for single cell analysis," in *2012 International Symposium on Micro-NanoMechatronics and Human Science (MHS)*, 2012, pp. 479–481.
- [56] C.-L. Lin, Y.-H. Lee, C.-T. Lin, Y.-J. Liu, J.-L. Hwang, T.-T. Chung, and P. L. Baldeck, "Multiplying optical tweezers force using a micro-lever," *Opt. Express*, vol. 19, no. 21, pp. 20 604–20 609, Oct 2011.

- [57] Y. J. Jeong, T. W. Lim, Y. Son, D.-Y. Yang, H.-J. Kong, and K.-S. Lee, "Proportional enlargement of movement by using an optically driven multi-link system with an elastic joint," *Opt. Express*, vol. 18, no. 13, pp. 13 745–13 753, Jun 2010.
- [58] S. Ushiba, K. Masui, N. Taguchi, T. Hamano, S. Kawata, and S. Shoji, "Size dependent nanomechanics of coil spring shaped polymer nanowires," *Scientific Reports*, vol. 5, no. 1, p. 17152, Nov 2015. [Online]. Available: <https://doi.org/10.1038/srep17152>
- [59] A. A. Bui, A. B. Stilgoe, I. C. Lenton, L. J. Gibson, A. V. Kashchuk, S. Zhang, H. Rubinsztein-Dunlop, and T. A. Nieminen, "Theory and practice of simulation of optical tweezers," *Journal of Quantitative Spectroscopy and Radiative Transfer*, vol. 195, pp. 66–75, 2017, laser-light and Interactions with Particles 2016. [Online]. Available: <https://www.sciencedirect.com/science/article/pii/S0022407316306422>
- [60] T. A. Nieminen, A. B. Stilgoe, N. R. Heckenberg, and H. H. Rubinsztein-Dunlop, "Approximate and exact modeling of optical trapping," in *Optical Trapping and Optical Micromanipulation VII*, K. Dholakia and G. C. Spalding, Eds., vol. 7762, International Society for Optics and Photonics. SPIE, 2010, pp. 509 – 516.
- [61] T. A. Nieminen, N. R. Heckenberg, and H. Rubinsztein-Dunlop, "Computational modeling of optical tweezers," in *Optical Trapping and Optical Micromanipulation*, K. Dholakia and G. C. Spalding, Eds., vol. 5514, International Society for Optics and Photonics. SPIE, 2004, pp. 514 – 523.
- [62] A. Ashkin, "History of optical trapping and manipulation of small-neutral particle, atoms, and molecules," *IEEE Journal of Selected Topics in Quantum Electronics*, vol. 6, no. 6, pp. 841–856, 2000.
- [63] —, "Forces of a single-beam gradient laser trap on a dielectric sphere in the ray optics regime," *Biophysical Journal*, vol. 61, no. 2, pp. 569–582, 1992.
- [64] A. I. Lvovsky, *Encyclopedia of Optical and Photonic Engineering*. New York, NY, USA: Taylor and Francis, 2015, ch. Fresnel Equations, pp. 1–6.
- [65] K. C. Neuman and S. M. Block, "Optical trapping," *The Review of scientific instruments*, vol. 75, no. 9, pp. 2787–2809, Sep 2004, 16878180[pmid].
- [66] Y. Harada and T. Asakura, "Radiation forces on a dielectric sphere in the rayleigh scattering regime," *Optics Communications*, vol. 124, no. 5, pp. 529–541, 1996. [Online]. Available: <https://www.sciencedirect.com/science/article/pii/0030401895007539>

- [67] P. W. Smith, A. Ashkin, and W. J. Tomlinson, “Four-wave mixing in an artificial kerr medium,” *Opt. Lett.*, vol. 6, no. 6, pp. 284–286, Jun 1981. [Online]. Available: <http://opg.optica.org/ol/abstract.cfm?URI=ol-6-6-284>
- [68] G. Mie, “Beiträge zur optik trüber medien, speziell kolloidaler metallösungen,” *Annalen der Physik*, vol. 330, no. 3, pp. 377–445, 1908. [Online]. Available: <https://onlinelibrary.wiley.com/doi/abs/10.1002/andp.19083300302>
- [69] A. Salandrino, S. Fardad, and D. N. Christodoulides, “Generalized mie theory of optical forces,” *J. Opt. Soc. Am. B*, vol. 29, no. 4, pp. 855–866, Apr 2012. [Online]. Available: <http://opg.optica.org/josab/abstract.cfm?URI=josab-29-4-855>
- [70] A. Ashkin and J. M. Dziedzic, “Observation of light scattering from nonspherical particles using optical levitation,” *Appl. Opt.*, vol. 19, no. 5, pp. 660–668, Mar 1980. [Online]. Available: <http://opg.optica.org/ao/abstract.cfm?URI=ao-19-5-660>
- [71] F. Xu, K. Ren, G. Gouesbet, G. Gréhan, and X. Cai, “Generalized lorenz-mie theory for an arbitrarily oriented, located, and shaped beam scattered by a homogeneous spheroid,” *J. Opt. Soc. Am. A*, vol. 24, no. 1, pp. 119–131, Jan 2007. [Online]. Available: <http://opg.optica.org/josaa/abstract.cfm?URI=josaa-24-1-119>
- [72] K. F. Ren, G. Gréhan, and G. Gouesbet, “Prediction of reverse radiation pressure by generalized lorenz–mie theory,” *Appl. Opt.*, vol. 35, no. 15, pp. 2702–2710, May 1996. [Online]. Available: <http://opg.optica.org/ao/abstract.cfm?URI=ao-35-15-2702>
- [73] B. Sun, Y. Roichman, and D. G. Grier, “Theory of holographic optical trapping,” *Opt. Express*, vol. 16, no. 20, pp. 15 765–15 776, Sep 2008. [Online]. Available: <http://opg.optica.org/oe/abstract.cfm?URI=oe-16-20-15765>
- [74] P. Waterman, “Matrix formulation of electromagnetic scattering,” *Proceedings of the IEEE*, vol. 53, no. 8, pp. 805–812, 1965.
- [75] X. Qi, T. A. Nieminen, A. B. Stilgoe, V. L. Y. Loke, and H. Rubinsztein-Dunlop, “Comparison of t-matrix calculation methods for scattering by cylinders in optical tweezers,” *Opt. Lett.*, vol. 39, no. 16, pp. 4827–4830, Aug 2014. [Online]. Available: <http://opg.optica.org/ol/abstract.cfm?URI=ol-39-16-4827>
- [76] T. Nieminen, H. Rubinsztein-Dunlop, N. Heckenberg, and A. Bishop, “Numerical modelling of optical trapping,” *Computer Physics Communications*, vol. 142, no. 1, pp. 468–471, 2001, conference on Computational Physics

- 2000: "New Challenges for the New Millenium". [Online]. Available: <https://www.sciencedirect.com/science/article/pii/S0010465501003915>
- [77] T. Nieminen, H. Rubinsztein-Dunlop, and N. Heckenberg, "Calculation of the t-matrix: general considerations and application of the point-matching method," *Journal of Quantitative Spectroscopy and Radiative Transfer*, vol. 79-80, pp. 1019–1029, 2003, electromagnetic and Light Scattering by Non-Spherical Particles. [Online]. Available: <https://www.sciencedirect.com/science/article/pii/S0022407302003369>
- [78] V. L. Loke, T. A. Nieminen, N. R. Heckenberg, and H. Rubinsztein-Dunlop, "T-matrix calculation via discrete dipole approximation, point matching and exploiting symmetry," *Journal of Quantitative Spectroscopy and Radiative Transfer*, vol. 110, no. 14, pp. 1460–1471, 2009, xI Conference on Electromagnetic and Light Scattering by Non-Spherical Particles: 2008. [Online]. Available: <https://www.sciencedirect.com/science/article/pii/S0022407309000181>
- [79] T. A. Nieminen, V. L. Loke, A. B. Stilgoe, N. R. Heckenberg, and H. Rubinsztein-Dunlop, "T-matrix method for modelling optical tweezers," *Journal of Modern Optics*, vol. 58, no. 5-6, pp. 528–544, 2011.
- [80] G. Gouesbet, "T-matrix formulation and generalized lorenz–mie theories in spherical coordinates," *Optics Communications*, vol. 283, no. 4, pp. 517–521, 2010. [Online]. Available: <https://www.sciencedirect.com/science/article/pii/S0030401809010840>
- [81] T. A. Nieminen, N. du Preez-Wilkinson, A. B. Stilgoe, V. L. Loke, A. A. Bui, and H. Rubinsztein-Dunlop, "Optical tweezers: Theory and modelling," *Journal of Quantitative Spectroscopy and Radiative Transfer*, vol. 146, pp. 59–80, 2014, electromagnetic and Light Scattering by Nonspherical Particles XIV. [Online]. Available: <https://www.sciencedirect.com/science/article/pii/S0022407314001587>
- [82] K. Svoboda, C. F. Schmidt, B. J. Schnapp, and S. M. Block, "Direct observation of kinesin stepping by optical trapping interferometry," *Nature*, vol. 365, no. 6448, pp. 721–727, Oct 1993.
- [83] L. P. Ghislain and W. W. Webb, "Scanning-force microscope based on an optical trap," *Opt. Lett.*, vol. 18, no. 19, pp. 1678–1680, Oct 1993. [Online]. Available: <http://opg.optica.org/ol/abstract.cfm?URI=ol-18-19-1678>
- [84] A. A. M. Bui, A. V. Kashchuk, M. A. Balanant, T. A. Nieminen, H. Rubinsztein-Dunlop, and A. B. Stilgoe, "Calibration of force detection for arbitrarily shaped

- particles in optical tweezers,” *Scientific Reports*, vol. 8, no. 1, p. 10798, Jul 2018. [Online]. Available: <https://doi.org/10.1038/s41598-018-28876-y>
- [85] S. B. Smith, Y. Cui, and C. Bustamante, “Overstretching b-dna: The elastic response of individual double-stranded and single-stranded dna molecules,” *Science*, vol. 271, no. 5250, pp. 795–799, 1996. [Online]. Available: <https://www.science.org/doi/abs/10.1126/science.271.5250.795>
- [86] K. Berg-Sørensen and H. Flyvbjerg, “Power spectrum analysis for optical tweezers,” *Review of Scientific Instruments*, vol. 75, no. 3, pp. 594–612, Mar 2004. [Online]. Available: <https://doi.org/10.1063/1.1645654>
- [87] S. B. Smith, Y. Cui, and C. Bustamante, “[7] optical-trap force transducer that operates by direct measurement of light momentum,” in *Biophotonics, Part B*, ser. Methods in Enzymology. Academic Press, 2003, vol. 361, pp. 134–162. [Online]. Available: <https://www.sciencedirect.com/science/article/pii/S0076687903610098>
- [88] A. Farré and M. Montes-Usategui, “A force detection technique for single-beam optical traps based on direct measurement of light momentum changes,” *Opt. Express*, vol. 18, no. 11, pp. 11 955–11 968, May 2010. [Online]. Available: <http://opg.optica.org/oe/abstract.cfm?URI=oe-18-11-11955>
- [89] A. Ashkin, J. M. Dziedzic, and T. Yamane, “Optical trapping and manipulation of single cells using infrared laser beams,” *Nature*, vol. 330, no. 6150, pp. 769–771, Dec 1987. [Online]. Available: <https://doi.org/10.1038/330769a0>
- [90] K. Svoboda and S. M. Block, “Biological applications of optical forces,” *Annual Review of Biophysics and Biomolecular Structure*, vol. 23, no. 1, pp. 247–285, 1994, pMID: 7919782.
- [91] J. P. Mills, L. Qie, M. Dao, C. T. Lim, and S. Suresh, “Nonlinear elastic and viscoelastic deformation of the human red blood cell with optical tweezers,” *Molecular & Cellular Biomechanics*, vol. 1, no. 3, pp. 169–180, 2004. [Online]. Available: <http://www.techscience.com/mcb/v1n3/33588>
- [92] M. Capitanio and F. S. Pavone, “Interrogating biology with force: Single molecule high-resolution measurements with optical tweezers,” *Biophysical Journal*, vol. 105, no. 6, pp. 1293–1303, 2013. [Online]. Available: <https://www.sciencedirect.com/science/article/pii/S0006349513009144>
- [93] P. Grigaravičius, K. O. Greulich, and S. Monajembashi, “Laser microbeams and optical tweezers in ageing research,” *ChemPhysChem*, vol. 10, no. 1, pp. 79–85, Jan 2009.

- [94] S. Suei, A. Raudsepp, L. M. Kent, S. A. Keen, V. V. Filichev, and M. A. Williams, "Dna visualization in single molecule studies carried out with optical tweezers: Covalent versus non-covalent attachment of fluorophores," *Biochemical and Biophysical Research Communications*, vol. 466, no. 2, pp. 226–231, 2015. [Online]. Available: <https://www.sciencedirect.com/science/article/pii/S0006291X15305301>
- [95] M. J. McCauley and M. C. Williams, "Mechanisms of dna binding determined in optical tweezers experiments," *Biopolymers*, vol. 85, no. 2, pp. 154–168, 2007. [Online]. Available: <https://onlinelibrary.wiley.com/doi/abs/10.1002/bip.20622>
- [96] S. B. Smith, L. Finzi, and C. Bustamante, "Direct mechanical measurements of the elasticity of single dna molecules by using magnetic beads," *Science*, vol. 258, no. 5085, pp. 1122–1126, 1992. [Online]. Available: <https://www.science.org/doi/abs/10.1126/science.1439819>
- [97] R. Simmons, J. Finer, S. Chu, and J. Spudich, "Quantitative measurements of force and displacement using an optical trap," *Biophysical Journal*, vol. 70, no. 4, pp. 1813–1822, 1996. [Online]. Available: <https://www.sciencedirect.com/science/article/pii/S0006349596797461>
- [98] C.-H. Lien, M.-T. Wei, T.-Y. Tseng, C.-D. Lee, C. Wang, T.-F. Wang, H. D. Ou-Yang, and A. Chiou, "Probing the dynamic differential stiffness of dsdna interacting with reca in the enthalpic regime," *Opt. Express*, vol. 17, no. 22, pp. 20 376–20 385, Oct 2009.
- [99] C. Bouchiat, M. Wang, J.-F. Allemand, T. Strick, S. Block, and V. Croquette, "Estimating the persistence length of a worm-like chain molecule from force-extension measurements," *Biophysical Journal*, vol. 76, no. 1, pp. 409–413, 1999. [Online]. Available: <https://www.sciencedirect.com/science/article/pii/S0006349599772073>
- [100] M. Wang, H. Yin, R. Landick, J. Gelles, and S. Block, "Stretching dna with optical tweezers," *Biophysical Journal*, vol. 72, no. 3, pp. 1335–1346, 1997. [Online]. Available: <https://www.sciencedirect.com/science/article/pii/S0006349597787800>
- [101] C. Bustamante, J. F. Marko, E. D. Siggia, and S. Smith, "Entropic elasticity of λ -phage dna," *Science*, vol. 265, no. 5178, pp. 1599–1600, 1994. [Online]. Available: <https://www.science.org/doi/abs/10.1126/science.8079175>
- [102] G. V. Shivashankar, M. Feingold, O. Krichevsky, and A. Libchaber, "Reca polymerization on double-stranded dna by using single-molecule

- manipulation: The role of atp hydrolysis,” *Proceedings of the National Academy of Sciences*, vol. 96, no. 14, pp. 7916–7921, 1999. [Online]. Available: <https://www.pnas.org/doi/abs/10.1073/pnas.96.14.7916>
- [103] J. van Mameren, P. Gross, G. Farge, P. Hooijman, M. Modesti, M. Falkenberg, G. J. L. Wuite, and E. J. G. Peterman, “Unraveling the structure of dna during overstretching by using multicolor, single-molecule fluorescence imaging,” *Proceedings of the National Academy of Sciences*, vol. 106, no. 43, pp. 18 231–18 236, 2009. [Online]. Available: <https://www.pnas.org/doi/abs/10.1073/pnas.0904322106>
- [104] S. K. Mohanty, A. Rapp, S. Monajembashi, P. K. Gupta, and K. O. Greulich, “Comet Assay Measurements of DNA Damage in Cells by Laser Microbeams and Trapping Beams with Wavelengths Spanning a Range of 308 nm to 1064 nm,” *Radiation Research*, vol. 157, no. 4, pp. 378 – 385, 2002.
- [105] H. Liang, K. Vu, P. Krishnan, T. Trang, D. Shin, S. Kimel, and M. Berns, “Wavelength dependence of cell cloning efficiency after optical trapping,” *Biophysical Journal*, vol. 70, no. 3, pp. 1529–1533, 1996. [Online]. Available: <https://www.sciencedirect.com/science/article/pii/S0006349596797163>
- [106] K. Neuman, E. H. Chadd, G. F. Liou, K. Bergman, and S. M. Block, “Characterization of photodamage to escherichia coli in optical traps,” *Biophysical Journal*, vol. 77, pp. 2856–2863, 1999.
- [107] M. P. Landry, P. M. McCall, Z. Qi, and Y. R. Chemla, “Characterization of photoactivated singlet oxygen damage in single-molecule optical trap experiments,” *Biophysical journal*, vol. 97, pp. 2128–2136, 2009.
- [108] A. Blázquez-Castro, “Optical tweezers: Phototoxicity and thermal stress in cells and biomolecules,” *Micromachines*, vol. 10, no. 8, 2019.
- [109] Y. Liu, D. Cheng, G. Sonek, M. Berns, C. Chapman, and B. Tromberg, “Evidence for localized cell heating induced by infrared optical tweezers,” *Biophysical Journal*, vol. 68, no. 5, pp. 2137–2144, 1995. [Online]. Available: <https://www.sciencedirect.com/science/article/pii/S0006349595803966>
- [110] E. J. Peterman, F. Gittes, and C. F. Schmidt, “Laser-induced heating in optical traps,” *Biophysical Journal*, vol. 84, no. 2, pp. 1308–1316, 2003. [Online]. Available: <https://www.sciencedirect.com/science/article/pii/S0006349503749467>

- [111] H. Nagar, T. Admon, D. Goldman, A. Eyal, and Y. Roichman, “Optical trapping below the diffraction limit with a tunable beam waist using super-oscillating beams,” *Opt. Lett.*, vol. 44, no. 10, pp. 2430–2433, May 2019. [Online]. Available: <http://opg.optica.org/ol/abstract.cfm?URI=ol-44-10-2430>
- [112] G. D. M. Jeffries, J. S. Edgar, Y. Zhao, J. P. Shelby, C. Fong, and D. T. Chiu, “Using polarization-shaped optical vortex traps for single-cell nanosurgery,” *Nano Letters*, vol. 7, no. 2, pp. 415–420, Feb 2007.
- [113] B. A. Kairdolf, A. M. Smith, T. H. Stokes, M. D. Wang, A. N. Young, and S. Nie, “Semiconductor quantum dots for bioimaging and biodiagnostic applications,” *Annual Review of Analytical Chemistry*, vol. 6, no. 1, pp. 143–162, 2013, pMID: 23527547.
- [114] A. Chowdhury, D. Waghmare, R. Dasgupta, and S. K. Majumder, “Red blood cell membrane damage by light-induced thermal gradient under optical trap,” *Journal of Biophotonics*, vol. 11, no. 8, p. e201700222, 2018. [Online]. Available: <https://onlinelibrary.wiley.com/doi/abs/10.1002/jbio.201700222>
- [115] K. König, Y. Tadir, P. Patrizio, M. W. Berns, and B. J. Tromberg, “Andrology: Effects of ultraviolet exposure and near infrared laser tweezers on human spermatozoa,” *Human Reproduction*, vol. 11, no. 10, pp. 2162–2164, Oct 1996.
- [116] Z. Liu, L. Wang, Y. Zhang, C. Liu, J. Wu, Y. Zhang, X. Yang, J. Zhang, J. Yang, and L. Yuan, “Optical funnel for living cells trap,” *Optics Communications*, vol. 431, pp. 196–198, 2019. [Online]. Available: <https://www.sciencedirect.com/science/article/pii/S0030401818308034>
- [117] B. Shao, L. Z. Shi, J. M. Nascimento, E. L. Botvinick, M. Ozkan, M. W. Berns, and S. C. Esener, “High-throughput sorting and analysis of human sperm with a ring-shaped laser trap,” *Biomedical Microdevices*, vol. 9, no. 3, pp. 361–369, Jun 2007. [Online]. Available: <https://doi.org/10.1007/s10544-006-9041-3>
- [118] T. Čižmár, M. Šiler, and P. Zemánek, “An optical nanotrap array movable over a millimetre range,” *Applied Physics B*, vol. 84, no. 1, pp. 197–203, Jul 2006.
- [119] B. Shao, S. C. Esener, J. M. Nascimento, M. W. Berns, E. L. Botvinick, and M. Ozkan, “Size tunable three-dimensional annular laser trap based on axicons,” *Opt. Lett.*, vol. 31, no. 22, pp. 3375–3377, Nov 2006. [Online]. Available: <http://opg.optica.org/ol/abstract.cfm?URI=ol-31-22-3375>
- [120] I. Manek, Y. Ovchinnikov, and R. Grimm, “Generation of a hollow laser beam for atom trapping using an axicon,” *Optics Communications*, vol. 147, no. 1,

- pp. 67–70, 1998. [Online]. Available: <https://www.sciencedirect.com/science/article/pii/S0030401897006457>
- [121] J. Arlt, K. Dholakia, J. Soneson, and E. M. Wright, “Optical dipole traps and atomic waveguides based on bessel light beams,” *Phys. Rev. A*, vol. 63, p. 063602, May 2001. [Online]. Available: <https://link.aps.org/doi/10.1103/PhysRevA.63.063602>
- [122] M. Dao, C. Lim, and S. Suresh, “Mechanics of the human red blood cell deformed by optical tweezers,” *Journal of the Mechanics and Physics of Solids*, vol. 51, no. 11, pp. 2259–2280, 2003, proceedings of a Symposium on Dynamic Failure and Thin Film Mechanics, honoring Professor L.B. Freund. [Online]. Available: <https://www.sciencedirect.com/science/article/pii/S0022509603001595>
- [123] M. R. Pollard, S. W. Botchway, B. Chichkov, E. Freeman, R. N. J. Halsall, D. W. K. Jenkins, I. Loader, A. Ovsianikov, A. W. Parker, R. Stevens, R. Turchetta, A. D. Ward, and M. Towrie, “Optically trapped probes with nanometer-scale tips for femto-newton force measurement,” *New Journal of Physics*, vol. 12, no. 11, p. 113056, nov 2010. [Online]. Available: <https://doi.org/10.1088/1367-2630/12/11/113056>
- [124] D. B. Phillips, S. H. Simpson, J. A. Grieve, R. Bowman, G. M. Gibson, M. J. Padgett, J. G. Rarity, S. Hanna, M. J. Miles, and D. M. Carberry, “Force sensing with a shaped dielectric micro-tool,” *EPL (Europhysics Letters)*, vol. 99, no. 5, p. 58004, sep 2012. [Online]. Available: <https://doi.org/10.1209/0295-5075/99/58004>
- [125] E. Avci, K. Ohara, C.-N. Nguyen, C. Theeravithayangkura, M. Kojima, T. Tanikawa, Y. Mae, and T. Arai, “High-speed automated manipulation of microobjects using a two-fingered microhand,” *IEEE Transactions on Industrial Electronics*, vol. 62, no. 2, pp. 1070–1079, 2015.
- [126] A. Mittas, F. M. Dickey, and S. C. Holswade, “Modeling an optical micromachine probe,” in *Ultrahigh- and High-Speed Photography and Image-based Motion Measurement*, C. B. Johnson, A. Davidhazy, T. G. Etoh, C. B. Johnson, D. R. Snyder, J. S. Walton, and J. S. Walton, Eds., vol. 3173, International Society for Optics and Photonics. SPIE, 1997, pp. 345 – 356. [Online]. Available: <https://doi.org/10.1117/12.294528>
- [127] P. J. Rodrigo, L. Gammelgaard, P. Bøggild, I. R. Perch-Nielsen, and J. Glückstad,

- “Actuation of microfabricated tools using multiple gpc-based counterpropagating-beam traps,” *Opt. Express*, vol. 13, no. 18, pp. 6899–6904, Sep 2005. [Online]. Available: <http://opg.optica.org/oe/abstract.cfm?URI=oe-13-18-6899>
- [128] M. Probst, C. Hürzeler, R. Borer, and B. J. Nelson, “A microassembly system for the flexible assembly of hybrid robotic mems devices,” *International Journal of Optomechatronics*, vol. 3, no. 2, pp. 69–90, 2009.
- [129] A. P. Gerratt, I. Penskiy, and S. Bergbreiter, “Integrated silicon-pdms process for microrobot mechanisms,” in *2010 IEEE International Conference on Robotics and Automation*, 2010, pp. 3153–3158.
- [130] C. W. Hull, “Apparatus for production of three-dimensional objects by stereolithography,” Mar 1986.
- [131] P. Galajda and P. Ormos, “Complex micromachines produced and driven by light,” *Applied Physics Letters*, vol. 78, no. 2, pp. 249–251, 2001.
- [132] M. Göppert-Mayer, “Über elementarakte mit zwei quantensprüngen,” *Annalen der Physik*, vol. 401, no. 3, pp. 273–294, Jan 1931. [Online]. Available: <https://doi.org/10.1002/andp.19314010303>
- [133] A. La Porta, B. J. Offrein, and I. M. Soganci, “Apparatus for production of three-dimensional objects by stereolithography,” 2013.
- [134] J. K. Hohmann, M. Renner, E. H. Waller, and G. von Freymann, “Three-dimensional μ -printing: An enabling technology,” *Advanced Optical Materials*, vol. 3, no. 11, pp. 1488–1507, 2015. [Online]. Available: <https://onlinelibrary.wiley.com/doi/abs/10.1002/adom.201500328>
- [135] J. Ma, W. Cheng, S. Zhang, D. Feng, T. Jia, Z. Sun, and J. Qiu, “Coherent quantum control of two-photon absorption and polymerization by shaped ultrashort laser pulses,” *Laser Physics Letters*, vol. 10, no. 8, p. 085304, jul 2013. [Online]. Available: <https://doi.org/10.1088/1612-2011/10/8/085304>
- [136] J. M. Kim and H. Muramatsu, “Two-photon photopolymerized tips for adhesion-free scanning-probe microscopy,” *Nano Letters*, vol. 5, no. 2, pp. 309–314, Feb 2005. [Online]. Available: <https://doi.org/10.1021/nl0480363>
- [137] S. Kawata, H.-B. Sun, T. Tanaka, and K. Takada, “Finer features for functional microdevices,” *Nature*, vol. 412, no. 6848, pp. 697–698, Aug 2001.
- [138] A. Accardo, M.-C. Blatché, R. Courson, I. Loubinoux, C. Vieu, and L. Malaquin, “Two-photon lithography and microscopy of 3d hydrogel scaffolds for neuronal

- cell growth,” *Biomedical Physics & Engineering Express*, vol. 4, no. 2, p. 027009, feb 2018. [Online]. Available: <https://doi.org/10.1088/2057-1976/aaab93>
- [139] R. Inukai, H. Takao, F. Shimokawa, and K. Terao, “On-site manipulation of single dna molecules using optically-driven microchopsticks,” in *2017 IEEE 30th International Conference on Micro Electro Mechanical Systems (MEMS)*, 2017, pp. 585–588.
- [140] E. Avci, M. Grammatikopoulou, and G.-Z. Yang, “Laser-printing and 3d optical-control of untethered microrobots,” *Advanced Optical Materials*, vol. 5, no. 19, p. 1700031, 2017.
- [141] B. Koss, S. Chowdhury, T. Aabo, S. K. Gupta, and W. Losert, “Indirect optical gripping with triplet traps,” *J. Opt. Soc. Am. B*, vol. 28, no. 5, pp. 982–985, May 2011. [Online]. Available: <http://opg.optica.org/josab/abstract.cfm?URI=josab-28-5-982>
- [142] S. Nakanishi, H.-B. Sun, and S. Kawata, “Elasticity of two-photon-fabricated nano-wires,” in *Nanoengineering: Fabrication, Properties, Optics, and Devices IV*, E. A. Dobisz and L. A. Eldada, Eds., vol. 6645, International Society for Optics and Photonics. SPIE, 2007, pp. 214 – 222.
- [143] H.-B. Sun, K. Takada, and S. Kawata, “Elastic force analysis of functional polymer submicron oscillators,” *Applied Physics Letters*, vol. 79, no. 19, pp. 3173–3175, 2001.
- [144] E. D. Lemma, F. Rizzi, T. Dattoma, B. Spagnolo, L. Sileo, A. Quattieri, M. De Vittorio, and F. Pisanello, “Mechanical properties tunability of three-dimensional polymeric structures in two-photon lithography,” *IEEE Transactions on Nanotechnology*, vol. 16, no. 1, pp. 23–31, 2017.
- [145] A. Raudsepp, L. M. Kent, S. B. Hall, and M. A. Williams, “Overstretching partially alkyne functionalized dsdna using near infrared optical tweezers,” *Biochemical and Biophysical Research Communications*, vol. 496, no. 3, pp. 975–980, 2018. [Online]. Available: <https://www.sciencedirect.com/science/article/pii/S0006291X18300998>
- [146] M. R. Griffiths, A. Raudsepp, K. M. McGrath, and M. A. K. Williams, “Measuring the interaction between a pair of emulsion droplets using dual-trap optical tweezers,” *RSC Adv.*, vol. 6, pp. 14 538–14 546, 2016. [Online]. Available: <http://dx.doi.org/10.1039/C5RA25073K>

- [147] D. P. Crimp and E. Avci, “Development of a micromanipulation platform with passive-active hybrid release strategy for single-cell separation,” in *2018 IEEE/ASME International Conference on Advanced Intelligent Mechatronics (AIM)*, 2018, pp. 986–990.
- [148] F. Arai, D. Ando, T. Fukuda, Y. Nonoda, and T. Oota, “Micro manipulation based on micro physics-strategy based on attractive force reduction and stress measurement,” in *Proceedings 1995 IEEE/RSJ International Conference on Intelligent Robots and Systems. Human Robot Interaction and Cooperative Robots*, vol. 2, 1995, pp. 236–241 vol.2.
- [149] L. Bergström, “Hamaker constants of inorganic materials,” *Advances in Colloid and Interface Science*, vol. 70, pp. 125–169, Jul 1997. [Online]. Available: <https://www.sciencedirect.com/science/article/pii/S0001868697000031>
- [150] R. P. Badman, F. Ye, W. Caravan, and M. D. Wang, “High trap stiffness microcylinders for nanophotonic trapping,” *ACS Applied Materials & Interfaces*, vol. 11, no. 28, pp. 25 074–25 080, Jul 2019.
- [151] A.-I. Bunea, E. L. Engay, M. Chouliara, A. R. Bañas, and J. Glückstad, “Rational design of light-controlled microrobots,” in *Advanced Manufacturing Technologies for Micro- and Nanosystems in Security and Defence*, A. Camposeo, Y. Dzenis, M. Farsari, and L. Persano, Eds., vol. 10804, International Society for Optics and Photonics. SPIE, 2018, pp. 1 – 9. [Online]. Available: <https://doi.org/10.1117/12.2325547>
- [152] J. Glückstad, “Sculpting the object,” *Nature Photonics*, vol. 5, no. 1, pp. 7–8, Jan 2011. [Online]. Available: <https://doi.org/10.1038/nphoton.2010.301>
- [153] D. B. Phillips, G. M. Gibson, R. Bowman, M. J. Padgett, S. Hanna, D. M. Carberry, M. J. Miles, and S. H. Simpson, “An optically actuated surface scanning probe,” *Opt. Express*, vol. 20, no. 28, pp. 29 679–29 693, Dec 2012. [Online]. Available: <http://opg.optica.org/oe/abstract.cfm?URI=oe-20-28-29679>
- [154] W. Wang, A. E. Chiou, G. J. Sonek, and M. W. Berns, “Self-aligned dual-beam optical laser trap using photorefractive phase conjugation,” *J. Opt. Soc. Am. B*, vol. 14, no. 4, pp. 697–704, Apr 1997. [Online]. Available: <http://opg.optica.org/josab/abstract.cfm?URI=josab-14-4-697>
- [155] M. Woerdemann, K. Berghoff, and C. Denz, “Dynamic multiple-beam counter-propagating optical traps using optical phase-conjugation,” *Opt. Express*, vol. 18, no. 21, pp. 22 348–22 357, Oct 2010. [Online]. Available: <http://opg.optica.org/oe/abstract.cfm?URI=oe-18-21-22348>

- [156] H. Ukita and K. Nagatomi, “Optical tweezers and fluid characteristics of an optical rotator with slopes on the surface upon which light is incident and a cylindrical body,” *Appl. Opt.*, vol. 42, no. 15, pp. 2708–2715, May 2003. [Online]. Available: <http://opg.optica.org/ao/abstract.cfm?URI=ao-42-15-2708>
- [157] S. Maruo and H. Inoue, “Optically driven micropump produced by three-dimensional two-photon microfabrication,” *Applied Physics Letters*, vol. 89, no. 14, p. 144101, 2006.
- [158] A. V. Kashchuk, A. A. Bui, S. Zhang, A. Houillot, D. Carberry, A. B. Stilgoe, T. A. Nieminen, and H. Rubinsztein-Dunlop, “Chapter 4 - optically driven rotating micromachines,” in *Light Robotics: Structure-Mediated Nanobiophotonics*, ser. Nanophotonics, J. Glückstad and D. Palima, Eds. Elsevier, 2017, pp. 99–128. [Online]. Available: <https://www.sciencedirect.com/science/article/pii/B9780702070969000045>
- [159] C.-L. Lin, G. Vitrant, M. Bouriau, R. Casalegno, and P. L. Baldeck, “Optically driven archimedes micro-screws for micropump application,” *Opt. Express*, vol. 19, no. 9, pp. 8267–8276, Apr 2011. [Online]. Available: <http://opg.optica.org/oe/abstract.cfm?URI=oe-19-9-8267>
- [160] P. Galajda and P. Ormos, “Rotors produced and driven in laser tweezers with reversed direction of rotation,” *Applied Physics Letters*, vol. 80, no. 24, pp. 4653–4655, Jun 2002.
- [161] A. La Porta and M. D. Wang, “Optical torque wrench: Angular trapping, rotation, and torque detection of quartz microparticles,” *Phys. Rev. Lett.*, vol. 92, p. 190801, May 2004.
- [162] J. Inman, S. Forth, and M. D. Wang, “Passive torque wrench and angular position detection using a single-beam optical trap,” *Opt. Lett.*, vol. 35, no. 17, pp. 2949–2951, Sep 2010.
- [163] S. C. Chapin, V. Germain, and E. R. Dufresne, “Automated trapping, assembly, and sorting with holographic optical tweezers,” *Opt. Express*, vol. 14, no. 26, pp. 13 095–13 100, Dec 2006. [Online]. Available: <http://opg.optica.org/oe/abstract.cfm?URI=oe-14-26-13095>
- [164] Y. Tanaka, H. Kawada, K. Hirano, M. Ishikawa, and H. Kitajima, “Automated manipulation of non-spherical micro-objects using optical tweezers combined with image processing techniques,” *Opt. Express*, vol. 16, no. 19, pp. 15 115–15 122, Sep 2008. [Online]. Available: <http://opg.optica.org/oe/abstract.cfm?URI=oe-16-19-15115>

- [165] S. Maruo, A. Takaura, and Y. Saito, “Optically driven micropump with a twin spiral microrotor,” *Opt. Express*, vol. 17, no. 21, pp. 18 525–18 532, Oct 2009. [Online]. Available: <http://opg.optica.org/oe/abstract.cfm?URI=oe-17-21-18525>
- [166] R. C. Gauthier, “Trapping model for the low-index ring-shaped micro-object in a focused, lowest-order gaussian laser-beam profile,” *J. Opt. Soc. Am. B*, vol. 14, no. 4, pp. 782–789, Apr 1997. [Online]. Available: <http://opg.optica.org/josab/abstract.cfm?URI=josab-14-4-782>
- [167] D. G. Grier and Y. Roichman, “Holographic optical trapping,” *Appl. Opt.*, vol. 45, no. 5, pp. 880–887, Feb 2006. [Online]. Available: <http://opg.optica.org/ao/abstract.cfm?URI=ao-45-5-880>
- [168] G. Brouhard, H. Schek, and A. Hunt, “Advanced optical tweezers for the study of cellular and molecular biomechanics,” *IEEE Transactions on Biomedical Engineering*, vol. 50, no. 1, pp. 121–125, 2003.
- [169] A. van der Horst and N. R. Forde, “Calibration of dynamic holographic optical tweezers for force measurements on biomaterials,” *Opt. Express*, vol. 16, no. 25, pp. 20 987–21 003, Dec 2008.
- [170] R. W. Gerchberg, “A practical algorithm for the determination of phase from image and diffraction plane pictures,” *Optik*, vol. 35, pp. 237–246, 1972.
- [171] R. D. Leonardo, F. Ianni, and G. Ruocco, “Computer generation of optimal holograms for optical trap arrays,” *Opt. Express*, vol. 15, no. 4, pp. 1913–1922, Feb 2007. [Online]. Available: <http://opg.optica.org/oe/abstract.cfm?URI=oe-15-4-1913>
- [172] E. Pleguezuelos, A. Carnicer, J. Andilla, E. Martín-Badosa, and M. Montes-Usategui, “Holotrap: Interactive hologram design for multiple dynamic optical trapping,” *Computer Physics Communications*, vol. 176, no. 11, pp. 701–709, 2007. [Online]. Available: <https://www.sciencedirect.com/science/article/pii/S0010465507002032>
- [173] P. Pozzi, L. Maddalena, N. Ceffa, O. Soloviev, G. Vdovin, E. Carroll, and M. Verhaegen, “Fast calculation of computer generated holograms for 3d photostimulation through compressive-sensing gerchberg–saxton algorithm,” *Methods and Protocols*, vol. 2, no. 1, 2019. [Online]. Available: <https://www.mdpi.com/2409-9279/2/1/2>
- [174] R. W. Bowman, G. M. Gibson, A. Linnenberger, D. B. Phillips, J. A. Grieve, D. M. Carberry, S. Serati, M. J. Miles, and M. J. Padgett, ““red tweezers”:

- Fast, customisable hologram generation for optical tweezers,” *Computer Physics Communications*, vol. 185, no. 1, pp. 268–273, 2014. [Online]. Available: <https://www.sciencedirect.com/science/article/pii/S0010465513002695>
- [175] A. H. Mack, M. K. Trías, and S. G. J. Mochrie, “Precision optical trapping via a programmable direct-digital-synthesis-based controller for acousto-optic deflectors,” *Review of Scientific Instruments*, vol. 80, no. 1, p. 016101, 2009.
- [176] M. T. Valentine, N. R. Guydosh, B. Gutiérrez-Medina, A. N. Fehr, J. O. Andreasson, and S. M. Block, “Precision steering of an optical trap by electro-optic deflection,” *Opt. Lett.*, vol. 33, no. 6, pp. 599–601, Mar 2008. [Online]. Available: <http://opg.optica.org/ol/abstract.cfm?URI=ol-33-6-599>
- [177] S. N. Antonov, “Acousto-optic deflector with a high diffraction efficiency and wide angular scanning range,” *Acoustical Physics*, vol. 64, no. 4, pp. 432–436, Jul 2018.
- [178] —, “Paratellurite-based acoustooptical deflectors. methods for increasing their efficiency and widening the scanning angle,” *Instruments and Experimental Techniques*, vol. 62, no. 3, pp. 386–392, Jul 2019. [Online]. Available: <https://doi.org/10.1134/S0020441219020155>
- [179] A. Constable, J. Kim, J. Mervis, F. Zarinetchi, and M. Prentiss, “Demonstration of a fiber-optical light-force trap,” *Opt. Lett.*, vol. 18, no. 21, pp. 1867–1869, Nov 1993. [Online]. Available: <http://opg.optica.org/ol/abstract.cfm?URI=ol-18-21-1867>
- [180] X. Zhao, N. Zhao, Y. Shi, H. Xin, and B. Li, “Optical fiber tweezers: A versatile tool for optical trapping and manipulation,” *Micromachines*, vol. 11, no. 2, 2020. [Online]. Available: <https://www.mdpi.com/2072-666X/11/2/114>
- [181] M.-J. Oh, F. Kuhr, F. Byfield, and I. Levitan, “Micropipette aspiration of substrate-attached cells to estimate cell stiffness,” *JoVE*, no. 67, p. e3886, Sep 2012.
- [182] Y. Tanaka, “Double-arm optical tweezer system for precise and dexterous handling of micro-objects in 3d workspace,” *Optics and Lasers in Engineering*, vol. 111, pp. 65–70, 2018. [Online]. Available: <https://www.sciencedirect.com/science/article/pii/S0143816618306432>
- [183] S. Bianchi and R. Di Leonardo, “Real-time optical micro-manipulation using optimized holograms generated on the gpu,” *Computer Physics*

- Communications*, vol. 181, no. 8, pp. 1444–1448, 2010. [Online]. Available: <https://www.sciencedirect.com/science/article/pii/S0010465510001232>
- [184] P.-K. Andrew, D. Fan, A. Raudsepp, M. Lofroth, U. Staufer, M. A. K. Williams, and E. Avci, “Design of optical micromachines for use in biologically relevant environments,” in *2020 IEEE/ASME International Conference on Advanced Intelligent Mechatronics (AIM)*, 2020, pp. 2039–2045.
- [185] R. D. Rodriguez, E. Lacaze, and J. Jupille, “Probing the probe: Afm tip-profiling via nanotemplates to determine hamaker constants from phase–distance curves,” *Ultramicroscopy*, vol. 121, pp. 25–30, 2012. [Online]. Available: <https://www.sciencedirect.com/science/article/pii/S0304399112001465>
- [186] R. S. Pieters, H.-W. Tung, D. F. Sargent, and B. J. Nelson, “Non-contact manipulation for automated protein crystal harvesting using a rolling microrobot,” *IFAC Proceedings Volumes*, vol. 47, no. 3, pp. 7480–7485, 2014, 19th IFAC World Congress. [Online]. Available: <https://www.sciencedirect.com/science/article/pii/S1474667016427916>
- [187] J. E. Melzer and E. McLeod, “Assembly of multicomponent structures from hundreds of micron-scale building blocks using optical tweezers,” *Microsystems & Nanoengineering*, vol. 7, no. 1, p. 45, Jun 2021. [Online]. Available: <https://doi.org/10.1038/s41378-021-00272-z>
- [188] J. Liu, C. Wu, G. Dai, F. Feng, Y. Chi, K. Xu, and W. Zhong, “Molecular self-assembly of a tyroservatide-derived octapeptide and hydroxycamptothecin for enhanced therapeutic efficacy,” *Nanoscale*, vol. 13, pp. 5094–5102, 2021. [Online]. Available: <http://dx.doi.org/10.1039/D0NR08741F>
- [189] Z. Li, Q. Fan, and Y. Yin, “Colloidal self-assembly approaches to smart nanostructured materials,” *Chemical Reviews*, vol. 122, no. 5, pp. 4976–5067, 2022, PMID: 34747588. [Online]. Available: <https://doi.org/10.1021/acs.chemrev.1c00482>
- [190] A.-I. Bunea, N. del Castillo Iniesta, A. Droumpali, A. E. Wetzel, E. Engay, and R. Taboryski, “Micro 3d printing by two-photon polymerization: Configurations and parameters for the nanoscribe system,” *Micro*, vol. 1, no. 2, pp. 164–180, 2021. [Online]. Available: <https://www.mdpi.com/2673-8023/1/2/13>
- [191] J. E. Curtis, B. A. Koss, and D. G. Grier, “Dynamic holographic optical tweezers,” *Optics Communications*, vol. 207, no. 1, pp. 169–175, 2002. [Online]. Available: <https://www.sciencedirect.com/science/article/pii/S0030401802015249>

- [192] J. Liesener, M. Reicherter, T. Haist, and H. Tiziani, "Multi-functional optical tweezers using computer-generated holograms," *Optics Communications*, vol. 185, no. 1, pp. 77–82, 2000. [Online]. Available: <https://www.sciencedirect.com/science/article/pii/S0030401800009901>
- [193] N. Malagnino, G. Pesce, A. Sasso, and E. Arimondo, "Measurements of trapping efficiency and stiffness in optical tweezers," *Opt. Commun.*, vol. 214, no. 1, pp. 15–24, 2002.
- [194] D.-Y. Chiou, M.-Y. Chen, M.-W. Chang, and H.-C. Deng, "Characterization and optimization design of the polymer-based capacitive micro-arrayed ultrasonic transducer," *Japanese Journal of Applied Physics*, vol. 46, no. 11, pp. 7496–7503, nov 2007. [Online]. Available: <https://doi.org/10.1143/jjap.46.7496>
- [195] Q. Hu, G. A. Rance, G. F. Trindade, D. Pervan, L. Jiang, A. Foerster, L. Turyanska, C. Tuck, D. J. Irvine, R. Hague, and R. D. Wildman, "The influence of printing parameters on multi-material two-photon polymerisation based micro additive manufacturing," *Additive Manufacturing*, vol. 51, p. 102575, 2022. [Online]. Available: <https://www.sciencedirect.com/science/article/pii/S2214860421007223>
- [196] C. A. Schneider, W. S. Rasband, and K. W. Eliceiri, "Nih image to imagej: 25 years of image analysis," *Nature Methods*, vol. 9, pp. 671–675, 2012.
- [197] A. Keloth, O. Anderson, D. Risbridger, and L. Paterson, "Single cell isolation using optical tweezers," *Micromachines*, vol. 9, no. 9, 8 2018.
- [198] M. Cruceanu, A. G. Stephen, P. J. Beuning, R. J. Gorelick, R. J. Fisher, and M. C. Williams, "Single dna molecule stretching measures the activity of chemicals that target the hiv-1 nucleocapsid protein," *Analytical Biochemistry*, vol. 358, pp. 159–170, 2006.
- [199] M. B. Rasmussen, L. B. Oddershede, and H. Siegumfeldt, "Optical tweezers cause physiological damage to escherichia coli and listeria bacteria," *Applied and Environmental Microbiology*, vol. 74, pp. 2441–2446, 2008.
- [200] K. König, "Laser tweezers are sources of two-photon effects," in *Multiphoton Microscopy and Fluorescence Lifetime Imaging Applications in Biology and Medicine*, K. König, Ed. Berlin, Germany: Walter de Gruyter GmbH, 2018, ch. 9, pp. 177–188.
- [201] A. Chowdhury, D. Waghmare, R. Dasgupta, and S. K. Majumder, "Red blood cell membrane damage by light-induced thermal gradient under optical trap," *Journal of Biophotonics*, vol. 11, no. 8, p. e201700222, 2018.

- [202] I. Krasnikov, A. Seteikin, and I. Bernhardt, “Thermal processes in red blood cells exposed to infrared laser tweezers ($\lambda = 1064$ nm),” *Journal of Biophotonics*, vol. 4, no. 3, pp. 206–212, 2011.
- [203] S. Ayano, Y. Wakamoto, S. Yamashita, and K. Yasuda, “Quantitative measurement of damage caused by 1064-nm wavelength optical trapping of escherichia coli cells using on-chip single cell cultivation system,” *Biochemical and Biophysical Research Communications*, vol. 350, no. 3, pp. 678 – 684, 2006.
- [204] R. Omori, T. Kobayashi, and A. Suzuki, “Observation of a single-beam gradient-force optical trap for dielectric particles in air,” *Opt. Lett.*, vol. 22, no. 11, pp. 816–818, Jun 1997.
- [205] M. D. Summers, D. R. Burnham, and D. McGloin, “Trapping solid aerosols with optical tweezers: A comparison between gas and liquid phase optical traps,” *Opt. Express*, vol. 16, no. 11, pp. 7739–7747, May 2008.
- [206] S. Maruo, K. Ikuta, and H. Korogi, “Force-controllable, optically driven micro-machines fabricated by single-step two-photon microstereolithography,” *Journal of Microelectromechanical Systems*, vol. 12, no. 5, pp. 533–539, Oct 2003.
- [207] C. G. Baumann, S. B. Smith, V. A. Bloomfield, and C. Bustamante, “Ionic effects on the elasticity of single dna molecules,” *Proceedings of the National Academy of Sciences*, vol. 94, no. 12, pp. 6185–6190, 1997.
- [208] M. R. Griffiths, A. Raudsepp, K. M. McGrath, and M. A. K. Williams, “Measuring the interaction between a pair of emulsion droplets using dual-trap optical tweezers,” *RSC Adv.*, vol. 6, pp. 14 538–14 546, 2016.
- [209] F. M. Fazal, D. J. Koslover, B. F. Luisi, and S. M. Block, “Direct observation of processive exoribonuclease motion using optical tweezers,” *Proceedings of the National Academy of Sciences*, vol. 112, no. 49, pp. 15 101–15 106, 2015.
- [210] M. Gauthier, S. Régnier, P. Rougeot, and N. Chaillet, “Analysis of forces for micromanipulations in dry and liquid media,” *Journal of Micromechatronics*, vol. 3, pp. 389–413, 2006.
- [211] R. S. Fearing, “Survey of sticking effects for micro parts handling,” *Proceedings 1995 IEEE/RSJ International Conference on Intelligent Robots and Systems. Human Robot Interaction and Cooperative Robots*, vol. 2, pp. 212–217, 1995.
- [212] B. V. Derjaguin, N. V. Churaev, and V. M. Muller, *The Derjaguin—Landau—Verwey—Overbeek (DLVO) Theory of Stability of Lyophobic Colloids*. Boston, MA: Springer US, 1987, pp. 293–310.

- [213] S. H. Behrens and D. G. Grier, “The charge of glass and silica surfaces,” *The Journal of Chemical Physics*, vol. 115, no. 14, pp. 6716–6721, 2001.
- [214] S. Maruo, O. Nakamura, and S. Kawata, “Three-dimensional microfabrication with two-photon-absorbed photopolymerization,” *Opt. Lett.*, vol. 22, no. 2, pp. 132–134, Jan 1997.
- [215] I. Shishkin, H. Markovich, Y. Roichman, and P. Ginzburg, “Auxiliary optomechanical tools for 3d cell manipulation,” *Micromachines*, vol. 11, no. 1, 2020.
- [216] M. Grammatikopoulou and G. Yang, “Three-dimensional pose estimation of optically transparent microrobots,” *IEEE Robotics and Automation Letters*, vol. 5, no. 1, pp. 72–79, Jan 2020.
- [217] W. Kuhn, “Über die gestalt fadenförmiger moleküle in lösungen,” *Kolloid-Zeitschrift*, vol. 68, no. 1, pp. 2–15, Feb 1934. [Online]. Available: <https://doi.org/10.1007/BF01451681>
- [218] S. A. Harris, “Modelling the biomechanical properties of dna using computer simulation,” *Philosophical Transactions of the Royal Society A: Mathematical, Physical and Engineering Sciences*, vol. 364, no. 1849, pp. 3319–3334, Dec 2006. [Online]. Available: <https://doi.org/10.1098/rsta.2006.1906>
- [219] O. Kratky and G. Porod, “Röntgenuntersuchung gelöster fadenmoleküle,” *Recueil des Travaux Chimiques des Pays-Bas*, vol. 68, no. 12, pp. 1106–1122, 1949. [Online]. Available: <https://onlinelibrary.wiley.com/doi/abs/10.1002/recl.19490681203>
- [220] A. A. Kornyshev and S. Leikin, “Electrostatic interaction between helical macromolecules in dense aggregates: An impetus for dna poly- and mesomorphism,” *Proceedings of the National Academy of Sciences*, vol. 95, no. 23, pp. 13 579–13 584, 1998. [Online]. Available: <https://www.pnas.org/doi/abs/10.1073/pnas.95.23.13579>
- [221] A. Brunet, C. Tardin, L. Salomé, P. Rousseau, N. Destainville, and M. Manghi, “Dependence of dna persistence length on ionic strength of solutions with monovalent and divalent salts: A joint theory–experiment study,” *Macromolecules*, vol. 48, no. 11, pp. 3641–3652, Jun 2015. [Online]. Available: <https://doi.org/10.1021/acs.macromol.5b00735>
- [222] P.-K. Andrew, A. Raudsepp, D. Fan, U. Staufer, M. A. K. Williams, and E. Avci, “Optical microlever assisted dna stretching,” *Opt. Express*, vol. 29, no. 16, pp. 25 836–25 847, 2021.

- [223] M. Sarshar, W. Wong, and B. Anvari, “Comparative study of methods to calibrate the stiffness of a single-beam gradient-force optical tweezers over various laser trapping powers,” *Journal of Biomedical Optics*, vol. 19, no. 11, pp. 1 – 13, 2014. [Online]. Available: <https://doi.org/10.1117/1.JBO.19.11.115001>
- [224] S. Wu, J. Serbin, and M. Gu, “Two-photon polymerisation for three-dimensional micro-fabrication,” *Journal of Photochemistry and Photobiology A: Chemistry*, vol. 181, no. 1, pp. 1 – 11, 2006. [Online]. Available: <http://www.sciencedirect.com/science/article/pii/S1010603006001237>
- [225] S. Hu, H. Xie, T. Wei, S. Chen, and D. Sun, “Automated indirect transportation of biological cells with optical tweezers and a 3d printed microtool,” *Applied Sciences*, vol. 9, no. 14, 2019. [Online]. Available: <https://www.mdpi.com/2076-3417/9/14/2883>
- [226] I. Shishkin, H. Markovich, Y. Roichman, and P. Ginzburg, “Auxiliary optomechanical tools for 3d cell manipulation,” *Micromachines*, vol. 11, no. 1, 2020. [Online]. Available: <https://www.mdpi.com/2072-666X/11/1/90>
- [227] I. Grexa, T. Fekete, J. Molnár, K. Molnár, G. Vizsnyiczai, P. Ormos, and L. Kelemen, “Single-cell elasticity measurement with an optically actuated microrobot,” *Micromachines*, vol. 11, no. 9, 2020.
- [228] A.-I. Bunea and J. Glückstad, “Strategies for optical trapping in biological samples: Aiming at microrobotic surgeons,” *Laser & Photonics Reviews*, vol. 13, no. 4, p. 1800227, 2019. [Online]. Available: <https://onlinelibrary.wiley.com/doi/abs/10.1002/lpor.201800227>
- [229] H.-C. Chiu, K. D. Koh, M. Evich, A. L. Lesiak, M. W. Germann, A. Bongiorno, E. Riedo, and F. Storici, “Rna intrusions change dna elastic properties and structure,” *Nanoscale*, vol. 6, pp. 10 009–10 017, 2014. [Online]. Available: <http://dx.doi.org/10.1039/C4NR01794C>
- [230] H. Chen, S. P. Meisburger, S. A. Pabit, J. L. Sutton, W. W. Webb, and L. Pollack, “Ionic strength-dependent persistence lengths of single-stranded rna and dna,” *Proceedings of the National Academy of Sciences*, vol. 109, no. 3, pp. 799–804, 2012. [Online]. Available: <https://www.pnas.org/content/109/3/799>
- [231] G. Neuert, C. Albrecht, E. Pamir, and H. Gaub, “Dynamic force spectroscopy of the digoxigenin–antibody complex,” *FEBS Letters*, vol. 580, no. 2, pp. 505–509, 2006. [Online]. Available: <https://febs.onlinelibrary.wiley.com/doi/abs/10.1016/j.febslet.2005.12.052>

- [232] B. L. Aekbote, T. Fekete, J. Jacak, G. Vizsnyiczai, P. Ormos, and L. Kelemen, “Surface-modified complex su-8 microstructures for indirect optical manipulation of single cells,” *Biomed. Opt. Express*, vol. 7, no. 1, pp. 45–56, Jan 2016. [Online]. Available: <http://www.osapublishing.org/boe/abstract.cfm?URI=boe-7-1-45>
- [233] A. Raudsepp, M. A. Williams, and G. B. Jameson, “Modeling multiple duplex dna attachments in a force-extension experiment,” *Biophysical Reports*, vol. 2, no. 1, p. 100045, 2022. [Online]. Available: <https://www.sciencedirect.com/science/article/pii/S2667074722000027>
- [234] S. Pradhan, M. A. Williams, and T. K. Hale, “Changes in the properties of membrane tethers in response to hp1 α depletion in mcf7 cells,” *Biochem. Biophys. Res. Commun.*, vol. 587, pp. 126–130, 2022.
- [235] F. M. Fazal, D. J. Koslover, B. F. Luisi, and S. M. Block, “Direct observation of processive exoribonuclease motion using optical tweezers,” *PNAS*, vol. 112, no. 49, pp. 15 101–15 106, 2015.
- [236] C. J. Bustamante, Y. R. Chemla, S. Liu, and M. D. Wang, “Optical tweezers in single-molecule biophysics,” *Nat. Rev. Methods Primers*, vol. 1, no. 1, p. 25, 2021.
- [237] G. Leitz, E. Fällman, S. Tuck, and O. Axner, “Stress response in caenorhabditis elegans caused by optical tweezers: Wavelength, power, and time dependence,” *Biophys. J.*, vol. 82, no. 4, pp. 2224–2231, 2002.
- [238] E. Avci and G.-Z. Yang, “Development of a microhand using direct laser writing for indirect optical manipulation,” in *2016 IEEE/RSJ International Conference on Intelligent Robots and Systems (IROS)*. IEEE Press, 2016, p. 5125–5130.
- [239] F. Niesler and M. Hermatschweiler, “Two-photon polymerization — a versatile microfabrication tool,” *Laser Technik Journal*, vol. 12, no. 3, pp. 44–47, 2015.
- [240] G. Gouesbet, J. A. Lock, and G. Gréhan, “Generalized lorenz–mie theories and description of electromagnetic arbitrary shaped beams: Localized approximations and localized beam models, a review,” *J. Quant. Spectrosc. Radiat. Transf.*, vol. 112, no. 1, pp. 1–27, 2011.
- [241] T. A. Nieminen, V. L. Y. Loke, A. B. Stilgoe, G. Knöner, A. M. Brańczyk, N. R. Heckenberg, and H. Rubinsztein-Dunlop, “Optical tweezers computational toolbox,” *J. Opt.*, vol. 9, no. 8, pp. S196–S203, 2007.

- [242] I. C. D. Lenton, T. A. Nieminen, V. L. Y. Loke, A. B. Stilgoe, Y. Hu, G. Knöner, A. M. Brańczyk, N. R. Heckenberg, and H. Rubinsztein-Dunlop, “Optical tweezers toolbox,” <https://github.com/ilent2/ott>, 2020.
- [243] A. Raudsepp, M. Griffiths, A. J. Sutherland-Smith, and M. A. K. Williams, “Developing a video tracking method to study interactions between close pairs of optically trapped particles in three dimensions,” *Appl. Opt.*, vol. 54, no. 32, pp. 9518–9527, 2015.
- [244] C. W. Ha and D.-Y. Yang, “Rotational elastic micro joint based on helix-augmented cross-spring design for large angular movement,” *Opt. Express*, vol. 22, no. 17, pp. 20 789–20 797, 2014.
- [245] C.-L. Lin, Y.-H. Li, C.-T. Lin, C.-C. Chiang, Y.-J. Liu, T.-T. Chung, and P. L. Baldeck, “Preliminary study of lever-based optical driven micro-actuator,” in *Proc. SPIE*, J. Leng, Y. Bar-Cohen, I. Lee, and J. Lu, Eds., vol. 8409, International Society for Optics and Photonics. SPIE, 2012, pp. 589 – 594.
- [246] Y.-H. Lee, Y.-J. Liu, C. Tsou, M. Bouriau, P. Baldeck, and C.-L. Lin, “Optically driven gear-based mechanical microtransducer for a lab-on-a-chip,” *J. Neurosci. Neuroeng.*, vol. 2, pp. 58–60, 2013.
- [247] C.-N. Nguyen, K. Ohara, T. Takubo, Y. Mae, and T. Arai, “High-speed auto-focusing of multisized microobjects,” in *2012 IEEE International Conference on Automation Science and Engineering (CASE)*, 2012, pp. 34–39.
- [248] M. Schmid, D. Ludescher, and H. Giessen, “Optical properties of photoresists for femtosecond 3d printing: refractive index, extinction, luminescence-dose dependence, aging, heat treatment and comparison between 1-photon and 2-photon exposure,” *Opt. Mater. Express*, vol. 9, no. 12, pp. 4564–4577, 2019.
- [249] N. Mohandas, L. M. Kent, A. Raudsepp, G. B. Jameson, and M. A. K. Williams, “Progress toward plug-and-play polymer strings for optical tweezers experiments: Concatenation of dna using streptavidin linkers,” *ACS Omega*, vol. 7, no. 7, pp. 6427–6435, Feb 2022. [Online]. Available: <https://doi.org/10.1021/acsomega.2c00198>
- [250] T. Baldacchini, M. Zimmerley, C.-H. Kuo, E. O. Potma, and R. Zadoyan, “Characterization of microstructures fabricated by two-photon polymerization using coherent anti-stokes raman scattering microscopy,” *The Journal of Physical Chemistry B*, vol. 113, no. 38, pp. 12 663–12 668, Sep 2009. [Online]. Available: <https://doi.org/10.1021/jp9058998>

- [251] A. Žukauskas, I. Matulaitienė, D. Paipulas, G. Niaura, M. Malinauskas, and R. Gadonas, “Tuning the refractive index in 3d direct laser writing lithography: towards grin microoptics,” *Laser & Photonics Reviews*, vol. 9, no. 6, pp. 706–712, Nov 2015. [Online]. Available: <https://doi.org/10.1002/lpor.201500170>
- [252] C.-S. Shin, T.-J. Li, and C.-L. Lin, “Alleviating distortion and improving the young’s modulus in two-photon polymerization fabrications,” *Micromachines*, vol. 9, no. 12, p. 615, Nov 2018, 30467303[pmid]. [Online]. Available: <https://pubmed.ncbi.nlm.nih.gov/30467303>
- [253] W. Xiong, Y. S. Zhou, X. N. He, Y. Gao, M. Mahjouri-Samani, L. Jiang, T. Baldacchini, and Y. F. Lu, “Simultaneous additive and subtractive three-dimensional nanofabrication using integrated two-photon polymerization and multiphoton ablation,” *Light: Science & Applications*, vol. 1, no. 4, pp. e6–e6, Apr 2012. [Online]. Available: <https://doi.org/10.1038/lssa.2012.6>